BRITISH COLUMBIA
Ministry of Employment and Investment
Energy and Minerals Division
Geological Survey Branch

GEOLOGY AND PLATINUM-GROUP-ELEMENT MINERALIZATION OF ALASKAN-TYPE ULTRAMAFIC-MAFIC COMPLEXES IN BRITISH COLUMBIA

By G.T. Nixon, P.Geo., J.L. Hammack, P.Geo.,
C.H. Ash, P.Geo., L.J. Cabri, G. Case, J.N. Connelly,
L.M. Heaman, J.H.G. Laflamme, C. Nuttall,
W.P.E. Paterson and R.H. Wong, P.Geo.

BULLETIN 93

Canadian Cataloguing in Publication Data
Nixon, Graham T. (Graham Tom), 1948-
Geology and platinum group element mineralization of Alaskan-type ultramafic-mafic complexes in British Columbia

(Bulletin 93, ISSN 0226-9430)

Issued by Geological Survey Branch.
Includes bibliographical references: p.
ISBN 0-7726-1974-3

1. Platinum ores - British Columbia. 2. Geochemical prospecting - British Columbia. 3. Geology, Economic - British Columbia. I. Hammack, Janet L. (Janet Lee), 1955- II. Ash, C. III. British Columbia. Ministry of Employment and Investment. IV. British Columbia. Geological Survey Branch. V. Title. VI. Series: Paper (British Columbia. Ministry of Employment and Investment) ; 1993-2.

TN490.P7 N69 1997 553.4'22'09711 C93-092417-7

VICTORIA
BRITISH COLUMBIA
CANADA

MARCH 1997

SUMMARY

Alaskan-type or zoned ultramafic-mafic complexes in British Columbia occur within accreted volcanic-arc terranes of the Intermontane Belt of the Canadian Cordillera and are broadly coeval and cospatial with early Mesozoic arc volcanic rocks of Quesnellia and Stikinia. The data on Alaskan-type complexes presented in this report includes previously published work on the Tulameen, Polaris, Lunar Creek, Wrede Creek, and Johanson Lake bodies in the Quesnel Terrane, and the Hickman, Gnat Lakes and Menard Creek complexes in northern Stikinia.

Where their external geometry can be determined, Alaskan-type complexes form transgressive sills (*e.g.*, Polaris) or stock-like intrusions (*e.g.*, Wrede) with locally well-developed thermal aureoles. Igneous textures are well preserved and cumulus minerals include olivine, chromite, clinopyroxene, hornblende and feldspar with minor phlogopite/biotite, magnetite, apatite and sphene. The principal ultramafic lithologies are dunite, wehrlite, olivine clinopyroxenite, clinopyroxenite, hornblende clinopyroxenite and hornblendite; and thin, discontinuous layers of chromitite are contained in dunite. Mafic to intermediate feldspathic rocks (hornblende gabbro-diorite to syenite) cut by late-stage hornblende-feldspar-quartz pegmatites are exposed in most complexes. Internal zoning may be assymetrical (*e.g.*, Polaris) or crudely symmetrical (*e.g.*, Wrede, Tulameen) and contacts between lithologies are sharp to gradational. Centimetre-scale modal layering is generally rare but locally conspicuous at Tulameen and Lunar Creek. The fieldwork results indicate that previous concepts relating the origin of Alaskan-type intrusions to diapiric re-emplacement of ultramafic cumulates existing at depth are no longer tenable. Rather, these Alaskan-type intrusions were emplaced high in the crust (subvolcanic?) where cumulate sequences developed *in situ* and recorded the progressive differentiation of primitive, and in some cases potassic, mafic magmas. Remobilization of early olivine-rich cumulates and chromitite horizons in the magma chamber was effected by slumping or reworking of poorly consolidated cumulate horizons in response to convection currents, gravitational instability or tectonic (earthquake) activity.

New U-Pb isotopic analyses on zircons separated from late-stage feldspathic pegmatites in the Lunar Creek and Polaris complexes yield mid-Triassic (237±2(2σ) Ma) and late Early Jurassic (186±2 Ma) dates, respectively. These data attest to the longevity of plutonism and coeval volcanism in the accreted arc terranes of Quesnellia and Stikinia. Furthermore, correlation of regional structures with ductile fabrics developed in the thermal aureole at the base of the Polaris complex indicates that early, eastward-verging contractional deformation related to docking of accreted terranes with ancestral North America apparently began during the final stages of cooling of the Polaris complex (*i.e.*, earliest Toarcian).

The economic potential of Alaskan-type complexes has been evaluated with respect to platinum-group elements (PGE). The highest abundances of PGE occur in chromitites in the Tulameen and Wrede Creek complexes, and reflect the accumulation of discrete platinum-group minerals (PGM), principally platinum-iron alloys, in magmatic cumulates. The chromitites are characterized by very high platinum:palladium and platinum:copper ratios. Normalized PGE abundances of platiniferous chromitites have "M-shaped" patterns with peaks at platinum and iridium separated by an intervening trough at ruthenium. These unusual geochemical traits serve to distinguish Alaskan-type complexes from other geological environments.

The textures and compositions of platinum-group minerals, and coexisting silicate, oxide and base metal minerals in PGE-enriched chromitites of the Tulameen Complex and spatially associated placers have been examined in detail. The principal Pt-Fe-Cu-Ni alloys in chromitites are "tetraferroplatinum" [Pt(Fe,Ni,Cu)] and "isoferroplatinum" [$Pt_{2.5}(Fe,Ni,Cu)_{1.5}$] whereas placers commonly contain "isoferroplatinum [Pt_3Fe to $Pt_{2.6}(Fe,Cu,Ni)_{1.4}$], native and ferroan platinum. Most alloys (except tulameenite, Pt_2FeCu), and minor laurite (RuS_2) and ehrlichmanite (OsS_2), are interpreted to represent a primary high-temperature paragenesis. Other PGM, notably platinum arsenides and antimonides and rhodium-iridium sulpharsenides, platinian copper, and small quantities of base metal sulphides, arsenides, antimonides, oxides and native metals, are secondary and formed by metasomatic replacement and localized remobilization of PGE during serpentinization and regional metamorphism. The compositions of chromite and olivine in platinum nuggets are identical to grains in chromitites and indicate quite conclusively that PGE in the placers were derived from mineralized chromitites in the dunite core of the Tulameen complex. The origin of these PGE-enriched chromitites in Alaskan-type intrusions is related to segregation of predominantly Pt-Fe alloys from primitive magmas during conditions that enhanced the precipitation of chromite (*e.g.*, increase in the fugacity of oxygen). There is no evidence for subsolidus concentration of PGE by either exsolution from chromite or desulphurization of primary magmatic sulphides.

The mineralogy and geochemistry of PGE in Alaskan-type intrusions have important implications for exploration. The provenance of PGM in placer deposits may be uniquely characterized by the compositions of coexisting gangue minerals such as chromite and olivine. In addition, the distinctive "M-shaped" PGE abundance patterns of mineralized chromitites provide a definitive signature of an Alaskan-type source. Since the PGE are predominantly concentrated in relatively inert alloys, they are expected to be fairly robust during weathering and transportation. Therefore, these observations should encourage the careful analysis of panned concentrates when prospecting for the source of placer PGE.

TABLE OF CONTENTS

MAPS (in pocket)

FIGURES

PHOTOS

TABLES

CHAPTER 1 INTRODUCTION

Alaskan-type ultramafic-mafic complexes in British Columbia are potential hosts for commercially exploitable deposits of platinum metals (Rublee, 1986; Evenchick *et al.*, 1986) as well as commodities such as chrome, nickel, cobalt, asbestos and jade. In 1987, the British Columbia Geological Survey initiated a project designed to update the geological database for Alaskan-type complexes in British Columbia in order to more fully evaluate their economic potential, particularly with respect to platinum-group elements (PGE). The project was made possible by funding provided by the Mineral Development Agreement (1985-1990) between Canada and the Province of British Columbia. This report summarizes previously published and unpublished results of geological fieldwork and geochronological, mineralogical and geochemical investigations of Alaskan-type complexes conducted between 1987 and 1992 (*cf.* Appendix A). It includes practically all of the known major Alaskan-type occurrences, including the Tulameen, Polaris, Wrede Creek and Lunar Creek complexes, and many minor bodies such as Johanson Lake, Menard Creek, Gnat Lakes and Hickman. The Tulameen complex warrants special attention because it has served as a type example of the Alaskan-type association in British Columbia (Findlay, 1963; 1969).

The Alaskan-type complexes and their associated placers are considered to be the most favourable environment for PGE in the Cordillera (Evenchick *et al.*, 1986; Hulbert *et al.*, 1988; Nixon and Hammack, 1991). To date, however, only the platinum-rich placers derived from the Tulameen complex in southern British Columbia have been exploited economically, yielding some 680 000 grams of impure platinum nuggets between 1885 and 1932 (O'Neil and Gunning, 1934). Evidence is presented in this study for a direct link between PGE-enriched placers and chromitite-hosted PGE mineralization in the bedrock. More importantly, this work has led to the recognition of important new exploration techniques for determining the nature of the source of placer PGE based on the geochemical signature of panned concentrates and mineralogy of platinum nuggets.

ALASKAN-TYPE COMPLEXES: GENERAL NATURE AND TECTONIC SETTING

The Alaskan-type complexes are named for a distinctive suite of ultramafic-mafic intrusions distributed along a narrow, northerly trending belt, 600 kilometres long, in southeastern Alaska (Figure 1.1). They were previously described from the Ural Mountains in the former Soviet Union (*e.g.*, Duparc and Tikonowitch, 1920) and are well known in both orogenic settings and stable platforms (*e.g.*, Aldan Shield in the former Soviet Union; Choco District, Colombia; Youbdo, Ethiopia; Goodnews Bay, Alaska; Fifield-Owendale District, New South Wales, Australia; *cf.* Taylor, 1967; Cabri, 1981; Johan *et al.*, 1989; Slansky *et al.*, 1991).

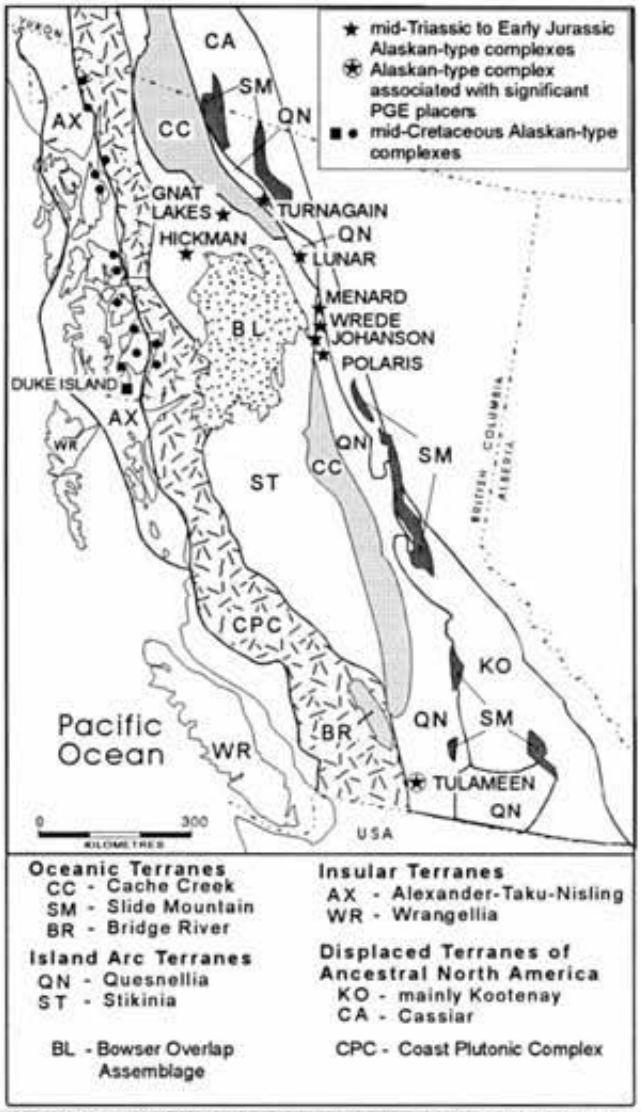

Figure 1.1. Distribution of major Alaskan-type ultramafic-mafic complexes and coeval volcanic rocks in British Columbia and southeastern Alaska in relation to tectonostratigraphic terranes of the Cordillera.

Commonly used synonyms include Alaskan-Ural, Uralian, concentrically zoned or just zoned complexes. Their salient geologic and petrographic features have been summarized by Taylor (1967), and the Duke Island ultramafic intrusion remains the best-documented example (Irvine, 1974a).

One of the key internal attributes of Alaskan-type complexes is a zonal distribution of rock types such that olivine-rich lithologies in the interior grade outward into pyroxenitic and/or gabbroic to dioritic rocks at the margins. This pattern may be crudely concentric but this is not a universal trait (Taylor, 1967). Primary mesoscopic layering and sedimentary structures such as those so spectacularly developed at

Duke Island (Irvine, 1974a) are seldom observed and appear atypical of Alaskan-type complexes in general. In part, however, such features may have been obscured or modified by post-cumulus recrystallization and remobilization.

Ultramafic lithologies characteristic of Alaskan-type complexes lie along the olivine-clinopyroxene join shown in Figure 1.2. The classification scheme is essentially that recommended by the IUGS Subcommision on the Systematics of Igneous Rocks as summarized by Le Maitre (1989). However, it was found beneficial in the field to arbitrarily subdivide extensive wehrlitic lithologies into olivine wehrlite (65 to 90 % olivine; 10 to 35 % clinopyroxene) and wehrlite (40 to 65 % olivine; 35 to 60 % clinopyroxene). Early cumulate minerals in Alaskan-type complexes are typically represented by forsteritic olivine, chromite, diopsidic clinopyroxene and rare phlogopitic mica, whereas hornblende, biotite, magnetite and plagioclase (together with accessory apatite, sphene and ilmenite) commonly predominate in the more evolved rocks. Orthopyroxene is characteristically absent which has been taken to indicate an alkalic affinity for the parental magmas (Irvine, 1974a). The gabbroic to dioritic rocks may be mildly alkaline or calcalkaline, or tholeiitic, and not necessarily genetically linked with ultramafic cumulates (Irvine, 1974a). Not all of the characteristic rock types are represented in each intrusion which can make their Alaskan-type affinity difficult to establish, particularly if only hornblende-rich and feldspathic differentiates are exposed.

Occurrences of the major Alaskan-type complexes in British Columbia are shown in Figure 1.1. Other smaller bodies are also known, particularly in the northern part of the province in the Wrede-Polaris region. In an attempt to formally apply recommendations contained in the North American Stratigraphic Code, Woodsworth *et al.* (1991) used the term "Polaris Ultramafic Suite" to describe all Alaskan-type complexes in British Columbia which were considered to be Late Triassic in age. Recent isotopic dating, however, has established intrusion ages ranging from mid-Triassic for the Lunar Creek complex, for example, to late Early Jurassic in the case of the Polaris complex. Also, there are significant exposures of genetically-related mafic-intermediate cumulate sequences exposed in the upper part of the Polaris complex, for example, in addition to the more voluminous ultramafic lithologies, and in some complexes mafic lithologies predominate almost to the exclusion of ultramafic counterparts. At this time, therefore, we have decided to retain the informal term "Alaskan-type complex" (Irvine, 1974a) to designate all such intrusive suites in British Columbia and have indicated the relative abundance of ultramafic versus mafic lithologies in any single complex by use of the adjectival qualifers ultramafic-mafic, where ultramafic rocks predominate, and mafic-ultramafic where the opposite is true.

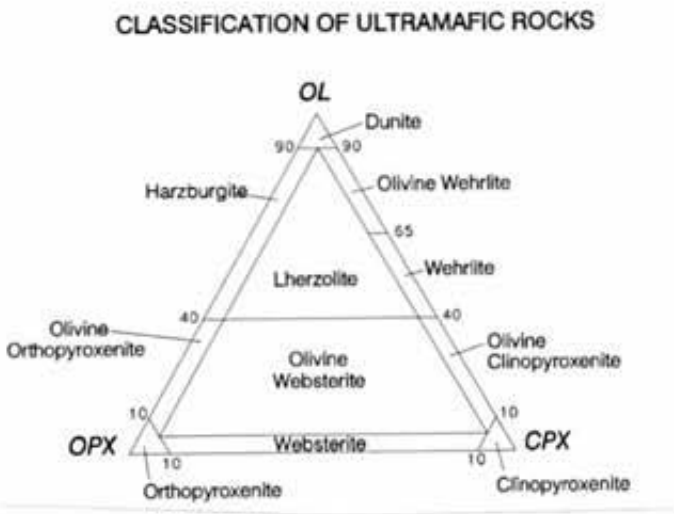

Figure 1.2. Classification of ultramafic rocks (modified after Le Maitre, 1989). Lithologies encountered in Alaskan-type complexes in British Columbia lie along the olivine-clinopyroxene join; other common rock types include hornblende clinopyroxenite (10-50% hornblende, 10-50% clinopyroxene) clinopyroxene hornblendite (10-50% clinopyroxene, 10-50% hornblende) and hornblendite (<10% clinopyroxene).

Without exception, all of the Alaskan-type complexes in British Columbia lie within the allochthonous terranes of the Intermontane Belt, specifically Quesnellia and Stikinia, that were amalgamated and accreted to the cratonic margin of ancestral North America in the Mesozoic (Gabrielse and Yorath, 1991; Wheeler and McFeeley, 1991). Their distribution is spatially associated with Late Triassic to Early Jurassic volcanic-arc rocks of the Nicola, Takla and Stuhini groups (Figure 1.1) with which they have been genetically related (Irvine, 1974b, 1976; Mortimer, 1986). The size of individual intrusive bodies ranges from less than one square kilometre to sixty square kilometres, and outcrop patterns vary from round or elliptical to markedly elongate. The latter intrusions are generally elongated parallel to the predominant structural grain of the region. Some intrusions exhibit well-developed contact metamorphic aureoles of amphibolite grade; others appear to be completely fault-bounded. The geology and noble metal geochemistry of specific complexes is examined prior to an overall assessment of their economic potential and tectonic significance.

ACKNOWLEDGMENTS

This project was made possible by funding from the Canada - British Columbia Mineral Development Agreement (1985-1990). The contributions of the junior authors were as follows: Jan Hammack wrote the chapters on the Wrede and Lunar Creek complexes and also mapped parts of the Johanson Lake and Polaris complexes; Chris Ash, Jim Connelly, Glenn Case, Carol Nuttall and Bill Paterson contributed their mapping expertise; Jim Connelly first deduced the kinematics of ductile faulting at Polaris; Russ Wong generously shared unpublished mapping and analytical data for Wrede Creek; Larry Heaman provided U-Pb isotopic dates for Polaris and Lunar Creek; and Louis Cabri and Gilles Laflamme collaborated on the study of platinum mineralization at Tulameen, provided electron microprobe data for platinum-group minerals and base metals, and supplied the beautiful scanning electron microscope photomicrographs.

Logistics in the field were made safe and enjoyable by numerous people. In particular, we wish to thank Sandy Jay-

cox and associates (Smithers), Keith Buchanan (Northern Mountain Helicopters), Tom Brooks (Canadian Helicopters), and especially Steve Blower for capable and cheerful assistance in the field at Tulameen. Thanks are also extended to Dennis Bohme (formerly of Newmont Exploration Ltd.) who made available maps and geochemical data for Tulameen; Colin Godwin (The University of British Columbia) who donated rocks and thin sections from Wrede Creek; Dr. J.A. Mandarino (Royal Ontario Museum) for supplying the platinum-bearing nuggets; Mr. J.M. Beaulne (Canada Centre for Mineral and Energy Technology) for preparing polished sections; Peter Roeder and Dave Kempson (Queen's University) for providing access to electron-microprobe facilities; Dick Player for thin sections and photographic reproduction; and Wes Johnson (former head of the former Analytical Sciences Laboratory of the former B.C. Ministry of Energy, Mines and Petroleum Resources), Gwendy Hall (Geological Survey of Canada), Eric Hoffman (Activation Laboratories) and Mario Bergeron (Institut National de la Recherche Scientifique) for their analytical expertise in performing PGE analyses on Tulameen samples.

Our ongoing education with respect to the nature and significance of Alaskan-type complexes and their platinum-group element mineralization derives in large part from the work of others. Particularly insightful discussions were entertained by Chris Findlay, Murray Duke, Larry Hulbert, John Scoates and Colin Dunn of the Geological Survey of Canada, Kay Fletcher (The University of British Columbia), Steve Cook (Ministry of Employment and Investment), Jacqui Rublee (Ottawa-Carlton Centre for Graduate Studies), and Charlie Greig (University of Arizona). We are also indebted to Hu Gabrielse and Jim Monger of the Geological Survey of Canada for sharing their ideas and extensive knowledge of the Cordillera.

The manuscript benefited from reviews in whole or in part by Sarah-Jane Barnes, Craig Bow, Bob Martin, Bill McMillan, Peter Roeder, and Mike Zientek. We thank Martin Taylor, Pierino Chicorelli, John Armitage and Verna Vilkos for drafting, Brian Grant and John Newell for editorial comments and Janet Holland for typing and layout.

CHAPTER 2 HICKMAN COMPLEX

The Hickman ultramafic-mafic complex (57°16′N, 131°05′W) is located approximately 150 kilometres south-southwest of Dease Lake and 55 kilometres south of Telegraph Creek (Figure 2.1). The project area is covered by 1:50 000 topographic maps 104G/6 and 104G/3. Access to the region is by air from Dease Lake to an airstrip at the confluence of the Scud and Stikine rivers, and from there by helicopter. The region has excellent, though rugged, rock exposures that skirt receding mountain glaciers at altitudes between 1200 and 2800 metres.

REGIONAL GEOLOGY AND GEOCHRONOMETRY

The Hickman complex lies near the eastern edge of the Coast Mountains in the Intermontane Belt. It is situated in northern Stikinia, a tectonostratigraphic terrane comprising middle Paleozoic to Mesozoic sedimentary, volcanic and plutonic rocks (Figure 2.1). The complex is named for Mount Hickman which lies at its western edge. The area is underlain by Late Triassic to Middle Jurassic granitoid rocks of the Hickman batholith and volcanic lithologies assigned to the Upper Triassic Stuhini Group (Figure 2.2; Souther, 1972; Holbeck, 1988; Brown and Gunning, 1989).

The Hickman batholith (1200 km^2) is a composite body incorporating the Late Triassic (Carnian-Norian) Nightout and Hickman plutons (Stikine Suite granitoids of Woodsworth *et al.*, 1991) and Middle Jurassic (Bajocian-Bathonian) Yehiniko pluton (Three Sisters Suite) which intrudes the other two. Potassium-argon and rubidium- strontium geochronometry on mineral separates and whole rocks yield dates of 228±16 (2σ; K-Ar on hornblende), 221±16 (K-Ar on hornblende), and 178×±22 Ma (Rb-Sr, whole rock) for the Nightout, Hickman and Yehiniko plutons, respectively (Holbeck, 1988). The Hickman pluton underlies some 300 square kilometres at the southern limit of the Hickman batholith. Two phases of this pluton are recognized within the map area: a main granodioritic to monzonitic phase and a mafic, more gabbroic phase.

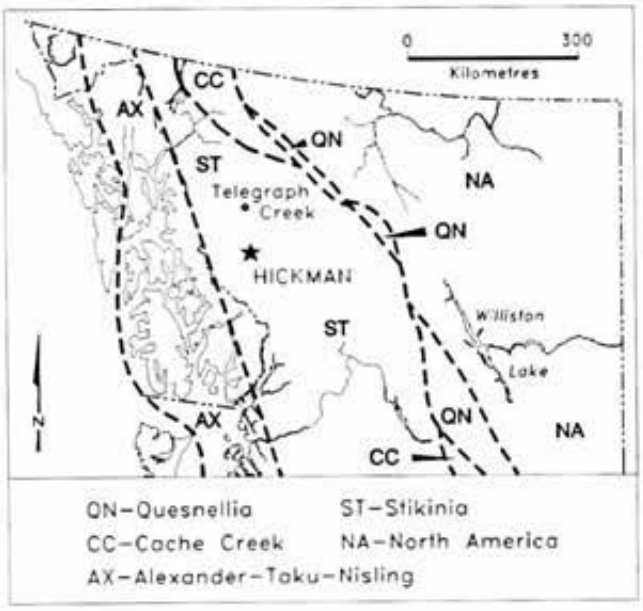

Figure 2.1. Location of the Hickman ultramafic-mafic complex in relation to major tectonostratigraphic terranes in northern British Columbia.

The ultramafic-mafic rocks were originally considered to form an integral part of the Hickman pluton (Souther, 1972). However, more recent mapping by Holbeck (1988) and Brown and Gunning (1989), in addition to our work, indicates that Mount Hickman itself is underlain by volcanic and volcaniclastic rocks that extend northeastward along the western margin of the ultramafic-mafic complex. We have therefore decided to treat the Hickman complex as a separate entity rather than assume genetic links with the Hickman pluton for which there is currently no strong evidence.

The Stuhini Group east of Mount Hickman generally forms elongate outcrops that are bounded by north-trending normal faults or intruded by batholithic rocks. Regionally, the Stuhini Group is characterized by mafic to intermediate augite-phyric flows, sills and volcaniclastic rocks with subgreenschist metamorphic assemblages. The upper part of the succession contains hornblende-plagioclase-phyric andesitic flows, heterolithic volcanic breccias and conglomerates, and rare felsic tuffs capped by fossiliferous limestones of Norian to Carnian age. These rocks appear to be correlative with similar lithologies that occur 100 kilometres to the northeast around the margin of the Hotailuh batholith (Anderson, 1983; 1988).

The structural and metamorphic history of the region is complex (*cf.* Brown and Gunning, 1989). At least two phases of pre-Permian folding are recognized, and deformation also occurred in post-Early Jurassic time with southwesterly directed folding and thrusting. The latter phase of compression involved the margins of the Hickman pluton and the Stuhini Group. Faulting in the region appears to have continued into the Late Tertiary.

COUNTRY ROCKS

STUHINI GROUP

Volcanic assemblages of uncertain age (Holbeck, 1988) almost completely surround the ultramafic complex. In the north, the contact with ultramafic rocks is faulted, but to the east a sharp intrusive contact has been recognized between weakly hornfelsed volcanic rocks and marginal gabbros of the Hickman complex (M.H. Gunning, personal

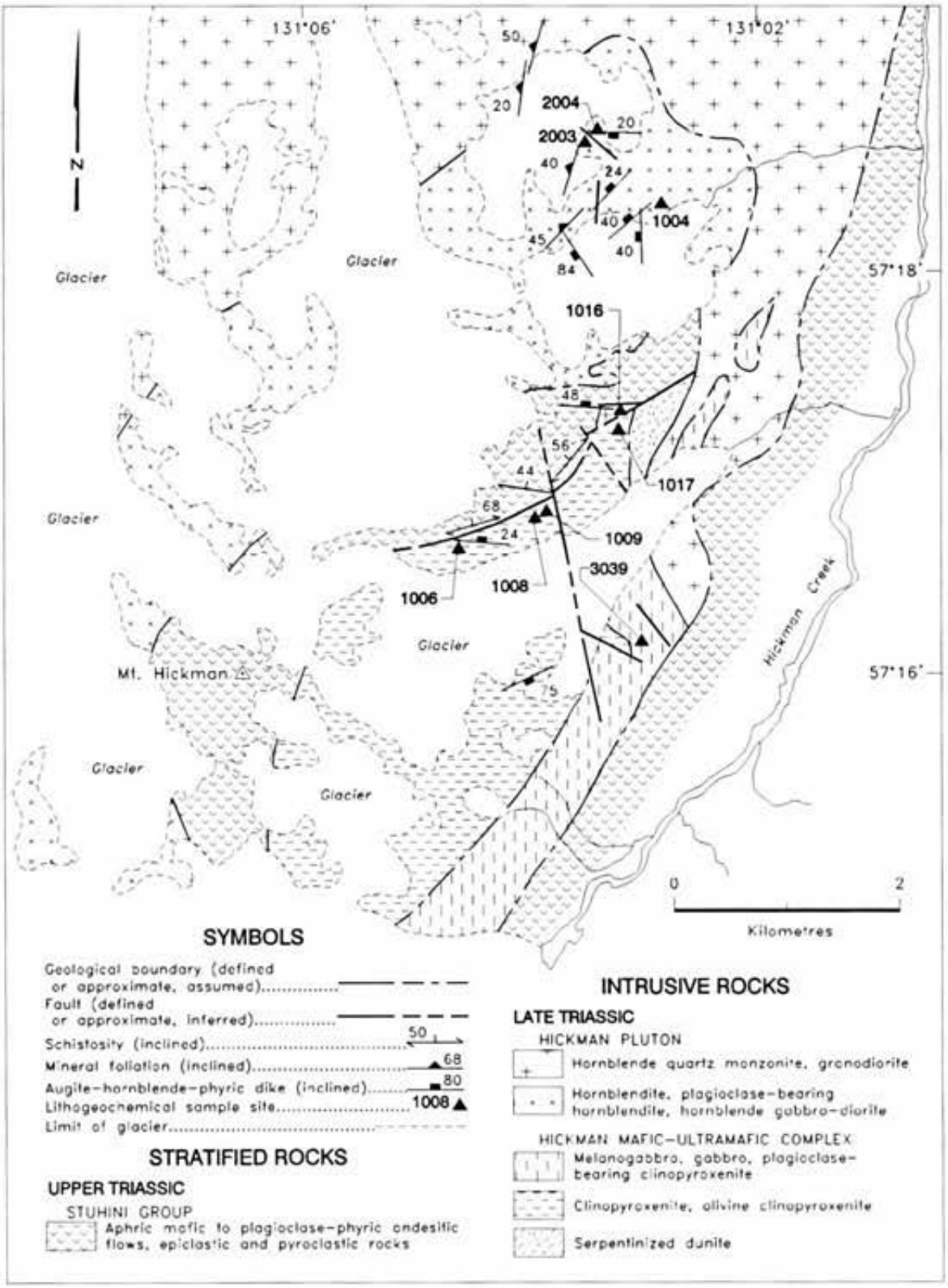

Figure 2.2. Geologic map of the Hickman mafic-ultramafic complex showing distribution of geochemical sample sites.

communication, 1988). The exact position and nature of the western contact just east of Mount Hickman is not known.

The volcanic stratigraphy comprises predominantly mafic aphyric flows with subordinate porphyritic andesites and minor intercalated volcaniclastic material. The rocks are generally dark greenish to medium grey or maroon, and are locally bleached pale green to buff. Andesitic flows contain phenocrysts of plagioclase (20 vol%) up to 3 millimetres in length, and pyroxene and/or amphibole (<5 vol%). These lithologies are included within the Stuhini Group, although doubt remains as to their exact stratigraphic position.

HICKMAN PLUTON

The main phase of the Hickman pluton delineates the northeastern margin of the ultramafic complex. It comprises a pale grey to pinkish grey weathering medium-grained hornblende biotite monzonite to granodiorite which grades into a more melanocratic phase towards the core of the pluton. The granitoid rocks become finer grained and enriched in biotite towards their contacts and irregular apophyses of fine-grained biotite monzonite locally cut the volcanic assemblages.

The mafic phase of the pluton is largely composed of medium to coarse-grained black hornblendite, plagioclase-bearing hornblendite, and dark to light grey hornblende gabbro to diorite with minor biotite. Prismatic hornblende crystals (<1 cm in length) in the more melanocratic rocks locally define an igneous lamination, probably a flow foliation, that wraps around inclusions. The xenolith suite comprises angular to rounded blocks of hornblendite, hornblende gabbro and grey-green pyritic diorite and large rafts of hornfelsed sedimentary rocks.

HICKMAN COMPLEX: ULTRAMAFIC-MAFIC ROCKS

The main outcrops of mafic and ultramafic rocks that comprise the Hickman complex are found immediately east of Mount Hickman, which itself is underlain by volcanic rocks of uncertain age (Holbeck, 1988), possibly correlative with the Stuhini Group. The complex covers 11 square kilometres and forms an elongate body trending northeast with maximum dimensions of about 6 by 3 kilometres (Figure 2.2). The ultramafic-mafic rocks are spatially associated with the Hickman pluton.

DUNITE

A small wedge of altered dunite is exposed at the northern end of the complex in fault contact with volcanic rocks and intruded by the main phase of the Hickman pluton. The rock is dark to pale grey weathering, moderately magnetic, and cut by numerous white calcite veins (<6 cm in width) especially near contacts. Two samples collected within 10 metres of the contact are thoroughly serpentinized. In thin section, olivine is seen to be completely replaced by serpentine and grain boundaries are coated with secondary magnetite dust. Tiny euhedral chromite crystals (1 vol%) are dispersed throughout the rock.

OLIVINE CLINOPYROXENITE AND CLINOPYROXENITE

The central part of the Hickman complex is predominantly composed of dark grey-green to brownish weathering, coarse to medium-grained clinopyroxenite containing minor olivine (up to 20 vol%) and interstitial magnetite (5 to 10 vol%), accessory biotite (<1 vol%) and rare hornblende. The rock is generally massive and uniform except close to faults where anastomizing veins of carbonate, serpentine, talc and clay minerals are found. Some fault zones are silicified and contain disseminated sulphides. In northern outcrops, the modal proportion of olivine appears to decrease to the east, away from the dunite. Locally, the clinopyroxenite is enriched in biotite which forms crystals up to 1 centimetre across. Clinopyroxenites gradually become feldspathic towards the contact with marginal gabbros. Generally, olivine and clinopyroxene occur as cumulus minerals that locally exhibit adcumulus growth. Iron-titanium oxides and biotite, with or without hornblende, form an intercumulus framework.

GABBROIC ROCKS

Gabbroic rocks crop out in a narrow belt 500 metres wide along the eastern margin of the complex. These marginal gabbros are dark to medium grey, equigranular rocks containing subequal proportions of plagioclase and clinopyroxene, and minor hornblende (5 vol%), biotite (usually <5 vol%) and magnetite. The gabbros are cut locally by leucocratic plagioclase-rich dikes several centimetres in width.

CONTACT RELATIONSHIPS

The age of emplacement of the Hickman complex is constrained by intrusive relationships, stratigraphic correlations and isotopic dating. The complex is truncated on the north by the main phase of the Hickman pluton (Stikine Suite) dated at approximately 221±16 Ma or Late Triassic (Holbeck, 1988), and intrudes volcanic rocks that are Upper Triassic equivalents of the Stuhini Group or older. Thus, the Hickman complex is considered to be Late Triassic in age.

Internally, the complex comprises several distinct lithologies that include dunite, olivine clinopyroxenite to clinopyroxenite and gabbroic rocks. The contact between dunite and olivine clinopyroxenite appears to be sharply transitional, and that between clinopyroxenite and the gabbroic rocks is sharp to gradational over several metres. The latter transition is marked by a gradual increase in the modal proportion of plagioclase (<15 vol%).

DIKES

Mafic to intermediate dikes of variable mineralogy and texture intrude the ultramafic and granitoid rocks. They are the youngest intrusions in the map area and are of Late Triassic age or younger. The dominant orientation is east-west with moderate dips to the north. Dark grey mafic dikes (<1 m in width) are weakly vesicular and either aphyric or contain sparse plagioclase microphenocrysts (<1 mm). Medium to pale grey porphyritic dikes (2 to 4 m in width) with large (<3 cm) phenocrysts of hornblende and augite (10 to 20%

by volume) and sparse plagioclase commonly exhibit chilled margins and multiple injection. These dikes mineralogically resemble typical Stuhini Group volcanic rocks although they postdate emplacement of the Hickman pluton and presumed Stuhini Group equivalents that host the ultramafic complex.

STRUCTURE AND METAMORPHISM

Faults trending west-southwest and north to northwest are the prominant structural features in the map area. A moderately dipping (60°), west-southwest-trending fault separates the northern margin of the Hickman complex from the volcanic rocks. The fault zone is about 30 metres wide, strongly foliated, and weakly mineralized. This fault may belong to a regional set of west-striking normal faults with north-side-down displacement (Brown and Gunning, 1989). North-trending faults have much narrower tectonized zones and may be related to east-west brittle extension in the Tertiary. One such structure offsets the west-southwest-trending fault with an east-side-down sense of displacement.

MINERALIZATION

The Hickman complex lies within a metallogenic belt that encompasses the eastern margin of the Coast Mountains and hosts precious metal and base metal deposits, notably prophyry copper-molybdenum and copper-gold deposits, and structurally controlled epigenetic gold veins. The regional metallogeny has been reviewed by Brown and Gunning (1989).

Mineralization within the map area appears to be dominantly controlled by faulting. The west-southwest-trending fault zone is silicified and locally carbonatized, and weathers a deep orange-brown at its western end due to the presence of disseminated sulphides, mostly pyrite (<5 vol%). Northerly trending faults appear to be unmineralized though fault zones are locally silicified. The age of the mineralization may be Early to Middle Jurassic (Brown and Gunning, 1989).

GEOCHEMISTRY

Analytical results for noble metals in the Hickman complex, porphyritic dikes and the mafic phase of the Hickman pluton are given in Table 2.1. The noble metals were preconcentrated by fire assay from 3-gram splits of 200 grams of rock powder (-200 mesh) and analyzed by inductively coupled plasma emission spectroscopyby Acme Analytical Laboratories, Vancouver. Accuracy was checked by in-house standard FA-5X (supplied by Acme) which contains 100, 100, 20 and 100 ppb platinum, palladium, rhodium, and gold respectively, and during analysis gave 98, 101, 20 and 100 ppb of each element respectively. Analytical precision (and any nugget effect) was monitored by hidden duplicates and internal standards.

The abundance of PGE in the mafic and ultramafic rocks is relatively low. Platinum abundunces are highest in olivine clinopyroxenite whereas gold has an affinity for sulphide-bearing and carbonatized rocks. Proximity to faults may account for the anomalously high gold content of sample GN-88-1009.

TABLE 2.1
NOBLE METAL ABUNDANCES IN THE HICKMAN COMPLEX AND ASSOCIATED ROCKS

Sample No.	Rock Type	Sulphides (vol. %)	ppb[1] Pt	Pd	Au
HICKMAN ULTRAMAFIC-MAFIC COMPLEX					
GN-88-1008	Ol clinopyroxenite	-	18	2	3
GN-88-1009	Ol clinopyroxenite	<5	9	2	87
GN-88-1017	Ol clinopyroxenite	-	2	2	1
GN-88-1006	Clinopyroxenite	-	2	2	3
GN-88-3039	Gabbro-diorite (carbonatized)	-	5	28	13
HICKMAN PLUTON - Mafic Phase					
GN-88-2003	Hb gabbro-diorite	-	1	2	1
GN-88-1004	Diorite	<5	1	17	8
DIKES					
GN-88-1016	Cpx-Hb porphyry	-	1	2	2
GN-88-2004	Cpx-Hb porphyry	-	1	2	1

Detection limits: Pt and Au, 1 ppb; Pd 2 ppb
[1] Rh is at or below detection limit (2 ppb) in all samples
Ol, olivine; Cpx, clinopyroxene; Hb, hornblende;
- sulphides not detected

SUMMARY

The Hickman ultramafic-mafic complex is situated in the northern part of the Stikine Terrane and is spatially associated with Upper Triassic volcanic and epiclastic assemblages of the Stuhini Group. Isotopic dating and geological relationships indicate that the complex is Late Triassic in age, *i.e.*, older than 221 to 228±16 Ma (2σ). This Alaskan-type complex is spatially associated with a large granitoid intrusion (Hickman batholith) but appears to be an entirely separate entity with no direct genetic ties to the batholithic rocks. Emplacement within the volcanic pile preceded granitic intrusion.

The complex exhibits an extensive suite of Alaskan-type lithologies, including dunite, olivine-bearing clinopyroxenites, and gabbros. Internal contacts between the various lithologies are gradational; external contacts are commonly affected by ductile and brittle faults. A distinctive mineralogical feature is the presence of phlogopitic mica in olivine clinopyroxenites. This mineral, for example, also makes an early appearance in dunitic and pyroxenitic cumulates of the Polaris and Tulameen complexes (Chapters 8 and 9).

Sulphide mineralization in the vicinity of the complex is predominantly associated with fault zones. Assay results for the precious metals suggest that these sulphides may carry interesting gold values (up to 0.087 g/t). However, there is no evidence within the mineralized zones for remobilization of PGE which have concentrations in the mafic and ultramafic rocks that appear to be low in comparison to their abundances in other Alaskan-type complexes.

CHAPTER 3 GNAT LAKES COMPLEX

The Gnat Lakes mafic-ultramafic complex (50°11.5'N, 129°51'W) is located some 30 kilometres south of Dease Lake on Highway 37, the Stewart-Cassiar Highway (Figure 3.1). It is situated at the southwestern margin of the Cry Lake map sheet (104I). The complex is named for Lower and Upper Gnat Lakes, and lies approximately 3 kilometres south of Upper Gnat Lake. A four-wheel-drive access road climbs west from the highway to treeline near the western margin of the complex. On the whole, the complex is poorly exposed and has a maximum outcrop area of about 2 square kilometres.

REGIONAL GEOLOGY AND GEOCHRONOMETRY

The Gnat Lakes complex lies in northern Stikinia (Figure 3.1). It has traditionally been included as part of the composite Hotailuh batholith (Hanson and McNaughton, 1936) which has been studied in detail by Anderson (1983). The batholith is composed of at least four distinct granitoid plutons, two of which, the Three Sisters and Cake Hill plutons, occur within the study area (Figure 3.2). These plutons belong to the Middle Jurassic Three Sisters and Late Triassic Stikine granitoid suites respectively (Woodsworth *et al.*, 1991).The main outcrops of mafic-ultramafic rocks are completely enclosed by metavolcanic and metasedimentary rocks of the Stuhini Group which lie within an embayment at the northwestern margin of the batholith. In addition, small isolated exposures of ultramafic rocks form pendants within the Three Sisters pluton about 2.5 kilometres to the south, and occur in the Cake Hill pluton 14 kilometres south-southeast and 18 kilometres east-northeast of the Gnat Lakes ultramafite (Anderson, 1983). The complex has no unique signature on the regional aeromagnetic map due to the overwhelming aeromagnetic response associated with a northwest-trending apophysis of the Three Sisters pluton (Anderson, 1983).

Figure 3.1. Location of the Gnat Lakes mafic-ultramafic complex in relation to major tectonostratigraphic terranes in northern British Columbia.

Potassium-argon dating of hornblende in hornblendite and hornblende clinopyroxenite of the Gnat Lakes complex has yielded isotopic ages of 230±10 (2σ) and 227±14 Ma respectively, or earliest Upper Triassic (Carnian) (Anderson, 1983; Stevens *et al.*, 1982). These dates are identical (within error) to K-Ar isotopic ages obtained on hornblende in the Cake Hill pluton (220±11, 218±11 and 227±14 Ma; Stevens *et al.*, 1982) which, according to Anderson (1983), is intruded by the Gnat Lakes body. However, the latter relationship could not be confirmed. A quartz monzonite of the potassic marginal phase of the Three Sisters pluton has been dated by K-Ar and U-Pb geochronometry at a locality approximately 3 kilometres west of the Gnat Lakes complex. Zircon fractions lying essentially on concordia yield a preferred U-Pb isotopic age of 170±1 Ma (Anderson *et al.*, 1982) which is concordant with a K-Ar date of 169±11 Ma for hornblende in the same sample (Stevens *et al.*, 1982). The age of the Stuhini Group is established as Late Triassic on the basis of ammonite faunas recovered from epiclastic sequences at the northern margin of the Hotailuh batholith (Anderson, 1980).

COUNTRY ROCKS

STUHINI GROUP

The Stuhini Group is composed of volcanic flows and breccias, subvolcanic intrusive rocks, and tuffaceous sandstones, siltstones and shales that appear variably metamorphosed to upper greenschist-grade mineral assemblages. The volcanic rocks are relatively well exposed above treeline immediately west of the mafic-ultramafic body. The predominant rock type is a dark greenish grey porphyry characterized by euhedral phenocrysts (<1 cm) of augite±plagioclase±amphibole set in a finer grained matrix. These augite porphyries form flows and massive shallow intrusions and are incorporated as angular fragments in volcanic breccias and thinly bedded tuffs and epiclastic rocks. Similar lithologies appear in stratigraphic sections measured by Anderson (1980) about 3 kilometres farther west and along the northern margin of the Hotailuh batholith. In thin section, clinopyroxene and hornblende phenocrysts are commonly rimmed and replaced along fractures by actinolitic amphibole, and plagioclase is extensively saussuritized. Locally, secondary amphibole and biotite form rounded ra-

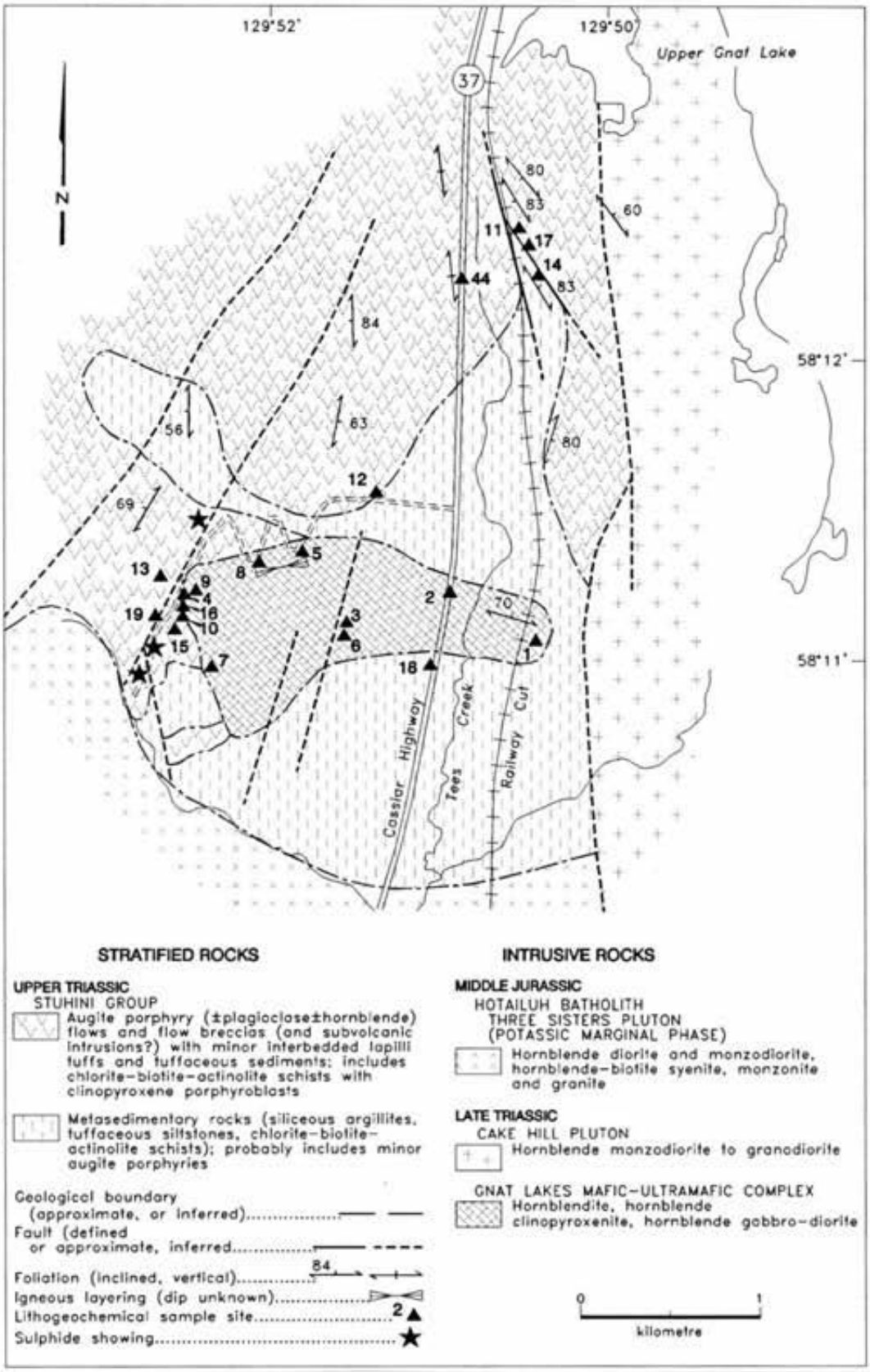

Figure 3.2. Geologic map of the Gnat Lakes mafic-ultramafic complex showing distribution of geochemical sample sites and sulphide showings.

diating crystal aggregates. Rare glomeroporphyritic clots contain intergrowths of augite, hornblende, plagioclase, iron-titanium oxides and apatite, with or without sphene.

In road and railway cuts north of the mafic-ultramafic complex, augite porphyries are strongly schistose and mylonitic. Under the microscope, relict augite phenocrysts exhibit flaser textures with pressure shadows and are altered extensively to tremolite-actinolite. The fine-grained matrix is recrystallized to actinolite, biotite, chlorite and sericite, which define the foliation, and carbonate, iron-titanium oxides and minor sulphides.

Metasedimentary rocks within the Stuhini Group include grey-green to rusty brown or buff-weathering tuffaceous sandstones, siltstones and black argillites, variably silicified and locally epidotized and pyritic. Near the southwestern margin of the Gnat Lakes complex these rocks have been recrystallized to fine-grained chlorite-biotite-actinolite-feldspar schists.

CAKE HILL PLUTON (STIKINE PLUTONIC SUITE)

Outcrops of the Late Triassic Cake Hill pluton were examined south of Upper Gnat Lake in the eastern part of the map area. The rock is a pink to buff-weathering medium-grained equigranular hornblende syenite to monzonite and monzodiorite with accessory magnetite and sphene. The predominant lithology in the central part of the pluton is hypidiomorphic granodiorite (Anderson, 1983). A penetrative foliation is defined locally by alignment of partially chloritized mafic minerals.

THREE SISTERS PLUTON (THREE SISTERS PLUTONIC SUITE)

The potassic marginal phase of the Middle Jurassic Three Sisters pluton crops out along the highway and in railway cuts to the south of the Gnat Lakes complex. It is composed of pale pink to white-weathering medium-grained hornblende monzonite to hornblende biotite syenite or quartz syenite cut by aplite and diabase dikes. The rocks are generally massive and well jointed. In thin section, plagioclase is seen to be partially altered to sericite and epidote, and hornblende (25 vol%) is chloritized. Accessory phases include biotite (<1%), iron-titanium oxides (<3%) and sphene.

GNAT LAKES COMPLEX: MAFIC-ULTRAMAFIC ROCKS

The Gnat Lakes complex comprises medium-grained grey-green hornblende clinopyroxenite, black hornblendite, dark to medium grey feldspathic hornblendite, hornblende gabbro and rare pyroxene gabbro. The predominant lithologies appear to be feldspathic hornblendite and hornblende gabbro or diorite. These rocks are locally pegmatitic with prismatic amphibole crystals reaching 3 centimetres in length.

Ultramafic rocks are well exposed in a railway cut at the eastern edge of the complex (Figure 3.2). Here, a continuous gradation is observed from variably carbonatized hornblende clinopyroxenite in the north to saussuritized hornblende gabbro in the south. However, the crude zonation from pyroxenitic core to hornblendite-hornblende gabbro margin, as inferred by Anderson (1983), could not be confirmed. Rudimentary igneous layering involving hornblende clinopyroxenite and feldspathic hornblendite grading into hornblende gabbro was observed in glacially polished outcrops along the access road. The rocks exhibit no tectonic foliation, yet in places the layering is contorted and appears to have been remobilized prior to complete solidification. Layered horizons are commonly intersected by irregular, locally derived leococratic veins that appear to have been generated by coalescence of residual gabbroic liquids. Veins of similar style and origin are also observed in the Tulameen complex (Chapter 9).

PETROGRAPHY AND MINERAL CHEMISTRY

As seen in thin section, hornblende clinopyroxenite contains cumulus clinopyroxene with intercumulus hornblende (20 vol%), iron-titanium oxides (5 to 10%) and minor sphene (1%). Cumulus clinopyroxene is also present in pyroxene gabbro but is replaced by cumulus amphibole in hornblendite, feldspathic hornblendite and hornblende gabbro. Plagioclase is a cumulus and intercumulus phase in the gabbroic rocks which also contain interstitial iron-titanium oxides (2 - 5 vol%), apatite (<1%) and sphene (<1%). Secondary minerals include epidote, carbonate, chlorite, sericite and sulphides, largely pyrite.

Anderson (1983) provided electron microprobe data for clinopyroxene and amphibole phenocrysts in Gnat Lakes ultramafic rocks, augite-plagioclase porphyry dikes, and augite±hornblende±plagioclase porphyries of the Stuhini Group. Overall, phenocryst compositions are similar. Clinopyroxenes (diopsidic augite to magnesium-rich salite) exhibit little zoning and have low TiO_2 (<1 wt%) and moderate Al_2O_3 (generally 2.5 to 5 wt%) and consequently relatively low octahedral alumina, indicative of crystallization within the crust. However, clinopyroxene compositions alone provide tentative evidence for their magmatic affinity (subalkaline versus alkaline) and tectonic environment (*see* Anderson, 1983).

Primary amphibole compositions are predominantly ferroan pargasite (Leake, 1978) with low TiO_2 and uniformly high K_2O (1 to 1.6 wt%). Amphiboles in Gnat Lakes hornblendite are zoned outwards towards actinolitic hornblende. Their levels of potash enrichment and potassium:sodium ratios are similar to those detected in amphiboles from hornblende clinopyroxenites and gabbroic rocks of the Tulameen complex (G.T. Nixon, unpublished data). Evidently, the liquids with which these crystals last equilibrated were relatively potassic. In general, these data support Anderson's contention that Gnat Lakes mafic and ultramafic rocks are likely comagmatic with Stuhini Group volcanism.

CONTACT RELATIONSHIPS

Despite poor outcrop, intrusive relationships in the map area are well known. A sharp intrusive contact between metasedimentary schists of the Stuhini Group and Gnat Lakes body is exposed at the southwestern margin of the complex. Hornblende gabbro and hornblendite decrease in grain size

as the contact is approached, indicating the presence of a marginal chill zone. These observations, together with the Carnian isotopic age (227±14 Ma), suggest that the Gnat Lakes complex is a high-level intrusion coeval with Stuhini Group volcanism. The augite plagioclase porphyry dikes, presumably the hypabyssal equivalents of Stuhini lavas, must be of various ages as they cut all of the Late Triassic lithologies including the Gnat Lakes complex.

Relationships between mafic-ultramafic and granitic rocks are well exposed in railway cuts at the eastern extremity of the complex. Irregular dikes of pink aplite and fine to medium-grained syenite have invaded hornblende clinopyroxenite and hornblende gabbro to produce localized agmatites. Irregular bodies of medium-grained hornblende-biotite syenite to monzonite also intrude the western part of the Gnat Lakes complex. Anderson (1983) considered these intrusions to be apophyses of the potassic marginal phase of the Three Sisters pluton, and therefore Middle Jurassic in age. Other minor intrusions into the Gnat Lakes body include dikes of pale buff dacite containing phenocrysts of hornblende, plagioclase and quartz, and diabase dikes with abundant plagioclase microphenocrysts and iron-titanium oxides (4 vol%).

STRUCTURE AND METAMORPHISM

The structure of the map area is poorly understood due to the lack of marker horizons. Major northerly to northeasterly trending lineaments observed on aerial photographs are interpreted as faults. Outcrops located near such lineaments may display a subparallel foliation or localized mylonitic fabric. The western margin of the Cake Hill pluton appears to be fault bounded.

A steeply dipping regional foliation, defined by amphiboles and micas, has been detected in all lithologies but is poorly developed or absent in the more massive augite porphyries and intrusive rocks. In the northeastern part of the map area, this foliation trends northwesterly, consistent with fabrics farther east that characterize the northwestern part of the Hotailuh batholith (Anderson, 1979). Farther west, foliations swing north to northeasterly, possibly influenced by faulting. In general, the mineral foliation reflects regional inhomogeneous deformation accompanied by variably developed metamorphic assemblages attaining upper greenschist grade. The timing of this deformation is uncertain; it may be synchronous with Late Triassic plutonism or associated with southwesterly verging folds and associated thrust faults of Middle Jurassic (post-Toarcian) to Cretaceous age (Monger *et al.*, 1978; R.G. Anderson, personal communication, 1988).

MINERALIZATION

Minor amounts of disseminated sulphides are distributed throughout the map area but mineralization is preferentially developed near faults.

Sulphides in the mafic and ultramafic rocks generally form no more than 5 vol% of the rock and comprise finely disseminated pyrite and rare chalcopyrite. Most of the mineralized outcrops occur near the western margin of the complex. No net-textured sulphides were observed.

Granitoid rocks commonly contain disseminated sulphides (<3 vol%) and thin (0.5 mm) discontinuous stringers of sulphide and chlorite along joint planes. Disseminated pyrite is also found in diabase dikes cutting the granitic rocks.

Control of mineralization by faults is seen at several localities. A fault contact between black argillite and schistose augite porphyry is well exposed in a railway cut in the northern part of the map area. Here, the abundance of disseminated sulphide in the argillite, intensity of carbonate veining and degree of silicification increase towards the fault.

The most important mineralization occurs along a major north-northeasterly trending fault in the Stuhini Group near the western limit of the mafic-ultramafic complex (Figure 3.2). In the mid-1960s, a program of geologic mapping, prospecting and trenching, and an induced polarization survey, were carried out on a number of mineral showings distributed along the fault (Roed, 1966a, b; Malinsky, 1966; Reynolds, 1967). Mineralized zones comprise massive pyrite, chalcopyrite, and minor pyrrhotite and arsenopyrite in a gangue of siderite, limonite, hematite and smoky quartz.

The age of the mineralization is not well constrained. On the whole, the association of mineralization with brittle phenomena such as faults and joints suggests that the mineralizing event(s) occurred late in the history of regional deformation (presumably post-Toarcian).

GEOCHEMISTRY

Whole-rock analyses of Gnat Lakes mafic-ultramafic rocks taken from Anderson (1983), and assay results for platinum, palladium, rhodium, and gold, are given in Tables 3.1 and 3.2 respectively. The occurrence of cumulate textures in the ultramafic rocks, and thus accumulative origin, precludes the use of whole-rock compositions as a means of classification (*e.g.*, Irvine and Baragar, 1971). The hornblende clinopyroxenites and hornblendites have high total iron and titania, reflecting in part the abundance of intercumulus iron-titanium oxides, and high alkalies and iron:magnesium ratios. These compositions compare rather closely with those of similar rocks in the Tulameen complex (Table 3.1). Their relatively high K/Na ratio is a trait shared by the majority of Stuhini Group volcanic rocks and porphyry dikes (Anderson, 1983). However, the latter rocks are altered (2 to 4 wt% H_2O and up to 5 wt% CO_2) and have clearly suffered some degree of alkali mobility (Na_2O/K_2O >12 in extreme cases), which renders rigorous geochemical comparisons uncertain.

The tenor of noble metals in mafic-ultramafic lithologies of the Gnat Lakes complex, Stuhini Group volcanic and metasedimentary rocks, and sulphide-bearing quartz veins is given in Table 3.2. Analytical methods and accuracy are described in Chaper 2. Abundances overall are relatively low. Typical economic PGE deposits have an average platinum grade of 5 to 10 grams per tonne (Macdonald, 1986). An anomalously high gold value occurs in a sulphide sample collected from a showing located on the fault near the west-

TABLE 3.1
MAJOR AND TRACE ELEMENT COMPOSITION OF GNAT LAKES ULTRAMAFIC ROCKS

	Gnat Lakes				Tulameen	
Rock	1	2	3	4	5	
Type	Hb	Hb	Hb Cpx	Hb Cpx	Hb Cpx (Range)	
Weight %						
SiO_2	45.00	41.60	39.80	39.60	40.74	(3.84)
TiO_2	1.24	1.58	1.97	2.06	1.48	(1.23)
Al_2O_3	5.80	6.70	11.10	6.50	5.06	(3.29)
Fe_2O_3	6.40	9.60	6.00	13.30	11.59	(6.92)
FeO	8.60	9.90	10.00	9.90	8.84	(2.67)
MnO	0.26	0.20	0.23	0.20	0.22	(0.04)
MgO	11.70	11.07	8.70	10.54	12.58	(2.13)
CaO	17.80	15.48	13.57	15.74	16.86	(1.92)
Na_2O	0.68	0.81	1.60	0.74	0.61	(0.84)
K_2O	0.48	0.55	0.72	0.42	0.53	(1.31)
P_2O_5	0.33	0.35	1.53	0.10	0.05	(0.10)
H_2O_T	1.80	1.30	2.20	0.70	1.03	(0.48)
CO_2	bd	0.70	0.50	0.10	0.16	(0.38)
S	bd	0.21	0.80	bd	0.03	(0.04)
Cl	0.05	0.11	0.10	0.06	na	
F	0.04	0.05	0.14	0.04	na	
Total	100.18	100.16	98.76	100.00	99.77	
ppm						
Rb	0	70	100	30		
Sr	270	240	400	140		
Ba	200	650	200	150		
U	0.4	na	na	na		
Zr	21	58	53	39		
Y	bd	44	41	50		
Cr	110	120	27	160		
Co	64	57	53	76		
Ni	63	91	33	150		
V	450	560	530	750		
Cu	13	210	250	17		
Zn	50	80	130	140		

Hb = Hornblendite; Hb Cpx = Hornblende clinopyroxenite; H_2O_T = total water; na = not analyzed; bd = below detection limit. Columns 1-4 are analyses from Anderson (1983, Table 2-4-2). Column 5 is the arithmetic mean (and range) for 4 hornblende clinopyroxenites from the Tulameen complex (Findlay, 1969, Table 4).

TABLE 3.2
NOBLE METAL ABUNDANCES IN THE GNAT LAKES COMPLEX AND ASSOCIATED ROCKS

Sample Location*	Sample No.	Rock Type	Sulphide (vol. %)	ppb[1] Pt	Pd	Au
GNAT LAKES COMPLEX						
1	GN-88-0005	Hb clinopyroxenite	-	1	20	1
1	GN-88-0006	Hb clinopyroxenite	-	1	17	6
2	GN-88-0001	Hornblendite	-	2	35	3
3	CA-88-0006	Hornblendite	<5	4	2	1
4	GN-88-1029	Hornblendite	Tr	1	11	2
5	GN-88-0009	Feldspathic hornblendite	Tr	2	19	6
6	CA-88-0005	Feldspathic hornblendite	Tr	6	2	1
7	GN-88-4018C	Feldspathic hornblendite	<5	11	17	2
1	GN-88-0007	Hb gabbro-diorite	<5	1	2	2
8	GN-88-1022	Hb gabbro-diorite	-	2	19	8
9	GN-88-1030	Hb gabbro-diorite	5-10	1	2	1
10	GN-88-4006	Hb gabbro-diorite	<5	1	2	1
STUHINI GROUP - Metavolcanic Rocks						
11	GN-88-0003	Cpx porphyry schist	-	2	25	1
12	GN-88-0008	Cpx-Plag porphyry schist	-	3	22	1
13	GN-88-1025A	Cpx porphyry (silicified)	Tr	2	29	25
14	GN-88-2025B	Cpx porphyry schist	<5	5	22	1
15	GN-88-4004	Cpx porphyry schist	Tr	3	26	1
16	GN-88-4007	Cpx-Plag porphyry	-	1	13	4
STUHINI GROUP - Metasedimentary Rocks and Veins						
17	GN-88-0004	Argillite	5	1	5	3
18	CA-88-0003	Metasediment (silicified)	<5	26	20	1
14	GN-88-2025A	Quartz vein in argillite	15-20	7	18	1
14	GN-88-2025A[2]			7	15	1
19	GN-88-1026	Pyrite-chalcopyrite	ore	1	4	824

Detection limits: Pt and Au, 1 ppb; Pd 2 ppb
**See Figure 3.2*
[1] Rh is at or below detection limit (2 ppb) in all samples
[2] Duplicate analysis
Plag = plagioclase; Hb = hornblende; Cpx = clinopyroxene; Tr = trace sulphides; - sulphides not detected. Samples designated schist contain abundant tremolite-actinolite, biotite, chlorite and sericite±carbonate.

ern edge of the complex. However, there is no evidence to suggest remobilization of PGE within the fault zone. It is interesting to note that Stuhini Group augite porphyries are as enriched in palladium as rocks of the Gnat Lakes complex. In general, there is no correlation between the amount of pyritic sulphides in a rock and the abundance of noble metals.

In the Gnat Lakes intrusive suite, the abundance of PGE is slightly lower, on average, in gabbros than in ultramafic rocks, which in turn are distinctly impoverished in PGE relative to their counterparts in the Tulameen complex (Chapter 9). From an economic potential viewpoint, the best prospects in the vicinity of the Gnat Lakes complex would appear to be structurally controlled gold-bearing sulphide deposits.

SUMMARY

The Gnat Lakes mafic-ultramafic complex is situated within northern Stikinia and is spatially associated with Upper Triassic volcanic and epiclastic assemblages of the Stuhini Group. Isotopic dating and geological relationships indicate that the complex is Late Triassic in age. Like the Hickman complex, the Gnat Lakes complex is exposed within an enclave of country rocks surrounded by a large granitoid pluton, the Hotailuh batholith. Only the more differentiated phases of the Alaskan-type association are present: hornblende clinopyroxenite, hornblendite and gabbro. Fortunately, this body has been well studied, and whole-rock and mineral chemistry support an Alaskan-type affinity. Internal contacts among the various lithologies are gradational; intrusive contacts with hostrocks have been observed.

Weakly developed sulphide mineralization in the vicinity of the complex is predominantly associated with fault zones. Assay results for the PGE are not encouraging, although gold abundances in grab samples attain 0.8 gram per tonne. The age of the mineralization is Early Jurassic (Toarcian) or younger.

CHAPTER 4 LUNAR CREEK COMPLEX

The Lunar Creek mafic-ultramafic complex (57°55′N, 127°28′W) lies within the Stikine Ranges of the Omineca Mountains, approximately 1 kilometre northwest of the headwaters of Lunar Creek (Figure 4.1). The area is covered at a scale of 1:250 000 by the Finlay River map sheet (94E) and 1:50 000 topographic maps (94E/13 and 14). Aeromagnetic maps are not currently available. Lunar Creek drains southward into the Chuckachida River, a tributary of the Stikine River. Access to the complex was gained by helicopter from Sturdee airstrip in the Toodoggone River area, which is serviced by scheduled flights from Smithers, or by vehicle along a well-maintained dirt road linking Fort St. James to the Cheni mine. The complex lies entirely above treeline and is best exposed along ridge crests and high on valley walls. Glacial till and talus aprons cover lower valley walls and floors.

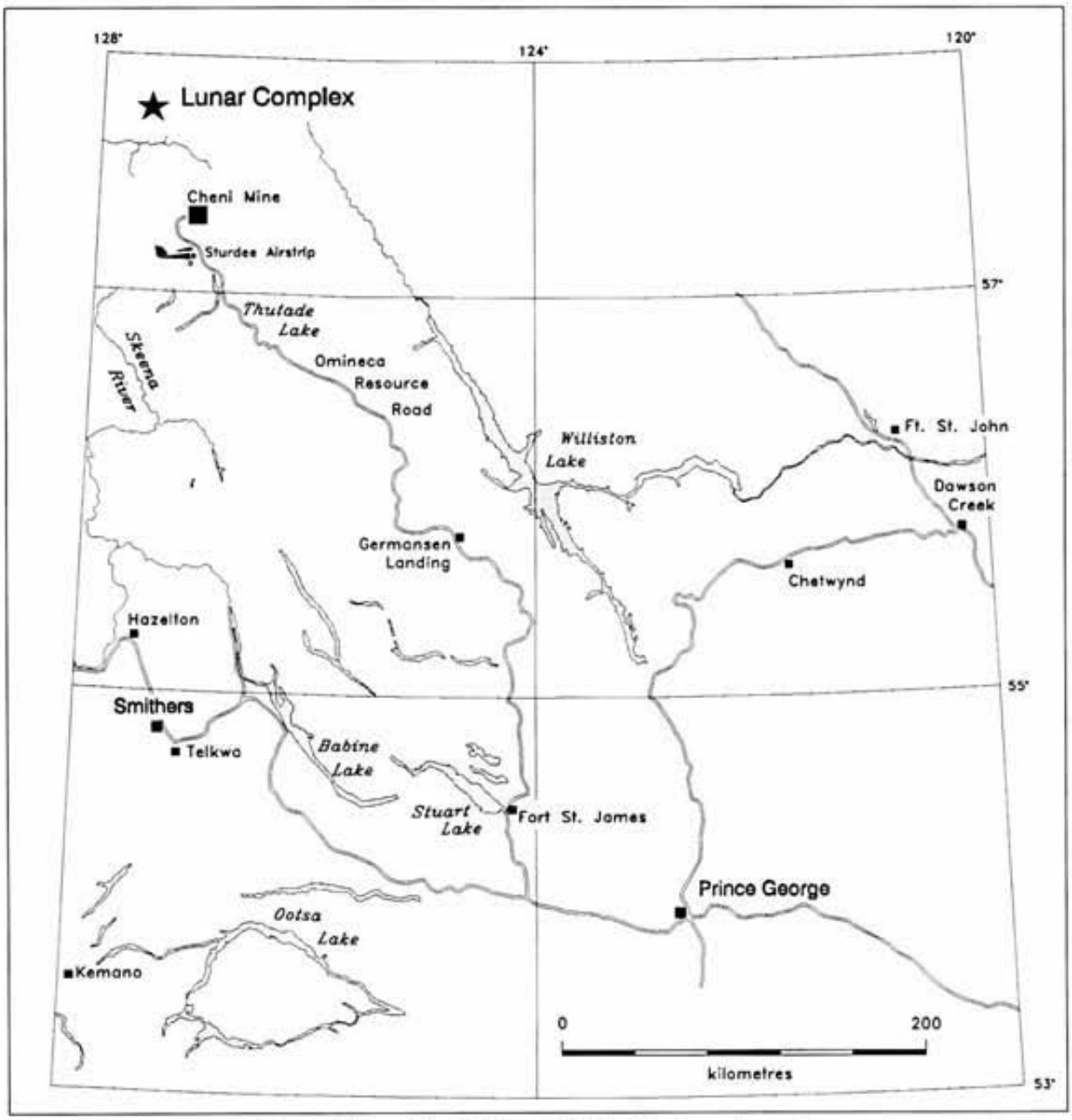

Figure 4.1. Location of the Lunar Creek mafic-ultramafic complex.

REGIONAL GEOLOGY AND K-Ar GEOCHRONOMETRY

The Lunar Creek complex is one of the largest of a series of Alaskan-type intrusions in northern British Columbia that form an arcuate trend around the northern and eastern margin of the Bowser Basin (Figure 1.1). The complex lies within Quesnellia at the boundary with the Stikine Terrane. This boundary is defined in the map area by the Kutcho fault which limits the western margin of the intrusion (Figure 4.2).

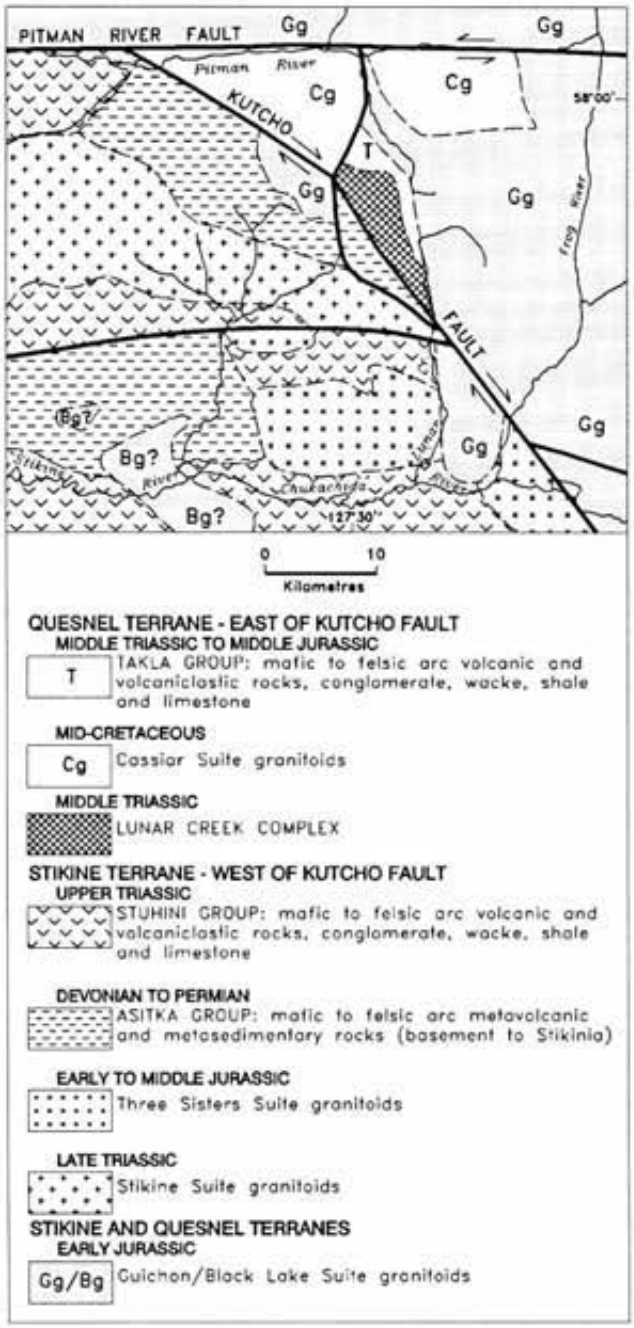

Figure 4.2. Regional geological setting of the Lunar Creek mafic-ultramafic complex.

The Lunar Creek complex was first recognized in 1973 during regional mapping by the Geological Survey of Canada (Gabrielse and Dodds, 1974). Later, more detailed mapping was completed by Irvine as part of a study of Alaskan-type complexes in the Finlay River area (Irvine, 1974b, 1976). Along its eastern margin, the complex lies in sheared contact with foliated augite-phyric volcanic rocks which, based on lithological similarities, are assigned to the Middle Triassic to Lower Jurassic Takla Group. Granitoids of the Early Jurassic Pitman batholith, part of the Guichon Suite of intrusions (Woodsworth *et al.*, 1991), intrude these volcanic rocks as well as ultramafic rocks of the complex. K-Ar determinations on hornblende from this batholith yield isotopic ages of 182±13 (2σ) Ma (Gabrielse *et al.*, 1980) and 190±8 Ma (Wanless *et al.*, 1979; Gabrielse *et al.*, 1980).

The Kutcho fault separates dioritic to gabbroic rocks of the Lunar Creek complex from Paleozoic and younger rocks within Stikinia. These Paleozoic rocks are believed to range in age from Devonian to Permian and are probably correlative with the Asitka Group (Thorstad, 1980; H. Gabrielse, personal communication, 1990). Arc-derived volcanic and clastic rocks of the Upper Triassic Stuhini Group are also represented west and south of the fault. The latter rocks have been intruded by granitoids of the Late Triassic Stikine batholith (Stikine Suite) as well as granitoids of the Early Jurassic Guichon and Black Lake suites. The Stikine batholith has yielded a K-Ar date on hornblende of 222±10 (2σ) Ma (Dodds *in* Wanless *et al.*, 1979; Anderson, 1984). Biotite obtained from the Mount Albert Dease pluton, part of the Three Sisters suite of intrusions found south of the mafic-ultramafic complex, has provided a K-Ar age of 167±6 (2) Ma (Dodds *in* Wanless *et al.*, 1979; Woodsworth *et al.*, 1991). The Three Sisters Plutonic Suite is spatially and temporally associated with volcanic and sedimentary rocks of the Lower to Middle Jurassic Hazelton Group.

COUNTRY ROCKS

Stratified rocks within the study area include both metavolcanic and metasedimentary rocks of the Takla Group, which crop out north and east of the complex, and a package of Paleozoic metavolcanic and metasedimentary rocks west of the Kutcho fault that appear to belong to the Asitka Group.

TAKLA GROUP

Rocks tentatively assigned to the Middle Triassic to Lower Jurassic Takla Group crop out north and east of the complex (Map 1 and Figure 4.3). To the north, augite plagioclase porphyry and volcanic wackes and siltstones have been metamorphosed to greenschist or lowermost amphibolite grade. To the east, the country rock is strongly sheared and metamorphosed, and varies from a medium-grained biotite schist to well-foliated amphibolite.

The contact between rocks of the Takla Group and the Lunar Creek complex is a ductile fault zone with mylonitic fabrics. Mylonitized metavolcanic rocks of the Takla Group are medium-dark grey to green-grey augite, augite-plagioclase and plagioclase-porphyritic actinolite schists. In thin

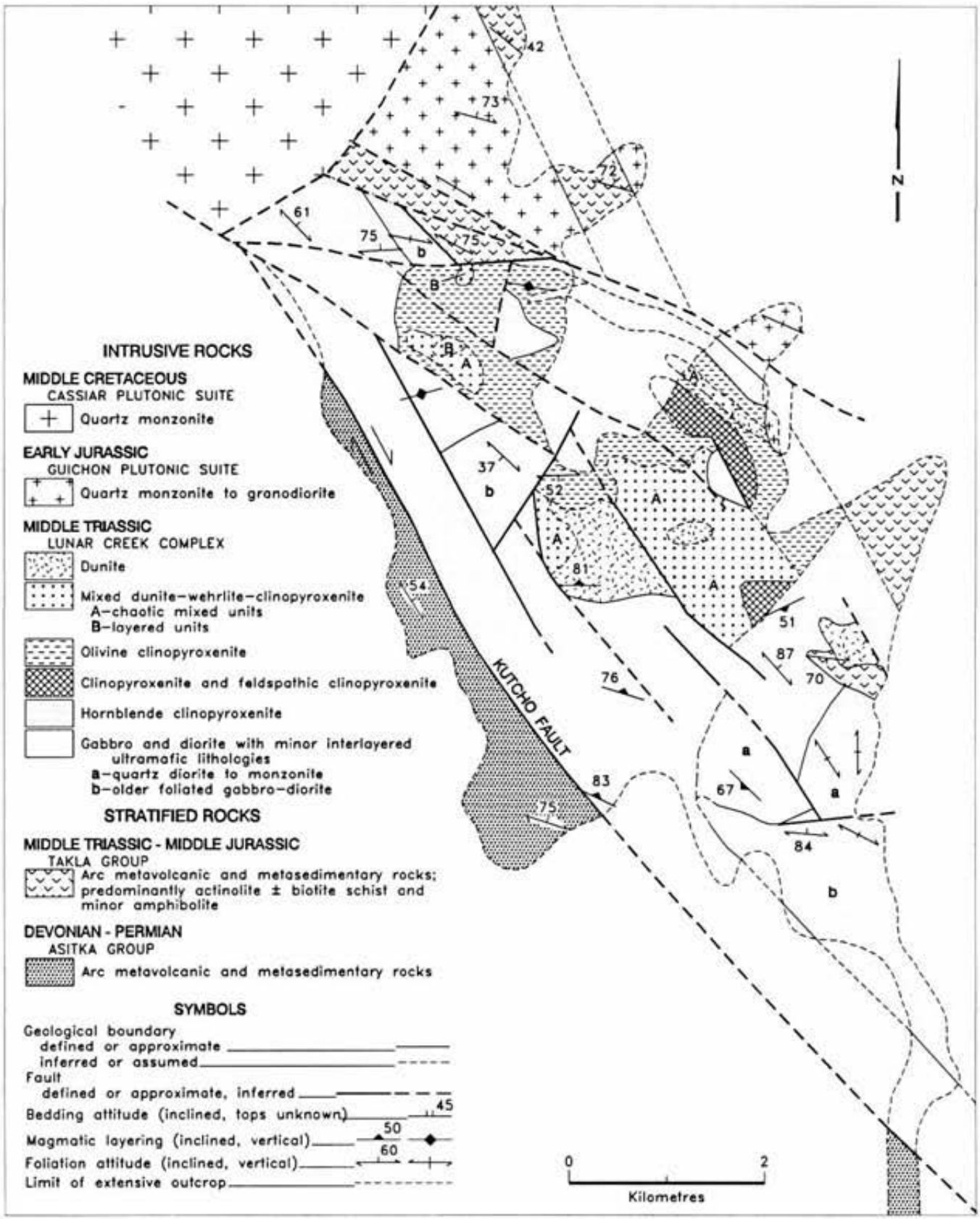

Figure 4.3. Generalized geology of the Lunar Creek mafic-ultramafic complex.

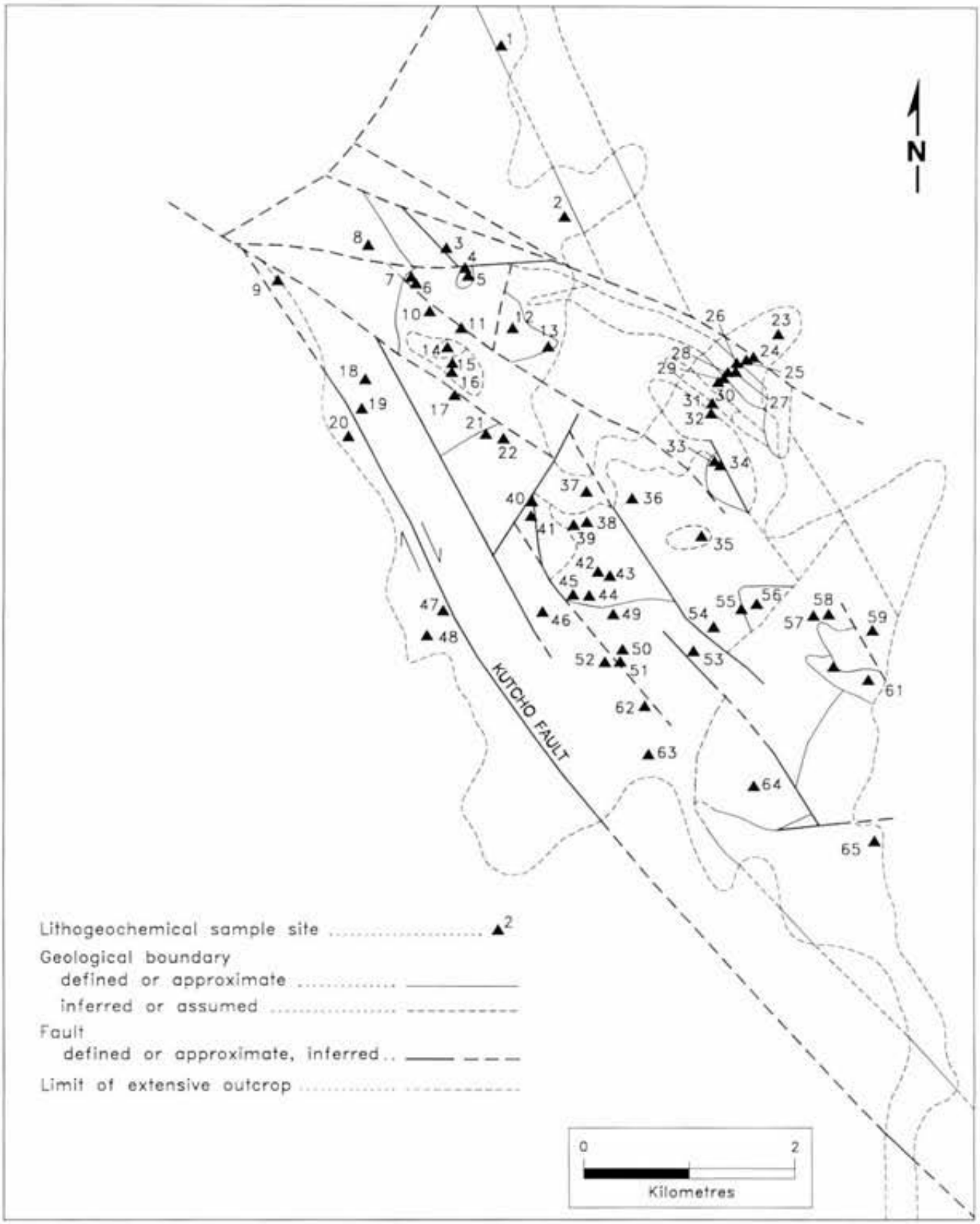

Figure 4.4. Location of lithogeochemical sample sites, numbered sequentially from north to south (*c.f.* Table 4.1). Symbols as in Figure 4.3.

section, augite augen, up to 0.7 centimetre in diameter, have been partially to completely altered to pale green actinolite. Actinolite is the most common constituent of the matrix, forming acicular laths parallel to the foliation. The remainder of the matrix consists of albite, epidote and clay minerals. Away from the mylonitic zone, the most common Takla Group lithology is dark grey augite porphyry that is metamorphosed to lower most amphibolite grade. In the northernmost part of the map area, medium to dark grey siltstones and fine-grained volcanic wackes at have also been metamorphosed to lower amphibolite grade. These rocks are well bedded, dip moderately toward the northeast and have a weak bedding-parallel foliation. Common constituent minerals are plagioclase, potassium feldspar, green pleochroic hornblende and abundant idioblastic biotite that is oriented within the foliation.

ASITKA GROUP

Paleozoic rocks west of the Kutcho fault have been tentatively assigned to the Asitka Group. Conodont analysis has shown that some of them are Mississippian in age (Thorstad, 1980), and may range from Devonian through to Permian (H. Gabrielse, personal communication, 1990). Regionally, lithologies include chlorite schist, sericite schist, phyllite, rhyolite flows and tuffs, chert, sandstone and carbonate (Thorstad, 1980). In the study area, these Paleozoic rocks crop out adjacent to the Kutcho fault. The lithologies include medium grey-green to dark grey quartz - potassium feldspar - actinolite schist, medium green-grey siliceous siltstone and medium grey, gritty micritic limestone with thin interbedded cherts. The rocks have been metamorphosed to upper greenschist facies assemblages.

LUNAR CREEK COMPLEX: MAFIC-ULTRAMAFIC ROCKS

The Lunar Creek complex is an elongate body which measures more than 11 kilometres in length and up to 4 kilometres in width. The northwesterly trending, major axis of the intrusion parallels the structural grain of the region.

Several attributes distinguish Lunar Creek from other Alaskan-type complexes in British Columbia:

- Two gabbroic-dioritic phases are present; the older one is ductily deformed and cut by a younger, undeformed phase that constitutes most of the complex.
- Cumulate layering in the ultramafic rocks is locally well developed, a rare feature in the Alaskan-type intrusions of British Columbia.
- Quartz-rich pegmatitic segregations are common in the gabbroic to dioritic rocks. This is also uncommon in Alaskan-type intrusions.

All the ultramafic lithologies which characterize Alaskan-type intrusions are represented at Lunar Creek. These include dunite, chromitiferous dunite, wehrlite, olivine wehrlite, olivine clinopyroxenite, clinopyroxenite and gabbroic-dioritic rocks. Of interest is the relatively low abundance of massive wehrlitic lithologies which are so abundant, for example, at the Polaris complex (Chapter 8). However, chaotically mixed wehrlite and clinopyroxenite domains are quite common. These chaotic domains generally occur in gradational contact with adjacent ultramafic lithologies and are most common at the transition between massive dunite and olivine clinopyroxenite. A petrologic study of the Lunar Creek complex has been completed by Nuttall (1991).

DUNITE

Massive dunite is exposed at three separate outcrops that have a combined total area of approximately 1.5 square kilometres (Map 1 and Figure 4.3). Dunite also occurs as irregular inclusions within chaotic mixed zones, interlayered with wehrlite, and as dikes within massive dunite, wehrlite and olivine clinopyroxenite (*e.g.*, Localities 5 and 14, Figure 4.4).

Dunite commonly weathers pale orange-brown and is medium grained. Outcrops are characteristically smooth and rounded. Contacts with clinopyroxene-rich lithologies (wehrlite and clinopyroxenite) are gradational and marked by a gradual increase in the abundance of clinopyroxene. Serpentinization is pervasive near faults and near contacts with gabbroic units and country rock. Away from these areas the rock is comparatively fresh and composed of virtually fresh, dark green olivine.

Although the contact between dunite and country rock was not seen, relationships at one locality suggest that it is intrusive (Locality 60, Figure 4.4). Here, dunite adjacent to the contact is weakly serpentinized but shows little evidence of shearing, implying that the contact is not ductily faulted. Furthermore, amphibolite-grade metamorphism of adjacent country rock may possibly represent part of a contact aureole.

The dunite bodies are commonly cut by swarms of anastomosing wehrlite, olivine clinopyroxenite, clinopyroxenite and rare dunite dikes (Photo 4.1). The dikes range in width from 1 to 20 centimetres and are most common near gradational contacts with clinopyroxene-rich lithologies.

Photo 4.1. Olivine clinopyroxenite to clinopyroxenite dikes in dunite.

CHROMITITE

Disseminated chromite is ubiquitous in dunite, typically forming 1 to 2% of the rock. Chromitite schlieren occur locally, generally in clusters of two or more (Photo 4.2). Individual schlieren range in thickness from 1 to 4 centimetres and in length from 20 to 30 centimetres. Locally, the schlieren are strongly magnetic, suggesting that some of the chromite has been altered to magnetite.

Photo 4.2. Deformed chromitite schlieren in dunite at Locality 44, Figure 4.4.

Photo 4.3. Layering of coarse-grained clinopyroxenite - olivine wehrlite offset by small syndepositional fault, mixed layered unit, south of Locality 5, Figure 4.4.

Chromitite schlieren are known to host PGE mineralization in the Tulameen (Chapter 10) and Wrede Creek complexes (Chapter 6). However, the relatively sparse amount of chromitite in the Lunar Creek complex does not bode well for the economic potential of PGE, at least with respect to the PGE-chromitite style of mineralization (Nixon and Hammack, 1991).

OLIVINE CLINOPYROXENITE AND CLINOPYROXENITE

Olivine clinopyroxenite is the most extensive of the ultramafic lithologies exposed at Lunar Creek (5 km^2). It is characterized by dark green to rusty brown, knobby-weathering outcrops. Fresh surfaces are dark green-grey and the rock is weakly magnetic. Clinopyroxene crystals vary from 2 millimetres to 3 centimetres in diameter, with an average grain size of approximately 0.5 centimetre. Olivine grain size is fairly constant at 1 to 2 millimetres. Locally, both minerals show cumulate textures. In some cases, clinopyroxene is intercumulus and poikilitically encloses olivine. Phlogopite exists locally as an accessory phase.

Contacts between olivine clinopyroxenite and other ultramafic lithologies are gradational, marked by variations in olivine content. A gradational relationship is also apparent between clinopyroxenite and feldspathic clinopyroxenite and is marked by the appearance of plagioclase as an intercumulus phase. Rare modal layering showing mineralogical and/or size grading of crystals has been observed locally in all of these lithologies (Photo 4.3).

Pods of dunite and wehrlite, up to 8 metres in diameter, are fairly common within the olivine clinopyroxenite unit, and are most common near gradational contacts with the chaotic mixed units described below. These pods may represent fragments of crystalline material that broke away from the walls or roof of the magma chamber, or they might be disrupted ultramafic dikes. Locally, pods have been flattened and stretched into schlieren which reach 1 metre in width and several metres in length. Locally these schlieren have a well-developed foliation parallel to their margins.

Hornblende clinopyroxenite is a comparatively rare rock type within this complex. Microscopic examination has shown that much of the hornblende observed in hand samples of clinopyroxenite is secondary, after clinopyroxene. Primary hornblende in clinopyroxenite was seen only at the narrow, gradational contacts between clinopyroxenite and hornblende clinopyroxene gabbro.

MIXED ULTRAMAFIC LITHOLOGIES

Mixed units comprise a variety of distinct ultramafic lithologies. Three varieties of mixed rocks are observed: layered units which are sequences of interlayered clinopyroxenite, olivine clinopyroxenite, wehrlite and dunite; chaotic units which consist of blocks of one ultramafic lithology mixed into another; and replacement zones which are sites where dunite has partially replaced clinopyroxenite.

LAYERED MIXED UNITS

Layering is locally well developed in peridotites of the Lunar Creek complex. Near Locality 5 (Figure 4.4), dunite, wehrlite, olivine clinopyroxenite and clinopyroxenite exhibit layering produced by modal and/or grain size variations. Most layering in this area is discontinuous and layers vary from less than 1 metre to several metres in thickness. Centimetre-scale layering and rhythmic layering are seen locally (Photo 4.4). Interlayered wehrlite, clinopyroxenite and rare dunite are seen farther south at Locality 14 (Figure 4.4). Here, dunite layers up to 2 metres thick, with rare chromite accumulations, grade into wehrlite. The dunite layers have sharp, nongradational contacts with adjacent olivine clinopyroxenite.

Features resembling soft-sediment deformation are well exposed at Locality 5 (Figure 4.4). Locally, large blocks, presumably derived from the walls and roof of the magma chamber, fell onto layered material resulting in compressed and distorted layering. Further crystallization within the chamber led to deposition of more layers, which drape over both the block and the distorted material. Angular unconformities caused by the truncation of layers were observed in several outcrops. These features bear many similarities to sedimentary structures described at Duke Island (Irvine, 1974a) and undoubtedly reflect similar processes, namely the deposition of cumulate crystals by convection currents.

Overall, there is no consistency in layer orientation between outcrops. Facing direction, determined by the truncation of layering and deformed layering below slumped blocks, is also variable. This suggests that significant rotation has occurred since deposition, presumably as a result of slumping within the magma chamber prior to complete solidification.

CHAOTIC MIXED ZONES

Chaotic mixed zones are more widespread than layered zones. They consist of blocks of massive olivine clinopyroxenite to clinopyroxenite, up to 5 metres in diameter, set in a matrix of wehrlite to dunite, or blocks of olivine wehrlite, dunite or wehrlite enclosed in clinopyroxenite. Blocks are typically angular to subrounded (rarely rounded) and commonly exhibit sharp contacts with their hosts. Contacts between mixed zones and massive peridotite are gradational and expressed by the appearance of scattered, irregular blocks in the massive hostrock. The mixed zones have been subdivided into wehrlite-dominated and clinopyroxenite-dominated domains (Figure 4.3).

Photo 4.4. Fine modal layering of olivine and clinopyroxene in mixed layered unit near Locality 5, Figure 4.4.

The chaotic mixed zones may represent density flows resulting from the spalling of cumulates from the walls and roof of the magma chamber. In some cases, these zones appear to have formed by dike intrusion into semiconsolidated cumulate sequences that were subsequently deformed plastically. Dikes of clinopyroxenite to wehrlite are very common in chaotic zones and add to the chaotic appearance of the outcrop by further subdividing large blocks. It is likely that some diking resulted from overpressuring of the underlying crystal mush, causing expulsion and upward migration of residual pore fluid through the cumulate pile. In fact, diking may have been promoted in chaotic zones, where slumping of large blocks from the chamber walls and roof resulted in rapid loading.

REPLACEMENT DUNITE

Locally, in clinopyroxene-rich lithologies, clinopyroxene crystals have been partially to completely replaced by olivine. This process resulted in the development of irregular bodies of dunite and wehrlite within clinopyroxenites and olivine clinopyroxenites. A similar replacement phenomenon has been documented at Duke Island in southeastern Alaska (Irvine, 1974a, 1986). Replacement dunite appears to have resulted from the migration of an olivine-rich magma through a porous, clinopyroxene-rich crystal mush. Disequilibrium between olivine-rich magma within the pore spaces and the adjacent clinopyroxene crystals led to wholesale replacement of clinopyroxene by olivine.

At Lunar Creek, replacement dunite is most common in olivine clinopyroxenite, particularly in the layered and chaotic mixed units. The effect is most spectacular in layered olivine clinopyroxenite that exhibits internal grading (Locality 5, Figure 4.4). Here, irregular bodies of replacement dunite are up to a metre wide and cut layering at a high angle. Coarse-grained layers show pervasive replacement along the layering, whereas finer grained layers are virtually unaffected. This strongly supports the hypothesis that porosity played an important role in the development of replacement dunite. The lower porosity of fine-grained layers restricted the amount of olivine-rich fluid in the pore spaces and thus limited the degree of replacement in these layers.

Passive infiltration through pore spaces is one mechanism for magma migration through the cumulate pile. Where cumulates were densely consolidated, and pore spaces were closed, magma movement was accomplished by diking. Ultramafic dikes are fairly common in all of the ultramafic lithologies observed at Lunar Creek, as well as in most other Alaskan-type intrusions. Dynamic processes within the magma chamber (slumping, infiltration, diking,

convection *etc.*) may explain the notable lack of mesoscopic layering in most of the ultramafic rocks of the complex, and the scarcity of such layering in general.

GABBROIC-DIORITIC ROCKS

Two suites of gabbroic to dioritic rocks are found at the Lunar Creek complex. The oldest is a strongly foliated hornblende clinopyroxene gabbro. Deformation of this unit predates intrusion of the main body of ultramafic cumulates and the emplacement of the younger suite of gabbroic rocks. The latter suite comprises massive equigranular gabbro and diorite which are virtually undeformed and appear to be the youngest rocks associated with the complex.

FOLIATED GABBRO-DIORITE

Weakly to strongly foliated hornblende clinopyroxene gabbro is similar in mineralogy to the younger unfoliated gabbros and diorites at Lunar Creek. However, crosscutting relationships demonstrate that this foliation predates crystallization of the massive gabbro. The age of deformation of the foliated gabbro is unknown, but it does appear to be an early phase of the ultramafic-mafic intrusion that was ductily deformed prior to emplacement of the remainder of the complex.

Foliated rock consists of alternating mafic and feldspathic foliae, typically less than 1 centimetre in width (Photo 4.5). Mafic layers are composed of black hornblende or dark green clinopyroxene or both. Feldspathic layers are composed of white plagioclase with rare quartz. Clinopyroxenes are subhedral to euhedral and commonly rimmed by hornblende.

Where original igneous layering is preserved it is parallel to foliation and is commonly boudinaged. Fabric orientation is variable throughout the complex. However, layering and foliation are crudely parallel to contacts with ultramafic components. This relationship is well exposed southeast of Locality 58 (Figure 4.4) where the fabric appears to arch over a large body of undeformed dunite.

Photo 4.5. Mylonitic fabrics in older, foliated gabbro-diorite, Unit 5c.

MASSIVE GABBRO-DIORITE

Gabbro, diorite and quartz diorite underlie a total area of approximately 16 square kilometres (Figure 4.3). Diorite to quartz diorite is well exposed along the western margin of the complex; gabbro-diorite forms a large body at the southeastern end of the complex and a narrow zone along its eastern margin. It is also found as thick units within interlayered clinopyroxenite-gabbro sequences (*e.g.*, 500 m north of Locality 12, Figure 4.4).

Gabbro-diorite occurs as massive, resistant, medium grey outcrops. Fresh rock varies in colour from medium grey to black; mafic minerals vary from 50 to 90 %. It is typically equigranular and medium to coarse grained, but fine-grained and pegmatitic varieties are also found. Subhedral to euhedral, cumulate hornblende and clinopyroxene are the common mafic components, and anhedral plagioclase occurs as an intercumulus phase. Minor net-textured sulphides were observed locally. Hornblende is typically more abundant than clinopyroxene, except near gradational contacts with ultramafic rocks. Igneous layering, in the form of alternating mafic and feldspathic layers, is fairly common (Photo 4.6). Locally, layers are leucocratic, with as little as 20% mafic minerals. Leucogabbro-leucodiorite also occurs as thick dikes which crosscut both gabbroic and ultramafic rocks.

Gabbro-diorite has a narrow gradational contact with ultramafic lithologies along the northeastern edge of the complex. In this area, gabbroic rocks form a thin wedge along the margin and lie in fault contact with Takla Group rocks to the northeast. Massive gabbro is also found in gradational contact with zones of interlayered olivine clinopyroxenite, clinopyroxenite, feldspathic clinopyroxenite, hornblende clinopyroxenite and gabbro. In addition, gabbro-diorite occurs as dikes which crosscut the foliated gabbro unit described above (Locality 22, Figure 4.4).

Diorite-quartz diorite intrudes ultramafic rocks as well as the foliated gabbro unit. Contacts with massive gabbro-diorite appear to be gradational. It is therefore believed to

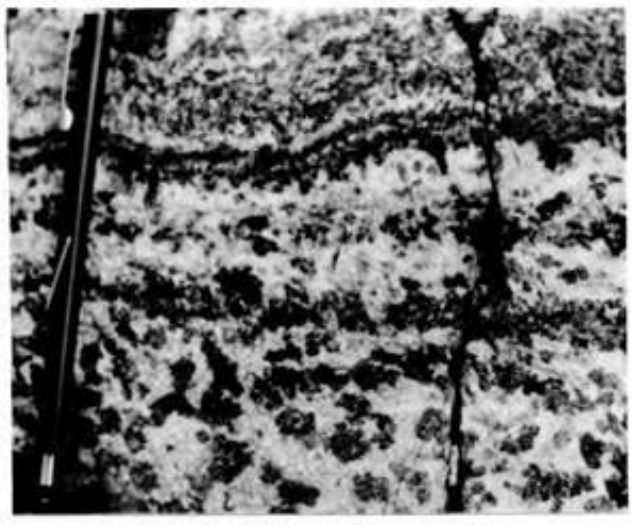

Photo 4.6. Fine modal layering of poikilitic hornblende and plagioclase in leucocratic layer within the gabbro-diorite of Unit 5a

be the youngest and most differentiated member of the Lunar Creek complex.

Rocks of diorite to quartz diorite composition form medium to light grey weathering, blocky outcrops. Fresh surfaces are medium grey in colour. Grain size varies from medium to coarse; the rock is locally pegmatitic. Hornblende, with or without biotite, comprises 30 to 50% of the rock. Variably altered plagioclase and quartz constitute the felsic component. Quartz varies in abundance from 1 to 25 vol% and is interstitial.

QUARTZ-FELDSPAR VEINS

Quartz-feldspar veins occur exclusively in ultramafic and mafic rocks of the complex. At one locality they pinch out into, and become continuous with, pegmatitic hornblende-bearing quartz diorite (Photo 4.7). They are therefore believed to represent late stage, silica-rich differentiates.

The veins range from 2 to 20 centimetres in width and most are approximately 4 centimetres wide. Typically, vein margins are lined with white plagioclase crystals up to 2 centimetres in diameter. Light grey quartz typically forms vein cores. Graphic feldspar-quartz intergrowths are commonly observed in the marginal zones.

GRANITOID ROCKS OF THE PITMAN BATHOLITH

Granitoid rocks north and east of the complex are associated with the Early Jurassic Pitman batholith, part of the Guichon Suite of intrusions (Gabrielse *et al.*, 1980). Granodiorite dikes emanating from the batholith intrude ultramafic and mafic rocks of the complex as well as Takla Group rocks to the north. Outcrops are commonly lichen covered and form resistant dark grey cliffs; where not covered by lichen, they are light grey. Fresh surfaces are light to medium grey and the rock is medium grained and equigranular. Composition varies from quartz monzonite to granodiorite. Mafic minerals, chloritized biotite and hornblende, comprise approximately 20 vol% of the rock and quartz varies from 10 to 25 vol%.

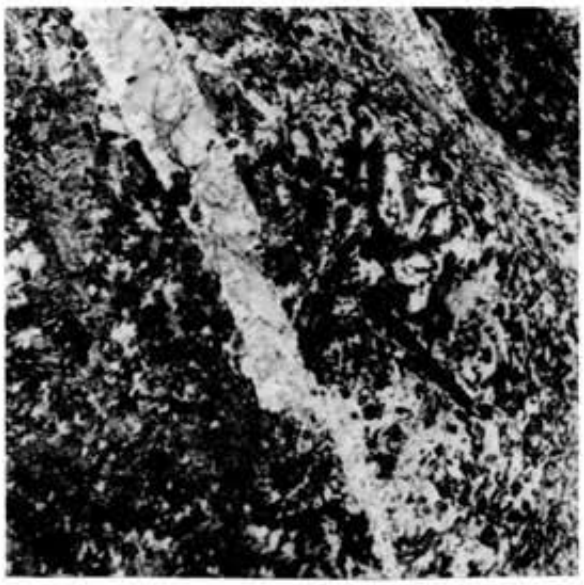

Photo 4.7. Zoned quartz-feldspar pegmatite vein cutting coarse-grained hornblende gabbro/diorite (upper left) and tapering into feldspathic groundmass (lower right) where it is continuous with its host (Unit 5b). Note concentration of quartz (pale grey) in centre of vein.

PLAGIOCLASE PORPHYRY DIKES

Plagioclase porphyry dikes intrude ultramafic and mafic rocks in the study area, and are intruded by hornblende microdiorite dikes described below. Euhedral to subhedral plagioclase phenocrysts up to 2 centimetres in diameter lie in a dark grey, fine-grained to aphanitic groundmass, which also contains hornblende microphenocrysts. In some dikes, plagioclase crystals are aligned and flattened parallel to the dike walls. These plagioclase porphyry dikes are believed to be derived from granitoids of the Early Jurassic Pitman batholith (Guichon Suite).

HORNBLENDE MICRODIORITE DIKES

Medium to dark grey hornblende microdiorite dikes of dubious affinity intrude granitic rocks of the Pitman batholith, plagioclase porphyry dikes, volcanic rocks of the Takla Group, and ultramafic-mafic rocks of the Lunar Creek complex (Photo 4.8). These dikes were not seen southwest of the Kutcho fault, but this area was not mapped in detail.

The dikes weather dark grey to pale brown and have an average width of approximately 50 centimetres. They are fine grained to aphanitic with microphenocrysts of euhedral hornblende and rare euhedral to subhedral white plagioclase. Dike margins are commonly foliated, implying at least some post-emplacement deformation.

U-Pb GEOCHRONOMETRY

Uranium-lead analyses of zircons separated from a potassium feldspar rich pegmatitic segregation in young, undeformed hornblende diorite were performed by L.M. Heaman in the Geochronology Laboratory, Royal Ontario Museum. Results are presented in Table 4.1 and Figure 4.5, and analytical techniques are summarized in Appendix B.

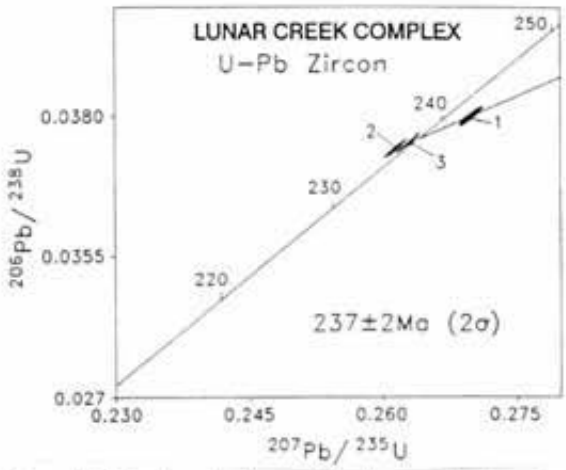

Figure 4.5. Uranium-lead concordia diagram for zircon from pegmatite of the Lunar Creek mafic-ultramafic complex..

Photo 4.8. Hornblende microdiorite dike cutting leucocratic gabbro-diorite Unit 5a and enclosing xenoliths of its host.

The zircon grains recovered from this sample vary considerably in size, morphology and colour. Three different zircon fractions were analyzed (#1-3 in Table 4.1 and Figure 4.5): large colourless prisms (#1); a fraction of tiny yellow prisms (#2); and a single large, colourless, euhedral prismatic grain (#3). The slightly yellow grains have a significantly higher uranium content (475 ppm) compared to the other two colourless fractions (300-350 ppm). The three zircon analyses are colinear with Fraction 1 showing a small inherited lead component. It is improbable that all the zircon analyses reflect inheritance as two quite different zircon populations (#2 and #3 in Table 4.1) yield identical $^{206}Pb/^{238}U$ ages. The single large grain is virtually concordant at 237 Ma, and taken together, the data indicate that the best estimate for the age of emplacement of the younger gabbro-diorite unit is 237±2 (2σ) Ma (Middle Triassic or Ladinian on the time scale of Harland *et al.*, 1990). Because this unit represents the youngest phase of the Lunar Creek intrusive suite, this date places a minimum age on the Alaskan-type ultramafic portion of the complex. The significance of the U-Pb geochronometry is discussed further in Chapter 11.

STRUCTURE

The Kutcho fault, which defines the boundary between the Quesnel and Stikine terranes, is one of many major transcurrent faults in the Cordillera. These faults were active possibly as early as Middle Jurassic and movements may have continued through to Eocene time (Gabrielse, 1985). The nature and magnitude of fault displacements are examined in more detail in Chapter 11.

Northwest-trending, steeply dipping faults, subparallel to the Kutcho fault, are the dominant structures in the study area. Steeply dipping northeast and east-trending faults are less abundant. Intense faulting has resulted in an outcrop pattern which is a mosaic of disrupted, disconnected blocks. This, together with the lack of distinctive marker horizons within the complex, has made details of the structure irresolvable at the present time.

At the north and east margin of the complex, Takla Group volcanic rocks and Pitman batholith (Guichon Suite)

TABLE 4.1
U-Pb ZIRCON RESULTS FOR THE LUNAR CREEK COMPLEX

Description		Weight	Concentration		Weight	Atomic Ratios**					Apparent Age (Ma)		
Sample Number	*Fraction	Sample (µg)	U (ppm)	Pb (ppm)	Common Pb (pg)	206Pb/204Pb	208Pb/206Pb	206Pb/238U	207Pb/235U	207Pb/206Pb	206Pb/238U	207Pb/235U	207Pb/206Pb
GN89-6122Z													
1	NM, a, cl, ab, (32)	282	302	11	11	23 947	0.0995	0.0380	0.2699	0.05154	240	243	265
2	NM, c, y, ab, (106)	69	475	18	179	8229	0.0974	0.0374	0.2614	0.05071	237	236	228
3	NM, a, cl, ab, (1)	13	342	13	14	1169	0.1055	0.0375	0.2627	0.05082	237	237	233

**Magnetic susceptibility: N, M=non-magnetic and magnetic at zero angle of side tilt on a Frantz isodynamic separator at a current of 1.0A and 10° forward tilt. Grain size (mesh): a=+100; c=-200+325; Colour: cl=colourless, y=yellow; ab=abrasion treatment.*
The numbers in parentheses correspond to the total number of grains analysed.
***Atomic ratios corrected for blank (Pb=5pg; U=2pg) and initial common Pb.*

granitoids, lie in fault contact with gabbroic rocks. All three lithologies are mylonitized along this fault. North of this contact, both the granitic and volcanic rocks have a steeply dipping, northwest-trending penetrative foliation. Bedding in Takla Group rocks dips moderately to the northeast.

Rocks adjacent to the Kutcho fault are not exposed. Approximately 250 metres southwest of the fault near Locality 47 (Figure 4.4), stratified rocks have a steeply dipping, northwest-trending, penetrative foliation that is subparallel to the trace of the fault. Bedding in these rocks dips moderately to the northeast. Diorite and quartz diorite, approximately 100 metres north of the fault, are extensively altered but not foliated.

An older episode of deformation is preserved in the foliated gabbro unit (Unit 5c, Figure 4.3). Crosscutting relationships show that ductile deformation in this unit predates intrusion of the main part of the complex. The outcrop distribution of the foliated gabbro unit is commonly controlled by faults. The orientation of the foliation appears to be fairly consistent within individual fault blocks, but varies between blocks. Outcrops near the north and south margins of the complex tend to have a steeply dipping, east-trending foliation, whereas most other outcrops have a steeply dipping, northwest-trending orientation. This fabric clearly predates regional contractional deformation in the Jurassic that affected this area, but its significance is not presently understood.

MINERALIZATION

Mineralization has been described near the eastern margin of the complex. A copper showing, hosted in skarn, and a porphyry-style alteration zone at the West property, were explored in the early 1970s and have been described in assessment reports. These claims covered minor garnet-epidote skarn that is locally enriched in copper (chalcopyrite, malachite and covellite; Jones, 1970). Malachite staining was also observed along fractures and foliation planes in biotite schists (Ryback-Hardy, 1972). Silt, soil and lithogeochemistry outlined several zones with modestly anomalous copper values. Skarn samples were also analysed for gold but were found to be barren (Jones, 1970). These showings are probably unrelated to the ultramafic complex and more likely associated with granitoids of the Pitman batholith to the east.

GEOCHEMISTRY

Analytical results for platinum, palladium, rhodium and gold in 84 representative rock samples from the Lunar Creek complex, its hostrocks, and various dikes and quartz veins in the map area are presented in Table 4.2. Sample localities are shown on Figure 4.4. The noble metals were preconcentrated by fire assay using 30-gram splits of approximately 200 grams of rock powder (-200 mesh) and analyzed by inductively coupled plasma emission spectroscopy by Acme Analytical Laboratories, Vancouver. Accuracy was checked by international and in-house standards, and analytical precision (and any nugget effect) monitored by hidden duplicates.

Platinum abundances are generally low except in dunites (up to 343 ppb) and a chromite-rich dunite (1017 ppb). Palladium abundances are low overall, and reach their highest values in gabbroic rocks (<90 ppb). With the exception of one weakly anomalous dunite (12 ppb), rhodium is at or near the limit of detection. Gold abundances attain their highest levels in gabbroic rocks (216 to 442 ppb) and show no correlation with PGE. Quartz veins close to the Lunar Creek complex are uniformly low in gold.

Anomalous abundances of platinum in chromitite and chromitiferous dunite are known in many other Alaskan-type intrusions (Chapter 10; Nixon and Hammack, 1991). The high platinum:palladium ratio (39) in chromite-rich dunite (Sample 7116B, Table 4.2) suggests a similar mineralogical association. Unfortunately, chromite is scarce and dunite is not abundant, which suggests that the Lunar Creek complex is not a prime target for further prospecting for PGE.

SUMMARY

The Lunar Creek complex is set in a unique structural environment, at the boundary between the accreted terranes of Quesnellia and Stikinia. Due to its close proximity to this major boundary, defined by the Kutcho fault, the complex is intensely faulted. Details of its internal structure are indeterminate at this time.

A wide range of Alaskan-type ultramafic and mafic lithologies are represented in the complex. Dunite forms only a minor proportion of the intrusion and concentrations of chromite are relatively sparse. Massive olivine clinopyroxenite is the most extensive rock type encountered. Hornblende clinopyroxenite is apparently confined to narrow gradational contacts between clinopyroxenite and gabbro. Irregular zones in which blocks of ultramafic cumulates have been chaotically mixed together are widespread. These features largely derive from the remobilization of partly consolidated crystal cumulates due to the action of density flows periodically recurring within the magma chamber. Some mixed zones, however, may have originated by the intrusion and subsequent remobilization of ultramafic dikes as their wallrocks deformed plastically. Magmatic layering comparable to that described at Duke Island (Irvine, 1974a) is locally well preserved in the ultramafic rocks. Layering such as this has not been seen in any other Alaskan-type intrusion in British Columbia.

The gabbroic to dioritic rocks in the Lunar Creek complex have been subdivided into two units. The oldest unit has a well-developed foliation which predates intrusion of the ultramafic rocks and the younger gabbro-diorite unit. The later phase is massive and includes rocks which range in lithology from gabbro to quartz diorite. This unit comprises the youngest rocks of the complex. A mineralogically prominent characteristic of the complex is the presence of quartz-rich pegmatitic segregations and veins, and the occurrence of interstitial quartz in the dioritic phases. Silica oversaturation in the felsic differentiates of Alaskan-type complexes appears to be comparatively rare.

The economic potential for PGE in the Lunar Creek complex appears to be low. Lithogeochemical analyses

TABLE 4.2
NOBLE METAL ABUNDANCES IN THE LUNAR CREEK COMPLEX AND ASSOCIATED ROCKS

Locality	Sample Number	UTM GRID ZONE 9V Northing	Easting	(ppb) Pt	Pd	Rh	Au
LUNAR CREEK COMPLEX							
Dunite							
14	GN-89-9077A	6421870N	589260E	41	6	<2	10
14	GN-89-9077B	6421870N	589260E	62	7	<2	11
14	GN-89-9077F	6421870N	589260E	343	10	<2	<1
35	GN-89-8096	6419960N	591800E	173	3	12	3
39	GN-89-9060	6420010N	590450E	41	4	<2	4
42	GN-89-7116B*	6419520N	590430E	1017	26	<2	<1
43	GN-89-9100B	6429480N	590850E	14	4	<2	<1
44	GN-89-9101	6419280N	590660E	18	3	<2	<1
Olivine Wehrlite and Wehrlite							
5	GN-89-9075B	6422695N	584275E	9	3	<2	9
14	GN-89-9077E	6421870N	589260E	15	<2	<2	4
14	GN-89-9077D	6421870N	589260E	60	12	<2	11
15	GN-89-9070B	6421620N	589300E	135	4	4	2
31	GN-89-9065	6421330N	591860E	85	3	<2	<1
36	GN-89-9080A	6420340N	591090E	29	3	<2	4
45	GN-89-7073A	6419250N	590440E	9	24	<2	47
Olivine Clinopyroxenite and Clinopyroxenite							
10	GN-89-6077	6422240N	589900E	13	<2	<2	5
11	GN-89-9076	6422060N	598225E	136	8	4	<1
15	GN-89-8070B	6421620N	589300E	57	9	<2	12
15	GN-89-9070A	6421620N	589300E	21	<2	<2	111
25	GN-89-9087	6421800N	592170E	41	4	<2	3
28	GN-89-9085	6421670N	592040E	40	6	<2	3
29	GN-89-9084	6421620N	592000E	28	5	<2	<1
30	GN-89-9066D	6421570N	591950E	26	4	<2	<1
33	GN-89-8082	6420760N	591890E	31	11	<2	3
37	GN-89-9064	6420385N	590590E	111	12	7	6
46	GN-89-7076A	6419085N	590150E	3	<2	<2	4
55	GN-89-8117B	6421310N	592290E	12	8	<2	3
59	GN-89-9113A	6418990N	593600E	55	3	<2	175
Hornblende Clinopyroxenite and Feldspathic Hornblende Clinopyroxenite							
13	GN-89-7092	6421890N	590180E	27	3	<2	94
27	GN-89-9068	6421710N	592120E	10	6	<2	12
52	GN-89-7099B	6418600N	590810E	7	12	<2	123
56	GN-89-8118	6419240N	592400E	15	16	<2	5
62	GN-89-7111	6418110N	591270E	34	63	<2	8
Clinopyroxene Hornblendite and Hornblendite							
40	GN-89-9056	6420290N	590010E	13	18	<2	4
41	GN-89-9058	6420150N	590010E	11	13	<2	3
Gabbro-Diorite							
24	GN-89-9090	6421850N	592300E	17	89	<2	8
49	GN-89-7097	6419070N	590880E	3	<2	<2	216
54	GN-89-8103	6418990N	591990E	8	16	<2	9
57	GN-89-9107	6419130N	593020E	<1	2	2	8
58	GN-89-9119	6419250N	593020E	15	8	<2	2
58	GN-89-9119	6419250N	593020E	10	8	<2	81

Diorite-Quartz Diorite							
8	GN-89-6110	6422890N	588240E	8	17	<2	64
9	GN-89-8080	6422510N	587290E	6	9	<2	4
17	GN-89-8043	6421340N	589330E	3	<2	<2	64
19	GN-89-8075	6421180N	588210E	2	<2	<2	18
51	GN-89-7107	6418590N	590990E	3	<2	<2	12
52	GN-89-7099A	6418600N	590810E	<1	<2	<2	2
64	GN-89-7120	6417320N	592400E	5	<2	<2	4
Leucogabbro-Leucodiorite							
7	GN-89-6107	6422600N	588670E	13	5	<2	373
34	GN-89-8084	6427600N	591940E	13	53	<2	10
51	GN-89-9106	6418590N	590990E	2	<2	<2	<1
Foliated Gabbro-Diorite							
4	GN-89-9073C	6422780N	584240E	12	3	<2	10
12	GN-89-9074B	6422060N	589950E	8	6	<2	2
21	GN-89-9049A	6420930N	589680E	8	7	<2	2
65	GN-89-6149	6416780N	593670E	9	9	<2	9
GUICHON SUITE GRANITOIDS AND MINOR INTRUSIONS							
Quartz Monzonite to Granodiorite							
2	GN-89-6094B	6423280N	590290E	<1	<2	<2	3
26	GN-89-9069	6421780N	592160E	3	<2	<2	11
Granodiorite Dikes							
26	GN-89-9069B	6421780N	592160E	<1	3	<2	14
30	GN-89-9066C	6421570N	591950E	<1	<2	<2	8
Leucogabbro-Leucodiorite Dikes							
6	GN-89-6078	6422530N	588725E	2	<2	<2	3
21	GN-89-9049	6420930N	589680E	<1	<2	<2	442
22	GN-89-8046	6420890N	589840E	31	4	<2	17
Plagioclase Porphyry Dikes							
30	GN-89-9066A	6421570N	591950E	<1	<2	<2	31
36	GN-89-9080B	6420340N	591090E	<1	<2	<2	<1
53	GN-89-6112B	6418700N	591730E	4	17	<2	21
55	GN-89-8117A	6421310N	592290E	4	6	<2	4
Hornblende Microgabbro-Microdiorite Dikes							
18	GN-89-8077	6421490N	588250E	<1	<2	<2	55
38	GN-89-9063	6420030N	590550E	6	<2	<2	142
50	GN-89-9105	6418720N	591010E	<1	<2	<2	43
53	GN-89-6112A	6418700N	591730E	<1	<2	<2	5
COUNTRY ROCKS							
Asitka Group Metavolcanic and Metasedimentary Rocks							
20	GN-89-8073	6420000N	588100E	<1	3	<2	20
47	GN-89-7085	6419060N	589115E	<1	<2	<2	133
48	GN-89-6124	6418790N	589080E	<1	<2	<2	15
Takla Group Metavolcanic and Metasedimentary Rocks							
1	GN-89-6090	6425050N	590550E	<1	<2	<2	4
23	GN-89-9094C	6422090N	592550E	<1	4	<2	5
23	GN-89-9094B	6422090N	592550E	9	8	<2	89
60	GN-89-9121	6418460N	593300E	10	5	<2	35
61	GN-89-9115	6418610N	593590E	4	<2	<2	37
Quartz Veins							
3	GN-89-6099	6422900N	589075E	2	<2	<2	17
16	GN-89-8069A	6421550N	589290E	3	<2	<2	3
16	GN-89-8069B	6421550N	589290E	2	<2	<2	<1
21	GN-89-8045B	6420930N	589680E	3	<2	<2	5
32	GN-89-8055A	6421250N	591860E	2	<2	<2	11
51	GN-89-9106C	6418590N	590990E	2	<2	<2	3
63	GN-89-7112	6417630N	591310E	2	3	<2	8

**Chromite-rich dunite*

Detection limits: Pt and Au, 1 ppb; Pd and Rh, 2 ppb.

Sample localities are shown on Figure 4.4.

were completed on 84 samples of assorted rock types from the map area. Anomalous abundances of platinum were detected in most ultramafic lithologies and dunite was particularly enriched. One sample of chromitiferous dunite contained 1017 ppb platinum, suggesting that platinum, probably in the form of platinum-iron alloys (Chapter 10), is intimately associated with chromitite. Unfortunately, chromitite horizons are rare and so economic concentrations of platinum, specifically the PGE-chromitite type of mineralization, appear unlikely.

CHAPTER 5 MENARD CREEK COMPLEX

The Menard Creek mafic-ultramafic complex (56°45.5′N, 126°29′W) is located in the Intermontane Belt of north-central British Columbia. It underlies part of the McConnell Range of the Omineca Mountains (94D/16), just north of Menard Creek for which it is named (Figure 5.1). Access to the area is by four-wheel-drive vehicle along a seemingly endless gravel road that leads north from Fort St. James to the Toodoggone River. A narrow spur road branches north toward the Menard complex just before Kilometre 423 on the main Cheni mine road. Alternatively, the area may be reached by helicopter from the Sturdee airstrip in the Toodoggone River area. The best exposures of the complex occur along serrated, locally precipitous ridges at elevations between 1900 and 2200 metres. Lichen cover on the crest of these ridges is fairly extensive.

REGIONAL GEOLOGY

Mafic-ultramafic rocks of the Menard Creek complex were initially included by Lord (1948) with the Early Cretaceous Omineca intrusions, a granitoid mass of batholithic proportions mainly composed of granodiorite to quartz diorite. Meyer and Overstall (1973) first identified the mafic-ultramafic nature of the complex during an exploration program to investigate an intense magnetic high over the body. Later, Irvine (1974b, 1976) identified the clinopyroxenites of the complex as an Alaskan-type association, produced the first detailed geological map and informally named the body the Menard Creek complex.

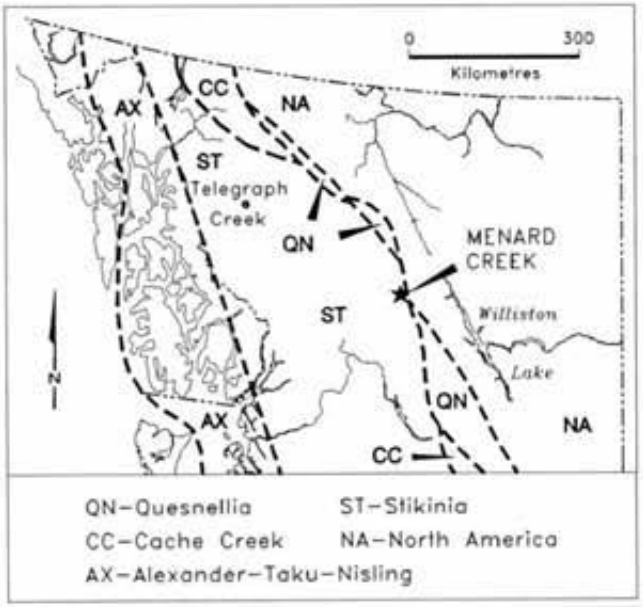

Figure 5.1. Location of the Menard Creek mafic-ultramafic complex in relation to major tectonostratigraphic terranes in northern British Columbia.

The complex (Figure 5.2) is a gabbro-clinopyroxenite body of probable Late Triassic age. It is surrounded by Middle Triassic to Lower Jurassic mafic volcanic rocks of the Takla Group. A possibly coeval high-level intrusive phase is represented by an augite and plagioclase-phyric dike swarm which intrudes the northern margin of the complex. Similar rock types have been described within the Savage Mountain Formation which is part of the "western assemblage" of Takla Group rocks that crop out to the west of the complex (Richards, 1976a).

The structure of the Takla Group is dominated by northerly to northwesterly trending faults and folds and at least two phases of deformation have been recognized (Bellefontaine and Minehan, 1988). The metamorphic grade of the Takla Group is greenschist to subgreenschist (Monger, 1977).

COUNTRY ROCKS: TAKLA GROUP

The Takla Group was initially described by Lord (1948) as an essentially Upper Triassic to Jurassic conformable assemblage of more than 10 000 metres of mafic volcanic and sedimentary rocks. Subsequent work by Richards (1976b), Monger, (1976, 1977), and Monger and Church (1977) refined this definition to include only rocks of Late Triassic age (upper Carnian to middle Norian). The Group was subdivided into two distinct facies, representing eastern and western assemblages, separated by a north-trending lineament, the Ingenika fault, which runs along the Ingenika River (Figure 5.2). The eastern belt of Takla Group rocks in central and northern Quesnellia are now known to range in age from Late Triassic to Early Jurassic (Souther, 1991). Near the Menard Creek complex, Takla Group rocks have been assigned to the eastern assemblage (Richards, 1976a) which includes mafic to intermediate lava flows, volcanic and epiclastic breccias, tuffaceous rocks and green phyllite, phyllitic schists and minor metasedimentary rocks.

MENARD CREEK COMPLEX: MAFIC-ULTRAMAFIC ROCKS

The Menard Creek complex is a roughly circular body covering almost 4 square kilometres. Its outcrop pattern is strongly controlled by faulting. The complex contains a mass of clinopyroxenite in its southwestern corner and a high proportion of gabbro. Igneous layering appears to be absent.

CLINOPYROXENITE

At the present level of exposure, clinopyroxenites, olivine-bearing clinopyroxenites, and olivine clinopyroxenites form 25 to 30% of the complex. They are grey to green-weathering, medium to coarse-grained (5 to 10 mm) or locally pegmatitic (<2 cm) rocks that are generally massive

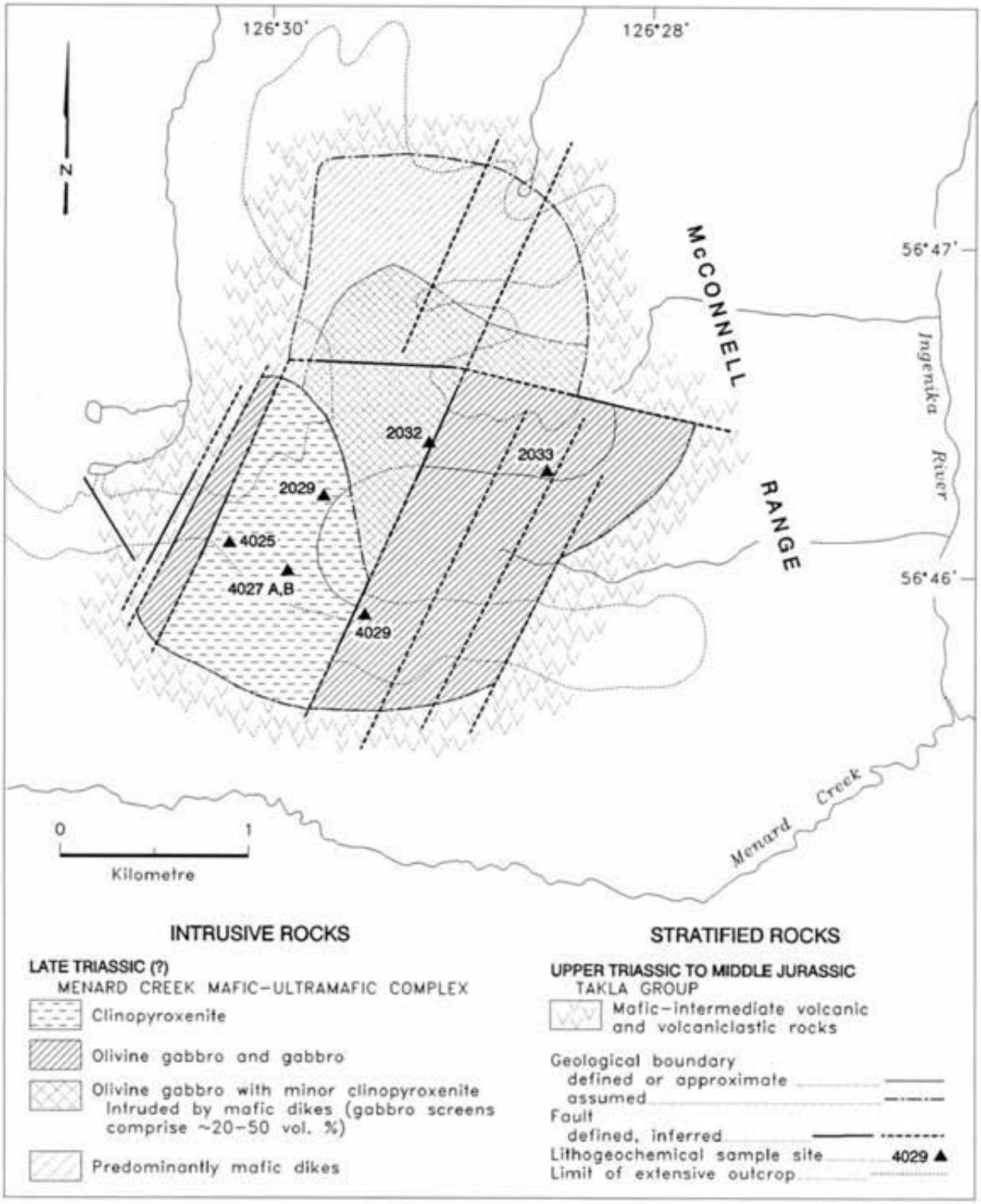

Figure 5.2. Geologic map of the Menard Creek mafic-ultramafic complex (in part after Irvine, 1976b) showing geochemical sample sites.

and isotropic. Varieties that contain olivine carry about 5 to 15 vol% and contacts between olivine-bearing and olivine-free clinopyroxenites appear gradational. Olivine grains are usually strongly altered and weather rusty brown.

In thin section, olivine and clinopyroxene exhibit cumulate textures and clinopyroxene locally displays adcumulate growth. Olivine is completely altered to a fine-grained assemblage of magnetite, serpentine and carbonate. Thin (0.5 to 1 mm) carbonate veinlets (2 to 3 vol% of the rock) are also common.

GABBROIC ROCKS

Pyroxene gabbro, variably enriched in magnetite, is the dominant lithology in the Menard complex. The principal outcrops occur along east-trending ridges in the eastern part of the body. The gabbro is a dark to pale grey, massive, medium-grained rock that is texturally rather uniform and strongly magnetic. It contains subequal proportions of clinopyroxene and plagioclase, and locally grades into more leucocratic or melanocratic variants.

A fault-bounded sliver of extensively epidotized and sericitized gabbro is exposed on the western margin of the clinopyroxenite unit. Melanocratic xenoliths of fine-grained mafic rocks are found within sheared and saussuritized gabbro, and may represent stoped blocks of Takla Group wallrocks. Locally these xenoliths are very abundant.

In thin section, clinopyroxenes are fresh whereas cumulus plagioclase is weakly to strongly altered to sericite (10 to 90 vol%). Magnetite (5 to 15 vol%) forms anhedral intercumulate grains, and subhedral crystals of serpentinized olivine (1 to 2 mm) occurs in trace amounts together with intercumulus biotite (<1 vol%).

MAFIC DIKES

At the northern margin of the complex, medium-grained equigranular gabbros, and a variety of gabbro with augite phenocrysts set in a fine-grained feldspathic matrix, are intruded by augite-phyric dikes that comprise up to 50% of the outcrop. Farther north, gabbro screens disappear and the dikes are sheeted.

Two texturally distinct varieties of dike rock can be identified. One contains conspicuously bladed subhedral crystals of plagioclase with subtrachytic texture that reach over a centimetre in length; the other carries subhedral to euhedral, roughly equidimensional phenocrysts of augite. However, both types of dike contain phenocrysts of plagioclase (<30 vol%), clinopyroxene (3 to 10%) and olivine (1%). In thin section, oscillatory zoned plagioclase phenocrysts are partially resorbed, augite is partly altered to chlorite and olivine is replaced by serpentine and chlorite. The groundmass is composed of finely crystalline clinopyroxene, feldspar and iron-titanium oxides (<20%).

CONTACT RELATIONSHIPS

Intrusive contacts between the Menard Creek complex and the Takla Group have not been identified, although it is likely that such relationships originally existed. Most contacts are represented by faults. However, the contact between clinopyroxenite and gabbro is well exposed and identified as transitional.

The mafic dikes clearly intrude the gabbros. The contact between the units is represented by an intrusive zone with up to 50% gabbro screens. Chilled margins provide good evidence for the chronology of dike intrusion. In all cases, augite porphyry dikes are chilled against dikes with bladed plagioclase textures, indicating that the latter are earlier. The timing of dike intrusion is uncertain, but they may represent feeders for Takla Group volcanism.

STRUCTURE AND METAMORPHISM

A system of northeasterly trending faults appears as well-defined lineaments on aerial photographs. The faults are recognized in the field by localized zones of strongly fractured rock and clay gouge. Near faults, alteration of the surrounding rock is locally severe, but no mineralization has been identified. Epidote and carbonate veining also becomes more intense within these fault zones.

MINERALIZATION AND GEOCHEMISTRY

Noble metal abundances for mafic and ultramafic rocks of the Menard Creek complex and mafic dikes are presented in Table 5.1. Platinum-group element abundances are generally low with weak enrichment of platinum in clinopyroxenites relative to gabbros. Anomalously high palladium in gabbro sample GN-88-4029 does not appear to coincide with the presence of sulphides and may be related to magnetite enrichment.

SUMMARY

The Menard Creek complex is close to the Ingenika fault at the eastern edge of Stikinia. In this respect, its tec-

TABLE 5.1
NOBLE METAL ABUNDANCES IN THE MENARD CREEK COMPLEX AND ASSOCIATED ROCKS

Sample No.	Rock Type	Sulphides (vol. %)	ppb[1] Pt	Pd	Au
MENARD CREEK COMPLEX					
GN-88-4025	Ol clinopyroxenite	-	7	2	1
GN-88-2029	Clinopyroxenite	-	6	4	1
GN-88-2033	Gabbro-diorite	Tr	1	6	1
GN-88-2033[2]	Gabbro-diorite<M>	Tr	1	6	1
GN-88-4029	Gabbro-diorite	-	1	41	2
MAFIC DIKES					
GN-88-4027A	Cpx porphyry	-	1	2	1
GN-88-4027B	Cpx porphyry	-	1	2	2
GN-88-2032	Cpx porphyry	-	1	8	1

Detection limits: Pt and Au, 1 ppb; Pd (2 ppb)
[1] Rh is at or below detection limit (2 ppb) in all samples
[2] Duplicate analysis
Ol, olivine; Cpx, clinopyroxene; Tr, trace sulphides; - sulphides not detected

tonic setting is very similar to the Lunar Creek complex (Chapter 4). The Menard Creek complex has been presumed to be Late Triassic in age and coeval with volcanic rocks of the Takla Group (equivalent in part to the Stuhini Group).

Although gabbroic rocks are the volumetrically dominant phase of the complex, olivine clinopyroxenite and clinopyroxenite are also present. In the absence of detailed study, perhaps its most distinctive Alaskan-type trait is the absence of cumulus orthopyroxene, abundance of magnetite clinopyroxenite and occurrence of biotite in the gabbroic rocks. Internal contacts between gabbro and clinopyroxenite are gradational. Intrusive contacts have not been positively identified. The complex was certainly emplaced high in the crust as it has been intruded by mafic dikes with chilled margins that likely fed Takla Group volcanism.

Abundances of PGE in the Menard Creek complex are uniformly low with the exception of palladium in a single sample. The prospects for PGE mineralization are not encouraging.

CHAPTER 6 WREDE CREEK COMPLEX

The Wrede Creek ultramafic-mafic complex (56°40′N, 126°08′W) is located in the Ingenika Range of the Omineca Mountains, approximately 400 kilometres north-northwest of Fort St. James (Figure 6.1). The area may be reached by well-travelled dirt road via Manson Creek and Germansen Landing. The complex is 8 kilometres north-northeast of Johanson Lake, and is named for Wrede Creek which lies about 4 kilometres beyond its northern margin (Figure 6.2). The region is serviced by chartered aircraft from Prince George or Smithers, via an airstrip at the northern end of the lake or from the Sturdee airstrip some 100 kilometres to the northwest in the Toodogonne River area. Access from Johanson Lake is by helicopter, or a poorly maintained, four-wheel-drive road leading to the southernmost exposures of ultramafic rocks. The map area is covered at a scale of 1:50 000 by NTS sheet 94D/9. Aeromagnetic survey maps are available at scales of 1:250 000 (Map 7778G-McConnell Creek) and 1:63 360 (Map 5272G-sheet 94D/9).

In the past, the Wrede Creek region has attracted considerable attention on account of its precious and base metal potential. The area experienced its first gold rush in 1899 with the discovery and subsequent exploitation of the McConnell Creek gold placers. Tiny platinum nuggets were reportedly found with the gold, but the placers never became as prominant a source of platinum as the rivers and creeks draining the Tulameen complex (O'Neill and Gunning, 1934; Rublee, 1986).

REGIONAL GEOLOGY AND GEOCHRONOMETRY

Reconnaissance mapping (1:250 000) and geological descriptions of the area were first completed by

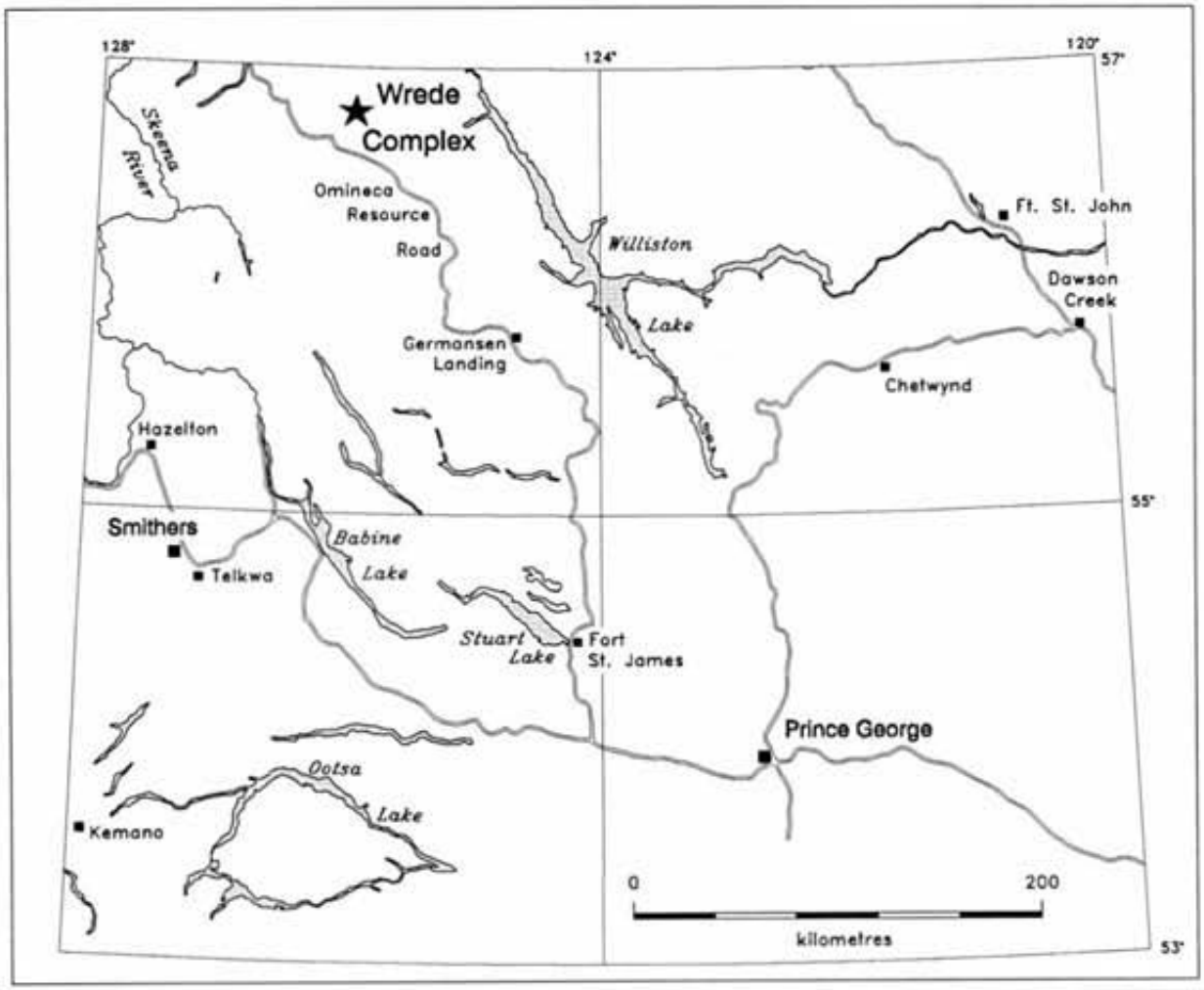

Figure 6.1. Location of the Wrede Creek complex.

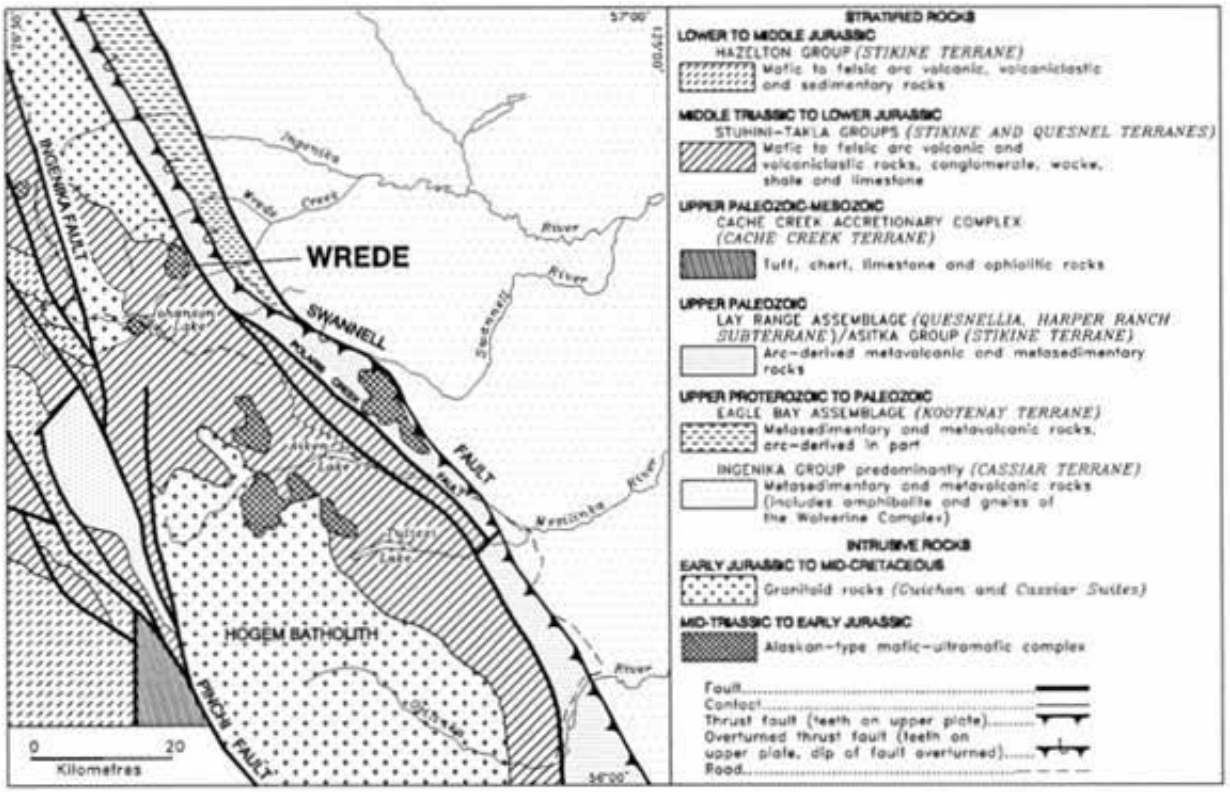

Figure 6.2. Regional geologic setting of the Wrede Creek ultramafic-mafic complex (modified after Irvine, 1974b; Richards, 1976b; and Monger, 1977).

Lord (1948). Subsequently, remapping of various parts of the McConnell Creek map sheet was undertaken by Richards (1976a, b), Monger (1977) and Church (1974, 1975). These authors also described the structure and stratigraphy of volcaniclastic and epiclastic rocks of the Middle Triassic to Lower Jurassic Takla Group, which hosts many of the Alaskan-type ultramafic complexes in the area (*see also* Bellefontaine and Minehan, 1988). Jurassic granitoid plutonism in the region has been described by Woodsworth (1976) and Woodsworth *et al.* (1991). Modern studies of the Alaskan-type complexes that occur within both the McConnell Creek and Aiken Lake map areas to the east, including the Wrede Creek ultramafic complex, were made by Irvine (1974a; 1976). Wong *et al.* (1985) and Irvine (1976) have presented the most detailed descriptions of the complex.

The Wrede Creek ultramafic-mafic complex intrudes volcanic and volcaniclastic rocks of the Middle Triassic to Lower Jurassic Takla Group of Quesnellia (Figure 6.2). To the west, the boundary between the Quesnel and Stikine terranes of the Intermontane Belt is delineated by the Pinchi-Ingenika fault system (Wheeler *et al.*, 1991). Type sections for the Takla Group, as presented by Monger (1977) and Monger and Church (1977), are exposed west of the Ingenika fault in Stikinia. East of the Wrede Creek complex, a high-angle fault separates these supracrustal volcano-sedimentary sequences from a tectonic sliver of rocks assigned to the upper Paleozoic Lay Range assemblage (Richards, 1976a, b; Monger, 1977). These rocks have recently been correlated with the Harper Ranch Subterrane which forms the basement of Quesnellia (Wheeler and McFeely, 1991; Monger *et al.*, 1991). Quesnellia is separated from pericratonic rocks of the Ingenika Group by the Swannell fault which, in part at least, is an imbricated thrust zone with evidence of southwesterly tectonic transport (Bellefontaine, 1989).

The Takla Group west of the Ingenika-Pinchi fault boundary exhibits subgreenschist metamorphism whereas correlative rocks to the east are characterized by greenschist-grade assemblages (Richards, 1976a, b; Monger, 1977). The predominant structural grain in the region is northwesterly. The main lithologies in the Ingenika Range west of the Wrede Creek complex include mafic to intermediate, plagioclase and augite-phyric, volcaniclastic and epiclastic rocks, subaqueous and minor subaerial lava flows, and interbedded black argillites, siltstones, sandstones and minor limestones (Bellefontaine and Minehan, 1988).

Irvine (1974a, 1976) considered that Alaskan-type complexes in north-central British Columbia were comagmatic with Late Triassic volcanic rocks of the Takla Group. Potassium-argon dating of two hornblende mineral separates from feldspathic pegmatites in the Wrede Creek complex appears to support this contention, yielding Late Triassic isotopic ages of 219±10 (1σ) and 225±8 Ma (Wong *et al.*, 1985).

Granitic rocks intrude both the Takla Group and Wrede Creek complex. K-Ar dating of hornblende has established a Middle Jurassic age of 172±6 (1σ) Ma for such intrusions in the Wrede Creek complex (Wong *et al.*, 1985). This is compatible with K-Ar dates on hornblende from plutons comprising part of the Hogem batholith to the south (*e.g.* the Duckling Creek syenite dated at 171±6 (1σ) Ma; Eadie, 1976). The Fleet Peak pluton, a diorite to monzodiorite body northwest of the Wrede Creek complex (Woodsworth, 1976), has yielded K-Ar dates on hornblende and biotite of 144±8 (2σ) Ma and 156±5 Ma, respectively (Wanless *et al.*, 1979). These plutons apparently belong to the Early to Middle Jurassic phases of the Guichon and Copper Mountain suites in Quesnellia (Woodsworth *et al.*, 1991).

COUNTRY ROCKS: TAKLA GROUP

The Wrede Creek complex lies within the predominantly subaqueous eastern facies of the Takla Group (Richards, 1976a, b). Adjacent to the complex, rocks of the Takla Group are predominantly brown to grey weathering, medium grey-green and dark grey augite and augite-plagioclase crystal tuffs, flows and volcanic breccias. These rocks are characterized by euhedral to subhedral black augite crystals up to 1 centimetre in diameter, and white to pale green, variably saussuritized plagioclase laths up to 5 millimetres in length. In thin section, clinopyroxene is seen to be partially or completely pseudomorphed by actinolite. Plagioclase is variably altered to sericite, epidote and carbonate. Actinolite is also abundant in the groundmass and locally assumes a weak preferred orientation. These mineral assemblages indicate regional metamorphism in the upper part of the greenschist facies.

WREDE CREEK COMPLEX: ULTRAMAFIC-MAFIC ROCKS

The Wrede Creek ultramafic-mafic complex occupies an area of approximately 10 square kilometres. It exhibits a crudely concentric zonation of rock types that constitute a complete gradation of lithologies from dunite in the core to gabbro at the margins (Map 2 in pocket; Figure 6.3). The dunite grades outwards through a narrow wehrlitic transition zone into olivine clinopyroxenite and clinopyroxenite. These units in turn pass into hornblende-rich gabbroic or dioritic rocks at the periphery of the complex. Minor olivine-hornblende and hornblende clinopyroxenite and hornblendite are present locally.

Dunite is well exposed along the crest of a northwesterly trending ridge, whereas outcrops of other map units at lower elevations are much more limited and exposure in valleys is poor. In a region of little outcrop at the eastern margin of the body, the position of the contact between the complex and its wallrocks has been estimated from aeromagnetic data. The geometry of the intrusion is poorly constrained, but based on a limited number of short diamond-drill holes at the southern margin of the complex, the body appears to represent a high-level intrusive stock (Wong *et al.*, 1985).

DUNITE

Dunite is the dominant lithology of the Wrede Creek complex and is well exposed (5 km^2) along a major northwesterly trending ridge at the centre of the map area. On weathered surfaces, dunite is characteristically orange-brown, yellow-orange or buff, and contains disseminated, variably magnetic, euhedral to subhedral chromite crystals (up to 1 mm in diameter) that weather with positive relief. The rock is generally medium grained and consists of black, glassy olivine crystals with minor chromite (1 to 5 vol%); fine-grained varieties are dark-grey.

Thin section analysis of dunite reveals an equigranular texture, or rare inequigranular fabric in which small olivine crystals (0.5 to 1 mm) comprising up to 80% of the rock are interstitial to, and poikilitically enclosed within, coarse olivine crystals (up to 5 mm across). Clinopyroxene was not observed within the dunite except at the gradational contact between dunite and clinopyroxenite (well exposed at Locality 5, Figure 6.3). The black colour of the olivine crystals is attributed to an abundance of tiny, opaque, rod-like inclusions which range from 2 to 5 microns in length, which are evenly distributed throughout the crystal and have a preferred orientation that is crystallographically controlled. Attempts to establish the composition of these inclusions by microprobe analysis have been unsuccessful but we believe that they are an exsolution phenomenon (magnetite?) related to oxidation during slow cooling of the dunite. The lack of these inclusions within dunite dikes which cut the dunite body suggests that dike intrusion postdates oxidation.

Microfractures are prominent along crystal boundaries and within crystals, and have acted as loci for serpentinization. On average, olivine is approximately 5% serpentinized, but the degree of alteration varies widely, ranging from thin envelopes surrounding microfractures, to complete serpentinization, particularly in samples collected near brittle shear zones. Altered areas are composed of antigorite, secondary magnetite and minor brucite, talc and carbonate.

Tabular zones of bright orange weathering, medium green-grey, carbonate-quartz alteration are common throughout the dunite. Such zones are composed mainly of ankerite and minor magnesite, and have abundant, closely spaced, white chalcedony veins which are locally folded (Photo 6.1). Minor disseminated bornite and pyrite were observed in one of these zones at the southwestern end of the dunite outcrop (Locality 19, Figure 6.3). The alteration most likely occurs along faults, which possibly serve as channel-

Photo 6.1. Quartz-carbonate alteration in dunite showing folded chalcedony veins in outcrops approximately 300 metres south of Locality 5 in Figure 6.3.

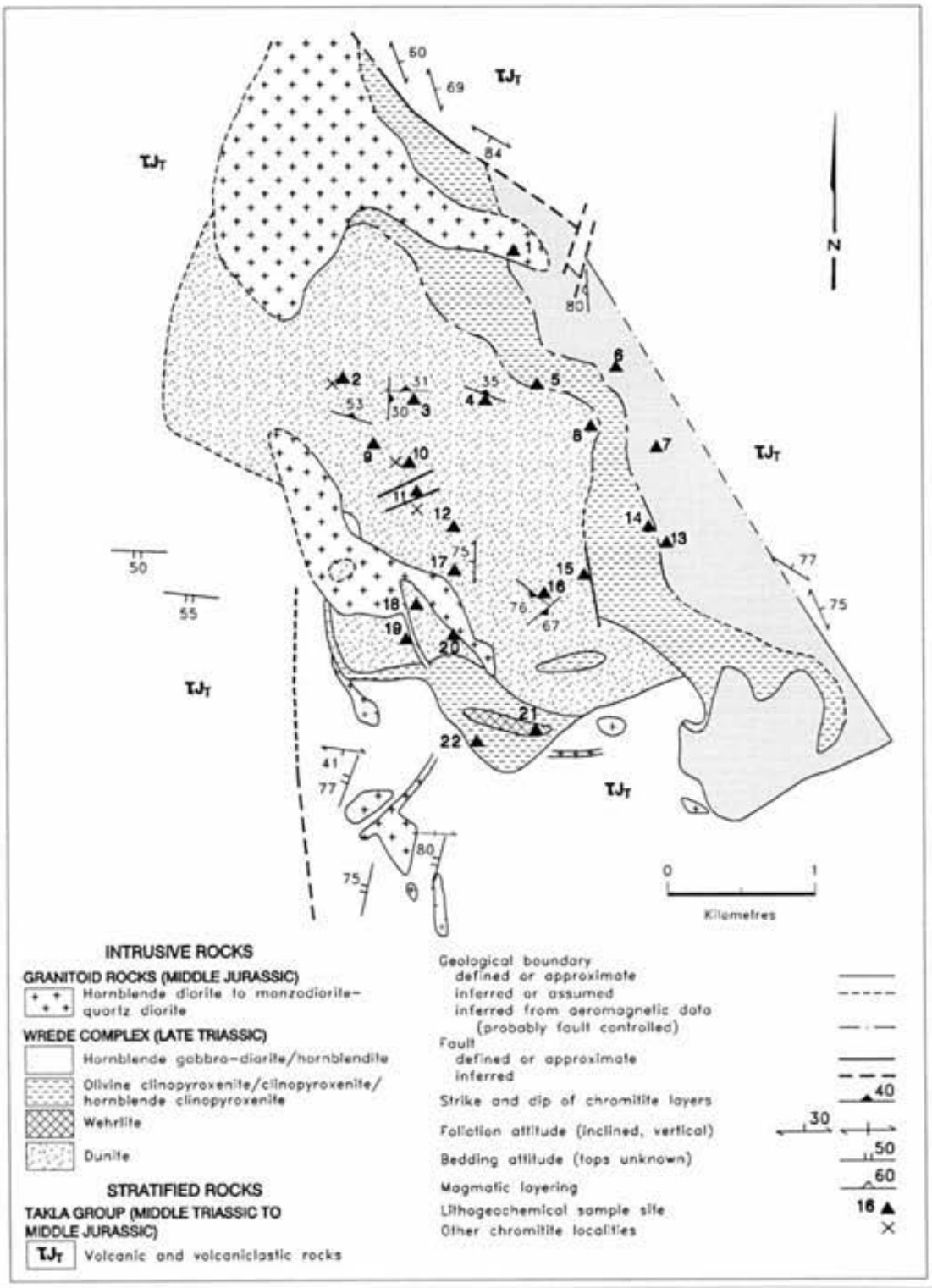

Figure 6.3. Generalized geology of the Wrede Creek ultramafic-mafic complex. Numbered locations represent geochemical sample sites listed in Table 6.1.

ways for the same fluids which introduced the sulphides so prevalent at the southern end of the complex (discussed below).

Microprobe analysis of olivines in the dunite indicates forsteritic compositions in the range of Fo_{88-92} (R.H. Wong, unpublished data). These analyses represent samples collected along an east-west traverse across the dunite core and provide no evidence for outward cryptic zonation.

CHROMITITE

Although chromite is ubiquitous as tiny euhedral crystals in dunite, it is concentrated locally into irregular pods and schlieren. Chromitite schlieren range from 0.1 to 5 centimetres in width and between 5 and 40 centimetres in length; most are less than 1 centimetre wide and 15 centimetres long. They are found as isolated bodies within the dunite, or more commonly in clusters forming chromitite-rich zones several metres in width (Photo 6.2; Locality 2 in Figure 6.3). It is common to find schlieren in various orientations within a single outcrop, indicating some degree of remobilization of previously consolidated chromite cumulates. However, in rocks with a locally penetrative foliation (*e.g.* Localities 16 and 18) schlieren are usually oriented in the plane of the fabric.

There appears to be no structural control reflected in the spatial distribution of chromitite-rich zones, most of which are separated by broad expanses of chromitite-free dunite. Chromitite schlieren appear to be absent within 200 metres of the dunite-clinopyroxenite contact, but this may be due to more limited outcrop in this part of the complex.

CLINOPYROXENITES

The clinopyroxenite unit includes olivine clinopyroxenite, clinopyroxenite, olivine-hornblende clinopyroxenite and hornblende clinopyroxenite. These lithologies typically form a complete gradation from olivine-rich phases adjacent to the dunite contact to hornblende-rich phases adjacent to the gabbro-hornblendite contact.

Clinopyroxenites form a semicontinuous rim around the dunite core of the complex (Figure 6.3). The apparent thickness of the clinopyroxenite unit varies from 50 metres at the southwestern end to 900 metres at the northern end of the complex. Along the eastern margin, clinopyroxenites are in gradational contact with clinopyroxene hornblendite and hornblende-clinopyroxene gabbro. To the south, clinopyroxenites intrude hornfelsed volcanic rocks of the Takla Group.

Photo 6.2. Zone of chromitite pods and schlieren at Locality 2 in Figure 6.3.

OLIVINE CLINOPYROXENITE AND CLINOPYROXENITE

Olivine clinopyroxenite and clinopyroxenite are usually coarse grained and composed of medium brown-green weathering, pale green, cumulus clinopyroxene and brown-weathering, black cumulus to intercumulus olivine. Olivine clinopyroxenite contains an average of approximately 30 vol% olivine, but modal variations range from 10 to 40 vol%. The modal abundance of olivine in clinopyroxenite averages about 5 vol%, but may vary between 0 and 10 vol%.

Olivine clinopyroxenite is most common near the dunite contact where it forms part of the gradation from dunite to clinopyroxenite. Locally, olivine forms up to 50% of the rock, which is more appropriately termed wehrlite. The olivine clinopyroxenite unit varies in width from approximately 2 metres at the eastern margin of the dunite body (approximately 200 m south of Locality 8 in Figure 6.3), to 250 metres at the southwestern edge of the dunite (100 m south of Locality 20) where it is in intrusive contact with hornfelsed country rock.

Clinopyroxenite is well exposed in the eastern part of the complex, where it is sandwiched between olivine clinopyroxenite to the west and hornblende-bearing clinopyroxenite to the east. The clinopyroxenite zone varies in thickness from approximately 100 to 200 metres.

In thin section, equigranular clinopyroxene (0.5 to 6 mm in diameter) exhibits cumulus textures, and olivine occurs as cumulus and intercumulus crystals and equigranular crystal clots which range from 0.5 to 1 millimetre across. Olivine is partially to completely serpentinized. Euhedral to subhedral chromite (0.5 to 1 mm) makes up less than 1 vol% of the rock.

Microprobe analyses of clinopyroxene from olivine clinopyroxenite yield diopsidic compositions with relatively low alumina (1.5 to 2.6 wt% Al_2O_3); olivine compositions range from Fo_{83-86} (R.H. Wong, unpublished data). Clinopyroxenes in clinopyroxenite are also diopsidic with 1 to 3 wt% alumina (R.H. Wong, unpublished data). These mineral compositions fall within the general range of silicate compositions in equivalent rock types of the Tulameen complex (Findlay, 1969; Nixon *et al.*, 1990a).

HORNBLENDE CLINOPYROXENITE AND OLIVINE-HORNBLENDE CLINOPYROXENITE

Hornblende clinopyroxenite is most extensive at the northern end of the complex where it reaches an apparent thickness of approximately 500 metres. In some exposures in the eastern part of the complex (100 m west of Locality 6, Figure 6.3), a complete gradation between clinopyroxenite and hornblende-bearing clinopyroxenite is observed. In this area hornblende-bearing clinopyroxenite

averages between 50 and 150 metres in width and grades into gabbro and hornblendite to the east.

Hornblende clinopyroxenite is medium brown weathering, and comprises about 20 to 50 vol% black hornblende and 50 to 80 vol% dark green clinopyroxene. Three main types are observed: a variety containing euhedral, cumulate hornblende crystals (up to 2 cm in length) surrounded by smaller grains (2 mm) of cumulus to intercumulus clinopyroxene; a coarse-grained variety comprising large crystals (1.5 cm) of cumulus clinopyroxene partially enclosed by intercumulus hornblende (1.5 cm); an equigranular coarse-grained variant of the second type with large (2 cm) interlocking crystals of subhedral cumulus hornblende and clinopyroxene. Locally, plagioclase appears as an intercumulus phase forming up to 5 vol% of the rock. A significant amount of both primary and secondary magnetite has made these hornblende-bearing lithologies strongly magnetic.

Thin section analysis of hornblende clinopyroxenite reveals fresh, pale brown pleochroic hornblende and unaltered clinopyroxene. Magnetite forms up to 2 vol% of the mode and occurs as small euhedra (0.1 to 1 mm) disseminated throughout the rock. Apatite (<1 vol%) occurs as an accessory phase.

Olivine within olivine-bearing hornblende clinopyroxenite was recognized only in thin section. Where present (*e.g.*, near Locality 13, Figure 6.3; and in a drillhole at the southern end of the complex; Wong *et al.*, 1985) it may form up to 10 or 15 vol% of the rock. Typically it occurs as small (0.5 to 1 mm), subhedral crystals completely pseudomorphed by secondary amphibole and magnetite, and poikolitically enclosed by clinopyroxene and hornblende.

HORNBLENDITE AND HORNBLENDE GABBRO-DIORITE

The hornblende gabbro-diorite to hornblendite unit includes rocks that contain variable proportions of hornblende, plagioclase and clinopyroxene, and that locally weather white to black depending on the modal abundance of feldspar. This unit occupies some 3.5 square kilometres at the eastern and southeastern periphery of the complex. Outcrop is sparse, particularly along the eastern margin of the body, and thus contact relationships are rarely seen. It appears, however, that gabbroic rocks are invariably in contact with pyroxenitic rocks toward the core of the complex, and in contact with country rocks externally. Where the contact between gabbro-diorite and pyroxenite rocks is observed (near Localities 6 and 7), it is gradational over a few metres. This contact is typified by a decrease in clinopyroxene and an increase in plagioclase as the gabbroic unit is approached. An intrusive contact between gabbroic rocks and country rocks is observed in a stream-cut approximately 500 metres east of Locality 1. Here, both the main gabbro-diorite body and numerous gabbroic dikes intrude country rocks that have been metamorphosed to lower amphibolite grade in the contact aureole (discussed below). Also at this locality, excellent examples of primary, centimetre-scale, rythmic layering are found within the hornblende gabbro. This texture is formed by modal variations in plagioclase and hornblende which form practically monomineralic layers from 2 millimetres to 2 centimetres thick (Photo 6.3).

Gabbroic rocks generally contain 10 to 40 vol% white to pale green, variably saussuritized plagioclase and euhedral to subhedral hornblende with cumulus to intercumulus textures. Locally, dark green cumulate clinopyroxene forms up to 30 vol% of the rock. Hornblendites typically have less than 5 vol% white to pale green feldspar interstitial to large (up to 2 cm) cumulus hornblende. In places, these rocks enclose pods of feldspathic clinopyroxene hornblendite with up to 50 vol% dark green clinopyroxene.

In thin section, the gabbroic to dioritic rocks are seen to be intensely altered. Pale green, pleochroic hornblende is locally altered to chlorite, clinopyroxenes are partially to completely transformed to uralite, and plagioclase is almost completely saussuritized. Plagioclase relicts with albite twinning are observed rarely. Minor phases include euhedral magnetite (up to 3 vol%) and apatite (1 vol%) with cumulate textures. Epidote is found as euhedral crystals in open-space fillings as well as in granular aggregates forming part of the plagioclase alteration.

MINOR INTRUSIONS

Minor intrusions within the complex include dikes of dunite, wehrlite, olivine clinopyroxenite and hornblende plagioclase pegmatite. With the exception of the latter, these dikes are mineralogically identical to the main lithologic units of the Wrede Creek complex, which they intrude, and appear to be rooted entirely within the intrusion.

ULTRAMAFIC DIKES

Ultramafic dikes composed of dunite, wehrlite and olivine clinopyroxenite, averaging approximately 10 centimetres in width, are found throughout the dunite body, but appear to be most common near the dunite-clinopyroxenite contact. Dunite and olivine wehrlite dikes that intrude olivine clinopyroxenite near the dunite-clinopyroxenite contact are particularly well exposed at Locality 5, and locally

Photo 6.3. Magmatic, centimetre-scale layering in hornblende gabbro in a stream-cut approximately 500 metres east of Locality 1 in Figure 6.3.

incorporate xenoliths of clinopyroxenite wallrocks. Also at this locality, olivine clinopyroxenite dikes cut earlier dikes of olivine wehrlite, attesting to a rather complex crystallization history. In areas where these dikes occur in high concentration (*e.g.* Locality 5), there is a resemblance to the wehrlitic/clinopyroxenitic mixed units described from the Polaris complex (Chapter 8).

In thin section, dunite dikes are seen to be composed of equigranular olivine crystals (0.5 mm) which poikilitically enclose smaller grains (<0.1 mm) of subhedral chromite that locally form up to 5 vol% of the rock. Olivine is variably serpentinized along closely spaced microfractures.

In olivine clinopyroxenite dikes, olivine occurs as glomerocrystic aggregates (0.5 mm) and as single crystals poikolitically enclosed by large clinopyroxenes (up to 2 cm in diameter). Olivine is typically completely serpentinized. In olivine clinopyroxenite dikes near the dunite-clinopyroxenite contact at Locality 5, olivine crystals appear to be entirely cumulate in origin, whereas olivine crystals in the host clinopyroxenite have both cumulus and intercumulus textures.

PEGMATITE DIKES

Buff-white weathering, hornblende plagioclase dikes with pegmatitic textures range from 1 to 5 metres wide and appear restricted to the dunite. They are characterized by fresh, euhedral, black hornblende crystals that measure up to 20 centimetres long and form 5 to 80 vol% of the rock. Pale greenish white, variably saussuritized plagioclase forms the remainder of the rock, together with accessory opaque oxides, apatite and sphene. Contacts between the pegmatite dikes and the dunite are everywhere sharp.

CONTACT AUREOLE

Metamorphism associated with intrusion of the Wrede Creek complex is reflected in an amphibolitic contact aureole developed in volcanic rocks of the Takla Group. The aureole is variable in width but is most extensive at the southern end of the complex where it is up to 400 metres wide. Sparse outcrop along the eastern margin of the complex shows some evidence of contact metamorphism, although the aureole does not appear to be as extensive as that to the south. Drillhole data from the southern end of the complex suggest that the intrusive contact dips gently to the south (Wong *et al.*, 1985). The relatively wide metamorphic aureole in this area may therefore be the surface expression of a contact at shallow depth.

In hand sample, hornblende hornfels is dark grey to black and fine grained. White-weathering subhedral feldspar and rare euhedral augite pseudomorphs help to distinguish this rock as a part of the wallrocks. In thin section, pleochroic green to blue-green hornblende or actinolitic hornblende crystals reach 1 millimetre in length and comprises 50 to 75 vol% of the rock. The matrix comprises fine-grained granoblastic feldspar, acicular actinolite and opaque oxides. Actinolitic amphibole probably formed in part at the expense of hornblende as a retrograde assemblage during regional greenschist facies metamorphism.

GRANITOID INTRUSIONS

Quartz monzonite, monzonite, quartz diorite and diorite dikes of Early or Middle to possibly Late Jurassic age intrude both the Wrede Creek complex and its hostrocks. These dikes vary from 2 to 250 metres wide and do not appear to have a preferred orientation.

Granitoid rocks in the area weather a distinctive buff-white and are white on fresh surfaces. Typically they are medium grained and equigranular, however, a porphyritic texture is developed locally. In hand sample, black hornblende (0 to 35 vol%) occurs as euhedral to subhedral laths up to 5 millimetres long. Plagioclase forms euhedral to subhedral white to pale green crystals. Potassium feldspar and quartz form very fine grained (<1 mm), white anhedral crystals which are easily overlooked in hand sample.

Thin sections of the granitoid rocks reveal zoning of plagioclase in some samples, particularly in plagioclase-porphyritic varieties. Plagioclase is moderately to strongly saussuritized and hornblende is commonly completely pseudomorphed by chlorite, epidote and calcite, although some relatively fresh varieties were found which have a pale green pleochroism. Where quartz and potassium feldspar are observed, they are unaltered and are interstitial to hornblende and plagioclase. All minerals are overprinted with very fine acicular actinolite which probably formed during upper greenshist grade regional metamorphism.

The southern end of the Middle(?) Jurassic Fleet Peak pluton lies approximately 3 kilometres to the north of the Wrede Creek complex. Accordingly, the granitoid intrusions in the vicinity of the complex probably belong to the younger phase of the Copper Mountain Plutonic Suite.

STRUCTURE AND METAMORPHISM

Regionally, faulting is the dominant deformation mechanism within rocks of the Takla Group (Richards, 1976b; Monger, 1977). Folds have been observed only in the less competent lithologies. Our limited structural observations in the vicinity of the Wrede Creek complex shed no light on the regional structure.

Faults manifest themselves as zones of foliated rock from 1 to 20 metres wide. A well-developed shear foliation parallels the northern margin of the complex and appears to be offset by brittle crossfaults in the south. The linear eastern boundary of the complex, inferred from aeromagnetic data, may represent a fault contact. Northwesterly trending faults occur just beyond the western and eastern margins of the complex (Wong *et al.*, 1985). As discussed above, a well-developed contact aureole in hostrocks at the southern perimeter of the complex provides strong evidence for an intrusive contact. The grade of regional metamorphism outside this aureole has attained upper greenschist facies, and has resulted in the formation of a relatively inconspicuous retrograde assemblage within the contact aureole.

MINERALIZATION

The Wrede Creek complex is associated with two unrelated types of mineralization. Most extensively explored is a porphyry copper-molybdenum prospect at the southern

TABLE 6.1
NOBLE METAL ABUNDANCES IN THE WREDE CREEK COMPLEX

Locality	Sample	Description	ppb Pt	Pd	Rh	Au
Chromitite						
2	GN-89-6006-1	Chromitite pod	248	<2	28	3
17	GN-89-6026	Chromitite pod	125	<2	6	2
16	GN-89-7027A	Chromitite pod	2002	5	17	4
10	GN-89-8000A	Chromitite pod	2388	12	72	29
3	GN-89-8002B	Chromitite pod	123	<2	5	<1
Dunite						
2	GN-89-6006-2	Dunite within chromite-rich zone	<1	<2	<2	<1
4	GN-89-6017A	Dunite within chromite-rich zone	<1	<2	<2	3
16	GN-89-7027B	Dunite within chromite-rich zone	19	<2	6	<1
10	GN-89-8000B	Dunite within chromite-rich zone	11	<2	<2	3
3	GN-89-8002A	Dunite within chromite-rich zone	14	<2	<2	63
12	GN-89-7005	Dunite	2	<2	<2	80
5	GN-89-6008-1	Dunite Dike	6	<2	<2	4
19	GN-89-6024	Carbonatized Dunite	5	<2	<2	8
Wehrlite and Clinopyroxenite						
21	GN-89-8020	Wehrlite	31	<2	<2	<1
5	GN-89-6008-2	Ol Clinopyroxenite	3	<2	<2	7
8	GN-89-8011	Ol Clinopyroxenite	26	<2	<2	2
15	GN-89-9030	Ol Clinopyroxenite	30	<2	<2	5
5	GN-89-6008-3	Ol Clinopyroxenite Dike	9	<2	<2	<1
22	GN-89-8018B	Clinopyroxenite	15	44	<2	2
14	GN-89-9026	Hb Clinopyroxenite	9	<2	<2	23
Gabbro-Diorite						
6	GN-89-7007A	Hb-Cpx Gabbro-diorite	4	3	<2	9
6	GN-89-7007B	Hb-Cpx Gabbro-diorite	15	12	<2	195
13	GN-89-7032	Hb-Cpx Gabbro-diorite	8	10	<2	5
7	GN-89-7011	Hb Gabbro-diorite	5	5	<2	10
1	GN-89-6023	Hornblendite	8	11	<2	7
Pegmatite						
9	GN-89-6004	Hb Pegmatite Dike	<1	<2	<2	7
11	GN-89-7001	Hb Pegmatite Dike	<1	<2	<2	26
18	GN-89-7041Z	Hb Pegmatite Dike	<1	<2	<2	23
20	GN-89-7043Z	Hb Pegmatite Dike	<1	<2	<2	4

Detection limits are 1 ppb for Pt and Au; 2 ppb for Pd and Rh. Sample localities are shown on Figure 6.3.
Abbreviations: Ol, olivine; Hb, hornblende; Cpx, clinopyroxene.

end of the complex. The second, discovered in this study, is represented by platinum enrichment within chromitite layers in the ultramafic rocks.

CHROMITE AND PLATINUM

Chromite is restricted to, and locally abundant in, the dunite core of the intrusion where it forms disseminations, pods and schlieren. The main chromitite outcrops, however, lack surface continuity but have not been tested at depth. Geochemical analyses (discussed below) indicate that these chromitites are significantly enriched in platinum. Platiniferous chromitites are now well known in other Alaskan-type bodies in British Columbia, notably the Tulameen complex (Chapters 9 and 10).

SULPHIDES

Wong *et al.* (1985) have described sulphide mineralization at the southern end of the complex. The sulphides are hosted by dioritic to granitic dikes which cut the complex, and also occur in the Takla Group and some pyroxenitic rocks adjacent to the contact. Mineralization is expressed as disseminations and fracture fillings of pyrite, chalcopyrite, molybdenite and bornite. The mineralized areas are covered by the NIK 1 to 9 claims which were staked in 1976 and explored by BP Minerals Limited. Exploration of the area

included 1:5000-scale geologic mapping, geochemical sampling of soils, stream sediments and rock chips, magnetometer and induced polarization surveys, 2550 metres of trenching, 3050 metres of percussion drilling, and 3100 metres of diamond drilling. Multi-element analysis of soils (Hoffman and Wong, 1986) delineated zones with anomalous copper and molybdenum. The most extensive sulphide mineralization was found within clinopyroxenite and hornfelsed country rocks at the southern contact of the intrusion. The sulphide mineralization appears to be structurally controlled and is most likely related to Jurassic granitoid plutonism.

Locally, disseminated bornite and pyrite are found in quartz-carbonate alteration zones within the dunite. The planar nature of these zones suggest that they are alteration envelopes surrounding faults. These zones may have been formed by hydrothermal fluids with metal concentrations bearing the signature of nearby granitoid plutons.

NOBLE METAL GEOCHEMISTRY

Analytical results for gold, platinum, palladium and rhodium in 29 lithogeochemical samples of the Wrede Creek ultramafic-mafic complex are presented in Table 6.1. Sample localities are shown in Figure 6.3. All analyses were done by inductively coupled plasma emission spectrometry at Acme Analytical Laboratories, Vancouver. Accuracy was checked by in-house standards, and analytical precision (and any nugget effect) monitored by hidden duplicates and internal standards. The noble metals were preconcentrated by fire assay from 30-gram aliquots of 200 grams of rock powder (-200 mesh).

Chromitite horizons in the core of the Wrede Creek complex are markedly enriched in platinum. Five samples of relatively high-grade chromitite ran between 120 and 2400 ppb platinum. Some of these samples also have significant abundances of rhodium; all are characterized by high platinum:palladium ratios, and one (Locality 10, Figure 6.3) contains some gold. Interestingly, the dunite samples, even where collected adjacent to chromitite layers, are low in PGE, although two specimens of dunite (Localities 3 and 12) have anomalous gold (60 to 80 ppb). In general, pyroxenitic rocks contain low abundances of PGE, hornblende-bearing varieties exhibit the lowest platinum:palladium ratios, and hornblende plagioclase pegmatites are low in the noble metals. The highest gold abundance occurs in a gabbro near the northeastern margin of the complex (Locality 6) but another sample from the same locality is markedly less enriched (Table 6.1).

Apart from the fact that the platiniferous chromitites are confined to the dunite core of the intrusion, they appear to have no systematic spatial distribution within the complex. Their economic significance is obviously strongly dependent upon the concentration of chromitite schlieren which, to date, remains to be more thoroughly tested.

SUMMARY

The Wrede Creek ultramafic-mafic complex fits well into the Alaskan-type classification. Cumulate textures, igneous layering, a crude concentric zonation and gradational contacts between ultramafic and mafic lithologies are consistent Alaskan-type features. The external geometry of the body is poorly constrained, but it may represent a stock-like intrusion. At the contact, Takla Group volcanic and volcaniclastic rocks have been hornfelsed to lower amphibolite grade. However, the contact effects have been largely overprinted by upper greenschist facies regional metamorphism.

Enrichment of PGE in chromitite pods and schlieren is encouraging and should warrant further exploration in order to determine the extent of these platiniferous chromitites. Of potentially added interest is the porphyry-style copper-molybdenum mineralization in the southern part of the complex. Renewed interest in base metal exploration may spur future investigation.

CHAPTER 7 JOHANSON LAKE COMPLEX

The Johanson Lake mafic-ultramafic complex (56°34.5′N, 126°13′W) is situated in the Omineca Mountains approximately 2 kilometres southwest of Johanson Lake, for which the complex is named (Figures 7.1 and 7.2). Access to the area is by a well-travelled dirt road stretching some 400 kilometres north from Fort St. James via Manson Creek and Germansen Landing. An airstrip at the northern end of Johanson Lake is in good repair and suitable for light aircraft. The complex is situated entirely above treeline and excellent exposures are to be found in cirque headwalls and at the crests of ridges between elevations of 1900 and 2300 metres. Talus aprons and glacial till blanket the lower slopes and valley floors.

The project area is covered at a scale of 1:250 000 by the McConnell Creek map sheet (NTS 94D) and 1:50 000 map sheet 94D/9. Aeromagnetic survey maps are available in the smaller scale (Map 7778G - McConnell Creek) and at a scale of 1:63 360 (Map 5272G - 94D/09).

The Johanson Lake complex is distinguished from other Alaskan-type complexes in the area by a lack of olivine-rich ultramafic lithologies (dunite, wehrlite and olivine clinopyroxenite). Instead, it is characterized by predominantly amphibole-bearing clinopyroxenites and gabbro-diorite. The gabbroic rocks appear to be volumetrically dominant and contain spectacular examples of comb layering as well as the more common centimetre-scale layering observed in the feldspathic phases of other complexes.

REGIONAL GEOLOGY AND GEOCHRONOMETRY

Geologic reconnaissance of the McConnell Creek map area was first completed by Lord (1948) who also described

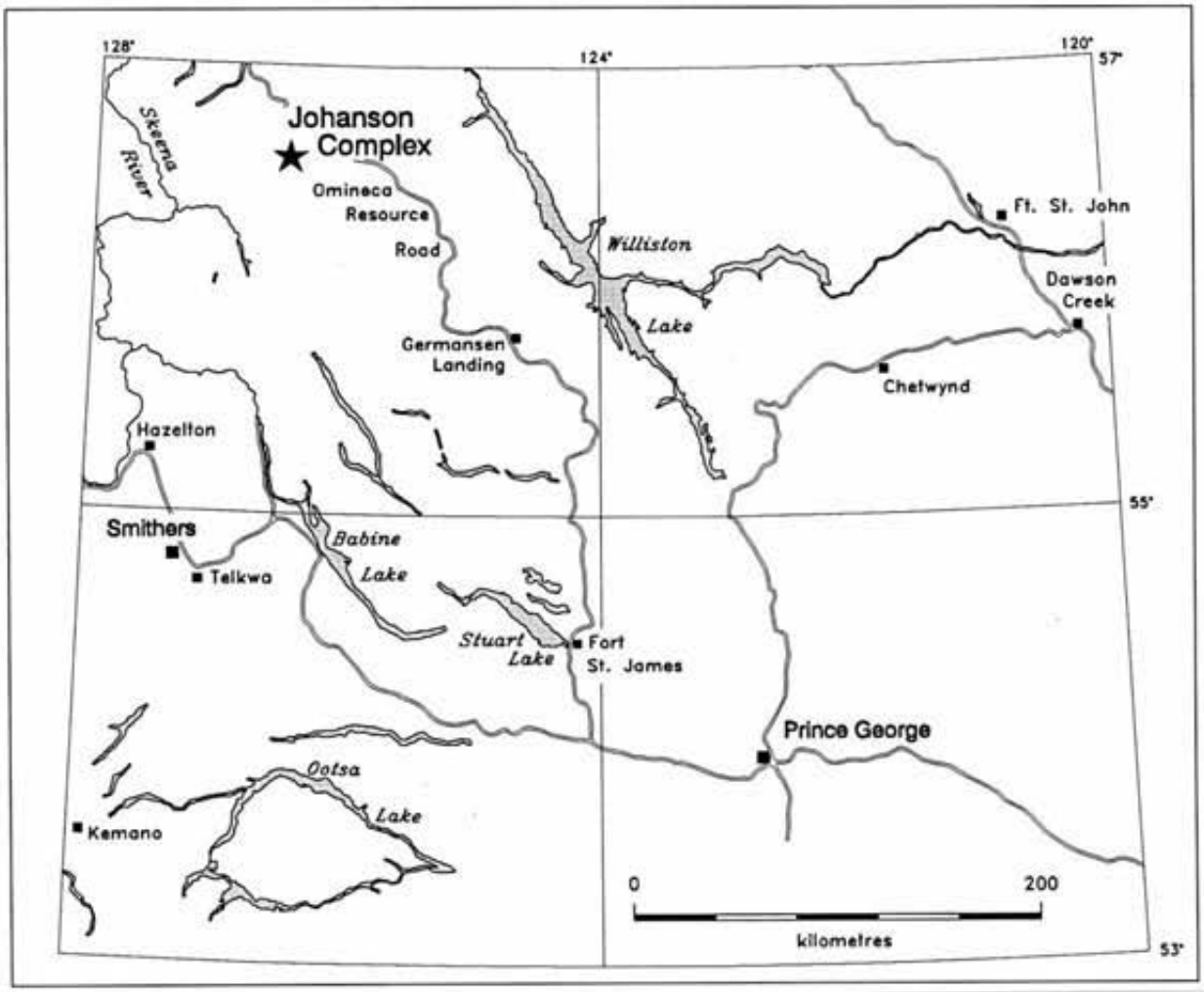

Figure 7.1. Location of the Johanson Lake mafic-ultramafic complex.

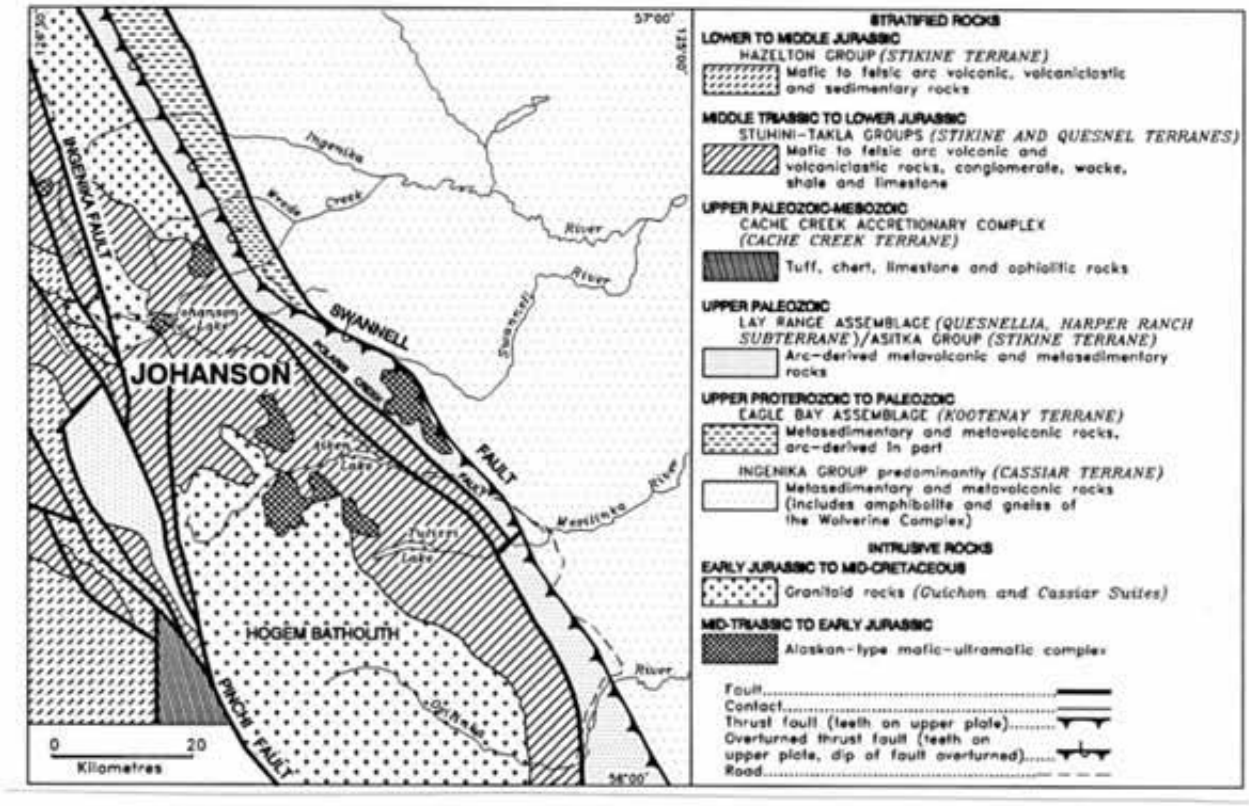

Figure 7.2. Geologic setting of the Johanson Lake mafic-ultramafic complex (modified after Irvine, 1974b; Monger, 1977; and Richards, 1976b).

many of the mineral prospects in the region. Much of the map sheet was later revised by Richards (1976a, b), Monger (1977) and Church (1974, 1975). The latter authors focused on the stratigraphy and structure of the Middle Triassic to Early Jurassic Takla Group which hosts the majority of the Alaskan-type complexes in the region. More recently, Bellefontaine and Minehan (1988) and Minehan (1989) published the results of geologic studies of the Takla Group in the southwestern part of the Ingenika Range approximately 8 kilometres north of Johanson Lake.

The most detailed investigations of Alaskan-type complexes in the region, including Johanson Lake, have been made by Irvine (1974b, 1976). Granitoid intrusions of predominantly Jurassic age in the area have been described by Woodsworth (1976) and Woodsworth *et al.* (1991).

The Johanson Lake complex lies within Quesnellia (Figure 7.2). The Quesnel terrane is bounded on the west by Stikinia along the line of the Pinchi-Ingenika fault system (Gabrielse, 1985; Wheeler *et al.*, 1991). Its eastern boundary is marked by the Swannell fault, in part a southwesterly directed thrust zone which places Upper Proterozoic miogeoclinal rocks (Ingenika Group) of ancestral North America on Quesnellia (Bellefontaine, 1989). West of the Ingenika-Pinchi fault system, Takla Group lithologies reach prehnite-pumpellyite grade assemblages whereas to the east these rocks have been metamorphosed to the greenschist facies (Richards, 1976b; Monger, 1977). The prevalent regional structures are represented by northwesterly trending, high-angle brittle faults and shear zones.

The Johanson Lake complex is hosted by the eastern facies of the Takla Group, an undifferentiated package of predominantly greenschist-grade, subaqueous mafic to intermediate volcaniclastic rocks interbedded with minor sedimentary material (Richards, 1976b; Monger, 1977; Bellefontaine and Minehan, 1988). These rocks are intruded by granitoid plutons of predominantly Jurassic age, the largest and possibly longest-lived of which is the composite Hogem batholith which is largely formed by Early to Middle Jurassic phases of the Guichon and Copper Mountain suites (Figure 7.2; Woodsworth *et al.*, 1991). A coarsely crystalline hornblendite from the Johanson Lake complex has yielded an early Late Triassic (early Carmian) K-Ar isotopic age on hornblende of 232±13 (2σ) Ma (Stevens *et al.*, 1982).

COUNTRY ROCKS: TAKLA GROUP

Middle Triassic to Early Jurassic country rocks of the Takla Group are well exposed in northeasterly trending ridges at the northern and southeastern margins of the complex, and farther south where they form a northwesterly trending ridge (Figure 7.3). At the faulted northern margin of the complex, the Takla Group is composed of metavolcanic and minor metasedimentary (epiclastic?) strata that dip to the north. The predominant lithologies are grey-green, well-cleaved, plagioclase-actinolite schists and massive,

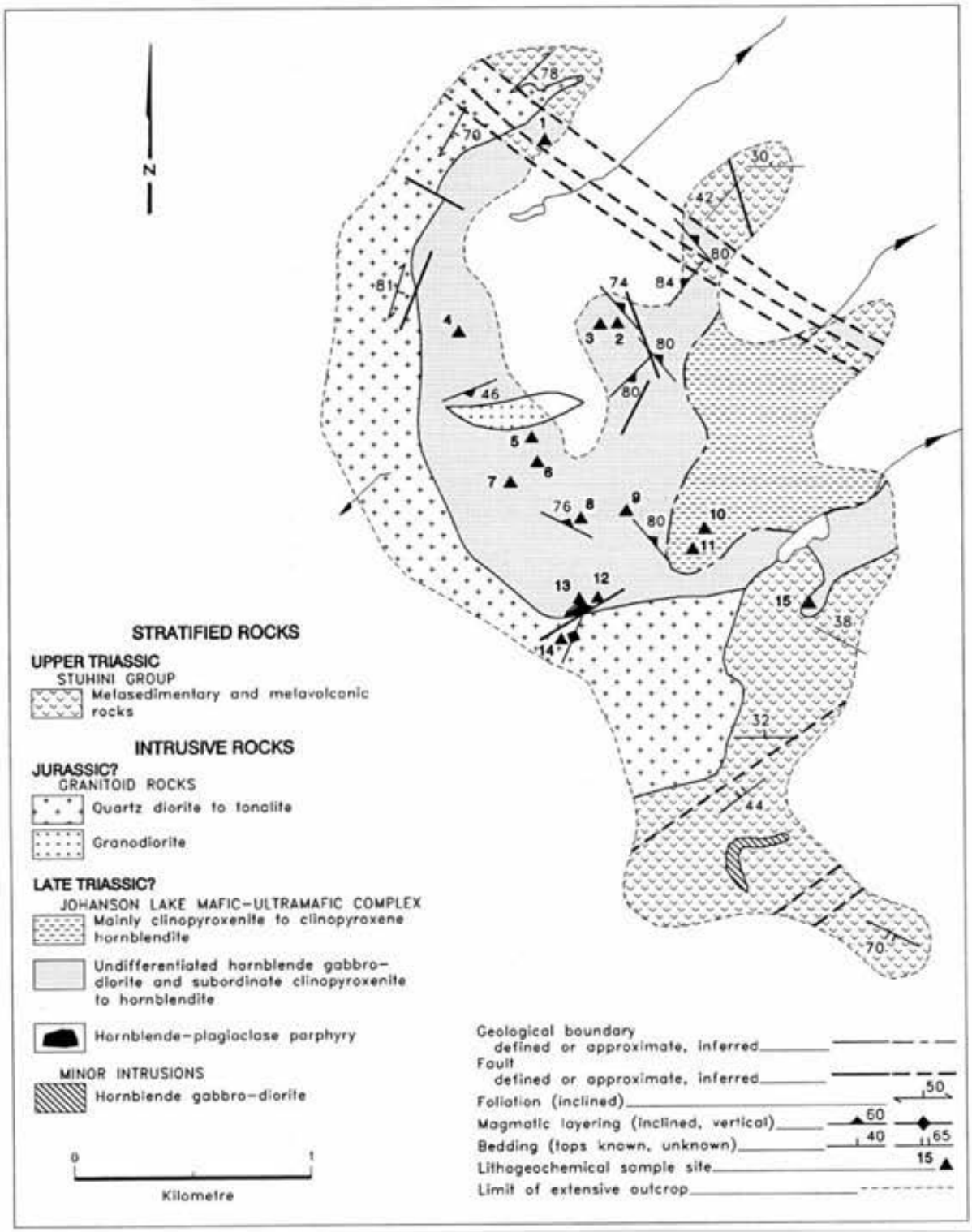

Figure 7.3. Generalized geology of the Johanson Lake mafic-ultramafic complex showing geochemical sample sites listed in Table 7.1.

mafic to intermediate flows that vary from aphanitic to plagioclase augite porphyries. In thin section, the latter rocks are seen to contain euhedral to subhedral phenocrysts or glomerocrysts (<4 mm across) of lamellar-twinned plagioclase and actinolite pseudomorphs after augite, set in a granoblastic matrix of plagioclase and actinolite (up to 50% of the matrix). Textures in aphanitic flows are also granoblastic and, locally, actinolite is pseudomorphous after rare mafic phenocrysts (up to 2 mm in length). Relict igneous plagioclase in these rocks commonly exhibits subgrain boundaries and shows only incipient alteration to clay minerals.

In the southern part of the map area, the Takla Group contains dark grey to rusty weathering, hornblende-augite-plagioclase-phyric lavas, massive crystal and crystal-lithic tuffs, volcanic breccias, altered amygdaloidal mafic flows, and thickly bedded, greenish grey, silicified siltstones and mudstones. These rocks have similar textures and metamorphic mineral assemblages to lithologies to the north. Graded bedding has been observed locally and suggests that the rocks are the right way up. The proportion of rusty weathering outcrop varies according to the abundance of pyrite, which locally reaches 10% of the rock, and occurs as disseminations and in quartz veins. On the whole, the country rocks of the Johanson Lake complex resemble Takla Group volcanic and volcaniclastic sequences north of Johanson Lake described by Bellefontaine and Minehan (1988) and Minehan (1989).

JOHANSON LAKE COMPLEX: MAFIC-ULTRAMAFIC ROCKS

The Johanson Lake mafic-ultramafic complex underlies an area of approximately 4 square kilometres (Figure 7.3). The major areas of outcrop are a prominent unnamed peak (2327 metres) in the southern part of the complex and several northeasterly to northerly trending ridges of rugged to gentle relief.

Previous work by Irvine established the predominantly gabbroic nature of the complex but showed a large unit of olivine clinopyroxenite occupying the southeastern part of the body (Irvine, 1976, Figure 15.3J). However, the area in question is underlain mostly by hornblende clinopyroxenite and clinopyroxene hornblendite with minor clinopyroxenite and melanocratic gabbro.

We have subdivided the complex into two main lithologic units: clinopyroxene and hornblende-rich ultramafic rocks with minor melanocratic gabbros; and hornblende±clinopyroxene gabbroic rocks with minor interlayered ultramafic lithologies. The latter map unit appears to be the most voluminous.

Intrusive contacts with the Takla Group are exposed at the southeastern margin of the complex. Internally, contacts between the major map units are usually sharply gradational, as are the contacts of interlayered minor rock types within each of the major units.

CLINOPYROXENITE

Small outcrops of medium grey-green, medium to coarse-grained clinopyroxenite occur at the northwestern extremity of the region underlain by mainly ultramafic lithologies, and in gabbroic rocks at Locality 3 in Figure 7.3. The clinopyroxenites contain pale brown-weathering, serpentinized olivine grains (2 - 5 vol%) distributed evenly throughout the rock and rare pods of olivine wehrlite to dunite up to 1 metre in length. These olivine-rich pods are elongate and irregular, and commonly exhibit a pronounced internal foliation in contrast to their massive pyroxenitic hostrocks. In thin section, subhedral to anhedral clinopyroxenes (up to 1 cm across) form an interlocking mosaic containing subhedral cumulus olivine crystals (5 - 10 vol%) up to 8 millimetres in diameter, and pale green, pleochroic, intercumulus hornblende (5 - 10 vol%). Olivines have been almost completely replaced by serpentine, magnetite and secondary amphibole (tremolite-actinolite). These olivine and hornblende-bearing clinopyroxenites represent the most primitive lithologies in the complex.

HORNBLENDE CLINOPYROXENITE AND CLINOPYROXENE HORNBLENDITE

A complete gradation exists between clinopyroxenite, hornblende clinopyroxenite (<50 vol% hornblende) and clinopyroxene hornblendite (<50 vol% clinopyroxene) in the ultramafic lithologies in the southeastern part of the complex. These rocks are medium to coarse grained and weather medium grey-green to dark greenish grey, depending on the clinopyroxene:amphibole ratio. In thin section, hornblende crystals (up to 3.5 cm) poikilitically enclose clinopyroxene and appear to be replacing corroded pyroxene relicts. Iron-titanium oxides, largely magnetite, occur in small amounts (<5 vol%). Clinopyroxenes have been partly replaced by actinolite-tremolite, and other secondary minerals include minor calcite and epidote. These ultramafic lithologies grade through melanocratic gabbros into surrounding gabbroic rocks.

GABBROIC TO DIORITIC ROCKS

The gabbroic to dioritic map unit in Figure 7.3 contains significant proportions of interlayered hornblende clinopyroxenites, clinopyroxene hornblendites, hornblendites and their feldspathic equivalents. Gabbroic pods are quite common within these ultramafic lithologies. The dominant rock type is medium-grained to pegmatitic hornblende gabbro or diorite that weathers pale to dark grey or grey-green, and locally contains rusty zones rich in pyrite (2 - 3 vol%). Hornblende clinopyroxene gabbros occur locally and contain as little as 20% amphibole and up to 40% clinopyroxene. A complete gradation exists between these rock types.

The gabbroic unit is characterized by two types of layering. Medium-grained equigranular gabbroic rocks may exhibit centimetre-scale modal layering comprising alternating hornblende±clinopyroxene and plagioclase-rich horizons (Photo 7.1). In many places, pegmatitic zones have developed spectacular comb layering defined by acicular hornblende crystals up to 20 centimetres in length (Photos 7.2 and 7.3). Almost invariably, amphibole crystals are preferentially oriented at high angles (70-80°) to the trend of the layering. These comb-textured layers generally alternate with more equigranular, feldspathic layers (Photo 7.2). The boundaries between layers are curvilinear and sharply tran-

Photo 7.1. Centimetre-scale layering formed by modal variations in plagioclase and amphibole in hornblende gabbro-diorite. Magnet is 11 centimetres long.

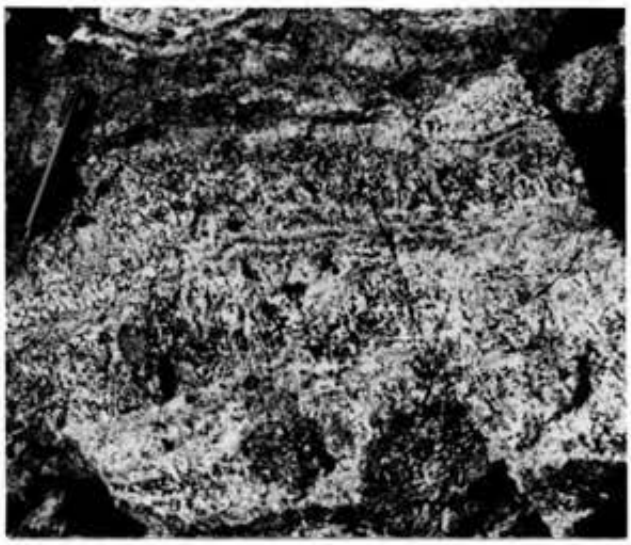

Photo 7.2. Comb layering in hornblende gabbro-diorite formed by acicular amphibole crystals oriented nearly perpendicular to more equigranular, centimetre-scale layers.

sitional, and the terminations of large prismatic hornblendes locally penetrate the adjacent layer (Photo 7.3). These features suggest that comb layering developed by *in situ* crystal growth under conditions where silicate melts became periodically supersaturated in amphibole.

In thin section, the gabbroic to dioritic rocks contain subhedral, brown to deep green pleochroic hornblende (20 - 50 vol%), subhedral to anhedral plagioclase (30 - 60%), euhedral to subhedral clinopyroxene (0 - 40%), and accessory iron-titanium oxides (<5%), apatite and minor sphene. Plagioclase is extensively saussuritized and generally occurs as intercumulus and cumulus material. Clinopyroxene invariably forms cumulus grains which are commonly partially altered to actinolite. Hornblende is generally a cumulus mineral but forms large (up to 2 cm) poikilitic intercumulus crystals in a rare variety of hornblende-megacrystic gabbro. Magnetite, apatite and sphene form

Photo 7.3. Well-developed comb layering in coarse-grained to pegmatitic hornblende gabbro-diorite. Note penetration of adjacent feldspathic layer by large amphibole crystal to right of magnet.

euhedral cumulus crystals up to 1 millimetre in length. Quartz may occur in minor amounts (<5%) in the groundmass of hornblende gabbros and appears to be largely primary.

HORNBLENDE-PLAGIOCLASE PORPHYRY

A medium grey, fine to medium-grained, porphyritic dioritic rock is exposed at the southern margin of the complex (Figure 7.3). It contains subequant saussuritized plagioclase (40 vol%), acicular hornblende crystals partly altered to biotite and actinolite, and minor quartz (5%). Locally the rock is sheared and enriched in chlorite and epidote, and cut by quartz veins. Intrusive contacts with coarse-grained gabbroic rocks are sharp and the porphyry contains irregular gabbro xenoliths (cognate?). Thin (1 to 2 cm) feldspathic veinlets cut the porphyry and adjacent gabbroic rocks and may represent more differentiated residual liquids derived from within the complex. The porphyry is distinguished from the adjacent quartz diorite/tonalite pluton by its more melanocratic character, and appears to represent a late marginal phase of the Johanson Lake complex.

MINOR INTRUSIVE ROCKS

Narrow dikes of hornblende-rich gabbro or diorite, hornblende pegmatite and fine-grained felsite cut mafic and ultramafic lithologies of the Johanson Lake complex. Hornblende plagioclase pegmatite dikes up to 3 metres wide cut clinopyroxene hornblendites interlayered with gabbroic rocks. Prismatic hornblende crystals (up to 15 cm long) are commonly arranged haphazardly in the centre of the intrusion but may lie parallel to wallrock contacts near the margins of the dike. These rocks are compositionally identical to the comb-layered pegmatite zones of the gabbroic unit.

Dark grey-green melanocratic microgabbro or microdiorite dikes less than a metre wide are observed locally.

They consist almost entirely of saussuritized plagioclase and hornblende variably altered to actinolite. Most textures are equigranular although a few dikes contain larger crystals of hornblende (up to 2 mm). These dikes are characterized by a conspicuous alignment of hornblende prisms parallel to their margins.

White to pink-weathering, aphanitic felsite dikes up to 0.5 metre wide cut gabbroic and ultramafic rocks alike. Mafic minerals form less than 5% of the rock and have been replaced by epidote, chlorite and carbonate. The origin of these rocks is uncertain but they bear a strong resemblance to rather widespread feldspathic veinlets that represent leucocratic differentiates of the gabbroic rocks.

A dike-like body of grey-green, medium-grained hornblende gabbro or diorite intrudes volcanic rocks of the Takla Group south of the Johanson Lake complex (Figure 7.3). The rock contains euhedral prismatic hornblende (50 vol%) and subequant plagioclase laths up to 2 millimetres long set in a fine-grained recrystallized feldspathic groundmass. Amphibole crystals define a pronounced flow fabric subparallel to the contacts of the intrusion. Plagioclase is saussuritized and hornblende partly replaced by actinolite. Euhedral to subhedral magnetite and apatite occur as accessory minerals, and secondary pyrite (1 - 2 vol%) is disseminated throughout the rock. This intrusion is probably coeval, and may be cogenetic, with hornblende-rich gabbroic rocks of the Johanson Lake Complex.

GRANITOID ROCKS

A large body of quartz diorite to tonalite delineates much of the western and southern margins of the Johanson Lake complex. Intrusive contacts with the Takla Group are well exposed in the northern and southern parts of the map area, but contact relationships with gabbroic rocks are not clear. We suspect that the Johanson Lake complex is older and tentatively consider the quartz diorite-tonalite to be post-Late Triassic and pre-Late Jurassic in age.

The quartz diorite-tonalite unit is a pale grey weathering, massive, medium-grained subequigranular rock containing variable proportions of anhedral quartz (10 - 30 vol%) with subgrain mosaics, euhedral to subhedral plagioclase (45 - 55 vol%), dark green pleochroic hornblende (10 - 20 vol%), minor biotite and iron-titanium oxides (<5%). Hornblende crystals are largely replaced by actinolite at their rims and some biotite appears to be secondary. Plagioclase is partly saussuritized and disseminated pyrite is common near fault zones.

A small body of pale pinkish grey weathering, medium-grained granodiorite intrudes the western part of the complex. It contains euhedral to subhedral, partly saussuritized plagioclase (50 vol%) up to 5 millimetres in length; anhedral quartz crystals (30 vol%) up to 2 millimetres across; subhedral to anhedral potassium feldspar (20%) up to 2 millimetres in length; and minor biotite and trace amounts of hornblende. The age of the granodiorite is uncertain but it has been tentatively assigned to the Jurassic.

STRUCTURE AND METAMORPHISM

The lack of distinctive marker horizons in the eastern facies of the Takla Group hampers interpretations concerning regional deformation. The attitude of bedding could have resulted from folding or rotation by faulting. Northwesterly trending, high-angle fault zones bounding the northern margin of the complex have incorporated metavolcanic country rocks as a thin fault-bounded slice within it.

The grade of metamorphism throughout the map area appears to have reached middle to upper greenschist facies. A sample of crystal tuff in the Takla Group near the fault contact with clinopyroxene hornblendite at the northeastern margin of the complex has granoblastic texture and a lowermost amphibolite (hornblende-plagioclase-quartz) grade mineral assemblage. Other volcanic rocks farther northwest along the same contact have uppermost greenschist grade assemblages. Faulting and retrograde regional metamorphism may, therefore, have obscured a weak, and as yet poorly defined, metamorphic aureole of lowermost amphibolite grade at the margins of the complex.

NOBLE METAL GEOCHEMISTRY AND MINERAL POTENTIAL

Analytical results for platinum, palladium, rhodium and gold in 15 lithogeochemical samples of the Johanson Lake mafic-ultramafic complex are presented in Table 7.1. Sample localities are shown in Figure 7.3. All analyses were conducted by inductively-coupled plasma emission spectroscopy at Acme Analytical Laboratories, Vancouver. Analytical methods and accuracy are described in Chapter 2.

The highest abundances of platinum and palladium, 41 and 88 ppb respectively, are found in hornblende plagioclase pegmatites within the gabbroic sequence. The tenor of gold peaks at 41 ppb in the gabbros and rhodium is below the detection limit in all samples. In general, palladium abundances are higher in gabbroic than pyroxenitic lithologies and the noble metals are uniformly low in quartz diorites. Unlike other Alaskan-type complexes in British Columbia, platinum shows no systematic decrease from ultramafic to gabbroic rocks. This may be due to the relatively small number of samples analyzed or the limited range of ultramafic lithologies represented. Another notable feature is the relatively high average abundance of gold in the Johanson Lake complex as a whole.

The distribution of noble metals bears no apparent relationship to the presence of sulphides (disseminated pyrite) or proximity to fault zones. The potential for economic concentrations of precious metals appears to be low.

SUMMARY

The Johanson Lake mafic-ultramafic complex is a relatively small (4 km^2) Alaskan-type intrusion hosted by augite-plagioclase-phyric mafic to intermediate volcanic and volcaniclastic rocks of the Middle Triassic to Early Jurassic Takla Group that forms part of Quesnellia. The complex is dominated by hornblende-bearing gabbroic rocks with lesser proportions of clinopyroxene hornblendite,

TABLE 7.1
NOBLE METAL ABUNDANCES IN THE JOHANSON LAKE COMPLEX

Locality	Sample	Rock Type	ppb Pt	Pd	Rh	Au
Clinopyroxenite and Hornblendite						
3	GN-89-9031	Ol-Hb-bearing clinopyroxenite	9	5	<2	4
9	GN-89-6034	Hb clinopyroxenite	6	5	<2	4
11	GN-89-9011	Hb clinopyroxenite	17	15		15
4	GN-89-8032	Feldspathic Hb clinopyroxenite	5	4	<2	7
12	GN-89-9009	Feldspathic Hb clinopyroxenite	<1	<2	<2	26
1	GN-89-9048	Feldspathic Cpx hornblendite	5	5	<2	10
Gabbro-Diorite						
5	GN-89-8027A	Hb-Cpx gabbro-diorite	19	22	<2	41
8	GN-89-6031	Hb-Cpx gabbro-diorite	5	13	<2	14
7	GN-89-8023	Cpx-Hb gabbro-diorite	20	7	<2	41
10	GN-89-8007	Cpx-Hb gabbro-diorite	15	33	<2	22
6	GN-89-8022	Hb gabbro-diorite	7	11	<2	13
Pegmatite						
2	GN-89-9034	Hb-Plag pegmatite	8	42	<2	21
13	GN-89-9001C	Hb-Plag pegmatite	41	88	<2	28
Qz Diorite						
15	GN-89-9004	Melanocratic Qz diorite	5	8	<2	<1
14	GN-89-9006Z	Qz diorite-tonalite	<1	<2	<2	<1

Abbreviations: Ol, olivine; Cpx, clinopyroxene; Hb, hornblende; Plag, plagioclase; Qz, quartz
Detection limits: 1 ppb for Pt and Au; 2 ppb for Pd and Rh. Sample localities are shown on Figure 7.3.

hornblende clinopyroxenite, hornblendite and clinopyroxenite. The pegmatitic gabbros exhibit spectacular comb layering that records *in situ* crystal growth from supersaturated liquids that crystallized within the central part of the intrusion.

The northeastern margin of the complex is fault-bounded and the western and southern margins are bordered by a quartz diorite to tonalite pluton of probable Jurassic age. A small body of granodiorite intrudes the western part of the complex, and other minor intrusive rocks include dikes of microdiorite to microgabbro, felsite, and hornblende plagioclase pegmatite.

The regional metamorphic mineral assemblages within the project area, which is within the eastern facies of the Takla Group west of the Pinchi-Ingenika fault system, indicate middle to upper greenschist facies conditions. However, vestiges of a metamorphic aureole of lower amphibolite grade at the northeastern margin of the complex may have been largely obscured by faulting and retrograde metamorphism.

The abundance of noble metals in representative samples of the mafic and ultramafic lithologies is relatively low and there is no evidence of economic mineralization.

CHAPTER 8 POLARIS COMPLEX

The Polaris ultramafic-mafic complex (56°30′N, 125° 40′W) is situated 10 kilometres northeast of Aiken Lake in the Omineca Mountains (Figure 8.1). It is one of the largest Alaskan-type intrusions in British Columbia, second only to the Tulameen complex (Chapter 9). Access is by dirt road extending some 335 kilometres north from Fort St. James via Manson Creek and Germansen Landing, reaching Aiken Lake via a well-maintained gravel road that leads to the Cheni mine in the Toodogonne River area. Alternatively, the area may be reached by flights from Smithers to the Sturdee airstrip situated approximately 130 kilometres northwest of Aiken Lake, and from there by helicopter. The complex underlies an area of approximately 45 square kilometres at the southern end of the Lay Range and is well exposed above treeline at elevations between 1600 and 2200 metres. It takes its name from Polaris Creek, a tributary of Lay Creek, both of which drain the western margin of the body and flow southwards into the Mesilinka River.

The project area is covered at a scale of 1:250 000 by the Mesilinka map sheet (NTS 94C) and 1:50 000 base maps (94C/5 and 12). Aeromagnetic survey maps are also available in the smaller (Map 7777G-Fort Grahame) and larger (Maps 9074G and 9075G) scales respectively.

REGIONAL GEOLOGY AND GEOCHRONOMETRY

The first systematic geological mapping of the Aiken Lake area was completed by Armstrong (1946), Armstrong and Roots (1948), and Roots (1954). Earlier, Lay (1932) had examined many of the mineral prospects in the region. More recent mapping in the Aiken Lake area and further south has been reported by Ferri *et al.* (1992a, b; 1993a, b). The first

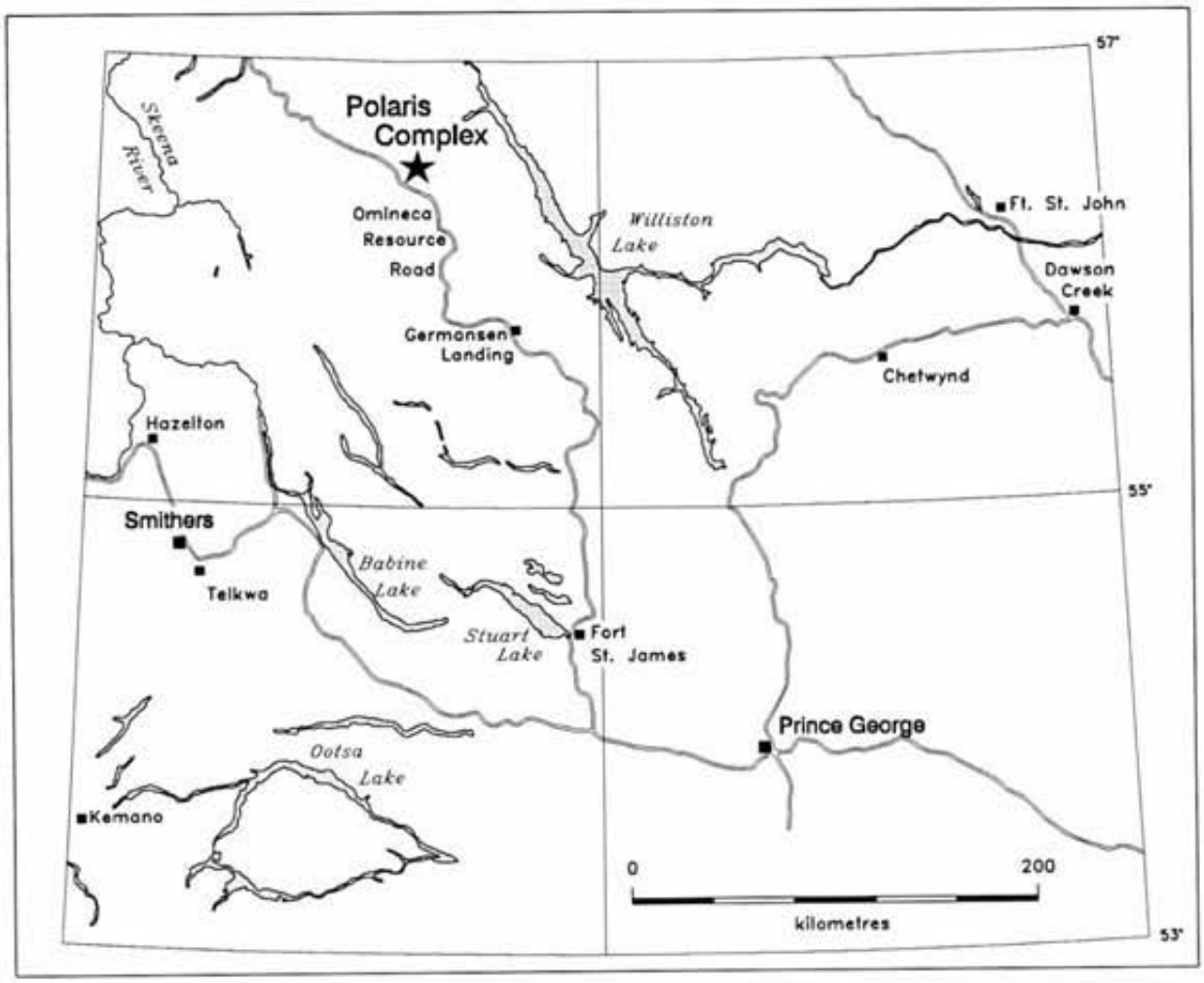

Figure 8.1. Location of the Polaris ultramafic-mafic complex.

detailed observations of the mafic and ultramafic rocks of the Polaris complex were made by Roots (1954). Modern petrologic studies and more detailed mapping of the complex were completed later by Irvine (1974a; 1976) and Foster (1974).

The Polaris complex is the largest of a number of Alaskan-type bodies in the region that intrude Quesnellia (Figure 8.2). It lies at the eastern margin of the Harper Ranch Subterrane of Quesnellia which is separated from Stikinia and Cache Creek Terrane to the west by the Pinchi-Ingenika fault system and bounded to the east by the Swannell Fault (Gabrielse, 1985; Wheeler *et al.*, 1991). The latter fault places variably metamorphosed, Paleozoic to Upper Proterozoic pericratonic rocks of the miogeocline (Cassiar Terrane) in thrust contact with Quesnellia (Mansy and Gabrielse, 1978; Bellefontaine, 1989; Ferri *et al.* 1993a, b)

Mafic and ultramafic rocks of the Polaris complex and smaller satellitic bodies intrude the Lay Range assemblage, a structurally complex sequence of arc-derived, predominantly clastic and volcaniclastic rocks of greenschist or ower grade assemblages (Monger, 1973, 1977; Richards, 1976a, b; Irvine, 1974a) that have been tentatively correlated with the Upper Devonian to Upper Permian Harper Ranch Subterrane considered as basement to Quesnellia (Monger *et al.*, 1991; Wheeler and McFeely, 1991).). Ferri *et al.* (1993a) informally subdivided the stratigraphy of the Lay Range assemblage into a Mississippian(?) to middle Pennsylvanian lower sedimentary division and a Middle Pennsylvanian to Permian upper mafic tuff division. Newly recognized Upper Devonian to Lower Mississippian sedimentary and pyroclastic strata exposed along the eastern margin of the Lay Range form the upper part of a westward-dipping homoclinal succession of Paleozoic strata that have been traced southwards into the informally named Big Creek group (Figure 8.3; Ferri *et al.*, 1992a). The Big Creek group is underlain by a succession of Middle Devonian and older, variably dolomitized carbonates that pass downwards into Lower Cambrian fine-grained siliciclastics, including orthoquartzite, described in detail by Ferri and Melville (1994). The contact between the Big Creek and older Paleozoic and Upper Proterozoic succession appears to be faulted throughout most of the Swannell River area (Figure 8.3).

The age of the Polaris complex is not well established by previous K-Ar determinations. Potassium-argon dates on biotite and hornblende in a "peridotite" yielded Jurassic isotopic ages of 167±9 (2σ) and 156±15 Ma (Wanless *et al.*, 1968). These dates have been considered too young by most workers who have stressed the spatial and petrological associations of Alaskan-type complexes in British Columbia with Upper Triassic to Lower Jurassic Takla-Nicola-Stuhini volcanic rocks of Quesnellia and Stikinia (*e.g.*, Monger, 1973; Irvine, 1974b, 1976; Woodsworth *et al.*, 1991). New U-Pb dates reported below confirm these inferences.

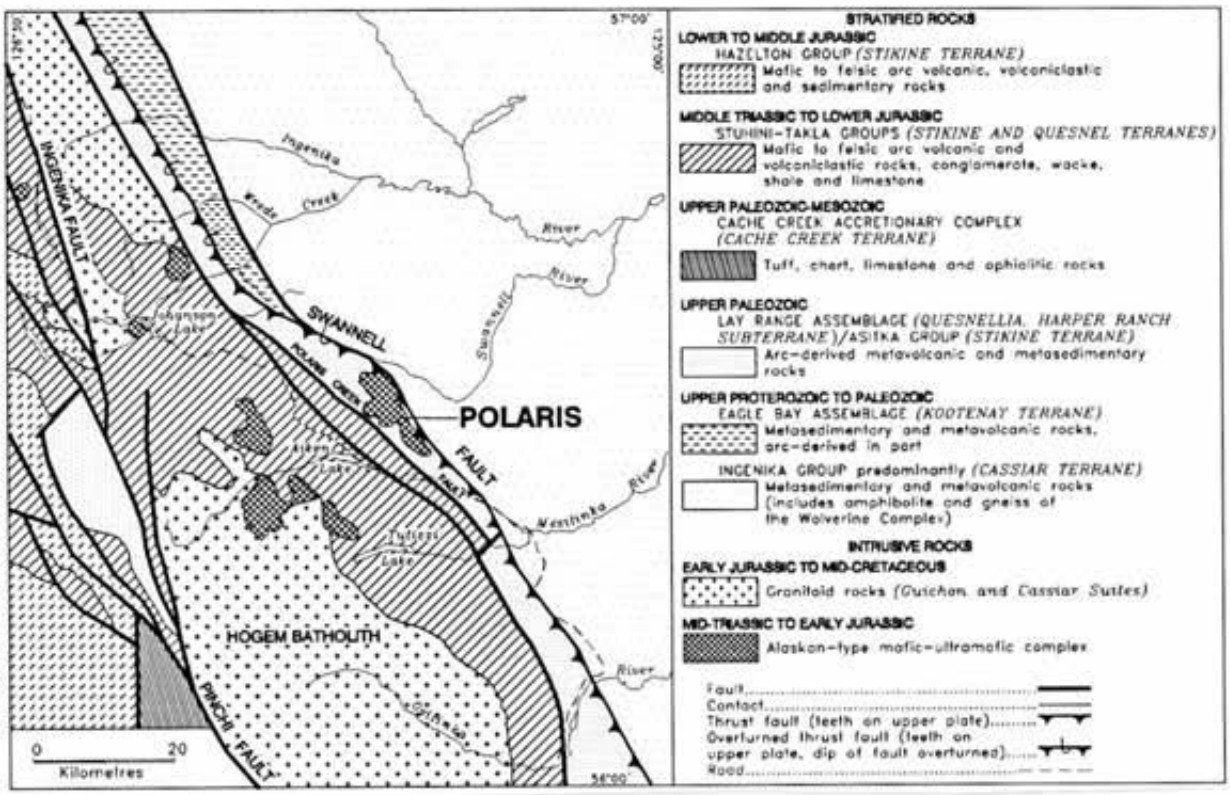

Figure 8.2. Geologic setting of the Polaris ultramafic-mafic complex (modified after Irvine, 1974b; Monger, 1977; and Richards, 1976b).

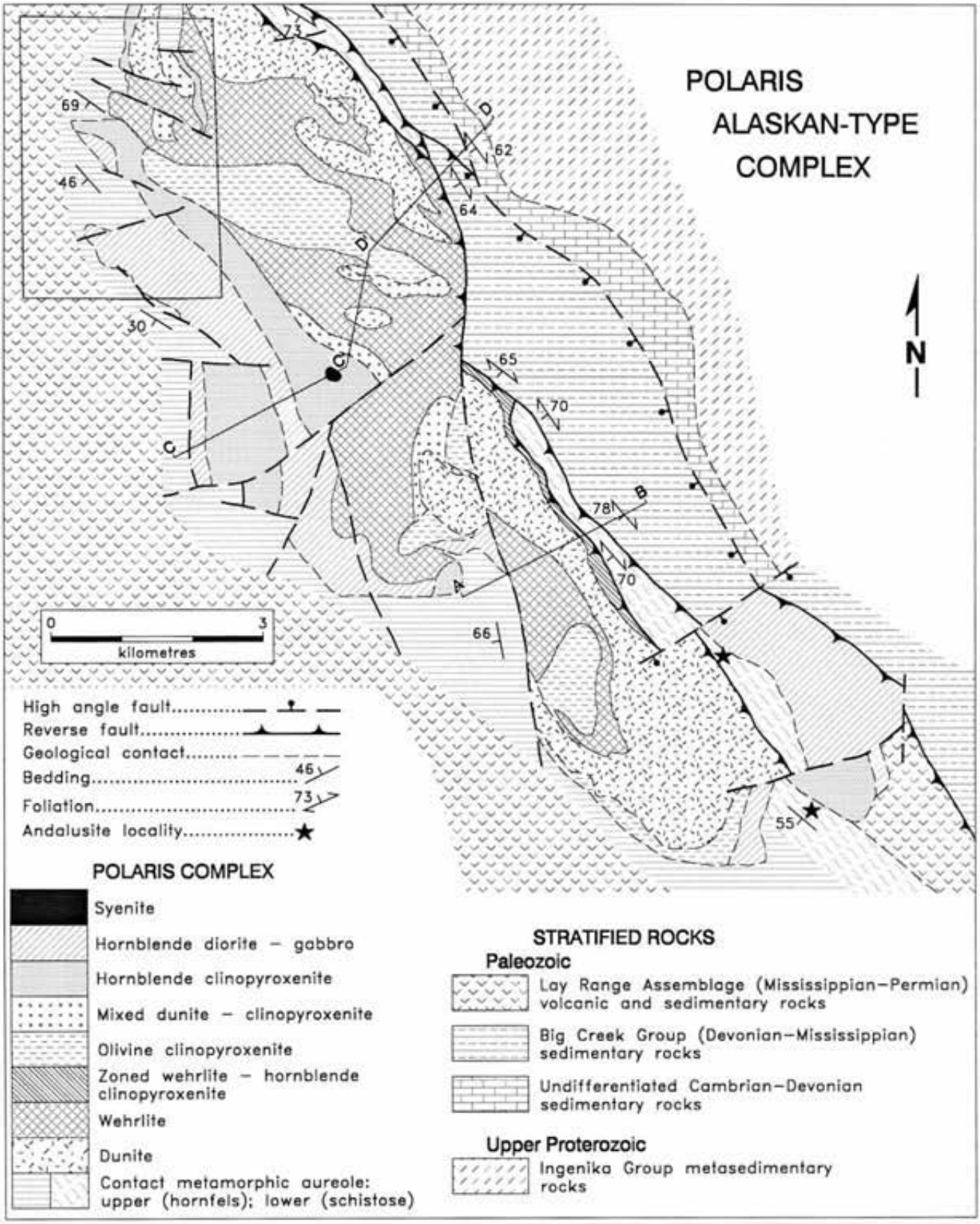

Figure 8.3. Generalized geology of the Polaris ultramafic-mafic complex. A-B and C-C'-D'-D indicate location of cross-sections in Figure 8.4. Inset shows location of Figure 8.5.

COUNTRY ROCKS: LAY RANGE ASSEMBLAGE

Roots (1954) noted that rocks which host the Polaris complex form a westward-dipping (40-50°), westward-facing homoclinal sequence (Maps 3 and 4 in pocket and Figures 8.3 to 8.6). The Lay Range assemblage is entirely fault-bounded and internally composed of a series of northwest-trending fault slices (Monger, 1973) and recumbent, northeasterly verging folds (Ferri *et al.*, 1993a). Northwest of the Polaris complex at the margin of the Lay Range, exposures of the lower sedimentary division comprise fine-grained clastics, chert, heterolithic conglomerate, limestone and lesser rhyolitic tuff and quartzite of probable continental derivation. Carbonates in this package have yielded mid-Pennsylvanian fossils, although younger Paleozoic or lowermost Mesozoic rocks may also be present (Monger, 1973; Monger and Paterson, 1974; Ferri *et al.*, 1993a). The mafic-ultramafic rocks are hosted entirely by the mafic tuff division which comprises mainly mafic to intermediate volcanic breccia and flows, well-bedded crystal and lithic tuff and volcanic wacke, lesser clastic rocks and carbonate, and rare rhyolitic ash-flow tuff. The pyroclastic rocks and tuffaceous sediments are generally feldspathic and locally contain clinopyroxene, hornblende and rare volcanic quartz. The flows are locally pillowed and amygdaloidal, and commonly carry plagioclase and clinopyroxene phenocrysts, not unlike their counterparts in the younger Takla Group.

Lithologies along the western margin of the complex are thickly to thinly bedded argillites, siltstones, sandstones and minor carbonates, lithic-crystal tuffs and massive lava flows. Grey-green thinly bedded or laminated volcanogenic siltstones and fine-grained wackes are well exposed along the western margin of the complex where they form some of the highest peaks. Sedimentary features such as graded bedding, channel scours, load and flame structures, and cross-laminations indicate tops to the west. Locally, the succession contains chocolate-brown mudstones and thin (<0.3 metre thick), lenticular, impure carbonates characterized by brown-weathering rinds. At one locality (77, Figure 8.5), a thin (0 - 4 m), medium grey layer of crystal-rich, nonwelded ash-flow tuff contains rip-up clasts (up to 12 cm in length) of grey-green siltstone that are weakly imbricated and preferentially oriented in the direction of flow. The top of the deposit is reworked and the basal part exhibits normal grading and has scoured underlying siltstones. Thus, it appears to have been emplaced in a subaqueous near-shore environment.

Country rocks exposed at the northeastern margin of the complex include black, fissile argillite and phyllite with interbedded, fine-grained lithic tuff and pale grey carbonate.

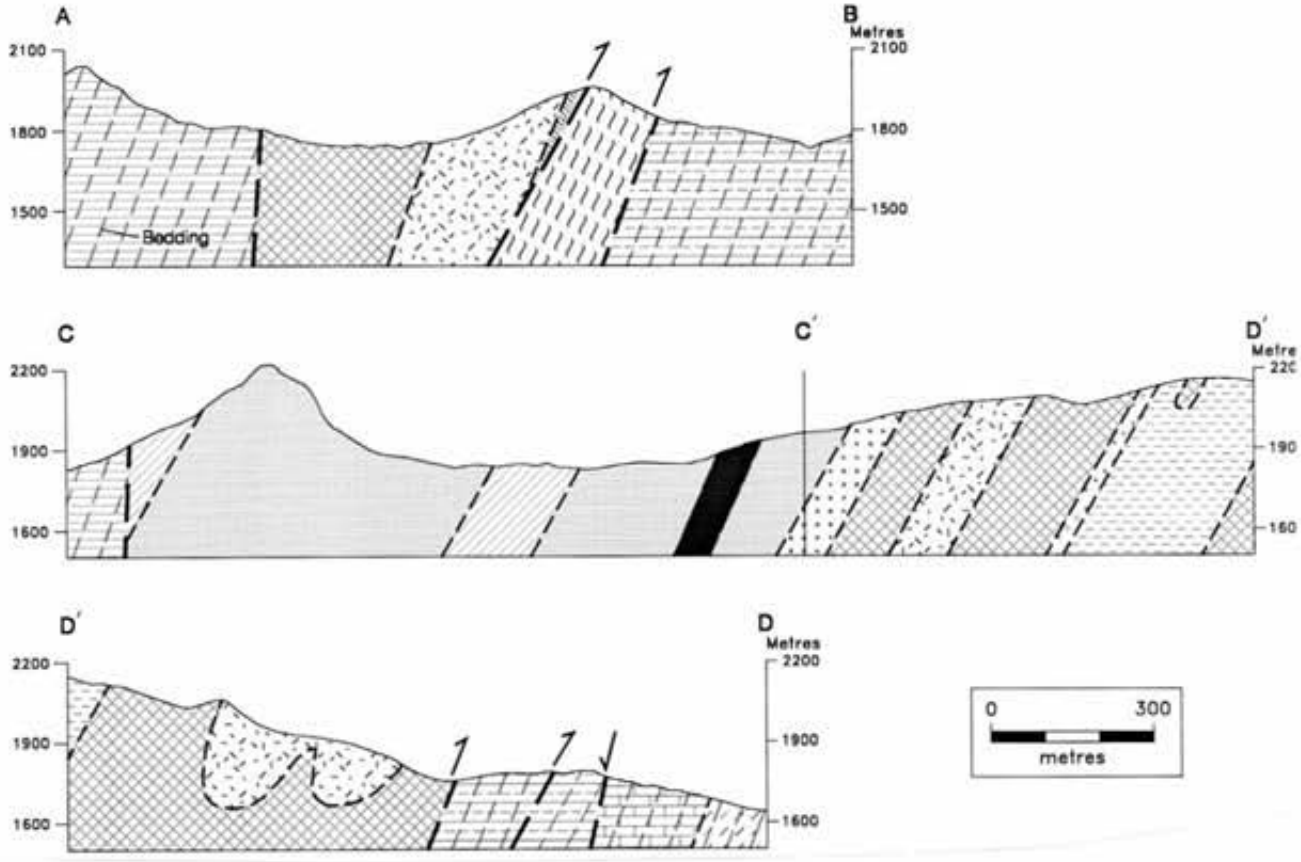

Figure 8.4. Schematic geologic cross-sections of the Polaris complex. *See* Figure 8.3 for locations.

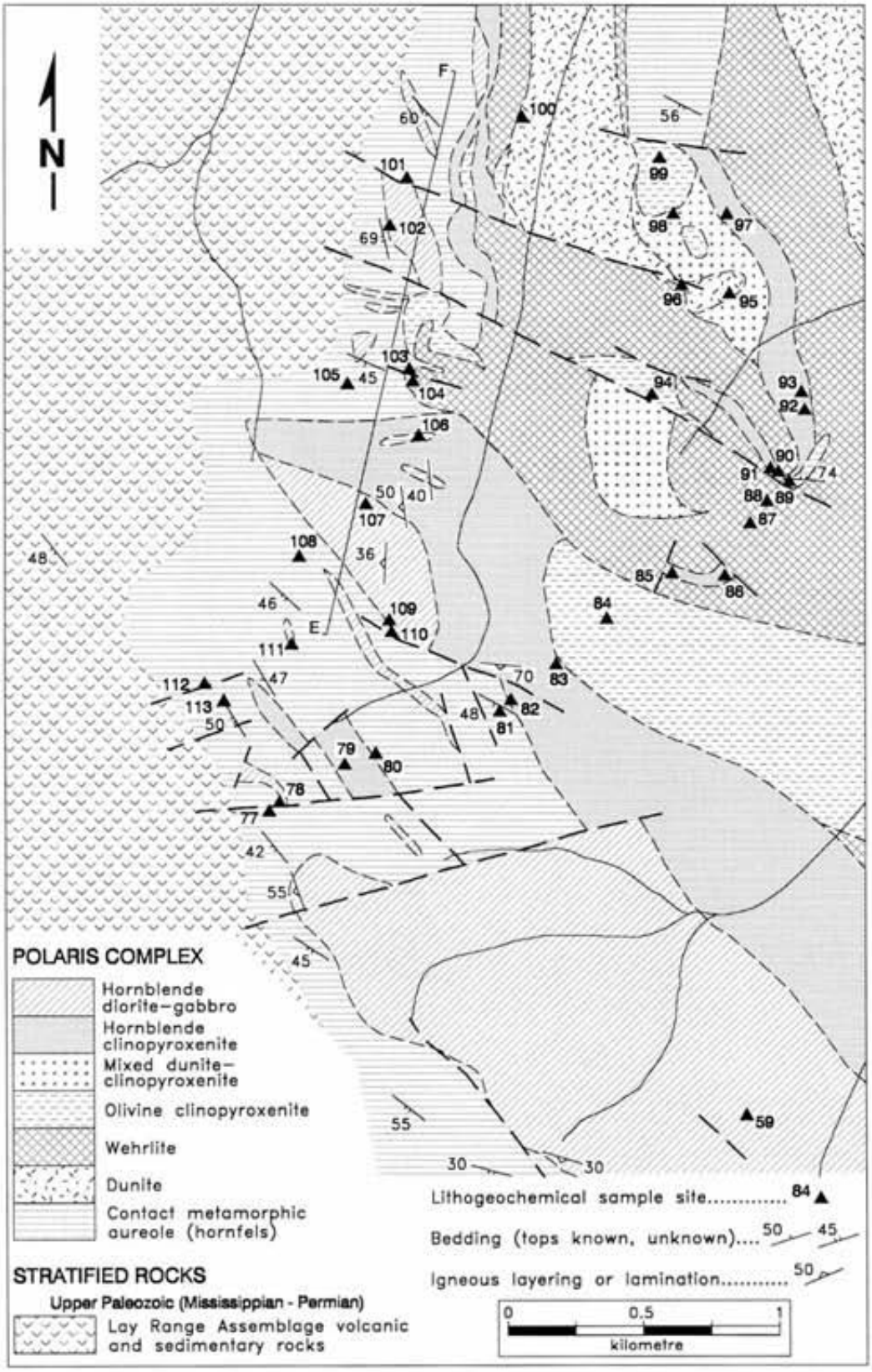

Figure 8.5 Generalized geology of the northwestern terminus of the Polaris complex (inset, Figure 8.3) showing intrusive relationships and geochemical sample sites. E-F is location of cross-section in Figure 8.6. Other symbols as in Figure 8.3.

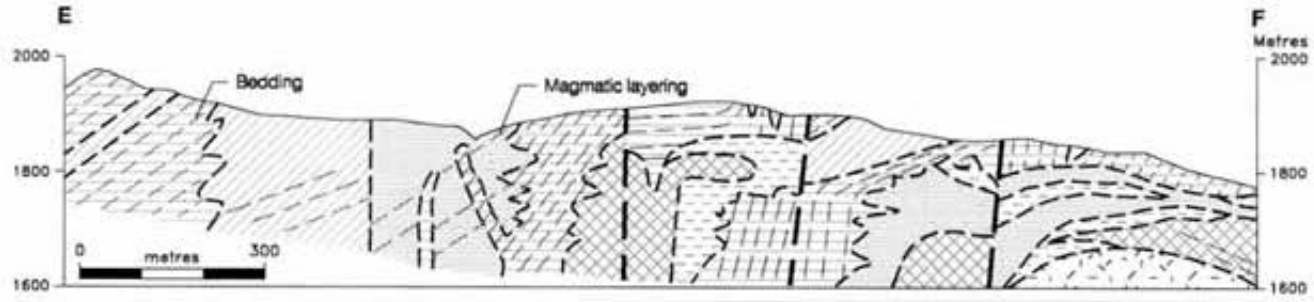

Figure 8.6. Schematic geologic cross-section of intrusive relationships at the northwestern end of the Polaris complex. *See* Figure 8.5 for location.

At the southeastern margin, black phyllite and massive, aphanitic to porphyritic lavas of mafic to intermediate composition lie in sheared contact with serpentinized dunite. The lavas locally enclose concentrations of cognate xenoliths (up to 8 cm across) of hornblende gabbro, hornblendite and feldspathic hornblendite in a hornblende-phyric host. These rocks appear to have hornblende-phyric andesitic counterparts occurring as dikes in Lay Range assemblage strata overlying the intrusion.

POLARIS COMPLEX: ULTRAMAFIC-MAFIC ROCKS

The Polaris ultramafic-mafic complex is an elongate sill-like body 14 kilometres long by 4 kilometres across at its broadest point, and exhibits a well-developed contact metamorphic aureole. Its northwesterly trending elongation is conformable with the regional structural grain. The northern and southern terminations of the body are largely obscured by glacial drift. Farther north in the Lay Range, thin sill-like ultramafic intrusions, presumably coeval with the Polaris complex, were mapped by Roots (1954). However, the complex does not appear to have a large subsurface extension judging from its distinctive aeromagnetic anomaly.

All of the lithologies that characterize Alaskan-type complexes are well represented in the Polaris complex (Figures 8.3 to 8.6). These include dunite, olivine wehrlite and wehrlite, olivine clinopyroxenite and clinopyroxenite, hornblende clinopyroxenite, hornblendite, gabbroic to dioritic rocks, late-stage pegmatites and fine to coarse-grained feldspathic phases. As in many other Alaskan-type complexes in British Columbia, phlogopitic mica appears in early cumulates, including dunite. Ultramafic lithologies are well exposed in the eastern and southern parts of the complex; gabbroic to dioritic hornblende-bearing rocks in the west.

DUNITE

The main mass of dunite forms northwest-trending ridges in the eastern half of the complex, and the floor and walls of a large glacially scoured depression in the south. Dunite weathers tan to pale yellowish brown and forms smooth, blocky outcrops that typically lack a penetrative fabric. Joint planes are commonly coated with pale green to black serpentine that locally appears asbestiform. Fresh surfaces vary from dark greenish grey to black as the degree of serpentinization increases. Complete serpentinization, however, only occurs close to fault zones and, on the whole, olivines are well preserved. In thin section, the dunite is generally medium grained and composed of weakly serpentinized olivines (<3 mm) and minor chromite (1 vol%) that exhibit cumulate textures, accompanied by minor rare cumulus and more common intercumulus phlogopite.

CHROMITITE

Concentrations of chromite are confined to the dunite except for minor occurrences in olivine wehrlite adjacent to dunite (Figure 8.3). Chromitites occur as irregular pods, centimetre-scale schlieren, and millimetre-thick, planar to curved laminae. Schlieren commonly range from 6 to 15 centimetres in length and 0.5 to 4 centimetres in width; laminae can rarely be traced for more than 0.5 metre. Roots (1954) found more extensive chromitite horizons measuring almost 4 metres long by 12 centimetres wide. Locally, coherent angular blocks of laminated chromitite up to 30 centimetres across are found juxtaposed in random orientation (Photo 8.1). In thin section, aggregates of chromite crystals commonly form networks or ring-like structures that partially to completely enclose cumulus olivines. Similar textures were documented by Clark (1978) from another Alaskan-type intrusion, the Turnagain River complex in

Photo 8.1. Disrupted block of layered chromitite in dunite cut by thin dunite dikes.

northern British Columbia. The irregular geometry of podiform chromitites, pinch-and-swell nature of schlieren, and random orientation of layered chromitites are due to remobilization of previously deposited chromite-rich cumulates early in the crystallization history of the intrusion.

OLIVINE WEHRLITE AND WEHRLITE

Extensive outcrops of wehrlitic rocks are found in the northern and central parts of the complex and prompted subdivision into mappable units of olivine wehrlite (90 - 65 vol% olivine, 10 - 35 vol% clinopyroxene) and wehrlite (65 - 40 vol% olivine, 35 - 60 vol% clinopyroxene; Figure 1.2). Wehrlitic lithologies weather pale brown to medium reddish brown and are massive to well jointed and weakly serpentinized; fresh surfaces are grey-green. These rocks commonly have a knobby texture due to recessive weathering of olivine relative to clinopyroxene. In places, anhedral to subhedral megacrystic clinopyroxenes (up to 8 cm across) with well-developed poikilitic textures impart a distinctive lustre mottling to the outcrop (Photo 8.2). Olivines typically occur as cumulus crystals whereas clinopyroxenes exhibit intercumulus and cumulus textures. These primary silicates are accompanied by accessory chrome spinel and trace amounts of phlogopite. Rarely, wehrlitic mineralogy appears to have formed by infiltration of clinopyroxene-rich magmas into an olivine-rich host, resulting in the formation of anastomosing three-dimensional networks of coarse-grained clinopyroxenite in the hostrock (Photo 8.3).

OLIVINE CLINOPYROXENITE AND CLINOPYROXENITE

Outcrops of olivine clinopyroxenite and clinopyroxenite are widely distributed throughout the ultramafic portion of the intrusion. Weathered surfaces are pale green to pale greyish green where enriched in clinopyroxene; olivine-rich areas appear rusty brown. The rocks are usually medium to coarse grained (3 to 10 mm) and grey-green on fresh surfaces. In pegmatitic zones, clinopyroxenes reach 8 centimetres in length and are rarely poikilitic. Locally, these zones contain olivine-rich areas or inclusions of wehrlite (<20 cm across) that are eratically distributed and mottle the outcrop with rusty brown patches. In thin section, euhedral to subhedral clinopyroxenes are commonly schillered and have inequigranular textures; most olivines appear subhedral and have cumulus or intercumulus textures. Phlogopite usually occurs as an accessory phase. Opaque oxides are notably reduced in abundance in olivine clinopyroxenites, and appear to be absent altogether in clinopyroxenites.

MIXED WEHRLITIC-PYROXENITIC UNITS

Mappable zones of intermixed olivine clinopyroxenite to clinopyroxenite and wehrlite to olivine wehrlite (and rarely dunite) are found locally near the margins of clinopyroxenite or wehrlitic bodies. They are particularly well developed in the central and northern parts of the intrusion (Figures 8.3 and 8.5). Contacts between the rock types are generally sharp. The most common type of mixed unit comprises a chaotic assemblage of angular to subangular blocks of clinopyroxenite, ranging from less than a metre to tens of metres in size, enclosed in an olivine-rich host. This texture appears to have originated either by intrusion of clinopyroxenite magma into a semiconsolidated host, or by remobilization of zones of clinopyroxenite dike injection. Another type of mixed zone is formed by concentrations of randomly oriented wehrlitic dikes cutting clinopyroxenite. The occurrence of mixed olivine-rich and pyroxenitic lithologies is also seen in the Lunar Creek and Tulameen complexes (Chapters 4 and 9) where they appear to have formed, in part at least, by slumping of coherent masses of dunite or clinopyroxenite cumulates that were plastically deformed during redeposition at lower levels in the magma chamber.

HORNBLENDE CLINOPYROXENITE AND HORNBLENDITE

This map unit comprises a gradation of rock types from hornblende clinopyroxenite through clinopyroxene hornblendite to hornblendite and feldspathic hornblendite. These hornblende-bearing ultramafic rocks are almost entirely restricted to the upper part of the complex where they are closely associated with gabbroic to dioritic rocks. Hornblende clinopyroxenite occurs as a pale green to brownish green weathering, medium to coarse-grained rock studded with black hornblende crystals. It contains cumulus clinopyroxene, cumulus or intercumulus hornblende, locally abun-

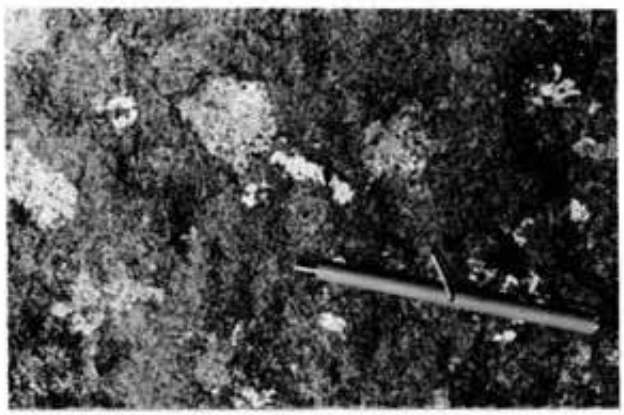

Photo 8.2. Megacrystic wehrlite exhibiting lustre mottling caused by subhedral poikilitic clinopyroxene. Magnet is 11 centimetres long. Photo by C. Nuttall.

Photo 8.3. Wehrlite formed by net veining of dunite near contact of clinopyroxenite and dunite bodies.

dant cumulus magnetite, accessory biotite and apatite, and intercumulus plagioclase appears in feldspathic variants. Hornblendite exhibits a black, coarse-grained to pegmatitic texture with crystals reaching 8 centimetres in length. Locally, the rock has a rudimentary lineation, or a marked lamination of prismatic hornblende crystals with no directional fabric. A thin sill of megacrystic hornblende clinopyroxenite that intrudes roof rocks at the northwestern margin of the complex (Figure 8.5) locally displays well-developed centimetre-scale layering of cumulus subequant hornblende and clinopyroxene. Olivine-bearing hornblende clinopyroxenites are comparatively rare. One such unit occupies a narrow transition zone between dunite-wehrlite and hornblende clinopyroxenite at the zoned eastern margin of the complex (Figure 8.4, cross-section A-B) and is distinguished by relatively abundant phlogopitic mica (5 vol%).

GABBROIC TO DIORITIC ROCKS

The feldspathic rocks comprise hornblende±clinopyroxene gabbros and/or diorites. They are restricted to the margins of the complex and are most voluminous near the roof. They also form thin sills penetrating metasedimentary rocks of the Lay Range assemblage. Outcrops are typically lichen covered and dark grey weathering; fresh surfaces are medium grey to greenish grey depending on the degree of saussuritization of the feldspars. The rocks are usually massive, medium grained and equigranular. Centimetre-scale modal layering formed by alternating amphibole and plagioclase-rich horizons is observed locally and, near the contacts at least, is usually concordant with the attitude of bedding in the hostrocks. In thin section, the gabbroic to dioritic rocks are composed of cumulus hornblende and rare clinopyroxene, cumulus to intercumulus plagioclase, accessory iron-titanium oxides, apatite and biotite, and sporadic secondary pyrite (<2 vol%).

Sills intruding the Lay Range assemblage have fine-grained chilled margins with crude columnar jointing, and may grade from medium-grained hornblende gabbro-diorite in the interior to hornblende porphyry at the contact.

DIKES AND VEINS

Dikes and veins of various ultramafic lithologies and syenite to leucomonzonite composition are widespread in the Polaris complex. There appears to be no systematic orientation to the pattern of dike intrusion. In large part, these dikes reflect the nature of, and temporal relationships between, major lithologic units.

Among the ultramafic rock types, centimetre to metre-wide dikes of olivine clinopyroxenite and clinopyroxenite are most common, and are found cutting dunite, olivine wehrlite and wehrlite (Photo 8.4). Dunite dikes, typically several centimetres in width, are only conspicuous where they penetrate chromitites (Photo 8.1); thin olivine wehrlite to wehrlite dikes less than 0.5 metre wide transect dunite, wehrlitic and pyroxenitic units. The latter dikes have local concentrations of clinopyroxene crystals at their margins, a feature also documented at the Turnagain complex (Clark, 1975). Thin (1 - 20 cm in width), medium to coarse-grained hornblendite to feldspathic hornblendite dikes have been observed cutting dunite, olivine clinopyroxenite, gabbro-diorite and metasedimentary strata of the Lay Range assemblage.

Leucocratic phases ranging from fine-grained, millimetre-wide feldspathic veinlets to pegmatitic hornblende-biotite-feldspar±quartz veins and segregation pods several centimetres across are common within the gabbroic rocks and adjacent ultramafic units. In a ridge traverse along section D'-C' (Figures 8.3 and 8.4), leucocratic dikes make their first appearance in dunite and wehrlitic lithologies and increase in abundance southward toward the gabbro-diorite units. Composite dikes in the ultramafic rocks locally exhibit hornblendite margins and quartzofeldspathic cores. Pegmatitic hornblende-feldspar-quartz segregation pods that formed by ponding of residual liquids are also common in hornblende clinopyroxenites near the roof of the intrusion (Photo 8.5). The occurrence of silica-oversaturated differentiates in the Polaris complex, particularly near the roof of the intrusion, may indicate late-stage contamination by siliceous wallrocks.

The overall sequence of dike intrusion, namely dunite, wehrlite, clinopyroxenite, hornblendite, gabbro-diorite and leucocratic residua, reflects the gross internal stratigraphy and general order of crystallization of major lithologic units

Photo 8.4. Bifurcating wehrlite and clinopyroxenite dikes in dunite. Note thin offshoot of clinopyroxenite dike cutting wehrlite at left of hammer handle.

Photo 8.5. Pegmatitic hornblende-feldspar segregation pod in hornblende clinopyroxenite.

in the complex. Locally ambivalent crosscutting relationships, such as those observed between olivine clinopyroxenite-clinopyroxenite and wehrlitic dikes, and hornblendite and gabbro-diorite, point to multiple intrusive events when magmas of a limited range of composition coexisted.

CONTACT RELATIONS AND INTRUSION GEOMETRY

Steep contacts, rudimentary internal zoning and the preservation of apparently up-domed "roof" rocks at the northwestern end of the complex have previously been used to support a stock-like geometry for the intrusion (Roots, 1954; Irvine, 1974b; Foster, 1974). Detailed examination of contact relationships in the north confirms these crosscutting relationships (Figures 8.5 and 8.6). However, the elongate shape of the complex, the nature of the western margin of the body where intrusive contacts are conformable with the strike and dip of metasedimentary hostrocks, the steep westward dip of zoned units at the eastern margin of the intrusion (Figure 8.4) and the asymetrical nature of the zoning, all indicate that the Polaris complex is a high-level sill-like intrusion. Postemplacement deformation has tilted the sill on end such that rocks forming the "roof" zone of earlier workers in fact are wallrocks at the transgressive northern contact of the sill. Swarms of small gabbroic to pyroxenitic sills that intrude the roof zone to the west mimic the geometry of the larger intrusion.

INTERNAL STRATIGRAPHY

In general, the gross internal distribution of rock types is systematically disposed about the margins of the intrusion. Dunite and olivine-bearing pyroxenitic rocks are concentrated near the base of the intrusion whereas hornblende-bearing pyroxenites and gabbro-diorite are well developed near the roof. In the east-central part of the intrusion, the base of the complex is progressively zoned downwards from dunite through wehrlitic and olivine clinopyroxenite to phlogopite-bearing olivine-hornblende clinopyroxenite (Figure 8.4). Contact relationships between the major lithologic units are sharp to gradational.

MECHANISM OF EMPLACEMENT

Irvine (1974a; 1976) was struck by the internal zoning (albeit complex) and evidence for disruption of layered chromitites and clinopyroxenites by olivine-rich lithologies. He suggested that these features could be most satisfactorily explained by diapiric re-emplacement of hot, thickly stratified, olivine-rich cumulates in a semi-solid state during regional tectonism. We have difficulty with this hypothesis for a number of reasons. In the first place, sharp undeformed intrusive contacts have been identified at the base and roof of the sill. Also, relationships among the wehrlitic and pyroxenitic lithologies (*i.e.*, mixed units) are locally quite complex and record a history of multiple intrusive events. As indicated earlier, the chaotic nature of mixed ultramafic lithologies and remobilized chromitite horizons can be explained adequately by periodic, syndepositional mass wasting of cumulates to lower levels in the magma chamber, events perhaps triggered by earthquakes and episodic magma recharge. Furthermore, we have found no evidence for injection of dunite and wehrlitic lithologies into gabbroic and hornblende-rich rocks which might be expected in Irvine's model. Rather, intrusive relationships dictate the reverse. Also we note the general asymmetry in the development of internal zoning; the widespread preservation of cumulate textures as opposed to tectonite fabrics; and the general lack of penetrative fabrics both within and near the margins of the body, except where faulted. Moreover, why a high-density mass of olivine-pyroxene cumulates would migrate "diapirically" to significantly higher levels in the crust rather than sink to the crust-mantle boundary in order to achieve isostatic compensation is not adequately explained. It is apparent from the mapping that the internal stratigraphy of cumulates developed *in situ* (*i.e.*, with respect to adjacent hostrocks) and represent the crystallization products of a magma chamber in the upper crust.

CONTACT AUREOLE

A contact aureole of amphibolite grade is well developed in volcanic and sedimentary rocks at the margin of the intrusion. The maximum width of the metamorphic aureole is not accurately known, but has been estimated to extend 50 to 150 metres away from the contact (Irvine, 1974b). The extent of hornfelsed rocks may be much greater than this, especially in the south (Roots, 1954).

In the north, metasedimentary rocks adjacent to the roof and margins of the complex have been recrystallized to an assemblage of hornblende, plagioclase and quartz±biotite±potassium feldspar. Large rafts and pendants of hornfelsed metasediments with well preserved bedding are locally conspicuous (*e.g.*, Figure 8.6). These amphibolitic rocks exhibit no penetrative schistosity except adjacent to faults. Their finer grain size and preservation of relict stratification generally serves to distinguish these amphibolites from coarser grained gabbro-diorite and hornblende-rich ultramafic rocks of the intrusion.

A narrow contact aureole developed in metavolcanic and metadsedimentary rocks has been mapped at the base of the intrusion (Figures 8.3 and 8.4). A pronounced mineral foliation is defined by amphibole and plagioclase±biotite±quartz that crystallized under amphibolite-grade conditions. Metasedimentary rocks underlying the amphibolitic contact aureole at the northeastern margin of the complex (Section D'-D, Figure 8.4), exhibit a single, well-developed schistosity that is conformable with fabrics in the aureole. This foliation is defined in thin section by biotite, muscovite, chlorite, quartz, plagioclase and minor carbonate. This mineral assemblage formed during mid-greenschist facies metamorphism. Thus, the grade of metamorphism appears to increase systematically towards the sheared ultramafic contact.

Ductile fault zones with mylonitic textures locally crosscut the footwall rocks and may exhibit pronounced mineral lineations plunging steeply (60 to 70°) downdip to the northwest. In thin section, the mylonitic fabric is defined by amphibole, plagioclase, quartz, epidote, carbonate and chlorite (retrograde?). Movement appears to have taken

place under upper greenschist to lowermost amphibolite-grade conditions.

Oriented specimens were collected from metavolcanic and metasedimentary rocks structurally below the basal fault in the central part of the complex (1 to 2 km north of Section A-B, Figure 8.4). The C/S fabrics and shear bands observed in outcrop are defined in thin section by chlorite and biotite, and quartz and plagioclase have been dynamically recrystallized into subgrains. These textures indicate that mylonitization was taking place during middle greenschist facies metamorphism. Kinematic indicators reveal that the hangingwall moved upward along southwest-dipping thrust planes. Mineral lineations plunging 65° to the northwest at the site of the C/S fabrics suggest that thrust movement, if parallel to the stretching lineation, was toward the southeast.

At the southeastern extremity of the complex, the basal fault zone places serpentinized dunite in fault contact with black carbonaceous schists containing porphyroblasts of andalusite (chiastolite) up to 3 millimetres across (Figure 8.3). Growth of andalusite formed in response to contact metamorphism. However, andalusite porphyroblasts have been ductily deformed, indicating that motion in the shear zone occurred during or after their growth. A second andalusite locality exhibiting similar textures occurs just beyond the southern tip of the intrusion (Figure 8.3). Andesitic lavas structurally underlying these carbonaceous phyllites lack a penetrative fabric but have undergone recrystallization of hornblende phenocrysts and groundmass consistent with lowermost amphibolite-grade metamorphism.

MINOR INTRUSIONS

Intrusions that have uncertain relationships with the Polaris complex include a sill-like hornblende diorite body at the northwestern edge of the map area (Figure 8.5), a syenitic intrusion in the central part of the complex (Figure 8.3), and mafic dikes cutting metasedimentary rocks of the Lay Range assemblage. The dioritic body is a grey-brown weathering, fine to medium-grained rock, locally epidotized, with crystals of hornblende, plagioclase and minor potassium feldspar. The syenitic intrusion is a cream-weathering, greyish white coarse-grained rock comprising alkali feldspar (perthitic), minor hornblende, clinopyroxene and sphene, and trace amounts of biotite. It is considered probable that the syenitic intrusions are felsic differentiates of the Polaris complex derived from liquids that did not experience wallrock contamination. The dikes are dark greenish grey on weathered and fresh surfaces, and generally less than 2 metres wide, although they locally swell to over 14 metres across. The thicker dikes have aphanitic chilled margins and hornblende-phyric interiors with up to 15 vol% phenocrysts. They are partly controlled by easterly oriented fault zones and are largely undeformed, appearing to postdate fault movement.

U-Pb GEOCHRONOMETRY

Uranium-lead analyses of zircons from the Polaris complex were done by Heaman in the Geochronology Laboratory at the Royal Ontario Museum. The zircons were separated from a quartz-hornblende-plagioclase pegmatite pod within hornblendite at the northwestern margin of the complex. Results are presented in Table 8.1 and Figure 8.7, and analytical techniques are summarized in Appendix B.

Zircons from the pegmatite are quite uniform in appearance, comprising colourless fragments and prisms that tend to be quite large (100 μm). The zircon grains analyzed have

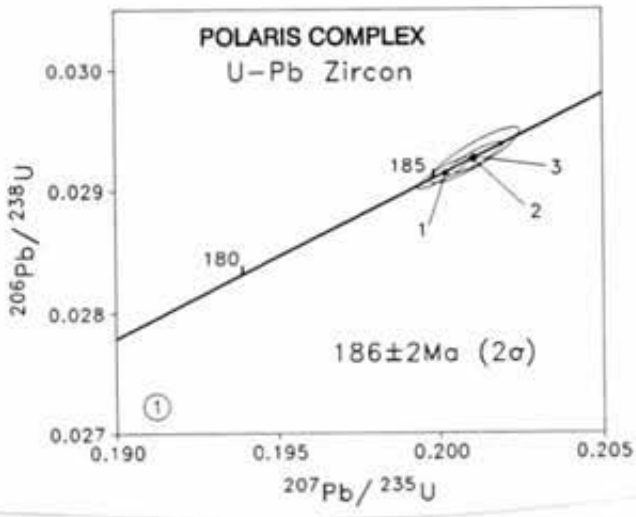

Figure 8.7. U-Pb concordia diagram for zircon in pegmatite from the Polaris complex.

TABLE 8.1
U-Pb ZIRCON RESULTS FOR THE POLARIS COMPLEX

Description	Weight	Concentration		Weight	Atomic Ratios**					Apparent Age (Ma)		
Sample Number *Fraction	Sample (ug)	U (ppm)	Pb (ppm)	Common Pb(pg)	206Pb/204Pb	208Pb/206Pb	206Pb/238U	207Pb/235U	207Pb/206Pb	206Pb/238U	207Pb/235U	207Pb/206Pb
GN89-6182Z												
1M, a, cl, ab, (61)	296	846	27	76	6500	0.2065	0.0292	0.2003	0.04978	186	185	185
2M, a, cl, ab, (90)	206	817	26	6	72, 092	0.2111	0.0292	0.2009	0.04986	186	186	188
3NM, a, cl, ab, (27)	129	795	25	5	>90, 000	0.1942	0.0293	0.2012	0.04986	186	186	188

Magnetic susceptibility: N, M=non-magnetic and magnetic at zero angle of side tilt on a Frantz isodynamic separator at a current of 1.0A and 10° forward tilt. Grain size (mesh): a=+100;Colour:cl=colourless, y=yellow;ab=abrasion treatment.

The numbers in parentheses correspond to the total number of grains analyzed.

***Atomic ratios corrected for blank (Pb=5pg; U=2pg) and intial common Pb.*

relatively high uranium contents (750 ppm). The results for three fractions (#1-3 in Table 8.1 and Figure 8.7) indicate a tight clustering of the data at 186±2 (2σ) Ma (late Early Jurassic or early Toarcian on the time scale of Harland *et al.*, 1990). This date is considered the best estimate for the zircon crystallization age since for samples this young, the $^{206}Pb/^{238}U$ ages are generally more precise and accurate. The U-Pb isotopic age of this pegmatite represents the final stages of solidification of the Polaris complex. The tectonic significance of the zircon dating is discussed in Chapter 11.

STRUCTURE AND METAMORPHISM

The Polaris complex is contained within a northwest-trending, southwest-facing and southwest-dipping homocline that represents a fault-bounded slice of Lay Range assemblage rocks (Harper Ranch Subterrane). High-angle, northwest-trending faults are well exposed in the northern and eastern parts of the map area. They are commonly marked by schistose zones, crush breccias and quartz-carbonate alteration, and cut both the Polaris complex and its hostrocks. Most of these faults have displacements of unknown sense and magnitude.

Roofrocks and wallrocks at the ends of the sill, lack a penetrative foliation. However, country rocks structurally beneath the complex, especially those adjacent to the basal ductile fault zone, are generally highly schistose or mylonitic. The increase in metamorphic grade towards the ultramafic contact, the presence of the regional foliation within the aureole, and the textural evidence for the localized development of mylonitic fabrics under amphibolite-grade conditions indicate that deformation occurred while the intrusion was still hot. Kinematic fabrics indicate that the Polaris complex has been transported tectonically, together with its adjacent wallrocks, as an allochthonous thrust slice emplaced eastwards onto the miogeoclinal margin of ancestral North America.

The eastward-verging structures in the Lay Range documented above and previously by Monger (1973) have counterparts in the Ingenika Group west of the Swannell fault, where they are represented by an early set of northwest-plunging, northeast-verging, tight to isoclinal folds (Bellefontaine, 1989). The Swannell fault is a later, northeast-dipping, southwest-verging, imbricate thrust zone with associated drag folds that emplaced variably metamorphosed miogeoclinal rocks on Quesnellia (Bellefontaine, 1989). The timing and significance of regional deformation and metamorphism are examined in Chapter 11.

ALTERATION AND MINERALIZATION

Fault zones in the Polaris complex and Lay Range assemblage are commonly affected by quartz-carbonate alteration and weather to a bright orange-brown rock locally enriched in limonite, hematite, goethite and sulphides (largely pyrite). Alteration of this type develops in faults of every orientation in every lithology, but appears best developed in northwesterly and easterly trending fault zones. In addition to quartz and ferrodolomite, Irvine (1974a) notes the presence of vesuvianite, and Roots (1954) records ankerite and mariposite. Sparse quantities of asbestiform serpentine are restricted to joint surfaces and faults.

The Polaris complex is notably devoid of sulphide mineralization. The only sulphides of note are exposed in several small reddish brown weathering outcrops of pyroxenitic rocks in the central part of the complex (Locality 43 in Figure 8.8). Here, net-textured primary sulphides, largely pyrrhotite, form immiscible blebs (up to 25 vol%) in a medium-grained clinopyroxenite. Disseminated secondary pyrite occurs locally in hornblende-rich ultramafic rocks and gabbro-diorite in amounts up to 2 vol%.

Chromitite is surprisingly sparse for the apparent size of the dunite mass. For example, in the Tulameen complex, which is a larger body but has a lower proportion of exposed dunite, chromitite is much more abundant. Likewise, the Wrede Creek complex appears to have more chromitite per square kilometre of exposed dunite than the Polaris intrusion. In both of the latter Alaskan-type bodies, PGE are associated with chromitite. Evidently, the apparent size of the dunite body is no guide to its chromite or PGE potential (Chapter 10). Magnetite is confined to the hornblende-bearing ultramafic and gabbroic to dioritic lithologies, but rarely exceeds 5 to 10 vol% of the rock and is of no economic significance.

GEOCHEMISTRY

Analytical results for gold, PGE and other elements in over 130 representative samples of the Polaris complex and its hostrocks are presented in Table 8.2. Sample localities are shown in Figures 8.5 and 8.8. Three different analytical methods were used in two independent laboratories: inductively coupled plasma (ICP) mass spectrometry, Acme Analytical Laboratories, Vancouver; instrumental neutron activation analysis (INAA), Institut National de la Récherche Scientifique, Université du Québec; and inductively coupled plasma emission spectrometry, also Acme Analytical Laboratories. Accuracy was checked by international and in-house standards, and analytical precision (and any nugget effect) monitored by hidden duplicates and internal standards. All samples were preconcentrated by fire assay from 30-gram (ICP) or 50-gram (INAA) splits of 200 grams of rock powder (-200 mesh).

Additional elements analyzed include sulphur, nickel, chromium, arsenic and antimony. Sulphur is generally low in abundance, and reaches a maximum value of 4.2 wt% in a clinopyroxenite (Locality 43, Table 8.2 and Figure 8.8) that contains net-textured sulphides and has weakly anomalous abundances of platinum and palladium. The only other sulphur-rich samples of note (<1 wt% sulphur) are gabbro-diorite and metasedimentary rocks which contain secondary pyrite and exhibit no enrichment in the noble metals. Nickel and chromium have relatively high abundances in ultramafic rocks, but the latter element is particularly sensitive to the abundance of chromite in olivine-rich rocks. The highest chromium abundances are in chip samples of high-grade chromitite; the chromitiferous dunites are represented by composite samples of small chromitite schlieren and host dunite. Thus, if the PGE are preferentially concentrated in chromitite, as in the case of the Tulameen complex (St.

TABLE 8.2
ABUNDANCES OF NOBLE METALS AND OTHER ELEMENTS
IN THE POLARIS COMPLEX AND ASSOCIATED ROCKS

Locality	Sample	Anal. Method	S wt %	Ni ppm	Cr ppm	As ppm	Sb ppm	Pt ppb	Pd ppb	Rh ppb	Ru ppb	Re ppb	Ir ppb	Os ppb	Au ppb
POLARIS COMPLEX															
Chromitite and Chromitiferous Dunite															
62	GN-88-1032	1	-	-	-	-	-	<1	<2	<2	-	-	-	-	<1.0
62	GN-88-1032	2	<0.02	1500	257955	<1.0	<0.20	<5	<5	7	<10	<5	8.70	4.8	<1.0
66	GN-88-1039	1	-	-	-	-	-	49	5	<2	-	-	-	-	<1.0
66	GN-88-1039	2	<0.02	2036	102308	<1.0	<0.20	121	<5	16	24	<5	33.00	18.0	<1.0
68	GN-88-1053	1	-	-	-	-	-	<1	<2	<2	-	-	-	-	<1.0
68	GN-88-1053	1*	-	-	-	-	-	<1	<2	3	-	-	-	-	<1.0
68	GN-88-1053	2	<0.02	1929	75107	<1.0	<0.20	<5	<5	6	10	<5	4.50	<3.0	<1.0
71	GN-88-1055B	1	-	-	-	-	-	28	<2	<2	-	-	-	-	<1.0
71	GN-88-1055B	1*-	-	-	-	-	-	72	5	<2	-	-	-	-	<1.0
71	GN-88-1055B	2	<0.02	1870	64710	<1.0	<0.20	75	<5	19	45	<5	88.00	51.0	<1.0
76	GN-88-1058A	1	-	-	-	-	-	<1	<2	<2	-	-	-	-	2.0
76	GN-88-1058A	1*	-	-	-	-	-	2	<2	<2	-	-	-	-	<1.0
76	GN-88-1058A	2	<0.02	2036	49612	<1.0	<0.20	<5	<5	3	31	<5	3.30	<3.0	<1.0
76	GN-88-1058B	1	-	-	-	-	-	2	<2	<2	-	-	-	-	<1.0
76	GN-88-1058B	2	<0.02	2322	39182	<1.0	<0.20	<5	<5	4	<10	<5	2.20	<3.0	<1.0
25	GN-88-1074	1	-	-	-	-	-	72	<2	<2	-	-	-	-	<1.0
25	GN-88-1074	2	<0.02	2331	58402	<1.0	0.37	-	-	-	-	-	-	-	<1.0
22	GN-88-1089	1	-	-	-	-	-	50	<2	<2	-	-	-	-	<1.0
22	GN-88-1089	2	<0.02	1641	75803	<1.0	<0.20	735	<5	24	32	<5	43.00	19.0	<1.0
63	GN-88-1031	1	-	-	-	-	-	<1	<2	<2	-	-	-	-	<1.0
63	GN-88-1031	2	<0.02	1660	155744	<1.0	<0.20	<10	<5	7	24	6	5.40	<3.0	<1.0
69	GN-88-1052	1	-	-	-	-	-	<1	<2	<2	-	-	-	-	<1.0
69	GN-88-1052	2	<0.02	2080	135880	<1.0	<0.20	<10	<5	5	<5	<5	9.30	6.0	<1.0
36	GN-88-1069B	1	-	-	-	-	-	5	5	<2	-	-	-	-	<1.0
36	GN-88-1069B	1*	-	-	-	-	-	3	6	<2	-	-	-	-	2.0
36	GN-88-1069B	2	<0.02	2176	27235	<1.0	<0.20	<5	<5	2	<10	<5	3.90	<3.0	<1.0
24	GN-88-1092	1	-	-	-	-	-	4	<2	<2	-	-	-	-	<1.0
24	GN-88-1092	2	<0.02	1896	29311	<1.0	<0.20	<5	<5	5	<15	<5	4.50	<3.0	<1.0
61	GN-88-2050	1	-	-	-	-	-	<1	4	<2	-	-	-	-	<1.0
61	GN-88-2050	2	<0.02	2024	224571	<5.0	<0.30	<10	<5	9	16	<5	10.00	5.0	<1.0
37	GN-88-2072	1	-	-	-	-	-	<1	3	<2	-	-	-	-	2.0
37	GN-88-2072	2	<0.02	2467	89573	<5.0	<0.30	<5	<5	14	12	<5	8.90	6.5	<1.0
46	GN-88-2073	1	-	-	-	-	-	<1	<2	<2	-	-	-	-	<1.0
46	GN-88-2073	2	<0.02	2692	28022	<5.0	<0.30	9	<5	5	<5	<5	4.50	<3.0	<1.0
44	GN-88-2077	1	-	-	-	-	-	<1	<2	<2	-	-	-	-	<1.0
44	GN-88-2077	2	<0.02	1803	211248	<5.0	0.36	<5	<5	12	39	<5	10.00	<3.0	<1.0
17	GN-88-2107A	1	-	-	-	-	-	5	<2	<2	-	-	-	-	<1.0
17	GN-88-2107A	2	<0.02	2282	65558	<5.0	<0.30	<10	<5	3	<15	<5	3.10	3.4	<1.0
21	GN-88-2113	1	-	-	-	-	-	3	<2	<2	-	-	-	-	<1.0
21	GN-88-2113	2	<0.02	2093	41928	<5.0	<0.30	<5	<5	6	<15	<5	27.00	15.0	<1.0
10	GN-88-3145	1	-	-	-	-	-	<1	<2	<2	-	-	-	-	<1.0
10	GN-88-3145	2	<0.02	1929	143079	<5.0	<0.30	<10	<5	9	<15	<5	11.00	9.3	<1.0
75	GN-88-4068	1	-	-	-	-	-	6	<2	<2	-	-	-	-	2.0
75	GN-88-4068	2	<0.02	1821	261896	<5.0	<0.30	15	<10	5	<15	<5	22.00	15.0	<1.0
5	GN-88-4098	1	-	-	-	-	-	2	<2	<2	-	-	-	-	<1.0
5	GN-88-4098	2	<0.02	2181	107468	<5.0	<0.30	<10	<5	11	<20	<5	21.00	12.0	<1.0
9	GN-88-4102	1	-	-	-	-	-	3	<2	<2	-	-	-	-	<1.0
9	GN-88-4102	2	<0.02	1974	48594	6.5	<0.30	9	<5	4	<20	<5	5.70	4.0	<1.0
8	GN-88-4103	1	-	-	-	-	-	2	<2	<2	-	-	-	-	<1.0
8	GN-88-4103	2	<0.02	2004	113463	<5.0	<0.30	18	<5	4	<20	<5	8.60	9.4	<1.0
Dunite															
72	GN-88-1054B	1	-	-	-	-	-	<1	<2	<2	-	-	-	-	2.0
72	GN-88-1054B	2	<0.02	1650	1213	1.1	0.25	<5	<5	2	<5	<5	2.70	<3.0	<1.0
71	GN-88-1055A	1	-	-	-	-	-	<1	<2	<2	-	-	-	-	<1.0
71	GN-88-1055A	2	<0.02	2228	4407	<1.0	<0.20	21	<5	<1	26	<5	5.20	<3.0	1.1
73	GN-88-1056A	1	-	-	-	-	-	6	<2	<2	-	-	-	-	2.0
73	GN-88-1056A	2	<0.02	1986	2339	<1.0	<0.20	<10	<5	2	25	<5	5.50	3.5	<1.0
74	GN-88-1057A	1	-	-	-	-	-	4	<2	<2	-	-	-	-	<1.0
74	GN-88-1057A	2	0.02	2293	2977	<1.0	<0.20	<10	<10	<1	22	<5	2.80	<3.0	<1.0
95	GN-88-2044	1	-	-	-	-	-	<1	3	<2	-	-	-	-	<1.0
96	GN-88-2048A	1	-	-	-	-	-	<1	<2	<2	-	-	-	-	<1.0
96	GN-88-2048A	2	<0.02	1723	3635	<5.0	<0.30	<5	<15	<1	17	<5	0.92	<3.0	<1.0
19	GN-88-2106	1	-	-	-	-	-	5	<2	<2	-	-	-	-	<1.0
19	GN-88-2106	2	0.03	2367	3969	5.4	<0.30	<5	<5	<1	<5	<5	1.30	<3.0	<1.0

Table 8.2 continued

Locality	Sample	Anal. Method	S wt %	Ni	Cr	As	Sb	Pt	Pd	Rh	Ru	Re	Ir	Os	Au
						ppm						ppb			
2	GN-88-4092A	1	-	-	-	-	-	2	<2	<2	-	-	-	-	<1.0
2	GN-88-4092A	2	0.07	1928	2952	<5.0	0.31	<5	<5	<1	<5	<5	0.90	<3.0	<1.0
6	GN-88-4097	1	-	-	-	-	-	2	<2	<2	-	-	-	-	2.0
6	GN-88-4097	2	<0.02	2448	28449	<5.0	<0.30	<5	<5	2	<15	<5	3.30	3.7	<1.0
100	GN-89-6220	3	-	-	-	-	-	<1	<2	<2	-	-	-	-	122.0
Olivine Wehrlite and Wehrlite															
72	GN-88-1054A	1	-	-	-	-	-	<1	<2	<2	-	-	-	-	<1.0
72	GN-88-1054A	2	<0.02	2175	3661	<1.0	<0.20	17	<5	3	27	<5	2.00	<3.0	<1.0
36	GN-88-1069A	1	-	-	-	-	-	<1	3	<2	-	-	-	-	<1.0
36	GN-88-1069A	2	<0.02	2026	3281	<1.0	<0.20	<10	<10	<1	20	<5	0.98	<3.0	<1.0
26	GN-88-1075	1	-	-	-	-	-	<1	<2	<2	-	-	-	-	<1.0
23	GN-88-1093A	1	-	-	-	-	-	7	<2	<2	-	-	-	-	2.0
23	GN-88-1093A	1*	-	-	-	-	-	3	<2	<2	-	-	-	-	3.0
23	GN-88-1093A	2	<0.02	1744	1096	2.3	<0.20	13	<5	2	<5	<5	3.00	3.8	<1.0
45	GN-88-2076	1	-	-	-	-	-	<1	<2	3	-	-	-	-	<1.0
45	GN-88-2076	2	<0.02	2521	99916	<5.0	<0.30	<10	<5	11	21	<5	6.90	4.8	<1.0
60	GN-88-4060	1	-	-	-	-	-	<1	<2	<2	-	-	-	-	<1.0
60	GN-88-4060	2	<0.02	2025	94789	6.9	<0.30	<15	<5	6	<40	<5	5.20	<3.0	<1.0
32	GN-88-4070A	1	-	-	-	-	-	7	<2	<2	-	-	-	-	<1.0
87	GN-89-8143	3	-	-	-	-	-	2	<2	<2	-	-	-	-	3.0
73	GN-88-1056B	1	-	-	-	-	-	3	4	<2	-	-	-	-	<1.0
73	GN-88-1056B	2	<0.02	1199	5284	<1.0	<0.20	<20	<10	<1	23	<5	1.60	<3.0	1.2
30	GN-88-4080A	1	-	-	-	-	-	2	12	<2	-	-	-	-	<1.0
30	GN-88-4080A	2	<0.02	1148	2298	<5.0	<0.30	9	12	<1	<5	<5	0.56	<3.0	<1.0
7	GN-88-4101	1	-	-	-	-	-	<1	<2	<2	-	-	-	-	<1.0
7	GN-88-4101	2	<0.02	1100	2764	<5.0	<0.30	<5	<5	<1	<10	<5	0.54	<3.0	<1.0
104	GN-89-6201	3	-	-	-	-	-	2	<2	<2	-	-	-	-	3.0
90	GN-89-8134	3	-	-	-	-	-	3	<2	<2	-	-	-	-	<1.0
Olivine Clinopyroxenite and Clinopyroxenite															
74	GN-88-1057B	1	-	-	-	-	-	<1	<2	<2	-	-	-	-	<1.0
74	GN-88-1057B	2	<0.02	442	4157	<1.0	<0.20	<20	<10	<1	22	<5	0.95	<3.0	<1.0
34	GN-88-1063	1	-	-	-	-	-	<1	<2	<2	-	-	-	-	<1.0
96	GN-88-2048B	1	-	-	-	-	-	<1	<2	<2	-	-	-	-	<1.0
96	GN-88-2048B	2	<0.02	359	1849	<5.0	<0.30	<10	<35	<1	<15	<5	<0.10	<3.0	<1.0
43	GN-88-2079	1	-	-	-	-	-	45	22	<2	-	-	-	-	3.0
43	GN-88-2079	2	4.24	556	726	<5.0	<0.30	53	25	<1	20	6	0.27	<3.0	3.2
88	GN-88-4042	1	-	-	-	-	-	<1	<2	<2	-	-	-	-	<1.0
64	GN-88-4052	1	-	-	-	-	-	5	<2	<2	-	-	-	-	<1.0
67	GN-88-4063A	1	-	-	-	-	-	<1	<2	<2	-	-	-	-	<1.0
67	GN-88-4063A	2	<0.02	249	1798	<5.0	0.46	<5	<5	<1	<5	<5	<0.10	<3.0	<1.0
33	GN-88-4069A	1	-	-	-	-	-	239	285	<2	-	-	-	-	7.0
32	GN-88-4070B	1	-	-	-	-	-	5	11	<2	-	-	-	-	<1.0
3	GN-88-4093	1	-	-	-	-	-	2	7	<2	-	-	-	-	<1.0
3	GN-88-4093	2	<0.02	529	2556	<5.0	<0.30	<5	<5	<1	<15	<5	0.20	<3.0	<1.0
98	GN-89-7130	3	-	-	-	-	-	4	<2	<2	-	-	-	-	14.0
98	GN-89-7131A	3	-	-	-	-	-	4	<2	<2	-	-	-	-	<1.0
99	GN-89-9173	3	-	-	-	-	-	50	70	7	-	-	-	-	13.0
55	GN-89-9141	3	-	-	-	-	-	<1	<2	<2	-	-	-	-	5.0
52	GN-89-9146B	3	-	-	-	-	-	13	7	<2	-	-	-	-	8.0
94	GN-89-9169B	3	-	-	-	-	-	<1	<2	<2	-	-	-	-	<1.0
35	GN-88-1064	1	-	-	-	-	-	8	13	<2	-	-	-	-	2.0
85	GN-89-8139	3	-	-	-	-	-	8	9	<2	-	-	-	-	5.0
Hornblende Clinopyroxenite, Clinopyroxene Hornblendite and Hornblendite															
48	GN-88-1077	1	-	-	-	-	-	5	<2	<2	-	-	-	-	2.0
48	GN-88-1077	2	<0.02	<150	<150	5.9	1.80	9	9	<1	7	<5	3.10	<3.0	<1.0
79	GN-88-4031A	1	-	-	-	-	-	11	35	<2	-	-	-	-	<1.0
79	GN-88-4031A	2	<0.02	251	732	<5.0	<0.30	12	24	1	<5	<5	0.13	<3.0	<1.0
79	GN-88-4031C	1	-	-	-	-	-	<1	5	<2	-	-	-	-	3.0
92	GN-88-4045	1	-	-	-	-	-	14	44	<2	-	-	-	-	<1.0
30	GN-88-4080B	1	-	-	-	-	-	2	16	<2	-	-	-	-	2.0
30	GN-88-4080B	2	<0.02	258	675	<5.0	<0.30	8	14	<1	<10	<5	0.15	<3.0	1.1
111	GN-89-7143B	3	-	-	-	-	-	13	12	<2	-	-	-	-	10.0
79	GN-89-9132B	3	-	-	-	-	-	16	20	<2	-	-	-	-	24.0
79	GN-89-9132C	3	-	-	-	-	-	6	8	<2	-	-	-	-	22.0
82	GN-89-9167B	3	-	-	-	-	-	48	14	7	-	-	-	-	174.0
57	GN-89-9139A	3	-	-	-	-	-	5	5	<2	-	-	-	-	9.0
56	GN-89-9140A	3	-	-	-	-	-	11	<2	<2	-	-	-	-	2.0
86	GN-89-8133A	3	-	-	-	-	-	7	12	<2	-	-	-	-	<1.0

Table 8.2 continued

Locality	Sample	Anal. Method	S wt %	Ni ppm	Cr ppm	As ppm	Sb ppm	Pt ppb	Pd ppb	Rh ppb	Ru ppb	Re ppb	Ir ppb	Os ppb	Au ppb
50	GN-88-1080B	1	-	-	-	-	-	4	<2	<2	-	-	-	-	2.0
83	GN-88-2040B	1	-	-	-	-	-	8	18	<2	-	-	-	-	<1.0
83	GN-88-2040B	1*	-	-	-	-	9	15	<2	-	-	-	-	<1.0	
83	GN-88-2040B	2	0.44	<150	<150	<5.0	<0.30	14	16	<1	17	<5	0.17	<3.0	<1.0
97	GN-88-2045	1	-	-	-	-	-	3	11	<2	-	-	-	-	<1.0
97	GN-88-2045	2	<0.02	<150	966	<5.0	<0.30	7	<10	<1	13	<5	0.14	<3.0	<1.0
38	GN-88-4082B	1	-	-	-	-	-	<1	14	<2	-	-	-	-	<1.0
38	GN-88-4082B	2	<0.02	167	228	<5.0	<0.30	7	13	<1	<5	<5	<0.10	<3.0	<1.0
40	GN-88-4086	1	-	-	-	-	-	<1	18	<2	-	-	-	-	<1.0
40	GN-88-4086	1*	-	-	-	-	-	<1	15	<2	-	-	-	-	<1.0
40	GN-88-4086	2	0.02	<150	287	<5.0	<0.30	6	10	<1	<5	<5	<0.10	<3.0	<1.0
93	GN-89-8147	3	-	-	-	-	-	<1	<2	<2	-	-	-	-	2.0
Gabbroic Rocks															
70	GN-88-1050A	1	-	-	-	-	-	2	<2	<2	-	-	-	-	2.0
50	GN-88-1080C	1	-	-	-	-	-	<1	<2	<2	-	-	-	-	5.0
59	GN-88-2094	1	-	-	-	-	-	3	8	<2	-	-	-	-	3.0
59	GN-88-2094	2	0.01	<150	154	<5.0	<0.30	7	6	<1	18	<5	<0.10	<3.0	1.4
58	GN-88-2095	1	-	-	-	-	-	<1	<2	<2	-	-	-	-	<1.0
58	GN-88-2095	2	<0.02	<150	255	<5.0	<0.30	<5	<5	<1	22	<5	<0.10	<3.0	<1.0
18	GN-88-2100B	1	-	-	-	-	-	2	<2	<2	-	-	-	-	11.0
18	GN-88-2100B	2	2.72	<150	<150	<5.0	1.20	<5	<5	<1	19	<5	<0.10	<3.0	3.8
18	GN-88-2100C	1	-	-	-	-	-	<1	<2	<2	-	-	-	-	<1.0
18	GN-88-2100C	2	<0.02	<150	315	<5.0	0.64	<5	<5	<1	20	<5	<0.10	<3.0	<1.0
20	GN-88-2115	1	-	-	-	-	-	4	<2	<2	-	-	-	-	<1.0
79	GN-88-4030B	1	-	-	-	-	-	2	20	<2	-	-	-	-	2.0
81	GN-88-4036	1	-	-	-	-	-	2	11	<2	-	-	-	-	4.0
81	GN-88-4036	2	<0.02	<150	184	7.9	<0.30	7	11	<1	<5	<5	<0.10	<3.0	<1.0
29	GN-88-4073A	1	-	-	-	-	-	<1	<2	<2	-	-	-	-	4.0
102	GN-89-6165	3	-	-	-	-	-	7	7	<2	-	-	-	-	47.0
107	GN-89-6195	3	-	-	-	-	-	8	9	<2	-	-	-	-	55.0
109	GN-89-7164	3	-	-	-	-	-	9	9	<2	-	-	-	-	42.0
108	GN-89-6193B	3	-	-	-	-	-	4	<2	<2	-	-	-	-	3.0
112	GN-89-9154	3	-	-	-	-	-	8	9	<2	-	-	-	-	5.0
83	GN-88-2040A	1	-	-	-	-	-	5	11	<2	-	-	-	-	<1.0
83	GN-88-2040A	2	2.29	<150	746	<5.0	<0.30	11	14	<1	18	8	0.14	<3.0	<1.0
91	GN-88-4043A	1	-	-	-	-	-	5	21	<2	-	-	-	-	9.0
31	GN-88-4072A	1	-	-	-	-	-	5	16	<2	-	-	-	-	<1.0
31	GN-88-4072A	1	0.30	<150	216	<5.0	<0.30	8	10	<1	<5	<5	<0.10	<3.0	<1.0
28	GN-88-4074	1	-	-	-	-	-	<1	14	<2	-	-	-	-	<1.0
39	GN-88-4089	1	-	-	-	-	-	<1	10	<2	-	-	-	-	<1.0
78	GN-89-9128C	3	-	-	-	-	-	11	8	<2	-	-	-	-	27.0
51	GN-89-9147	3	-	-	-	-	-	2	4	<2	-	-	-	-	4.0
80	GN-89-9148B	3	-	-	-	-	-	11	9	<2	-	-	-	-	5.0
80	GN-89-9148B	3*	-	-	-	-	-	11	9	<2	-	-	-	-	6.0
78	GN-89-9128A	3	-	-	-	-	-	2	3	<2	-	-	-	-	88.0
Hornblende-Feldspar Pegmatites and Felsic Dikes															
42	GN-88-2078	1	-	-	-	-	-	<1	<2	<2	-	-	-	-	<1.0
42	GN-88-2078	2	<0.02	204	<150	<5.0	<0.30	<5	<5	<1	13	<5	<0.10	<3.0	<1.0
65	GN-88-4053D	1	-	-	-	-	-	7	<2	<2	-	-	-	-	<1.0
29	GN-88-4073B	1	-	-	-	-	-	2	<2	<2	-	-	-	-	<1.0
29	GN-88-4073B	2	0.05	<150	<150	10.0	<0.30	<5	<5	<1	<5	<5	<0.10	<3.0	<1.0
27	GN-88-4076	1	-	-	-	-	-	2	<2	<2	-	-	-	-	<1.0
41	GN-88-4085	1	-	-	-	-	-	<1	<2	<2	-	-	-	-	<1.0
41	GN-88-4085	3	<0.02	<150	<150	<5.0	<0.30	<5	<5	<1	8	<5	<0.10	<3.0	<1.0
105	GN-89-6188	3	-	-	-	-	-	<1	<2	<2	-	-	-	-	60.0
82	GN-89-8123B-2	3	-	-	-	-	-	2	<2	<2	-	-	-	-	<1.0
82	GN-89-8123B-1	3	-	-	-	-	-	10	4	<2	-	-	-	-	<1.0
53	GN-89-9145Z	3	-	-	-	-	-	2	<2	<2	-	-	-	-	<1.0
54	GN-89-9143	3	-	-	-	-	-	<1	<2	<2	-	-	-	-	<1.0
LAY RANGE ASSEMBLAGE															
Metasedimentary and Metavolcaniclastic Rocks															
47	GN-88-2083	1	-	-	-	-	-	<1	6	<2	-	-	-	-	<1.0
49	GN-88-2088	1	-	-	-	-	-	2	4	<2	-	-	-	-	2.0
13	GN-88-2109	1	-	-	-	-	-	<1	<2	<2	-	-	-	-	3.0
13	GN-88-2109	2	1.32	<150	<150	5.5	<0.30	<5	<5	<1	<5	<5	<0.10	<3.0	1.6
11	GN-88-2110	1	-	-	-	-	-	3	<2	<2	-	-	-	-	<1.0

Table 8.2 continued

Locality	Sample	Anal. Method	S wt %	Ni	Cr	As	Sb	Pt	Pd	Rh	Ru	Re	Ir	Os	Au
				ppm				ppb							
101	GN-89-6162A	3	-	-	-	-	-	<1	<2	<2	-	-	-	-	83.0
101	GN-89-6162B	3	-	-	-	-	-	2	<2	<2	-	-	-	-	6.0
106	GN-89-6199	3	-	-	-	-	-	9	5	<2	-	-	-	-	<1.0
1	GN-89-6225	3	-	-	-	-	-	2	5	<2	-	-	-	-	3.0
110	GN-89-7147A	3	-	-	-	-	-	19	20	<2	-	-	-	-	76.0
4	GN-89-8155	3	-	-	-	-	-	2	<2	<2	-	-	-	-	12.0
103	GN-89-6202	3	-	-	-	-	-	<1	4	<2	-	-	-	-	43.0
110	GN-89-7147B	3	-	-	-	-	-	3	4	<2	-	-	-	-	5.0
89	GN-89-8136	3	-	-	-	-	-	<1	4	<2	-	-	-	-	4.0
79	GN-89-9132A	3	-	-	-	-	-	<1	<2	<2	-	-	-	-	19.0
80	GN-89-9148A	3	-	-	-	-	-	2	6	<2	-	-	-	-	3.0
82	GN-89-9167A	3	-	-	-	-	-	4	5	<2	-	-	-	-	4.0
Metavolcanic Rocks and Dikes															
14	GN-89-9175A	3	-	-	-	-	-	<1	<2	<2	-	-	-	-	4.0
12	GN-89-9176	3	-	-	-	-	-	<1	<2	<2	-	-	-	-	11.0
77	GN-89-9126C	3	-	-	-	-	-	3	<2	<2	-	-	-	-	214.0
113	GN-89-9153A	3	-	-	-	-	-	7	8	<2	-	-	-	-	10.0
QUARTZ VEINS AND QUARTZ-CARBONATE ALTERATION															
16	GN-88-2101	1	-	-	-	-	-	<1	<2	<2	-	-	-	-	<1.0
15	GN-88-2108	1	-	-	-	-	-	<1	<2	<2	-	-	-	-	2.0
84	GN-89-8126	3	-	-	-	-	-	2	<2	<2	-	-	-	-	7.0

*Analytical methods: 1=Inductively coupled plasma mass spectrometry, Acme Laboratories,Vancouver; 2=Instrumental neutron activation, Institut National de la Recherche Scientifique, Quebec; 3=Inductively coupled plasma emission spectrometry, Acme Laboratories,Vancouver. Detection limits:1 ppb for Pt and Au; 2 ppb for Pd and Rh; neutron activation detection limits vary with sample composition. *=Duplicate analysis. Sample localities are shown on Figures 8.5 and 8.7.*

Louis *et al.*, 1986; Chapter 9), and PGE-rich and PGE-depleted chromitites exist, there will be no simple correlation between the abundance of chromium and PGE in the sample population. The abundances of arsenic and antimony are generally low and show no correlation with PGE or gold.

The highest concentration of platinum (735 ppb) is found in chromitiferous dunite (Locality 22, Figure 8.8) and is accompanied by small but significant quantities of rhodium, ruthenium, iridium and osmium. Low abundances of sulphur, arsenic and antimony suggest that the PGE may be contained as discrete platinum-iron alloys as typifies the chromitite-PGE association in the Tulameen complex (St. Louis *et al.*, 1986; Nixon and Hammack, 1991). The tenor of platinum in a duplicate analysis is over fourteen times lower, and is attributed to a nugget effect, which appears to influence other samples (*e.g.* GN-88-1039, Locality 66). Rarely, abundances of iridium and osmium seem anomalously high (*e.g.* GN-88-1055B, Locality 71) and may indicate the presence of iridium-osmium(-ruthenium?) alloys which have been documented in other Alaskan-type associations (Harris and Cabri, 1973; Cabri and Harris, 1975). Anomalously high platinum and palladium (200 ppb) occur in a clinopyroxenite dike in the central part of the complex (GN-88-4069A, Locality 33). In general, palladium remains near or below detection limits in chromitites and olivine-rich ultramafic rocks, and increases in abundance in hornblende-bearing gabbroic to dioritic rocks. This behaviour is accompanied by a concomitant decrease in the platinum:palladium ratio, similar to trends in other Alaskan-type complexes (Nixon and Hammack, 1991).

Strongly anomalous abundances of gold (100 ppb) occur in an andesitic dike intruding metasedimentary sequences adjacent to a fault zone (Locality 77, Figure 8.5); in hornblendite at the roof of the complex (Locality 82); and in dunite near the margin of the intrusion (Locality 100). In fact, all of the gold anomalies (>20 ppb) are confined to the extreme northwestern end of the complex. Almost without exception, they exhibit a strong spatial relationship with intrusive contacts, although some are close to faults, and appear to favour mafic lithologies. No correlation is evident between the abundances of PGE and gold, which is generally low within the complex, and the few quartz veins and quartz-carbonate alteration zones sampled are barren. These data suggest that circulating fluids, possibly driven by convective cooling at the margins of the intrusion, scavenged gold from Lay Range assemblage rocks and deposited it near the contacts of the intrusion where mafic rocks may have acted as a chemical sink. The apparent spatial concentration of gold anomalies at the northwestern contacts is probably a reflection of sampling bias.

SUMMARY

The Polaris ultramafic-mafic complex is an instructive example of an Alaskan-type intrusion. It is one of the largest (45 km^2) of such bodies in British Columbia. Although spectacular mesoscopic layering, such as that found at Duke Island (Irvine, 1974a), is nowhere developed, relationships with the country rocks, and between ultramafic and more differentiated gabbroic to diorite rocks, are well exposed. In addition, all typical Alaskan-type lithologies are represented, including dunite, chromitite, wehrlite, olivine cli-

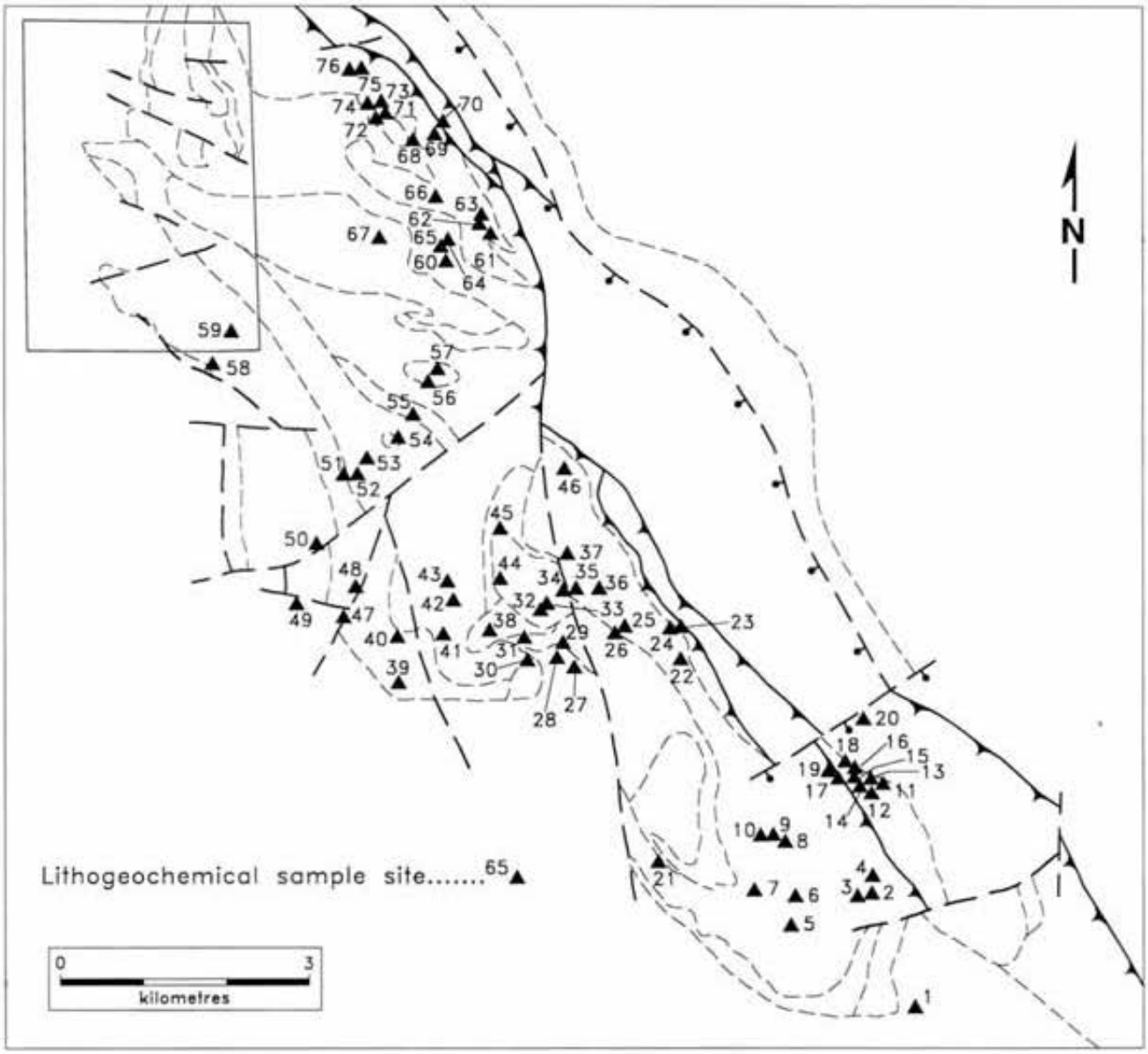

Figure 8.8. Location of geochemical sample sites listed in Table 8.2 (also *see* Figure 8.5). Symbols as in Figure 8.3.

nopyroxenite, clinopyroxenite, hornblende clinopyroxenite, hornblendite, gabbro-diorite and more leucocratic pegmatitic phases. Cumulate textures are widespread and well preserved, and an interesting petrologic feature is the occurrence of cumulus and intercumulus phlogopite in early cumulates (dunite), indicative of relatively potassium-rich parental magmas. A potentially important economic consideration is the chromitite-PGE association documented from other Alaskan-type intrusions.

Detailed mapping of the Polaris complex and its environs has established that the body is a westward-dipping, westward-facing transgressive sill that intrudes metasedimentary and metavolcanic rocks of the Upper Paleozoic Lay Range assemblage (Harper Ranch Subterrane) which forms the basement of Quesnellia. Intrusive contacts at the roof and margins of the sill are well exposed at the northwestern end of the complex. Here, minor coeval intrusions of gabbro-diorite and hornblende clinopyroxenite in the country rocks mimic the geometry of their larger counterpart. New U-Pb dates on zircon separates are concordant at 186±2 Ma and establish a late Early Jurassic (early Toarcian) age for the complex.

The internal stratigraphy of the Polaris complex is well exposed in cross-section. The lower margin of the sill is zoned outward over a narrow interval from dunite through wehrlite and olivine clinopyroxenite to phlogopite-bearing olivine-hornblende clinopyroxenite. Dunite occupies much of the lower part of the intrusion, and, in a gross sense, is succeeded upward by thickly stratified wehrlitic cumulates and clinopyroxenites, hornblende-bearing clinopyroxenites

and hornblendites, and hornblende-rich gabbroic to dioritic rocks which are well developed near the roof of the intrusion. Contacts between the main lithologic units are sharp to gradational. On a more local scale, there is evidence for complex multiple intrusive events between wehrlitic and pyroxenitic lithologies on the one hand, and between feldspathic differentiates and hornblende-rich ultramafic units on the other. Previously consolidated chromitite layers, and complex zones of intermixing of wehrlitic and clinopyroxenitic rocks, point to syndepositional remobilization of early cumulates by mass-wasting processes (*e.g.*, slumping and density flows) which deposited them lower down in the magma chamber. The widespread remobilization of chromitite concentrations, combined with their scanty occurrence, do not bode well for commercial exploitation of chromite in these rocks.

The Polaris complex is contained within a northwest-trending, westward-dipping homoclinal sequence of well-bedded country rocks with unambiguous sedimentary structures that face west. High-angle faults with predominantly northwesterly and westerly trends transect ultramafic and country rocks alike. A basal ductile thrust zone exposed at the eastern margin of the complex exhibits S/C fabrics which indicate tectonic transport to the east. The complex has therefore been tectonically uprooted and transported, together with its hostrocks, as an allochthonous slice, similar to the structure of rock packages documented in other parts of the Lay Range. Textural evidence indicates that eastward transport took place while the aureole was still hot. This deformation and metamorphism are apparently synchronous with the collision of accreted terranes of the Intermontane Belt, specifically Quesnellia, against the miogeocline of ancestral North America (Chapter 11).

Lithogeochemical assays for PGE, gold and associated elements yield some interesting but rather localized anomalies. Platinum attains a maximum abundance of 735 ppb in chromitite-bearing dunite, and is accompanied by minor iridium and osmium which reach maximum abundances of 88 and 51 ppb, respectively. A sample of clinopyroxenite yields anomalously high platinum and palladium of 239 and 285 ppb, respectively. The PGE have no apparent correlation with the abundances of other elements suggesting that they may be contained as discrete platinum-iron or iridium-osmium-ruthenium alloys. Gold anomalies (20 to 214 ppb) show a preference for mafic lithologies at the margins of the complex. This suggests that the mafic-ultramafic rocks may have acted as a chemical trap for mineralizing fluids circulating adjacent to the intrusion, and that the gold was derived from the country rocks.

CHAPTER 9 TULAMEEN COMPLEX

The Tulameen mafic-ultramafic complex (48°20'N, 120°50'W) underlies 60 square kilometres of forested terrain centred 23 kilometres due west of Princeton (Figure 9.1). It is the largest and most easily accessible Alaskan-type intrusion in British Columbia. Historically, the Tulameen has been the largest producer of platinum in the province, in the form of impure platinum nuggets (Chapter 10).

Physiographically, the region lies in a transition zone between the Cascade Mountains to the west and the Interior Plateau to the east. A paved highway connects Princeton with the communities of Coalmont and Tulameen where a network of well-maintained logging roads leads westward into the intrusion. The Tulameen River road provides access to a complete cross-section through the body, intersecting the central dunite approximately 10 kilometres west of the village of Tulameen. The area is covered by NTS map sheets 92H/7 and 92H/10 at a scale of 1:50 000.

REGIONAL GEOLOGY AND GEOCHRONOMETRY

The Tulameen complex is situated within the southwestern Intermontane Belt just east of the boundary between the Quesnel Terrane and Mount Lytton - Eagle Plutonic Complex. The area lies within a zone of Early Tertiary "transtensional" block faulting related to regional right-lateral transform motions along the Fraser River - Straight Creek fault system (Ewing, 1980; Monger, 1985, 1989). The complex has been the subject of detailed geological and petrological studies by Findlay (1963, 1969) and, more recently, Rublee (1994).

The geologic setting of the Tulameen complex is shown in Figures 9.1 and 9.2. The mafic-ultramafic rocks are hosted by metasedimentary and mafic to felsic metavolcanic lithologies that belong mainly to the western facies of the Upper Triassic (Carnian to lower Norian) Nicola Group (Preto, 1975, 1979; Price *et al.*, 1987). Volcanic assemblages in the Nicola Group contain calcalkaline and clinopyroxene-phyric shoshonitic lavas that evolved during Late Triassic arc magmatism (Mortimer, 1986). These rocks have been considered to be comagmatic with mafic-ultramafic rocks of the Tulameen suite (Findlay, 1969). The Tulameen complex and its hostrocks are unconformably overlain by terrigenous sedimentary and volcanic assemblages of the Early Tertiary (Eocene) Princeton Group and Miocene plateau basalts.

Regional structures trend approximately north-northwest and are characterized by a southwest-dipping foliation that parallels the eastern margin of, and extends into, the southern extension of the Mount Lytton batholith, or Eagle Plutonic Complex. This zone of deformation has been referred to as the "Eagle Shear Zone" by Greig (1992) and is related to a syn-intrusive Middle to Late Jurassic contractional deformation. The Tulameen complex forms an elongate body at the eastern margin of this shear zone concordant with the regional structural grain.

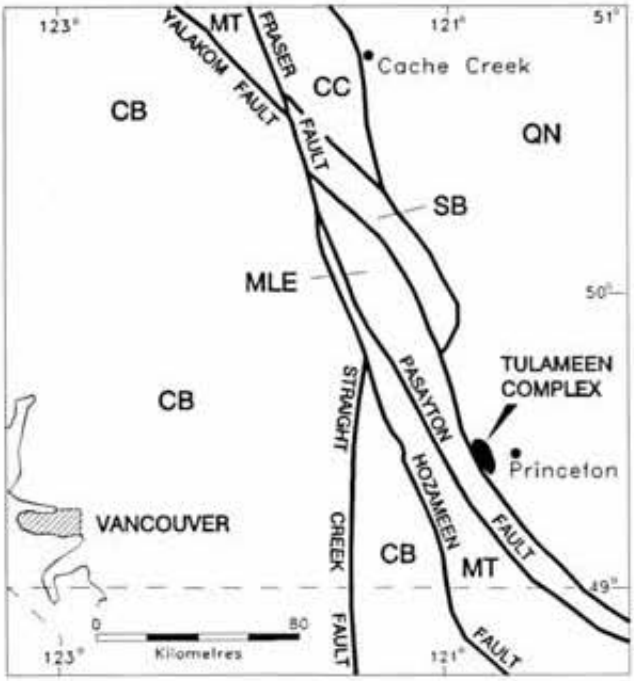

Figure 9.1. Location and generalized geologic setting of the Tulameen mafic-ultramafic complex in relation to tectonostratigraphic terranes (modified after Kleinspehn, 1985; Wheeler *et al.*, 1991).

Previously published K-Ar and $^{40}Ar/^{39}Ar$ dates for hornblendes from the Tulameen complex yield ages of 208 to 196 Ma (Roddick and Farrar, 1971, 1972; McDougall, 1974; dates recalculated according to the decay constants recommended by Steiger and Jäger, 1977) or latest Triassic to Early Jurassic according to the time scale of Harland *et al.* (1990). The younger dates have been considered too young due to loss of radiogenic argon during post-emplacement regional metamorphism, and the older dates a close

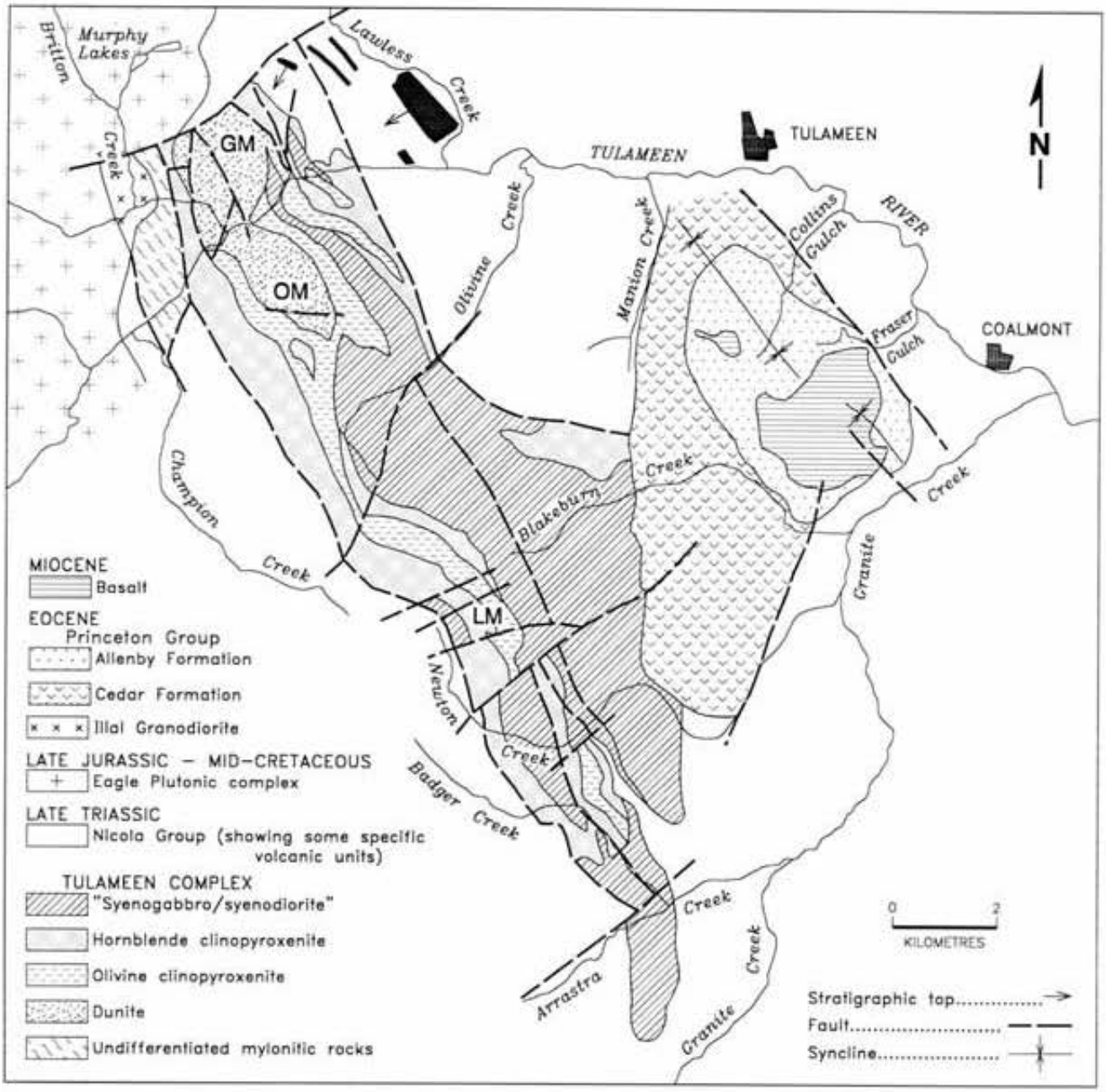

Figure 9.2. Generalized geology of the Tulameen complex (modified after Findlay, 1963 and Nixon, 1988).

approximation to the age of crystallization of the feldspathic part of the intrusion. A complex thermal history for the area has been confirmed by new K-Ar determinations on the Mount Lytton - Eagle Plutonic Complex where hornblende and biotite in samples collected near Murphy Lakes at the eastern margin of the complex (Figure 9.2) yielded highly discordant dates ranging from 57 to 130 Ma interpreted as a result of mid-Cretaceous and Early Tertiary thermal events (Greig, 1989; Greig *et al.*, 1992). A zircon separate from the same locality gave a U-Pb isotopic age of 157±4 Ma (Middle-Late Jurassic boundary) which was regarded as a minimum age of emplacement for the plutonic complex (Greig, 1989; Greig *et al.*, 1992). Two further U-Pb zircon determinations for the Mount Lytton Complex have given isotopic ages of 250±5 and 212±1 Ma (Friedman and van der Heyden, 1992; Parrish and Monger, 1992). A U-Pb zircon date in the range 204 to 212 Ma (latest Triassic–earliest Jurassic) for syenodiorite associated with the Tulameen complex was reported by Rublee and Parrish (1990) and Rublee (1994) and, taken together with the argon data, provides a good estimate for the crystallization age of the feldspathic part of the complex.

COUNTRY ROCKS

NICOLA GROUP

Rocks of the Nicola Group in the Tulameen region comprise black, thinly laminated argillites, green and brown tuffaceous siltstones and lapilli tuffs, dark grey-green aphyric to plagioclase-phyric pyroxene andesite and hornblende dacite flows, rare aphanitic rhyolites, cherts, chert breccias and dark grey limestones. All lithologies are regionally metamorphosed to greenschist grade. Chlorite-muscovite schists with minor biotite are common to the west of the ultramafic complex and marbles with weakly developed skarns commonly occur adjacent to the contact with the Eagle Plutonic Complex. Skarn mineralization includes traces of molybdenite, chalcopyrite, pyrite, covellite, bornite and chalcocite(?).

Beyond the northeastern margin of the intrusion, andesitic lavas preserve primary flowage features such as vesicle trains aligned within the flow foliation, chilled basal zones overlying baked sedimentary horizons, and basal flow breccias caught in "squeeze-ups". The latter two criteria indicate that these lavas are the right way up (Figure 9.2). A distinctive variety of porphyritic flow contains large (>1 cm) feldspar laths with subtrachytic texture previously referred to as "bladed feldspar porphyries" (Preto, 1975, 1979).

PRINCETON GROUP

The Princeton Group contains sub-greenschist grade lithologies of Eocene age that have been deformed and rotated by block faulting (Ewing, 1980; Monger, 1985). Rock types include thinly bedded coal seams and seat earths, fissile shales yielding plant remains, arkosic sandstones and conglomerates, polymictic laharic breccias, biotite rhyolite, hornblende-phyric dacite and locally pillowed olivine basalt flows and hyaloclastites. The Princeton Group is locally capped by subhorizontal amygdaloidal basalts of Miocene age that are unfaulted (Monger, 1985).

MOUNT LYTTON - EAGLE PLUTONIC COMPLEX

The Mount Lytton-Eagle Plutonic Complex comprises foliated to gneissic (syntectonic) tonalite-granodiorite and variably deformed (syntectonic to post-tectonic) muscovite granite. Granodiorite at the eastern margin of the complex is a medium to coarse-grained rock containing quartz, plagioclase, potassium feldspar and biotite. The granodiorite is weakly to intensely foliated, cut by quartz veins and locally encloses amphibolitic schlieren. Near the contact with Nicola rocks on the Tulameen River road, numerous aplite sills (<1 m) that are generally concordant with westward-dipping argillites and metasiltstones are probably rooted in the Eagle pluton. On Britton Creek, unfoliated biotite hornblende granodiorite contains randomly oriented xenoliths of amphibole-biotite-chlorite schist derived from adjacent mylonitic rocks. Recent mapping and K-Ar geochronometry in the region has identified this granitoid stock as a post-tectonic intrusion of Early Tertiary (Eocene) age (Greig, 1989). The age of the Eagle Plutonic Complex is regarded as Middle to Late Jurassic (Greig, 1989; Greig *et al.*, 1992).

TULAMEEN COMPLEX: MAFIC-ULTRAMAFIC ROCKS

Comprehensive reports of the geology and economic mineral occurrences in the Tulameen district are provided by Camsell (1913) and Rice (1947). The most complete accounts of the geology and petrology of the ultramafic complex are provided by Findlay (1963, 1969) and Rublee (1994). The geology of the Tulameen complex is shown on Map 5 (in pocket) and Figures 9.2 and 9.3. The distribution of mappable units observed in the field is as determined by Findlay (1963). However, we have a different view of relationships among some of the principal lithologic units and regarding the structural evolution of the complex. The principal ultramafic and mafic units comprise dunite, olivine clinopyroxenite, hornblende clinopyroxenite, and gabbroic to dioritic rocks.

DUNITE

Outcrops of dunite are restricted to the northern part of the complex at Grasshopper and Olivine mountains (Figure 9.3). The dunite is medium to dark grey where fresh, buff-weathering and well jointed. The primary mineralogy consists of forsteritic olivine, accessory chromite and rare diopsidic augite. Alteration products include serpentine, carbonate, magnetite and talc. In general, the degree of serpentinization decreases from east (80 vol% serpentine) to west (20%) where the lowest loss on ignition values (<2 wt% volatiles) are recorded (Findlay, 1963; White, 1987).

CHROMITITE

Concentrations of chrome spinel and massive chromitite appear to be distributed randomly throughout the dunite as discrete layers, nodular masses, and schlieren up to 1 metre long and 6 centimetres wide (Figure 9.3). Chromitite schlieren are commonly distinguished in outcrop by a pale alteration halo (0.1 to 1 cm wide). Associated with the chromite are microscopic grains of platinum minerals (*e.g.*, tulameenite, sperrylite), nickel-iron sulphides (*e.g.*, pentlandite, violarite, bravoite), chalcopyrite and pyrite as described in detail later (St. Louis *et al.*, 1986; *cf.* Chapter 10).

OLIVINE CLINOPYROXENITE

The principal outcrops of olivine clinopyroxenite envelop the dunite "core" and extend southwards along the central part of the complex. In addition, three discrete bodies of olivine clinopyroxenite that are distinctly elongate along the regional structural trend are exposed in the northeastern part of the intrusion. The fresh rock is medium to coarse grained and has a blotchy green and black appearance due to partially serpentinized olivine (<20 vol% serpentine) and deep green clinopyroxene. Sporadic pegmatitic masses contain crystals up to 8 centimetres across and olivine segregations locally form schlieren.

Breccias within the olivine clinopyroxenite unit are well exposed in the banks of the Tulameen River near the western margin of the dunite (Figure 9.3). Angular to rounded blocks (<0.5 m) of dunite, pyroxenite and interlayered dunite-pyroxenite (Photo 9.1) are enclosed in a ser-

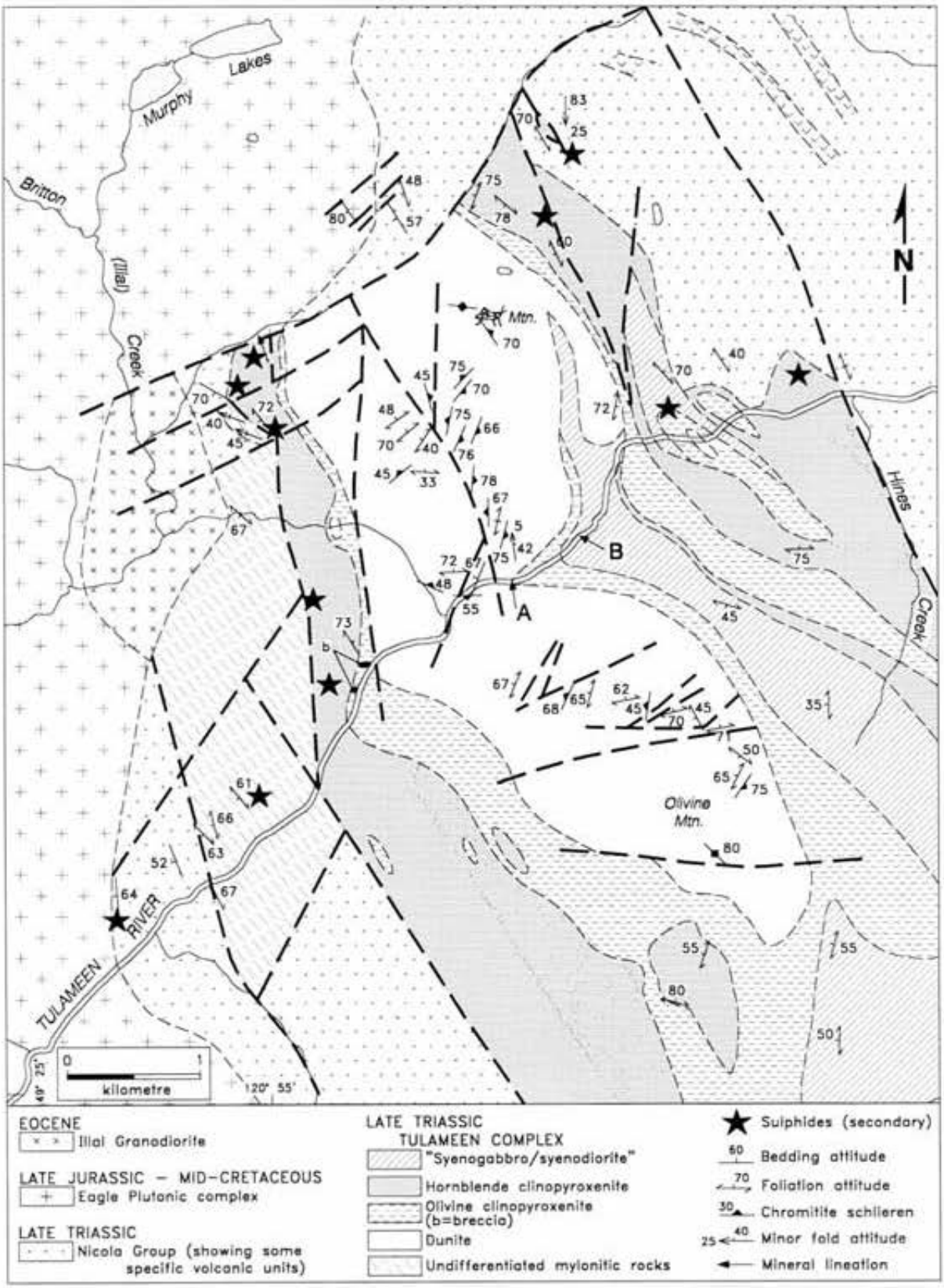

Figure 9.3. Detailed geologic map of the northern part of the Tulameen ultramafic complex (modified after Findlay, 1963 and Greig, 1989). A-B refers to the location of the measured stratigraphic section (Figure 9.4).

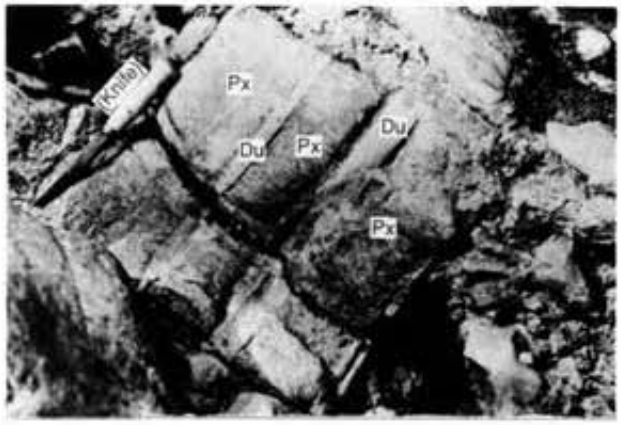

Photo 9.1. Angular block of layered dunite (Du) - clinopyroxenite (Px) in sulphide-rich serpentinized breccia within the westernmost olivine clinopyroxenite unit exposed in the Tulameen River bed.

pentinized, formerly pyroxene-rich matrix carrying calcite and disseminated sulphides (largely pyrite). On the eastern bank, the southern margin of a similar breccia is in contact with a body of dunite 8 metres thick which is succeeded southward by another breccia with clasts that are predominantly foliated (mylonitized?) gabbro in random orientation. All observed contacts between breccias and host pyroxenite dip moderately to steeply (30 to 70°) south. The cause of brecciation is not clear and may involve either tectonic or localized explosive activity.

HORNBLENDE CLINOPYROXENITE

Hornblende clinopyroxenite generally occurs at the periphery of the complex. This unit is continuous along the western margin of the intrusion but is more irregularly distributed in the east. The fresh rock is medium to coarse grained and contains diopsidic augite, hornblende, relatively abundant magnetite and minor biotite, apatite and disseminated sulphides; feldspathic variants are extremely rare. Medium-grained varieties commonly exhibit mineral foliations and/or hornblende lineations. Biotite locally forms coarse books (1 cm) and amphiboles commonly reach 1 to 3 centimetres in size. Accessory biotite and apatite occur in magnetite-rich layers 6 metres thick, that are poorly exposed in old workings on the southern slopes of Tanglewood Hill (Eastwood, 1959). Massive magnetite is also found as schlieren and podiform masses on Lodestone Mountain (Figure 9.2) and is commonly associated with coarse-grained hornblende and clinopyroxene segregations. This rudimentary igneous layering generally parallels mineral foliations developed in the region.

MINOR ULTRAMAFIC LITHOLOGIES

Rock types that do not generally form mappable units include peridotite, clinopyroxenite, hornblende olivine clinopyroxenite, hornblendite, "hybrid" rocks and mafic pegmatite. The latter rock contains large (6 cm) hornblende crystals with interstitial feldspar and usually passes gradationally into finer grained hornblendite. Mafic pegmatites are preferentially distributed near the margins of hornblende clinopyroxenite bodies (Findlay, 1963). Hybrid rocks are characterized by gabbroic xenoliths in various stages of assimilation and generally occur at gabbro-diorite contacts (Findlay, 1963). However, gabbroic xenoliths are also found at the summit of Lodestone Mountain.

GABBROIC TO DIORITIC ROCKS

The gabbroic to dioritic rocks were subdivided by Findlay (1963) into syenogabbro and syenodiorite. In the absence of more detailed study, Findlay's nomenclature is retained here but these rocks might equally well have been named diorite, monzonite, monzosyenite or variants thereof, due to the general absence of plagioclase compositions greater than An50 where recognizable (Findlay 1963).

The main mass of syenogabbro is distributed eccentrically on the eastern side of the complex. In the north, gabbroic rocks are commonly in direct contact with olivine clinopyroxenite but only rarely lie against dunite. In the south, well-foliated and/or strongly lineated fine to medium-grained gabbroic rocks extend southwards across Arrastra Creek but their southern limit is poorly defined. These rocks were formerly mapped as "Badger gneiss" by Findlay (1963) who considered them to be contact-metamorphosed equivalents of the Nicola Group. The syenodiorite is confined to the southeastern margin of the intrusion where it is unconformably overlain by the Princeton Group.

Essential minerals are plagioclase (andesine), clinopyroxene, hornblende and potassium feldspar with minor biotite and opaques and accessory apatite and sphene. Syenodiorite is more leucocratic than syenogabbro and contains slightly less calcic plagioclase (Findlay, 1963, 1969). Textures range from equigranular to foliated and some rocks exhibit strong mineral elongation. Most gabbroic rocks are extensively saussuritized and appear various shades of green; fresh rocks are pale to medium grey or pinkish grey, depending on the nature and proportion of the feldspar. Sulphide-rich hornblende-bearing gabbro-diorite (described below) occurs as thin units within olivine clinopyroxenite in the bed of the Tulameen River.

MAGMATIC STRATIGRAPHY: TULAMEEN RIVER SECTION

An almost continuous stratigraphic section (530 m) along the Tulameen River, beginning at the eastern margin of the dunite and passing through olivine clinopyroxenite into syenogabbro is presented in Figure 9.4. The section is cut by unfoliated hornblende-bearing dacitic and basaltic dikes, probable feeders for Tertiary lavas in the Princeton Group and Miocene basalts, and contains faults at the dunite-pyroxenite and pyroxenite - gabbro-diorite contacts. Two thin gabbro-diorite units are also well exposed within the pyroxenite.

OLIVINE CLINOPYROXENITE

The olivine clinopyroxenite unit is rather massive and characterized by abundant xenoliths of dunite ranging in size from a few centimetres to 10 metres or more. Xenoliths locally contain clinopyroxene megacrysts or crystal clots, and some of the larger bodies of dunite enclose pyroxenite xenoliths that appear to have been derived from their host.

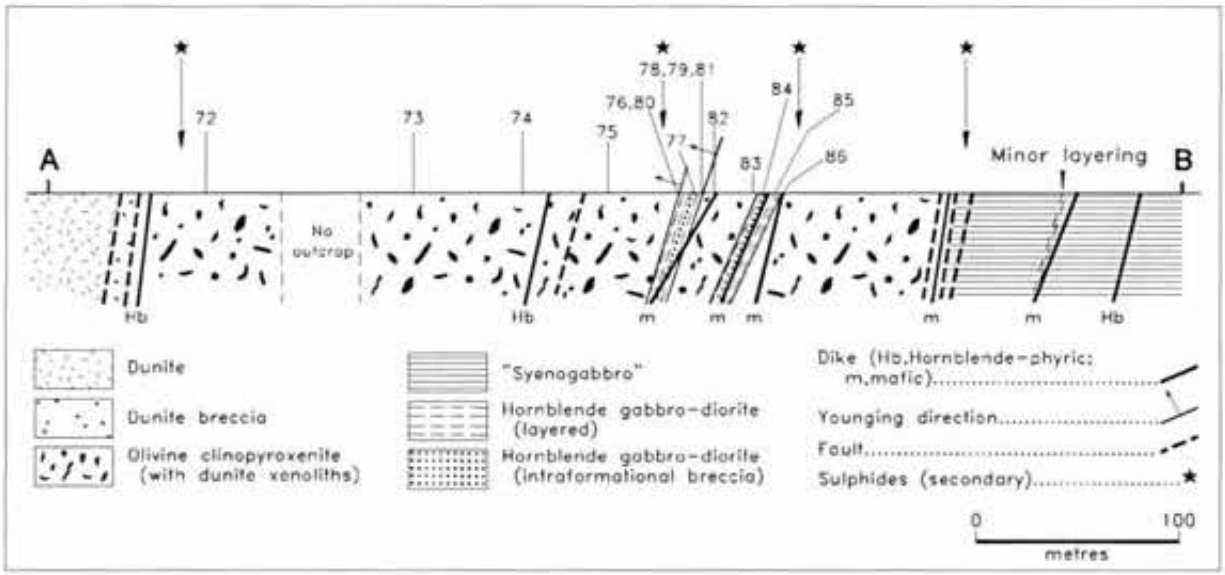

Figure 9.4. Stratigraphic section along the Tulameen River bed at the eastern margin of the dunite (*see* Figure 9.3 for location).

Photo 9.2. Intricately contorted ribbon-shaped xenolith of dunite (Du) in olivine clinopyroxenite (Px), Tulameen River section. Veins of carbonate and serpentine cut both xenolith and host.

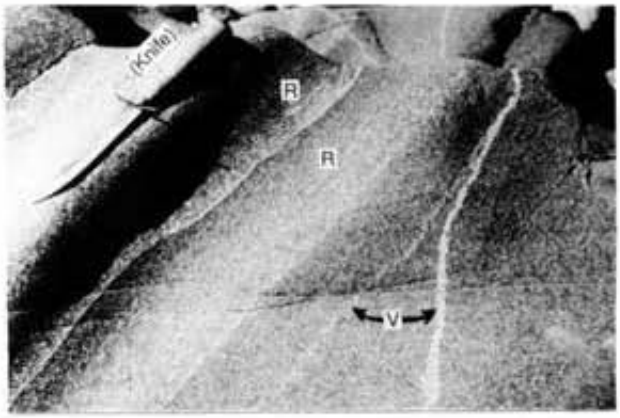

Photo 9.3. Reverse modal grading (R) of plagioclase and amphibole crystals in layered gabbro-diorite within olivine clinopyroxenite, Tulameen River section. Leucogabbro-leucodiorite segregation veinlets (V) are injected parallel to, and across, the layering.

Xenolith shapes are diverse: round, wispy, tabular, or distinctly elongate and contorted; contacts with their pyroxenite host are planar to irregular or crenulate (Photo 9.2). Rarely, dunite and pyroxenite are interlayered and appear to have behaved as cohesive blocks within the unit. However, the majority of xenoliths preserve features that suggest that they were deformed while hot and still capable of plastic deformation. The origin of these textures is probably related to episodic slumping of dunite-pyroxenite layered cumulates deposited elsewhere in the intrusion and emplaced at their present location by mass flowage down the cumulate slope.

GABBRO-DIORITE

Hornblende-bearing gabbro-diorite units within the olivine clinopyroxenite each contain three medium-grained subunits comprising a lower and upper layered sequence separated by gabbro-diorite breccia. Contacts with the olivine clinopyroxenite are sharp and depositional. The layered gabbro-diorite units preserve a wealth of sedimentary features including modal grading of plagioclase and ferromagnesian phenocrysts (largely amphibole) in which the density grading may be normal or reverse in different layers (Photo 9.3); and erosional unconformities which transect earlier layers (Photo 9.4). The latter features consistently indicate that stratigraphic tops face west towards the dunite "core". The brecciated layers contain rounded to angular gabbro-diorite blocks enclosed in a uniform gabbro-diorite mesostasis that may be slightly more leucocratic or melanocratic than the majority of the blocks. Most of the above features may be related to the action of magmatic convection currents or mass wasting of previously crystallized cumulates. Both gabbro-diorite units are enriched in sulphides which appear to be concentrated in the upper layered gabbro-diorite subunit.

Photo 9.4. Layered hornblende-bearing gabbro-diorite, Tulameen River section. Note erosional truncation of layering (E) indicating stratigraphic tops face right (upstream) or west.

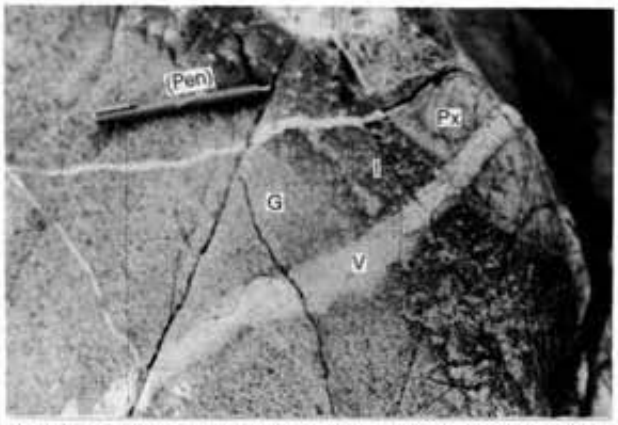

Photo 9.5. Segregation vein (V) of leucogabbro-leucodiorite cutting base of layered gabbro-diorite (G), underlying olivine clinopyroxenite unit (Px) and an intermediate uralitized zone (I). Note diffuse margins of vein in gabbro-diorite and sharp contacts in pyroxenite.

A prominent feature of the gabbro subunits is the presence of leucogabbro-leucodiorite veins and stringers containing acicular "quench" amphiboles. These veins crosscut and parallel the layering for short distances, and locally transect both the upper and lower contacts with the pyroxenite. Where this occurs, many veins that have diffuse margins in the gabbro-diorite form sharp contacts with the pyroxenite (Photo 9.5). These textural and mineralogical features indicate that leucocratic vein material formed when trapped intercumulus liquids migrated out of gabbro cumulates. Migration of intercumulus liquids in this case may well have been promoted by rapid loading of the cumulate pile caused by sudden deposition of cumulates from dunite-pyroxenite density flows.

CONTACT RELATIONSHIPS

NICOLA - ULTRAMAFIC ROCKS

Evidence of intrusion into the Nicola Group is rare. However, such relationships have been observed 0.5 kilometre south of Blakeburn Creek, near the gabbro-ultramafic contact, where rafts of Nicola metasedimentary rocks are intruded by gabbro and hornblendite, and in mafic pegmatite, exposed in logging cuts on the western slopes of Grasshopper Mountain, which contains angular xenoliths (<40 cm across) of hornblende dacite derived from Nicola wallrocks.

GABBROIC - ULTRAMAFIC ROCKS

Relationships between gabbroic and ultramafic rocks are complex. Intrusive breccias with a net-veined texture comprising gabbroic blocks set in a hornblende clinopyroxenite - hornblendite mesostasis were observed at several localities. In Newton Creek, thin (<15 cm) hornblende clinopyroxenite dikes intrude gabbro and both are crosscut by leucocratic gabbroic stringers (1 cm). In the Tulameen River, gabbro-diorite is interlayered with olivine clinopyroxenite and Findlay (1963) noted gabbroic dikes cutting hornblende clinopyroxenite. These relationships point to more than one episode of gabbro-diorite crystallization as opposed to remobilization of previously solidified gabbros (Findlay, 1969).

DUNITE - OLIVINE CLINOPYROXENITE

Thin (<20 cm) olivine clinopyroxenite dikes cut dunite on the southern flank of Olivine Mountain and north of the summit of Grasshopper Mountain near the dunite-pyroxenite contact. In addition, pyroxenite veins a few centimetres in width occur in clinopyroxene-bearing dunite exposed in the Tulameen River below the confluence with Britton Creek. These veins exhibit postemplacement boudinage and may represent clinopyroxene-rich intercumulus liquids that segregated and migrated through hot dunite at the brittle-ductile transition.

OLIVINE CLINOPYROXENITE - HORNBLENDE CLINOPYROXENITE

The only contact between hornblende clinopyroxenite and olivine clinopyroxenite examined in detail was that which crosses the Tulameen River near the western margin of the complex. Here, hornblende clinopyroxenite with pegmatitic masses of hornblende, clinopyroxene, biotite and magnetite grades into a medium to coarse-grained olivine clinopyroxenite cut locally by thin (<8 cm) dikes of finer grained pyroxenite.

SUMMARY OF CONTACT RELATIONSHIPS

Findlay (1963, 1969) concluded from his observations of contact relationships that the gabbroic and ultramafic parts of the complex represented two separate intrusions, an early gabbroic-dioritic mass invaded by an ultramafic body in which dunite was the last unit emplaced. One outcrop in the Tulameen River section that was used to support intrusion of dunite into olivine clinopyroxenite has been re-interpreted in this study as representing the products of magmatic debris flows that incorporated partly consolidated dunite-pyroxenite layered cumulate sequences. These relationships, and the occurrence of pyroxenite dikes cutting dunite, suggest that the dunite crystallized prior to the pyroxenites. The main body of gabbroic rocks to the east may largely predate emplacement of the ultramafic rocks, although localized gradational contacts are observed. Thin sequences of gabbro-diorite cumulates interlayered with

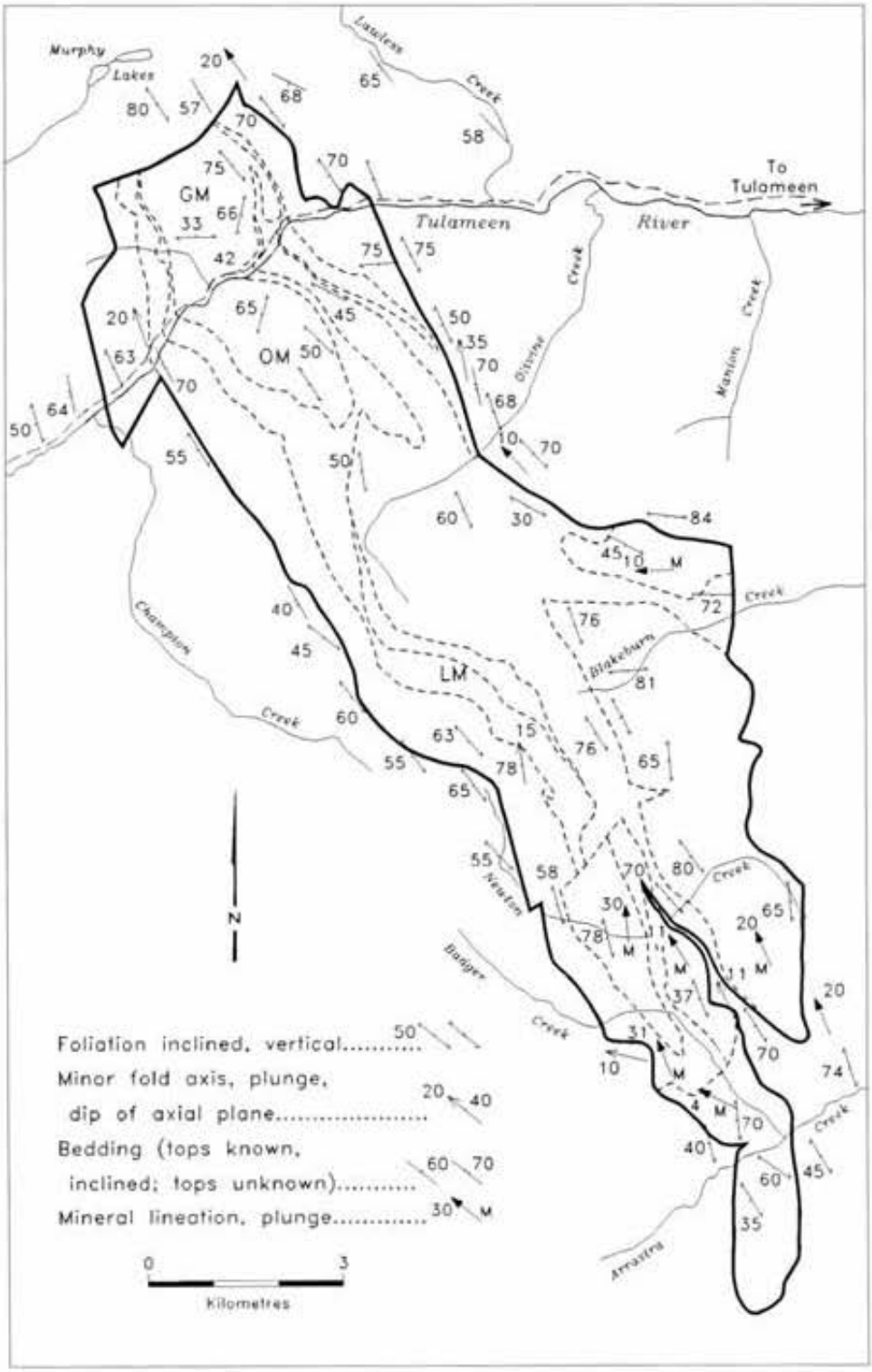

Figure 9.5. Representative measurements of structural fabrics in the Nicola Group and Tulameen ultramafic complex.

olivine clinopyroxenite, and gabbroic dikes cutting hornblende clinopyroxenite point to a protracted history of gabbro-diorite crystallization involving more than one influx of parental magma.

STRUCTURE

Structural data for the Tulameen complex and its hostrocks are given in Figure 9.5.

REGIONAL FOLIATION

A penetrative foliation, generally striking north-northwest and dipping steeply to the west, is especially pronounced in Nicola metasedimentary rocks and is also evident in the Mount Lytton-Eagle Plutonic Complex and mafic-ultramafic units of the Tulameen complex (Figure 9.5). Within the Nicola Group, the foliation is parallel to bedding and axial planar to eastward-verging minor isoclinal folds in thinly laminated argillites, tuffaceous siltstones and crosscutting quartz veins. The axes of these folds plunge gently (5 to 20°) to the north. Structures related to this phase of deformation are exposed on the Tulameen River road at the contact of the Eagle granodiorite and Nicola Group. Apophyses of granodiorite that intrude Nicola marbles are boudinaged and folded about axes lying within the plane of the regional foliation (Photo 9.6). These structures lie at the eastern margin of the Eagle Shear Zone, a ductile zone of Middle to Late Jurassic contractional deformation with eastward-verging regional kinematic indicators (Greig, 1992).

CHROMITITE SCHLIEREN

The distribution and structural controls of chromitite in the Tulameen complex have important economic implications. Extensive areas of dunite exhibit a weak to strong foliation that is variable in attitude but generally steeply inclined (Figure 9.4). Chromitite schlieren are locally oriented within the foliation and serve as structural indicators for strain within the dunite. The schlieren are generally 0.5 to 2 centimetres in width and 5 to 25 centimetres long. The most notable concentrations of chromitite were seen on the southern flanks of Grasshopper Mountain. Boudinaged chromitite layers and tight to isoclinal minor folds have been observed, as well as peculiar "ring structures" that may represent cross-sections through domical folds (Photo 9.7). Some of these structures are associated with the development of the foliation; other folds clearly postdate this fabric (Photo 9.8). In the latter case, the foliation is emphasized by micaceous alteration products (serpentine and talc) and serpentine veinlets have been folded. Evidently, the latter phases of ductile deformation took place at temperatures below the upper thermal stability limit of serpentine (<500°C).

Although data are sparse, there appears to be no concentric arrangement of either the foliation or chromitite schlieren within the dunite that might be expected during emplacement of a crystal mush (Findlay, 1963, 1969). However, there is some indication that radical changes in the attitude of the fabric are related to faulting, such as the change from northerly to predominantly easterly dipping structures across a north-trending fault bisecting Grasshopper Mountain (Figure 9.3). Despite these complexities, isoclinal folds in chromitite schlieren and the layer-parallel foliation within the dunite mimic structural elements in the country rocks. It seems reasonable to equate the locally penetrative fabric of the dunite with the regional foliation. Chromitite schlieren within the dunite presumably represent vestiges of formerly much more extensive cumulate layers.

Photo 9.6. Boudinaged and tightly folded dikes of Mount Lytton-Eagle granodiorite (G) penetrating thinly bedded, skarned marbles (M) and mica schists of the Nicola Group. Nicola schistosity is axial planar to folded dikes.

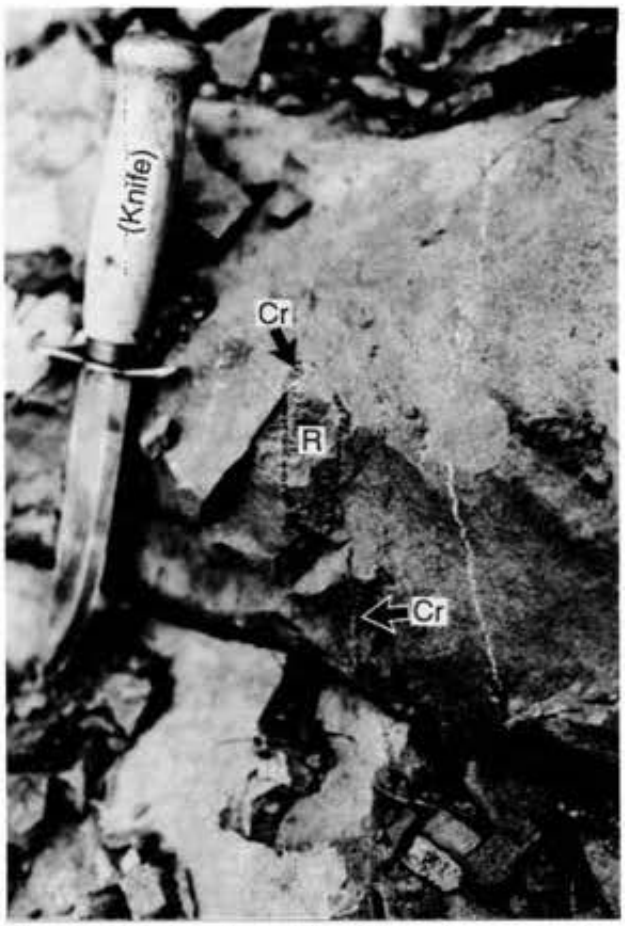

Photo 9.7. Chromitite layers (Cr) exhibiting ring structure (R) or "condom" fold in dunite, Grasshopper Mountain.

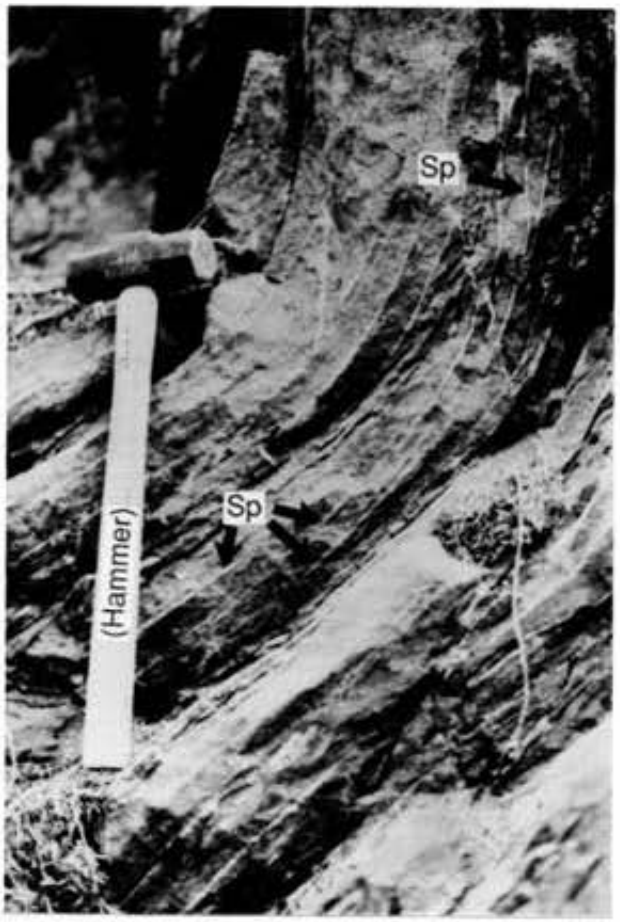

Photo 9.8. Hinge zone of rare minor fold in strongly foliated serpentinized dunite, Tulameen River road. Serpentine veinlets (Sp) lying within the foliation predate this folding event.

Photo 9.9. Tightly folded mylonitized gabbro-diorite at the northwestern extremity of the complex, west of Grasshopper Mountain.

BRITTLE AND DUCTILE FAULTS

High-angle faults are well exposed in the Tulameen River section (Figure 9.3). The eastern margin of the dunite is sheared and locally contains a cataclastic breccia comprising rounded dunite fragments set in a serpentinized matrix. A major high-angle fault at the contact between the major units of olivine clinopyroxenite and gabbroic rocks in the bed of the Tulameen River is marked by a mylonite zone 3.5 metres wide containing sheared quartz veins and disseminated pyrite. The gabbroic rocks near the fault zone are heavily saussuritized, locally pyritic, cut by veins of potassium feldspar, and rarely preserve primary cumulate layering. An unfoliated mafic dike intruding the mylonite zone confirms that ductile faulting was pre-Eocene.

All of the contacts between the Tulameen complex and Nicola Group observed in the field, with the few exceptions noted earlier, are ductily sheared or faulted. A package of strongly schistose to mylonitic rocks is distinguished at the northwestern margin of the complex (Figures 9.2 and 9.3). Phyllites, chlorite-muscovite-biotite±amphibole schists and mylonites characterized by well-developed flaser textures and amphibole augen are all represented. Contacts between the mylonitic rocks and Nicola Group are gradational and marked by increasing degrees of ductile strain whereas the ultramafic contact appears more sharply defined by faults. In a logging cut on the western side of Grasshopper Mountain, foliated gabbros with intense mineral elongation, schistose layers and quartz rodding have been tightly folded about minor fold axes plunging up to 45° west-northwest (Photo 9.9). These rocks were originally mapped by Findlay (1963) as part of the Nicola, but they clearly include retrograde bodies of hornblende clinopyroxenite and gabbro. The margin of the intrusion in this area is interpreted to represent a ductile shear zone that has subsequently undergone folding and faulting. A thin (2 m wide) shear zone with a similarly complex history occurs in hornblende clinopyroxenite about 100 metres south of the summit of Lodestone Mountain.

At the eastern margin of the complex, northeast of Grasshopper Mountain, metre-wide pods of hornblendite are imbricated with Nicola volcanic breccias along heavily chloritized high-angle shear zones. The attitude of the contact and the planar fabric in rocks at this boundary commonly appears concordant with the regional foliation. Farther south along the same shear zone, at Olivine Creek, the intensity of mineral elongation lineations in Nicola tuffs and minor gabbroic intrusions increases dramatically towards the contact. In general, lineations due to rodding and mineral streaking developed at the margins and locally within the intrusion are gently to moderately plunging (10 to 35°) to the northwest (Figure 9.5). Examination of kinematic indicators in the field suggests that major north-northwest-trending high-angle faults bounding the complex, and some fault zones within the complex, have a dextral component of motion (Rublee, 1994).

Brittle deformation of the Tulameen complex is commonly related to northeasterly to easterly trending high-angle faults manifested by zones of intense brecciation, clay fault gouge, quartz and carbonate veining, and manganese-

stained slickensided fault surfaces. Brecciated dunite is well exposed near the mouth of Britton Creek. Fragments are subangular to well rounded and cemented by coarsely crystalline serpentine (antigorite?) and finely comminuted dunite. The breccia is tectonic in origin and localized by a northeast-trending fault along the Tulameen River (Figure 9.3). A high-angle fault at the northern termination of the complex has caused extensive brecciation of all exposed lithologies including Tertiary dikes. Slickensides along the fault plane indicate a vertical component of motion.

MINERALIZATION AND GEOCHEMISTRY

The distribution and mineralogy of the PGE in bedrock and placer occurrences in the Tulameen district are treated in detail in Chapter 10. Newly discovered and previously recognized sulphide localities are shown in Figure 9.3. The most notable new showings occur in thin gabbro-diorite units within olivine clinopyroxenite in the Tulameen River section (Figure 9.4). Here, sulphides, predominantly pyrite, are disseminated throughout the rock and locally line fractures. All of these sulphides are confined to the heavily saussuritized gabbroic rocks and appear to be secondary in origin.

Analyses of PGE and other metals in 100 lithogeochemical samples from the Tulameen complex and Nicola Group are presented in Table 9.1. Sample locations are given in Appendix C and shown in Figure 9.6. Four geochemical laboratories were used and three different analytical methods, including instrumental neutron activation, inductively coupled plasma mass spectrometry and atomic absorption with a graphite furnace finish (*see* footnotes in Table 9.1). The highest abundances of PGE are found in chromitites and reach a maximum of 17.5 ppm platinum, 430 ppb iridium and 140 ppb rhodium in sample GN-87-40. Chromitites enriched in PGE contain low palladium (82 ppb or less) and are characterized by very high Pt/Pd ratios. Gold abundances are uniformly low apart from a single anomalous hornblende clinopyroxenite (102 ppb, Table 9.1). A distinct feature of the data is the large variation in the abundances of Pt, Pd and Au in different splits of the same sample. These variations appear much too large to be attributed to differences in analytical techniques or errors alone, and point to sample inhomogeneity caused by the presence of discrete platinum-group minerals (PGM). These minerals and the geochemical signatures they create are treated more fully in Chapter 10.

SUMMARY: STRUCTURAL AND EMPLACEMENT HISTORY

The Tulameen mafic-ultramafic complex records a prolonged and complex history of locally penetrative ductile and brittle deformation. Greenschist-grade assemblages prevalent in the Nicola Group east of the complex increase to amphibolite grade in the west as the contact with the Mount Lytton - Eagle Plutonic Complex is approached. The oldest structures recognized in both the Tulameen complex and host-rocks of the Nicola Group are a westward-dipping layer-parallel foliation and associated northwest-plunging minor isoclinal folds. These data are consistent with a Middle to Late Jurassic phase of eastward-verging contractional deformation(Greig, 1992; Greig *et al.*, 1992). Adjacent to the Tulameen complex, however, we have been unable to demonstrate any large-scale recumbent stratigraphy. Major ductile shear zones or faults oriented along the strike of the complex were indeed active prior to Early Tertiary intrusion of granitic stocks and dikes. Faulting in the Tulameen River section involving imbrication by thrusting or folding may partly explain the intricate repetition of clinopyroxenite and gabbro units in the northeastern and southern parts of the complex. Kinematic indicators within mylonitic fabrics in ductile faults at the margins of the complex provide evidence for a dextral sense of shear (Rublee, 1994). These fault movements may be related to early motion along the Fraser - Straight Creek fault system (Monger, 1985) but, unfortunately, the magnitude of displacement is unknown. Northeasterly and easterly trending cross faults are related to a Tertiary "transtensional" structural regime prevalent at this time in the southwestern Intermontane Belt (Monger, 1985).

Evidence for folding and thrusting of the Nicola Group by mid-Cretaceous time is found in the Cache Creek - Ashcroft area. Here, Travers (1978, 1982) documented structural elements in Nicola and Ashcroft strata that are remarkably similar to those described above in the Tulameen region. Furthermore, he demonstrated the presence of large-scale recumbent folding and easterly directed thrusting in response to eastward overthrusting of the Cache Creek Terrane on Quesnellia. Using these data, Monger (1985) speculatively linked the eastern boundary of the southern Mount Lytton - Eagle Plutonic Complex with its southwest-dipping gneissosity and adjacent concordant schist belt (Nicola Group) with the eastward-verging structures near Ashcroft. Our interpretation of the structure of the Tulameen complex and Nicola host-rocks is consistent with Monger's speculation that the two regions represent different structural levels of the same fold and thrust package.

Findlay (1963, 1969) interpreted ultramafic rocks of the Tulameen complex as reflecting an original igneous zonation formed in a "proto-stratiform" laccolith-like body in the order dunite, olivine clinopyroxenite, hornblende clinopyroxenite. The zonal configuration of units expressed in outcrop was formed subsequently during forceful emplacement of the dunite layer (or "core"), intruded as a partly consolidated crystal mush into the overlying pyroxenites (or "shell"). The dunite provided a "piston-like" locus of stress for deformation and tilting of overlying gabbroic and surrounding country rocks. Crystallization and emplacement were regarded as partly synchronous with regional deformation of Upper Triassic Nicola rocks in order to explain the lack of well-developed cumulate layering within the complex.

Uncertainties regarding the structural evolution of the Tulameen complex and the paucity of intrusive contacts precludes any firm assessment of original intrusion geometry, although a sill-like body modified by faulting appears reasonable. Gradational contacts among pyroxenite units (especially in the western half of the complex), interlayered

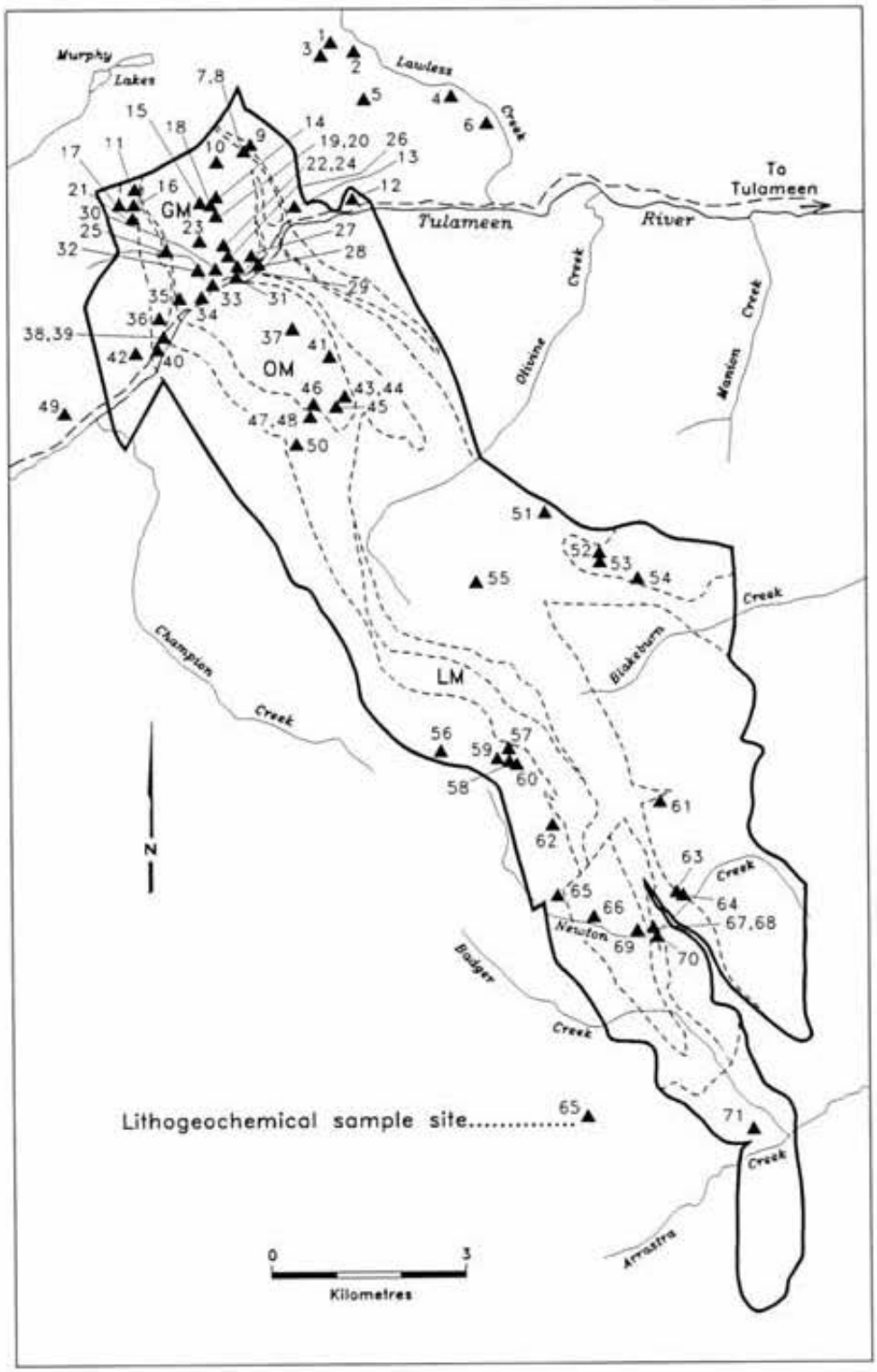

Figure 9.6. Location of lithogeochemical sample sites. Units as in Figures 9.2 and 9.5.

TABLE 9.1
ABUNDANCES OF NOBLE METALS AND OTHER ELEMENTS IN THE
TULAMEEN COMPLEX AND ASSOCIATED ROCKS

Locality	Sample	Anal. Method	Fe wt%	Cu	Zn	Ni	Cr	As	Sb	Pt	Pd	Rh	Ru	Ir	Os	Au
				ppm						ppb						
Chromitite and Chromitiferous Dunite																
26	GN-87-28	1	-	-	-	-	-	-	-	260.0	10.0	13.0	<5	4.1	3.0	11.0
26	GN-87-28	4	21.00	-	<500	884	74567	1.5	0.4	307.0	<15	10.0	43.0	13.0	<3	3.3
24	GN-87-29A	1	-	-	-	-	-	-	-	29.0	<5	2.0	<5	1.7	<2	<0.5
24	GN-87-29A	4	8.50	-	<500	1231	7775	<1	<0.2	60.0	55.0	2.0	<5	4.5	<3	<1
24	GN-87-29B	1	-	-	-	-	-	-	-	220.0	5.0	8.0	<5	11.0	<2	1.9
24	GN-87-29B	4	11.00	-	<500	1235	25378	<1	0.7	381.0	113.0	5.0	<5	23.0	<3	2.2
22	GN-87-30	2	-	4	40	1300	-	2.0	1.0	11.1	<0.5	-	-	-	-	2.4
22	GN-87-30	3	-	-	-	-	-	-	-	7.6	<0.1	-	-	-	-	0.7
22	GN-87-30	4	11.00	-	<500	1418	5752	<1	<0.2	16.0	72.0	<1	<5	2.1	<3	2.1
23	GN-87-32	2	-	18	83	387	-	4.0	<0.5	135.0	<0.5	-	-	-	-	3.6
23	GN-87-32	3	-	-	-	-	-	-	-	8.4	<0.1	-	-	-	-	1.3
23	GN-87-32	4	28.00	-	1695	1253	261110	4.1	0.5	<30	<30	11.0	37.0	76.0	6.0	1.2
23	GN-87-32*	3	-	-	-	-	-	-	-	11.6	<0.1	-	-	-	-	2.1
32	GN-87-33	2	-	9	67	396	-	2.0	<0.5	2060.0	5.6	-	-	-	-	12.4
32	GN-87-33	3	-	-	-	-	-	-	-	502.0	2.6	-	-	-	-	0.3
32	GN-87-33	4	25.00	-	1126	1000	223322	3.1	0.4	1316.0	<30	14.0	<5	223.0	14.0	1.3
33	GN-87-34	2	-	11	76	882	-	11.0	7.0	715.0	6.2	-	-	-	-	2.9
33	GN-87-34	3	-	-	-	-	-	-	-	608.0	6.4	-	-	-	-	1.1
33	GN-87-34	4	11.00	-	<500	926	20339	<1	0.5	749.0	82.0	3.0	<5	7.7	<3	2.2
32	GN-87-35	2	-	8	125	816	-	2.0	1.0	269.0	2.1	-	-	-	-	9.4
32	GN-87-35	3	-	-	-	-	-	-	-	312.0	2.6	-	-	-	-	1.2
32	GN-87-35	4	17.00	-	<500	1053	48334	<1	0.3	318.0	<30	9.0	17.0	15.0	<3	2.5
15	GN-87-36	1	-	-	-	-	-	-	-	6.0	16.0	<1	<5	0.3	<2	0.5
15	GN-87-36	2	-	3	41	1600	-	14.0	1.0	<1	<0.5	-	-	-	-	2.2
15	GN-87-36	3	-	-	-	-	-	-	-	1.8	<0.1	-	-	-	-	0.4
14	GN-87-37	1	-	-	-	-	-	-	-	1300.0	7.0	16.0	10.0	17.0	7.0	9.5
14	GN-87-37	2	-	5	33	1100	-	2.0	2.0	2445.0	8.8	-	-	-	-	11.9
14	GN-87-37	3	-	-	-	-	-	-	-	2003.0	8.1	-	-	-	-	2.9
18	GN-87-38	1	-	-	-	-	-	-	-	<79	<5	2.0	<5	6.2	<2	<0.5
18	GN-87-38	2	-	5	27	1500	-	2.0	0.5	16.8	<0.5	-	-	-	-	4.5
18	GN-87-38	3	-	-	-	-	-	-	-	22.8	<0.1	-	-	-	-	0.1
20	GN-87-40	1	-	-	-	-	-	-	-	13000.0	40.0	140.0	<20	430.0	37.0	17.0
20	GN-87-40	2	-	18	80	150	-	1.0	3.0	17541.0	71.2	-	-	-	-	55.2
20	GN-87-40	3	-	-	-	-	-	-	-	9869.0	64.9	-	-	-	-	22.1
20	GN-87-41	1	-	-	-	-	-	-	-	41.0	<5	<1	<5	0.5	<2	1.5
20	GN-87-41	2	-	2	32	1200	-	<1	0.6	66.6	2.2	-	-	-	-	40.7
20	GN-87-41	3	-	-	-	-	-	-	-	116.0	<0.1	-	-	-	-	<0.1
44	GN-87-80	1	-	-	-	-	-	-	-	57.0	<5	<1	<5	0.3	<2	1.5
44	GN-87-80	4	13.00	-	<500	992	2292	3.5	0.9	88.0	18.0	2.0	<5	0.7	<3	1.7
10	GN-87-146	1	-	-	-	-	-	-	-	2500.0	5.0	20.0	<10	17.0	8.0	2.5
10	GN-87-146	2	-	8	46	878	-	1.0	3.0	9297.0	73.3	-	-	-	-	32.3
10	GN-87-146	3	-	-	-	-	-	-	-	3189.0	23.4	-	-	-	-	3.8
19	GN-87-147	1	-	-	-	-	-	-	-	5600.0	75.0	56.0	<5	140.0	20.0	21.0
19	GN-87-147	2	-	17	127	105	-	2.0	3.0	7953.0	58.8	-	-	-	-	26.8
19	GN-87-147	3	-	-	-	-	-	-	-	5527.0	46.7	-	-	-	-	22.8
19	GN-87-147	4	22.00	-	681	796	135605	26.0	1.1	8348.0	<30	70.0	<15	243.0	50.0	40.0
19	GN-87-147*	3	-	-	-	-	-	-	-	5380.0	39.5	-	-	-	-	15.3
20	GN-87-148	1	-	-	-	-	-	-	-	5300.0	12.0	67.0	50.0	220.0	25.0	15.0
20	GN-87-148	3	-	-	-	-	-	-	-	4762.0	19.3	-	-	-	-	18.9
20	GN-87-148	4	17.00	-	<500	1062	105550	<1	5.8	7398.0	<15	68.0	<20	247.0	48.0	23.0
34	GN-87-159	1	-	-	-	-	-	-	-	810.0	8.0	11.0	39.0	6.5	3.0	1.7
34	GN-87-159	2	-	7	78	1100	-	2.0	<0.5	1073.0	25.0	-	-	-	-	5.8
34	GN-87-159	3	-	-	-	-	-	-	-	837.0	6.4	-	-	-	-	<0.1
34	GN-87-159*	3	-	-	-	-	-	-	-	1067.0	7.6	-	-	-	-	<0.1
72	GN-87-166+	2	-	9	69	729	-	1.0	3.0	450.0	2.1	-	-	-	-	4.3

Table 9.1 continued

Locality	Sample	Anal. Method	Fe wt%	Cu	Zn	Ni	Cr	As	Sb	Pt	Pd	Rh	Ru	Ir	Os	Au
				ppm						ppb						
Dunite																
27	GN-87-10	2	-	4	29	270	-	16.0	0.5	4.7	<0.5	-	-	-	-	2.9
27	GN-87-10	3	-	-	-	-	-	-	-	5.0	<0.1	-	-	-	-	<0.1
27	GN-87-10	4	3.80	-	<500	336	1497	<1	<0.2	17.0	13.0	2.0	<5	<0.1	<3	3.6
29	GN-87-11A	2	-	2	52	1200	-	3.0	2.0	7.1	<0.5	-	-	-	-	2.6
29	GN-87-11A	3	-	-	-	-	-	-	-	7.6	<0.1	-	-	-	-	0.3
29	GN-87-11A	4	8.70	-	<500	1134	1971	<1	0.6	<5	43.0	<1	60.0	1.3	<3	1.8
29	GN-87-11B	1	-	-	-	-	-	-	-	<9	14.0	<1	<5	0.3	<2	4.2
29	GN-87-11B	4	7.10	-	<500	1186	1382	2.9	0.2	<20	-	1.0	56.0	0.7	<3	<1
30	GN-87-12	1	-	-	-	-	-	-	-	18.0	17.0	<1	<5	0.4	<2	1.1
30	GN-87-12	4	12.00	-	803	887	1825	3.7	0.3	90.0	46.0	<1	12.0	0.6	<3	2.2
35	GN-87-24	2	-	11	54	945	-	19.0	1.0	420.0	3.3	-	-	-	-	3.7
35	GN-87-24	3	-	-	-	-	-	-	-	106.0	<0.1	-	-	-	-	<0.1
35	GN-87-24	4	8.80	-	<500	1036	1306	5.0	0.4	110.0	57.0	<1	42.0	0.9	<3	3.3
41	GN-87-48	1	-	-	-	-	-	-	-	53.0	16.0	<1	<5	0.2	<2	0.7
41	GN-87-48	4	7.80	-	506	904	1192	2.7	1.3	67.0	<5	<1	<5	0.4	<3	<1
37	GN-87-51	2	-	6	91	1900	-	1.0	1.0	61.4	21.5	-	-	-	-	59.1
37	GN-87-51	3	-	-	-	-	-	-	-	11.8	<0.1	-	-	-	-	<0.1
37	GN-87-51	4	9.80	-	<500	1795	2873	<1	<0.2	18.0	23.0	2.0	<5	1.2	<3	<1
43	GN-87-79	1	-	-	-	-	-	-	-	<9	<5	<1	<5	0.5	<2	0.6
43	GN-87-79	2	-	3	36	930	-	1.0	0.6	213.0	0.8	-	-	-	-	5.1
43	GN-87-79	3	-	-	-	-	-	-	-	175.0	<0.1	-	-	-	-	<0.1
46	GN-87-86	1	-	-	-	-	-	-	-	40.0	<5	<1	<6	0.2	<2	1.9
46	GN-87-86	2	-	5	42	867	-	14.0	2.0	90.8	0.9	-	-	-	-	3.0
46	GN-87-86	3	-	-	-	-	-	-	-	116.0	0.9	-	-	-	-	<0.1
82	GN-87-177	1	-	-	-	-	-	-	-	40.0	<5	<1	<5	0.2	<2	1.5
82	GN-87-177	2	-	35	73	855	-	26.0	2.0	28.3	<0.5	-	-	-	-	3.7
82	GN-87-177	3	-	-	-	-	-	-	-	27.1	<0.1	-	-	-	-	0.8
82	GN-87-177	4	9.30	-	<500	1036	<100	21.0	1.3	27.0	9.0	<1	<5	0.1	<3	1.2
Serpentinite																
18	GN-87-39	1	-	-	-	-	-	-	-	<5	<5	7.0	<5	0.2	<2	1.1
18	GN-87-39	4	5.30	-	<500	1386	3959	3.2	1.4	<5	41.0	<1	<20	<0.1	<3	<1
Olivine Clinopyroxenite																
48	GN-87-77	1	-	-	-	-	-	-	-	120.0	<5	<1	<5	0.1	12.0	1.8
48	GN-87-77	4	12.00	-	<500	591	645	1.6	1.3	117.0	19.0	1.0	<5	0.2	14.0	<1
47	GN-87-84	1	-	-	-	-	-	-	-	150.0	<5	<1	<5	<0.1	<2	2.4
47	GN-87-84	2	-	6	21	201	-	1.0	<0.5	190.0	2.2	-	-	-	-	3.3
47	GN-87-84	3	-	-	-	-	-	-	-	66.0	0.4	-	-	-	-	0.5
47	GN-87-84*	3	-	-	-	-	-	-	-	63.2	0.9	-	-	-	-	0.4
7	GN-87-143	2	-	4	31	300	-	5.0	0.7	6.9	0.5	-	-	-	-	45.8
7	GN-87-143	3	-	-	-	-	-	-	-	20.7	0.2	-	-	-	-	<0.1
7	GN-87-143	4	7.10	-	<500	342	735	4.4	0.4	7.0	34.0	<1	<5	<0.1	<3	<1
8	GN-87-144	2	-	2	46	660	-	1.0	<0.5	56.7	0.7	-	-	-	-	9.2
8	GN-87-144	3	-	-	-	-	-	-	-	48.0	0.4	-	-	-	-	1.2
8	GN-87-144	4	7.30	-	<500	699	2090	<1	0.3	60.0	52.0	2.0	<5	0.5	<3	1.3
9	GN-87-145	2	-	3	75	99	-	1.0	<0.5	3.2	4.7	-	-	-	-	9.6
9	GN-87-145	3	-	-	-	-	-	-	-	3.7	2.5	-	-	-	-	1.2
9	GN-87-145	4	19.00	-	<500	<100	<100	<1	0.3	<5	20.0	<1	<5	<0.1	<3	<1
31	GN-87-160	1	-	-	-	-	-	-	-	8.0	<5	<1	<5	<0.1	<2	1.7
31	GN-87-160	4	3.60	-	580	238	2017	<1	0.3	<20	<15	<1	<30	<0.1	<3	<1
25	GN-87-163	1	-	-	-	-	-	-	-	32.0	5.0	<1	<5	0.1	<2	0.9
25	GN-87-163	4	9.90	-	<500	988	2239	1.1	<0.2	35.0	<5	<1	24.0	0.2	<3	<1
73	GN-87-167	2	-	3	23	210	-	2.0	<0.5	8.3	<0.5	-	-	-	-	3.6
73	GN-87-167	3	-	-	-	-	-	-	-	7.5	<0.1	-	-	-	-	<0.1
73	GN-87-167	4	4.00	-	<500	304	1432	<1	<0.2	19.0	<15	<1	<5	0.2	<3	1.6
74	GN-87-168	1	-	-	-	-	-	-	-	<5	<5	<1	<5	<0.1	<2	3.4
74	GN-87-168	4	6.50	-	<500	189	1580	1.4	0.2	10.0	<10	<1	<5	<0.1	<3	2.1

Table 9.1 continued

Locality	Sample	Anal. Method	Fe wt %	Cu	Zn	Ni	Cr	As	Sb	Pt	Pd	Rh	Ru	Ir	Os	Au
				ppm						ppb						
75	GN-87-170	4	6.30	-	<500	204	1592	3.6	0.2	8.0	45.0	<1	11.0	0.2	<3	4.1
75	GN-87-170*	3	-	-	-	-	-	-	-	7.3	<0.1	-	-	-	-	1.5
79	GN-87-174	1	-	-	-	-	-	-	-	7.0	<5	<1	<5	<0.1	<2	7.9
79	GN-87-174	2	-	15	24	182	-	1.0	0.9	13.4	1.5	-	-	-	-	8.3
79	GN-87-174	3	-	-	-	-	-	-	-	9.1	<0.1	-	-	-	-	0.6
79	GN-87-174	4	2.00	-	<500	374	1274	<1	0.4	<20	<30	<1	<30	<0.1	<3	2.4
80	GN-87-175	1	-	-	-	-	-	-	-	7.0	<5	<1	<5	0.2	<2	2.6
80	GN-87-175	2	-	11	127	145	-	1.0	<0.5	1.0	2.4	-	-	-	-	3.5
80	GN-87-175	3	-	-	-	-	-	-	-	2.9	1.8	-	-	-	-	3.6
80	GN-87-175	4	8.20	-	<500	<100	1182	<1	<0.2	<5	43.0	<1	<5	0.2	<3	2.5
83	GN-87-179	1	-	-	-	-	-	-	-	8.0	<5	<1	<5	0.1	<2	1.4
83	GN-87-179	2	-	3	19	187	-	1.0	<0.5	7.8	<0.5	-	-	-	-	2.9
83	GN-87-179	3	-	-	-	-	-	-	-	5.6	<0.1	-	-	-	-	0.5
83	GN-87-179	4	2.80	-	<500	313	1208	<1	<0.2	<20	<5	<1	<30	<0.1	<3	2.6
45	GN-87-81	1	-	-	-	-	-	-	-	53.0	<5	<1	<5	0.3	<2	1.1
45	GN-87-81	4	4.30	-	<500	<100	2425	<1	0.2	20.0	<5	<1	<5	0.2	<3	2.2
Hornblende Clinopyroxenite																
12	GN-87-7	1	-	-	-	-	-	-	-	38.0	23.0	<1	<5	0.3	<2	0.5
12	GN-87-7	4	15.00	-	906	196	264	<1	0.4	60.0	78.0	<1	77.0	0.4	<3	1.5
36	GN-87-22	1	-	-	-	-	-	-	-	<5	12.0	<1	<5	<0.1	<2	1.4
36	GN-87-22	4	5.60	-	<500	106	3006	<1	0.6	<5	19.0	3.0	<5	<0.1	<3	3.9
16	GN-87-45	1	-	-	-	-	-	-	-	32.0	67.0	<1	<5	<0.1	<2	1.8
16	GN-87-45	2	-	269	92	207	-	<1	0.8	36.4	99.5	-	-	-	-	4.6
16	GN-87-45	3	-	-	-	-	-	-	-	35.3	92.6	-	-	-	-	4.8
50	GN-87-73	1	-	-	-	-	-	-	-	<5	<5	<1	<5	0.1	<2	2.4
50	GN-87-73	2	-	37	85	225	-	1.0	1.0	109.0	0.6	-	-	-	-	2.1
50	GN-87-73	3	-	-	-	-	-	-	-	1.8	1.8	-	-	-	-	0.3
53	GN-87-88	1	-	-	-	-	-	-	-	45.0	13.0	<1	<5	0.2	<2	1.3
53	GN-87-88	2	-	15	76	30	-	2.0	<0.5	128.0	8.0	-	-	-	-	102.0
53	GN-87-88	3	-	-	-	-	-	-	-	67.0	4.3	-	-	-	-	0.1
57	GN-87-93A	2	-	9	86	55	-	3.0	<0.5	4.7	0.5	-	-	-	-	11.2
57	GN-87-93A	3	-	-	-	-	-	-	-	5.7	0.4	-	-	-	-	1.3
57	GN-87-93A	4	22.00	-	856	<100	113	<1	0.2	12.0	<15	<1	7.0	0.1	<3	2.0
60	GN-87-97	2	-	6	82	76	-	1.0	<0.5	<1	1.6	-	-	-	-	7.3
60	GN-87-97	3	-	-	-	-	-	-	-	3.5	0.5	-	-	-	-	<0.1
56	GN-87-101	1	-	-	-	-	-	-	-	16.0	12.0	<1	<5	0.1	<2	0.6
56	GN-87-101	4	22.00	-	<500	<100	<100	<1	0.3	<5	25.0	<1	<5	<0.1	<3	<1
62	GN-87-102A	2	-	7	72	110	-	2.0	119.0	74.3	17.0	-	-	-	-	34.2
62	GN-87-102A	3	-	-	-	-	-	-	-	74.1	14.7	-	-	-	-	0.7
62	GN-87-102A	4	17.00	-	<500	130	193	<1	0.4	57.0	62.0	<1	<5	<0.1	<3	<1
62	GN-87-102B	2	-	5	70	120	-	1.0	0.5	17.9	3.9	-	-	-	-	3.8
62	GN-87-102B	3	-	-	-	-	-	-	-	20.6	4.0	-	-	-	-	<0.1
62	GN-87-102B	4	12.00	-	<500	202	438	<1	0.4	18.0	8.0	<1	<5	<0.1	<3	<1
55	GN-87-114	1	-	-	-	-	-	-	-	17.0	5.0	<1	<5	<0.1	<2	0.9
54	GN-87-117	1	-	-	-	-	-	-	-	9.0	<5	<1	<5	<0.1	<2	7.3
54	GN-87-117	4	11.00	-	<500	<100	<100	<1	0.4	10.0	7.0	<1	<5	<0.1	<3	1.3
63	GN-87-127	1	-	-	-	-	-	-	-	<9	<5	<1	<5	<0.1	<2	0.9
63	GN-87-127	4	15.00	-	<500	103	166	<1	0.3	6.0	11.0	<1	<5	<0.1	<3	<1
68	GN-87-129	1	-	-	-	-	-	-	-	11.0	22.0	<1	<5	<0.1	<2	1.6
68	GN-87-129	2	-	199	68	102	-	1.0	<0.5	12.6	16.0	-	-	-	-	9.7
68	GN-87-129	3	-	-	-	-	-	-	-	11.0	10.7	-	-	-	-	6.2
40	GN-87-150	1	-	-	-	-	-	-	-	<11	<5	<1	<5	<0.1	<2	<0.5
40	GN-87-150	4	9.70	-	<500	198	1335	1.8	<0.2	22.0	6.0	<1	<20	0.2	<3	2.1
38	GN-87-151	1	-	-	-	-	-	-	-	18.0	<5	<1	<5	0.2	<2	<0.5
38	GN-87-151	4	5.50	-	797	103	829	<1	0.3	18.0	14.0	<1	<20	0.3	<3	1.3

Table 9.1 continued

Locality	Sample	Anal. Method	Fe wt %	Cu	Zn	Ni	Cr	As	Sb	Pt	Pd	Rh	Ru	Ir	Os	Au
				ppm						ppb						
Hornblende Clinopyroxenite - Mylonitic																
42	GN-87-149	1	-	-	-	-	-	-	-	17.0	<5	<1	<5	0.3	<2	4.4
42	GN-87-149	2	-	57	80	83	-	6.0	1.0	17.6	11.4	-	-	-	-	3.1
42	GN-87-149	3	-	-	-	-	-	-	-	11.9	9.2	-	-	-	-	<0.1
Hornblende Clinopyroxenite - Pegmatitic																
39	GN-87-152	2	-	5	61	112	-	<1	<0.5	1.6	1.8	-	-	-	-	2.9
39	GN-87-152	3	-	-	-	-	-	-	-	1.1	0.8	-	-	-	-	0.7
39	GN-87-152	4	22.00	-	<500	285	194	1.2	0.4	14.0	6.0	<1	<5	0.1	<3	2.2
Hornblendite																
52	GN-87-90	1	-	-	-	-	-	-	-	<5	14.0	<1	<5	<0.1	<2	2.9
52	GN-87-90	4	18.00	-	<500	<100	201	3.3	0.5	82.0	33.0	<1	<5	<0.1	<3	6.0
63	GN-87-126	1	-	-	-	-	-	-	-	<5	40.0	<1	<5	0.2	<2	3.7
63	GN-87-126	4	19.00	-	<500	131	245	2.0	0.3	27.0	17.0	<1	<5	<0.1	<3	<1
67	GN-87-128A	1	-	-	-	-	-	-	-	7.0	12.0	<1	<5	<0.1	<2	3.3
67	GN-87-128A	4	14.00	-	657	148	<100	4.5	1.0	<5	40.0	<1	<5	<0.1	<3	<1
65	GN-87-131	1	-	-	-	-	-	-	-	18.0	14.0	<1	<5	0.2	<2	0.6
65	GN-87-131	4	22.00	-	<500	<100	<100	<1	0.2	24.0	<5	<1	<5	0.2	<3	<1
Hornblendite with Sulphides																
11	GN-87-55	1	-	-	-	-	-	-	-	<5	5.0	<1	<5	<0.1	<2	3.4
11	GN-87-55	4	19.00	-	1655	<100	<100	9.1	0.5	8.0	33.0	<1	<5	<0.1	<3	4.4
Gabbro-Diorite																
71	GN-87-3	1	-	-	-	-	-	-	-	<5	<5	<1	<5	<0.1	<2	1.1
71	GN-87-3	2	-	37	79	6	-	2.0	0.8	4.5	4.2	-	-	-	-	4.3
71	GN-87-3	3	-	-	-	-	-	-	-	4.3	1.4	-	-	-	-	<0.1
13	GN-87-9	1	-	-	-	-	-	-	-	16.0	58.0	<1	<5	0.5	<2	0.8
13	GN-87-9	2	-	105	83	13	-	3.0	1.0	8.3	18.7	-	-	-	-	4.8
13	GN-87-9	3	-	-	-	-	-	-	-	7.6	15.2	-	-	-	-	1.8
51	GN-87-92	1	-	-	-	-	-	-	-	<5	<5	<1	<5	<0.1	<2	3.0
51	GN-87-92	4	7.50	-	<500	<100	<100	6.0	0.7	<5	<30	4.0	<20	<0.1	<3	2.8
61	GN-87-124	2	-	47	89	8	-	3.0	1.0	4.1	14.1	-	-	-	-	6.3
61	GN-87-124	3	-	-	-	-	-	-	-	3.1	9.5	-	-	-	-	0.5
61	GN-87-124	4	13.00	-	<500	<100	<100	2.6	0.7	<5	9.0	<1	12.0	<0.1	<3	3.3
64	GN-87-125	1	-	-	-	-	-	-	-	9.0	19.0	<1	<5	<0.1	<2	0.6
64	GN-87-125	4	15.00	-	1111	<100	<100	1.9	1.0	10.0	18.0	<1	<5	<0.1	<3	<1
69	GN-87-130	1	-	-	-	-	-	-	-	6.0	10.0	<1	<5	<0.1	<2	1.8
69	GN-87-130	4	10.00	-	<500	131	<100	1.1	0.5	8.0	21.0	<1	<5	<0.1	<3	4.8
66	GN-87-132	1	-	-	-	-	-	-	-	<5	<5	<1	<5	<0.1	<2	3.5
66	GN-87-132	2	-	138	78	12	-	1.0	<0.5	<1	8.8	-	-	-	-	9.8
66	GN-87-132	3	-	-	-	-	-	-	-	1.4	4.8	-	-	-	-	2.2
70	GN-87-133	1	-	-	-	-	-	-	-	<5	5.0	<1	<5	<0.1	<2	1.6
70	GN-87-133	2	-	29	106	16	-	2.0	0.5	<1	8.9	-	-	-	-	4.4
70	GN-87-133	3	-	-	-	-	-	-	-	1.5	6.5	-	-	-	-	1.6
77	GN-87-172	1	-	-	-	-	-	-	-	<5	<5	<1	<5	<0.1	<2	2.7
77	GN-87-172	2	-	108	106	26	-	<1	<0.5	<1	<0.5	-	-	-	-	8.4
77	GN-87-172	3	-	-	-	-	-	-	-	0.2	0.2	-	-	-	-	1.6
77	GN-87-172	4	13.00	-	<500	<100	176	<1	<0.2	9.0	22.0	<1	<5	<0.1	4.0	2.1
78	GN-87-173	1	-	-	-	-	-	-	-	9.0	<5	<1	<5	0.3	<2	6.1
78	GN-87-173	2	-	110	85	111	-	1.0	<0.5	3.2	1.9	-	-	-	-	5.4
78	GN-87-173	3	-	-	-	-	-	-	-	1.6	0.4	-	-	-	-	<0.1
78	GN-87-173	4	7.60	-	<500	169	232	1.1	0.4	<5	26.0	<1	<20	<0.1	<3	1.5
86	GN-87-182	1	-	-	-	-	-	-	-	<5	<5	<1	<5	<0.1	<2	4.1
86	GN-87-182	4	9.20	-	911	<100	<100	6.4	0.3	<5	32.0	<1	<5	<0.1	<3	1.4

Table 9.1 continued

Locality	Sample	Anal. Method	Fe wt %	Cu	Zn	Ni	Cr	As	Sb	Pt	Pd	Rh	Ru	Ir	Os	Au
				ppm						ppb						
28	GN-87-183	1	-	-	-	-	-	-	-	<5	<5	<1	<5	0.1	<2	5.2
28	GN-87-183	2	-	44	89	283	-	1.0	<0.5	<1	2.4	-	-	-	-	3.6
28	GN-87-183	3	-	-	-	-	-	-	-	1.1	<0.1	-	-	-	-	0.3
28	GN-87-183	4	8.20	-	<500	279	579	<1	<0.2	<5	11.0	<1	<5	0.2	<3	1.7
Hornblende Gabbro-Diorite with Sulphides																
76	GN-87-171	1	-	-	-	-	-	-	-	<5	<5	<1	<5	<0.1	<2	1.7
76	GN-87-171	4	8.60	-	<500	150	260	3.8	<0.2	<5	18.0	<1	<5	<0.1	<3	3.3
81	GN-87-176	1	-	-	-	-	-	-	-	<5	11.0	<1	<5	0.2	<2	1.5
81	GN-87-176	4	7.40	-	<500	263	348	3.2	<0.2	<5	59.0	<1	<15	0.1	<3	1.9
84	GN-87-180	1	-	-	-	-	-	-	-	<20	<5	<1	<5	0.1	<2	2.0
84	GN-87-180	2	-	78	76	115	-	4.0	<0.5	2.9	0.9	-	-	-	-	3.5
84	GN-87-180	4	8.90	-	<500	254	407	4.8	<0.2	<15	21.0	<1	<25	0.1	<3	3.1
85	GN-87-181	1	-	-	-	-	-	-	-	<5	<5	<1	<5	0.1	<2	1.9
85	GN-87-181	2	-	20	95	191	-	1.0	<0.5	<1	<0.5	-	-	-	-	3.4
85	GN-87-181	3	-	-	-	-	-	-	-	2.7	<0.1	-	-	-	-	1.4
85	GN-87-181	4	7.20	-	<500	394	423	1.2	0.5	<5	18.0	<1	19.0	0.2	<3	2.4
Hornblende Gabbro - Diorite (Mylonitic)																
67	GN-87-128C	2	-	145	180	1000	-	8.0	1.0	5.0	10.7	-	-	-	-	4.2
67	GN-87-128C	3	-	-	-	-	-	-	-	3.6	7.3	-	-	-	-	1.2
67	GN-87-128C	4	16.00	-	<500	240	310	<1	0.4	<5	12.0	<1	<5	<0.1	<3	2.0
21	GN-87-185A	1	-	-	-	-	-	-	-	<5	<5	<1	<5	0.2	<2	2.2
21	GN-87-185A	4	7.60	-	<500	394	603	5.0	0.3	<5	14.0	<1	<5	0.3	<3	3.0
17	GN-87-187	1	-	-	-	-	-	-	-	11.0	<5	<1	<5	0.1	<2	2.5
17	GN-87-187	2	-	68	58	123	-	1.0	<0.5	<1	0.8	-	-	-	-	3.4
17	GN-87-187	3	-	-	-	-	-	-	-	2.2	1.1	-	-	-	-	1.6
17	GN-87-187	4	3.20	-	<500	228	166	<1	0.3	<5	<5	8.0	<20	0.2	<3	2.1
Magnetite																
53	GN-87-87	2	-	24	300	183	-	100.0	2.0	444.0	18.3	-	-	-	-	68.1
53	GN-87-87	3	-	-	-	-	-	-	-	343.0	17.4	-	-	-	-	0.7
53	GN-87-87	4	87.00	-	684	<100	537	1.4	<0.2	311.0	44.0	2.0	<5	0.6	3.0	1.5
58	GN-87-93B	1	-	-	-	-	-	-	-	<5	<5	<1	<5	<0.1	<2	1.9
58	GN-87-93B	2	-	4	99	74	-	25.0	1.0	2.0	0.9	-	-	-	-	9.9
58	GN-87-93B	3	-	-	-	-	-	-	-	3.7	1.1	-	-	-	-	1.7
58	GN-87-93B	4	19.00	-	<500	190	246	19.0	0.7	<5	35.0	<1	15.0	<0.1	<3	1.9
59	GN-87-103	1	-	-	-	-	-	-	-	14.0	11.0	<1	<5	<0.1	<2	<0.5
59	GN-87-103	2	-	15	92	780	-	1.0	1.0	17.9	2.1	-	-	-	-	4.3
59	GN-87-103	3	-	-	-	-	-	-	-	18.2	1.8	-	-	-	-	0.6
59	GN-87-103	4	77.00	-	<500	144	439	<1	<0.2	8.0	10.0	<1	<5	<0.1	<3	<1
Nicola Group Volcanic Rocks																
49	GN-87-19	2	-	6	34	4	23	3	0.5	-	-	-	-	-	-	-
49	GN-87-20	2	-	31	95	3	11	2	0.5	-	-	-	-	-	-	-
21	GN-87-56	2	-	11	63	10	19	3	0.5	-	-	-	-	-	-	-
5	GN-87-59	2	-	87	68	41	57	1	0.7	-	-	-	-	-	-	-
3	GN-87-60	2	-	188	93	52	62	1	0.5	-	-	-	-	-	-	-
1	GN-87-68	2	-	298	44	8	27	3	0.5	-	-	-	-	-	-	-
2	GN-87-69	2	-	48	67	90	251	1	0.7	-	-	-	-	-	-	-
4	GN-87-70	2	-	151	56	10	42	5	0.5	-	-	-	-	-	-	-
6	GN-87-71	2	-	70	81	64	161	1	0.5	-	-	-	-	-	-	-

Table 9.1 continued

Analyses of noble metals made on 50g splits of rock powder using fire-assay preconcentration followed by:

1 - Instrumental neutron activation (Activation Laboratories Ltd., Ancaster, Ontario); E. Hoffman, analyst.

2 - Atomic absorption spectrometry - graphite furnace finish (Analytical Laboratories, B.C. Ministry of Energy, Mines and Petroleum Resources, Victoria, British Columbia); W. Johnson, analyst.

3 - Inductively coupled plasma mass spectrometry (Geochemical Laboratories, Geological Survey of Canada, Ottawa); G.E.M. Hall, analyst.

4 - Instrumental neutron activation (Institut National de la Recherche Scientifique, Georessources, Sainte-Foy, Quebec); M. Bergeron, analyst.

* Duplicate Subsample + Extensively serpentinized

Samples with As <80 ppm analyzed by method 2 were rerun using 0.5 g of rock powder and a hydride extraction technique; Sb analyses were done on the same hydride solution.

Detection limits: 1 ppb for Pt and Au; 2 ppb for Pd and Rh; neutron activation detection limits vary with sample composition

Sample locations are given in Appendix C and shown on Map 5 and Figure 9.6.

dunite-pyroxenite cumulates, and evidence for a common petrogenetic affiliation (Findlay, 1969), support Findlay's concept of a single differentiated intrusive body. However, emplacement of ultramafic units as a high-temperature crystal mush is unlikely to preserve the delicate modal layering observed in thin gabbroic units within olivine clinopyroxenite. In addition, igneous cumulate textures are widely preserved and tectonite fabrics localized in ductile shear zones. The general lack of magmatic layering is at least partly attributable to periodic remobilization and slumping of cumulate sequences penecontemporaneous with deposition. Some chromitite schlieren, however, have undergone tectonic reworking by flowage during serpentinization of host dunite and regional metamorphism. Moreover, it seems unlikely that the rise of dense cumulates was triggered by regional contractional deformation in the Jurassic to Cretaceous since crystallization of the feldspathic phases of the Tulameen complex has been dated as latest Triassic to earliest Jurassic (Rublee, 1994). It is more likely that the diapiric re-emplacement mechanism for Alaskan-type complexes is invalid, as shown earlier for the Polaris complex (Chapter 8).

CHAPTER 10 PLATINUM-GROUP-ELEMENT MINERALIZATION

Alaskan-type ultramafic-mafic complexes and spatially associated placers are well-known hosts for platinum-group element (PGE) deposits (*e.g.*, Aldan Shield and Ural Mountains, USSR; Youbdo, Ethiopia; Choco District, Columbia; and Goodnews Bay, Alaska; *cf.* Cabri, 1981) and represent one of the most favourable environments for PGE in the Cordillera (Evenchick *et al.*, 1986; Rublee, 1986). The PGE typically occur as a dominant commodity (Cabri, 1981).

Based on mineralogical associations in lode occurrences, three subtypes of PGE deposits are recognized worldwide, all of which contain discrete platinum-group minerals (PGM) (*cf.* Nixon and Hammack, 1991). The chromitite-PGE association appears to be the most important and widespread; a magnetite-PGE subtype is known from at least two complexes, Tulameen in British Columbia and Lower Coon Mountain in northern California (Gray *et al.*, 1986); and in a newly recognized subtype from Fifield, Australia, the PGE are associated with clinopyroxenites (Johan *et al.*, 1989). In all three associations, base metal sulphides are of little importance.

NOBLE METAL GEOCHEMISTRY OF ALASKAN-TYPE COMPLEXES

Strongly anomalous abundances of PGE in Alaskan-type intrusions in British Columbia have been reported previously from the Tulameen (Findlay, 1963; St. Louis *et al.*, 1986) and Wrede Creek (Chapter 6) complexes, and less pronounced anomalies have been detected in the Polaris complex (Chapter 8). Normalized noble metal abundance patterns for rocks from Alaskan-type complexes in British Columbia and other magmatic environments are plotted in Figures 10.1 to 10.5. In general, Alaskan-type complexes exhibit a distinctive M-shaped PGE-abundance pattern in which a number of specific features are evident:

- Chromitites contain the highest absolute abundances of platinum (and iridium) and have high Pt/Pd ratios. This is a typical Alaskan-type feature (Cabri, 1981) and reflects the accumulation of discrete PGM, predominantly platinum-iron alloys, rather than solid solution of PGE in silicates and oxides (St. Louis *et al.*, 1986 ; discussed below).
- The abundances of PGE are much lower in other rock types, and the abundance of palladium increases with differentiation, reaching a maximum in pyroxenites. This is accompanied by a concomitant decrease of the Pt/Pd ratio.
- Gold is generally uniformly low, although gabbroic to dioritic rocks at the Johanson Lake and Wrede Creek complexes appear anomalously enriched (Figure 10.3); however, absolute abundances of gold remain low.
- The patterns for magmatic sulphides in the Turnagain coŸŸplex exhibit a fairly smooth enrichment in PGE with a positive slope (one pattern is notably erratic) culminating at palladium (Figure 10.4; Nixon *et al.*, 1989). The relatively low overall abundances of PGE are somewhat surprising in view of the known affinity of PGE for sulphides. As sulphide immiscibility was reached relatively early in the crystallization history of this intrusion (Clark, 1980), it is probable that the mantle source region was depleted in PGE.
- Magnetite horizons in hornblende clinopyroxenites of the Tulameen complex are locally enriched in platinum relative to the other PGE (Figure 10.1). Although it is possible that platinum is contained in magnetite solid solutions, the presence of dispersed PGM cannot be ruled out. This unusual feature is a good example of the comparatively rare magnetite-PGE association (Subtype 2 of Nixon and Hammack, 1991) and accounts for localized platinum soil anomalies detected by prospectors over hornblende clinopyroxenites in some parts of the Tulameen complex.
- The M-shaped patterns for Alaskan-type complexes are quite unique in comparison to rocks from other geologic environments. Note that ophiolitic assemblages typically have patterns of opposite slope, and this is also true for British Columbia ophiolites (Talkington and Watkinson, 1986). The distinctive character of PGE abundances in Alaskan-type intrusions has important ramifications for exploration for PGE deposits in Cordilleran settings. The geochemistry of the PGE is reflected in the presence of discrete PGM as described below.

PLATINUM-GROUP MINERALS IN THE TULAMEEN COMPLEX AND ASSOCIATED PLACERS - A CASE STUDY

In southern British Columbia, platinum and gold-bearing placers in the Tulameen-Similkameen river systems historically have been significant producers of PGE, yielding an estimated 620 kilograms of impure platinum between 1889 and 1936 (O'Neill and Gunning, 1934; Rice, 1947). The source of the platinum has been traced to ultramafic rocks of the Tulameen Alaskan-type complex whereas the origin of the gold has traditionally been related to a younger episode of regional vein-type mineralization. According to Rice (1947), the ratio of alluvial platinum to gold increases from about 1:4 in the lower reaches of the Tulameen and Similkameen rivers to about 1:1 in the vicinity of the mafic-ultramafic complex.

Modern studies of the Tulameen district have documented a number of discrete PGM in both placer and lode occurrences (*e.g.*, Cabri *et al.*, 1973; Raicevic and Cabri, 1976; St. Louis *et al.*, 1986). In particular, St. Louis *et al.* identified several species of PGM, including platinum-iron

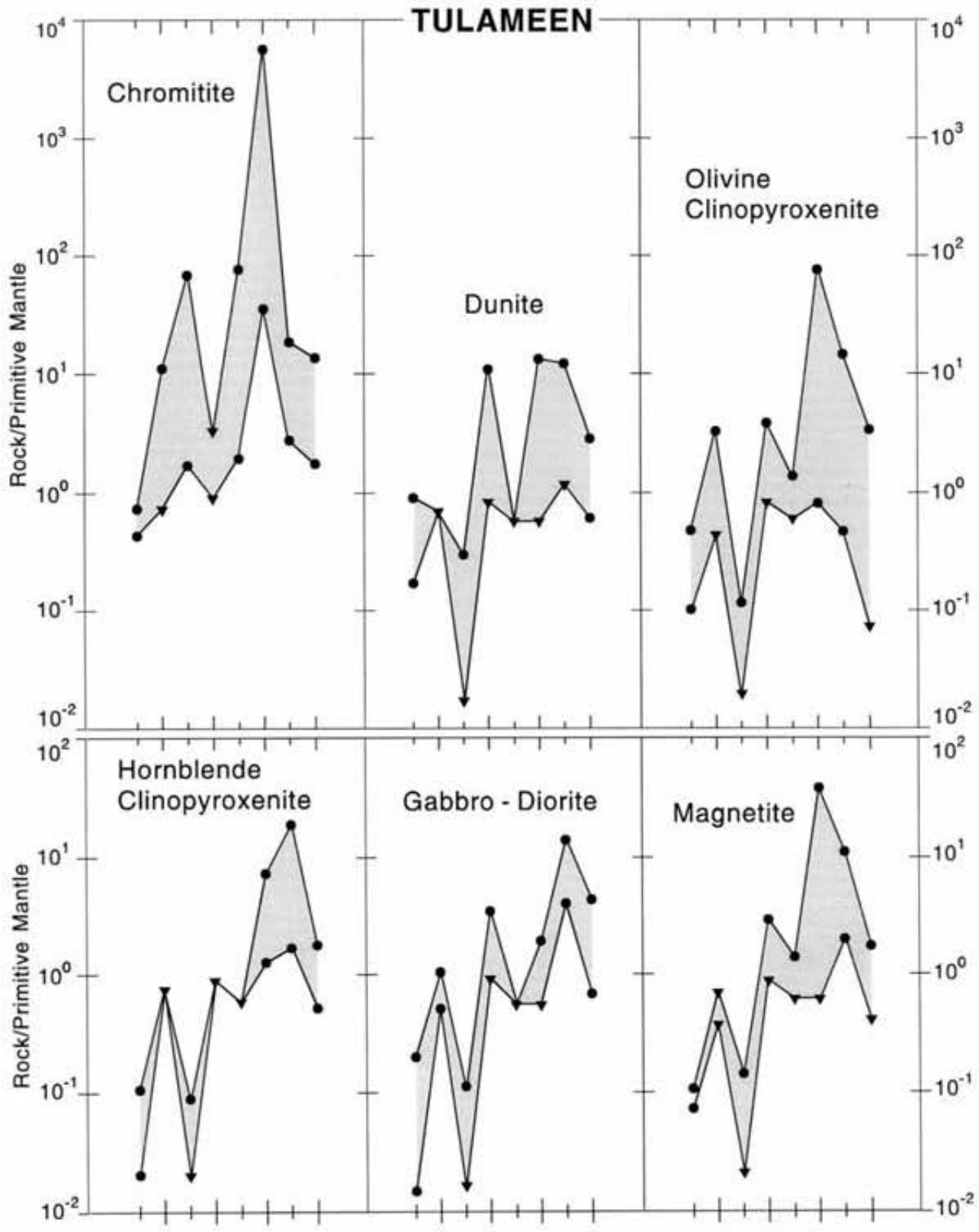

Figure 10.1. Range of mantle-normalized noble metal patterns in major rock types of the Tulameen complex. Normalizing values are mantle abundances (C1 chondrite x 0.00815) from Barnes *et al.* (1988) given in ppb unless otherwise indicated: Ni, 2000 ppm; Os, 4.2; Ir, 4.4; Ru, 5.6; Rh, 1.6; Pt, 8.3; Pd, 4.4; and Au, 1.2. Inverted triangles are values below detection limits.

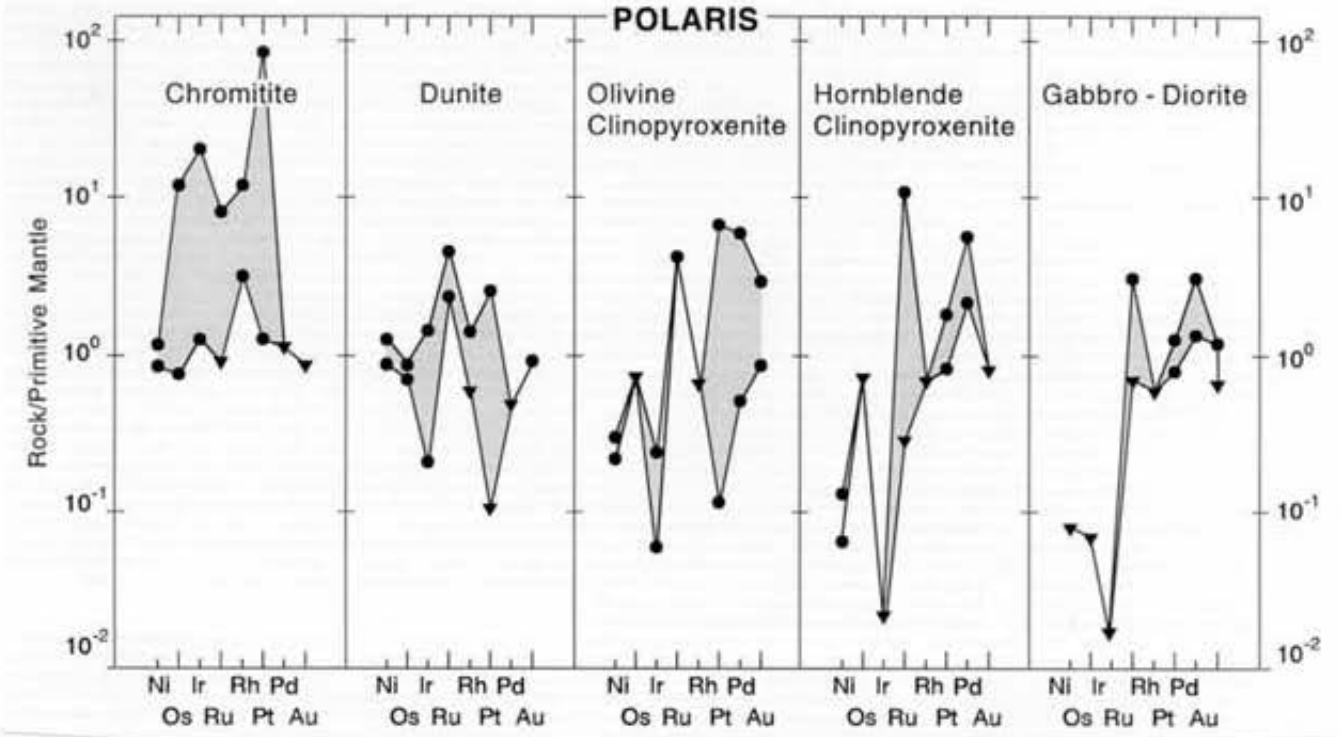

Figure 10.2. Range of mantle-normalized noble metal patterns in major rock types of the Polaris complex. Normalizing values and symbols as in Figure 10.1.

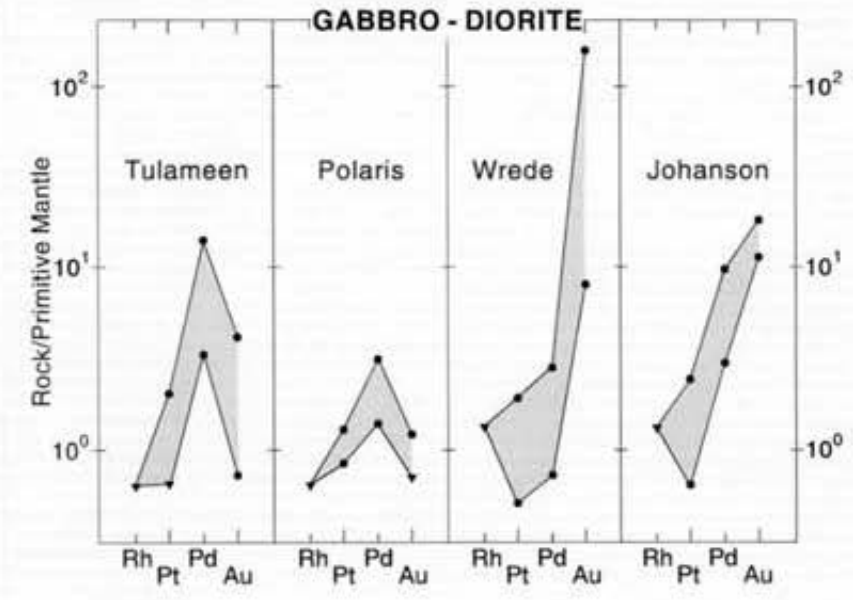

Figure 10.3. Range of mantle-normalized noble metal patterns in gabbroic to dioritic rocks of Alaskan-type complexes in British Columbia. Normalizing values and symbols as in Figure 10.1 except sulphide symbols which distinguish individual samples.

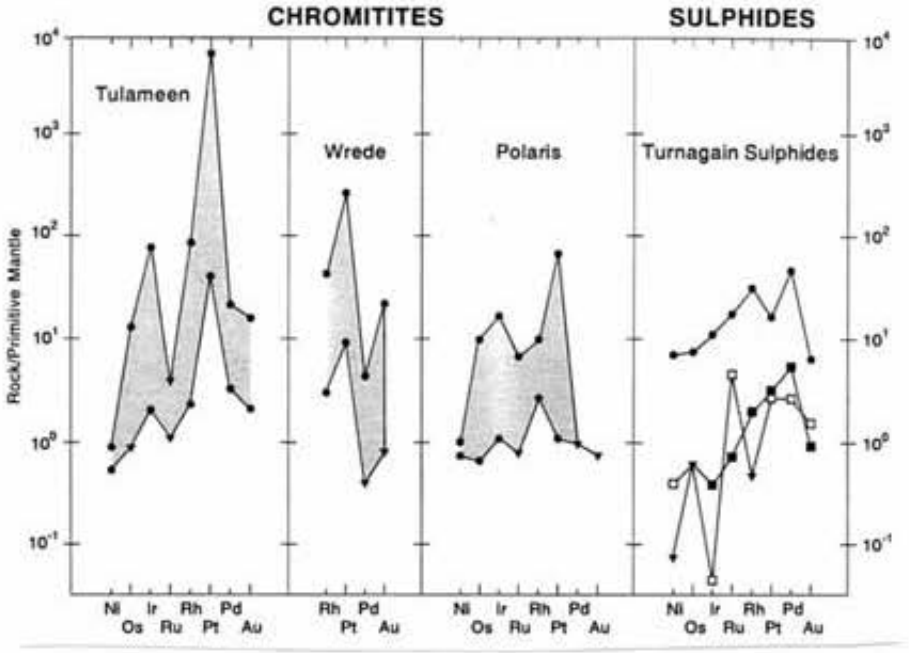

Figure 10.4. Range of mantle-normalized metal patterns in chromitites and magmatic sulphides of Alaskan-type complexes. Normalizing values and symbols as in Figure 10.1 except sulphide symbols which distinguish individual samples.

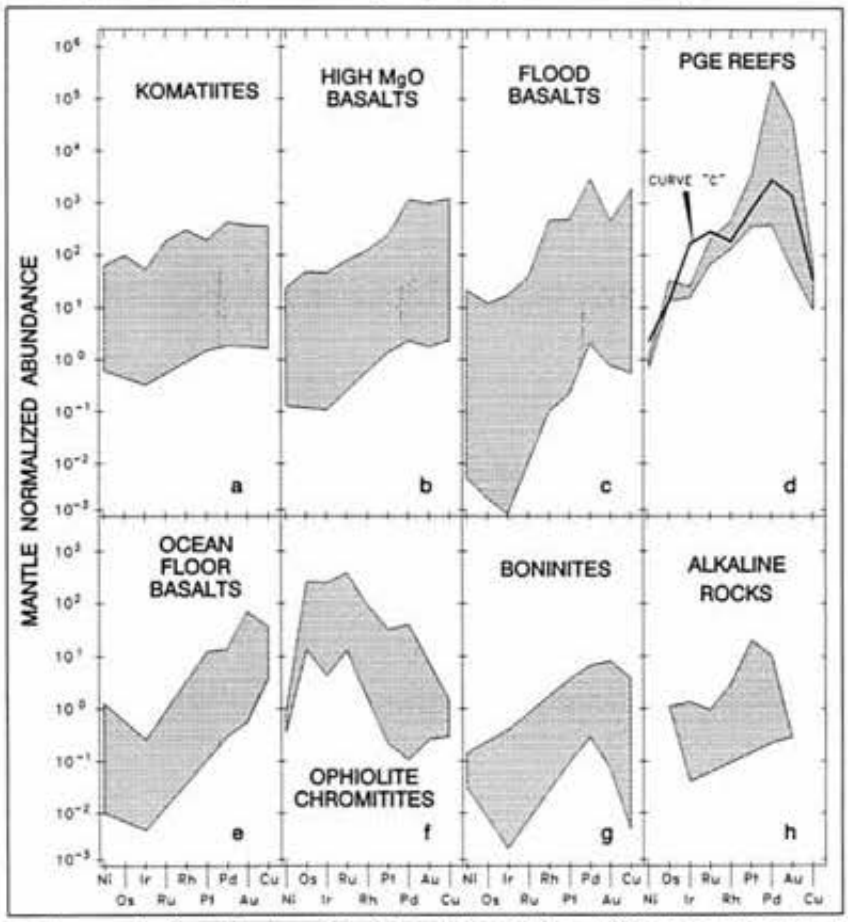

Figure 10.5. Range of mantle-normalized metal patterns for a) komatiites and the sulphides associated with them; b) high-MgO basalts and the sulphides associated with them; c) flood basalts and the sulphides associated with them; d) PGE reefs (with the Pt-enriched chromites from the Cliff locality of the Unst ophiolite shown as curve C); e) ocean floor basalts; f) podiform chromitites from ophiolites; g) boninites and low-TiO_2 basalts; and h) alkaline rocks (after Barnes *et al.*, 1988). Normalizing values as in Figure 10.1.

alloys and platinum antimonides and arsenides. We have further characterized the speciation and composition of the PGM and coexisting spinels, silicates and various base metal minerals in Tulameen chromitites and associated placer material using scanning electron microscopy and quantitative electron-microprobe methods. Analytical details are given in Appendix D. The results are described below and discussed relative to the origin of PGE mineralization in both lode and placer deposits. These data demonstrate quite convincingly that *in situ* PGE mineralization and alluvial platinum share a common heritage.

CHROMITITE SPECIMENS

Chromitite samples were collected from three different sites on Grasshopper Mountain in the northern part of the dunite body (Figures 9.2, 9.3 and 10.6). Previous work by Mr. D. Bohme, formerly of Newmont Exploration Limited, had outlined areas of platiniferous chromitite on the southern slopes of Grasshopper Mountain, and earlier St. Louis *et al.* (1986) had documented PGE-rich chromitites in a northeast-southwest traverse across the summit of the mountain. In this study, chromitites from Grasshopper Mountain were resampled as part of an effort to more thoroughly evaluate the PGE potential of Alaskan-type complexes in British Columbia (Nixon, 1990). The abundances of PGE in well-analyzed platiniferous chromitites are given in Table 10.1.

The chromitites typically form bulbous or irregular masses less than 10 centimetres across, or occur as thin, discontinuous schlieren 1 to 4 centimetres wide by up to 4 metres in length. The core of these bodies consists of massive chromite that has indistinct crystal outlines and is locally crosscut by irregular fractures. The margins of chromitites contain large (1-2 mm) subhedral to euhedral chromite crystals interspersed with olivine, and exhibit a sharp gradation into tiny (<20 μm) grains of euhedral spinel (1 vol%) in enveloping dunite. The margins of some schlieren exhibit rings of euhedral chromite granules that surround larger crystals of cumulate olivine, similar to textures documented elsewhere (*e.g.*, the Turnagain Alaskan-type complex in north-central British Columbia; Clark 1975, 1980). The formation of massive chromitite appears to have proceeded by coalescence of chromite grains of variable size during recrystallization and annealing at elevated temperatures in the manner described by Eales (1987). Disruption and redistribution of chromitite horizons within the dunite appears to have been accomplished by intermittent slumping and redeposition of formerly stratified cumulates at a relatively early stage of solidification of the magma chamber (Chapter 9).

PLACER NUGGETS

The nuggets were obtained from a variety of sources; some have been studied previously by Cabri and co-workers (Cabri *et al.*, 1973; Harris and Cabri, 1973; Cabri and Hey, 1974; Cabri and Feather, 1975; Raicevic and Cabri, 1976). The samples comprise rounded to subrounded monomineralic grains or polymineralic aggregates that reach 7 millimetres in diameter and have a metallic luster. The Lincoln nugget was purchased from a local collector and is named for the "Lincoln mine", a former placer operation on the Tulameen River situated about 0.8 kilometre below the mouth of Britton Creek (formerly Eagle Creek). The "Holland" nugget was obtained from the Tulameen River by the late Dr. S. S. Holland, formerly of the British Columbia Department of Mines (Ministry of Energy, Mines and Petroleum Resources). Sample M12410 is a vial of numerous placer grains obtained from the Royal Ontario Museum, Toronto. This material was collected from a site on the Tulameen River believed to be just upstream from the confluence with Lawless (Bear) Creek (Figure 9.1). Three relatively large nuggets (M12410-1, 2, and 3) were selected for study.

PETROGRAPHY AND MINERALOGY OF CHROMITITES

Chromitites within the dunite core of the Tulameen complex contain essential chromiferous spinel and minor, variably serpentinized olivine. PGE-rich chromitites exhibit a variety of discrete PGM, the proportion of which, in replicate polished sections, is highly variable and no doubt

TABLE 10.1
ABUNDANCES* OF PLATINUM-GROUP ELEMENTS IN CHROMITITES OF THE TULAMEEN COMPLEX

Sample	Pt	Pd	Rh	Ru	Ir	Os
GN87-146[1]	2500	5	20	<10	17	8
GN87-146[2]	9297	73	-	-	-	-
GN87-146[3]	3189	23	-	-	-	-
GN87-147[1]	5600	75	56	<5	140	20
GN87-147[2]	7953	59	-	-	-	-
GN87-147[3]	5527	47	-	-	-	-
GN87-147[3]	5380	39 (duplicate subsample)				
GN87-147[4]	8348	<30	70	<15	243	50
GN87-148[1]	5300	12	67	50	220	25
GN87-148[3]	4762	19	-	-	-	-
GN87-148[4]	7398	<15	68	<20	247	48
Average chromitite**	3410	<83	40	-	100	40
	(2220)		(20)		(40)	(20)

Concentrations in ppb - not determined.

Analyses made on 50-g splits of rock powder using fire-assay preconcentration of noble metals followed by:

[1] instrumental neutron activation (Activation Laboratories Ltd., Ancaster, Ontario)

[2] atomic absorption spectrometry-graphite furnace finish (Analytical Laboratories, B.C. Ministry of Energy, Mines and Petroleum Resources, Victoria, British Columbia)

[3] inductively coupled plasma mass spectrometry (Geochemical Laboratories, Geological Survey of Canada, Ottawa)

[4] instrumental neutron activation (Institut National de la Récherche Scientifique, Georessources, Sainte-Foy, Quebec)

***Mean value (standard error of the mean) from St. Louis et al., 1986, Table 4.*

Sample locations: GN87-146: 230m NW of Grasshopper Mountain summit at 1420 m (Lat. 49°32.7′N, Long. 120°53.9′W); GN87-147: southern slope of Grasshopper Mountain at 1370 m (Lat.49°32.3′N, Long. 120°54′W); GN87-148: 740 m SSW of Grasshopper Mountain summit at 1340m (Lat. 49°32.2′N, Long. 120°54′W).

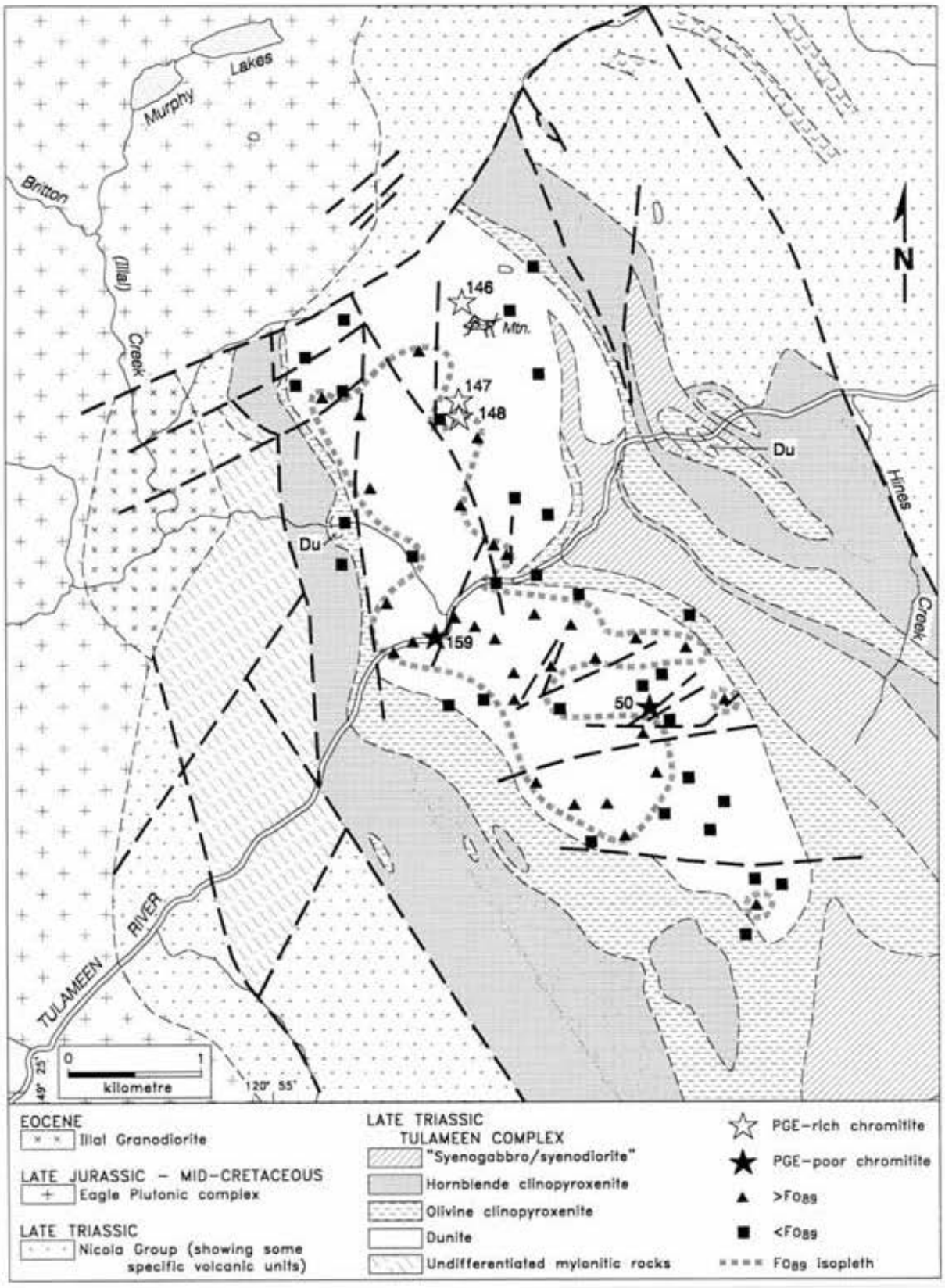

Figure 10.6. Geological map of the dunite core of the Tulameen complex showing olivine compositions (after Findlay, 1963) and chromitite localities documented in this study. Total range of olivine compositions in dunite is Fo_{88-92}. Du, dunite.

causes the significant range of PGE abundances noted above. Both PGE-rich and PGE-poor chromitites contain minor quantities of base metal sulphides and arsenides, and trace amounts of native metals and metal oxides. Serpentinization is generally moderately pronounced in the dunite within a few millimetres of the chromitite contact. Chromitite pods are also commonly traversed by hairline fractures filled with serpentine, chlorite, magnetite, carbonate and minor base metals and base metal sulphides.

PLATINUM-GROUP MINERALS

The PGE in chromitites are distributed primarily among Pt-Fe-Ni-Cu alloys, the most common PGM, and geversite, rhodium-iridium sulpharsenides, sperrylite, platinian copper, platinum oxide, erlichmanite and laurite, listed in order of decreasing abundance. The PGM are found as discrete grains or complex polymineralic intergrowths.

The nomenclature of the Pt-Fe-Ni-Cu alloys is problematical as there is a lack of data for phase relations in this system, and even relationships along the Pt-Fe binary join are imprecisely known (Cabri and Feather, 1975). Identification of platinum alloy species requires characterization of crystal structure as well as phase composition (Cabri and Feather, 1975) but no x-ray-diffraction data have been obtained due to the small grain size of the PGM. However, based on stoichiometric considerations and previous work, we tentatively recognize three species of alloys (Tables 10.2A and B.).

Platinum-iron-nickel-copper alloys, or simply platinum alloys, have been positively identified in more than 30 euhedral to subhedral grains (<35 μm), and most are encapsulated by chromite (Photos 10.1-10.3). Their compositions are plotted in Figure 10.7. Most grains plot near the centre of a triangle bounded by PtFe (tetraferroplatinum), Pt_2FeCu (tulameenite) and Pt_2NiFe (ferronickelplatinum) (Figure 10.7D) and are not unlike alloy compositions from other occurrences worldwide such as Noril'sk, in the former Soviet Union (Genkin and Evstigneeva, 1986) and the former Onverwacht mine, Transvaal (Cabri *et al.*, 1977). The latter authors reported on the composition of a tetragonal alloy approximately midway along the join Pt_2FeCu-Pt_2NiFe ($Pt_2FeNi_{0.5}Cu_{0.5}$; Figure 10.7D) and suggested that it might represent a nickel and copper-rich variety of tetraferroplatinum.

The majority of the grains of Pt-Fe-Ni-Cu alloys analyzed in chromitites are stoichiometrically close to Pt(Fe, Ni, Cu), with minor iridium (0.17 - 4.8 wt%), palladium (<0.53 wt%) and rhodium (<0.57 wt%) substituting for platinum (Table 10.2A). We tentatively regard this composition as representative of tetraferroplatinum, even though significant quantities of nickel (3.4 - 5.9 wt%) and copper (2.3 - 4.7 wt%) distinguish it from the ideal PtFe

TABLE 10.2A
ELECTRON-MICROPROBE DATA ON PLATINUM ALLOY INCLUSIONS
IN CHROMITITES, TULAMEEN COMPLEX

Anal. No.	Grain Size (μm)	Weight per cent										Atomic Proportions										
		Pt	Rh	Pd	Ir	Os	Fe	Cu	Ni	Sb	Total	Pt	Rh	Pd	Ir	Os	Sum	Fe	Cu	Ni	Sb	Sum
1. Pt (Fe, Ni, Cu) - tetraferroplatinum?																						
1	12 x 32	76.8	n.d.	n.d.	0.46	n.d.	13.4	4.7	4.1	0.23	99.69	1.007			0.006		1.013	0.614	0.189	0.179	0.005	0.987
2*	4 x 8	76.6	0.26	0.30	0.25	n.d.	13.7	3.2	4.6	n.d.	98.91	1.016	0.006	0.007	0.003		1.032	0.634	0.13	0.203		0.967
3	4 x 8	77.2	0.34	0.30	0.38	n.d.	13.9	2.9	4.3	n.d.	99.32	1.026	0.009	0.007	0.005		1.047	0.645	0.118	0.19		0.953
4+	6 x 8	77.1	0.26	0.29	0.17	n.d.	13	3.2	4.7	n.d.	98.72	1.034	0.007	0.007	0.002		1.050	0.609	0.132	0.21		0.951
5	15 x 20	72.6	0.43	0.50	3.50	n.d.	14.8	3.3	3.9	n.d.	99.03	0.951	0.010	0.012	0.046		1.020	0.677	0.133	0.17		0.980
6	10 x 10	73.3	0.38	0.50	1.90	n.d.	14.2	2.8	5.9	n.d.	98.98	0.948	0.009	0.012	0.025		0.994	0.641	0.111	0.254		1.006
7	20 x 25	74.2	0.4	0.53	2.80	n.d.	15.2	3.2	3.4	n.d.	99.73	0.970	0.001	0.013	0.037		1.030	0.694	0.128	0.148		0.970
8	8 x 15	71.5	0.57	0.49	4.80	n.d.	14.7	2.8	5	n.d.	99.86	0.923	0.014	0.012	0.063		1.012	0.663	0.111	0.215		0.989
9	5 x 6	74.5	0.31	0.15	0.35	n.d.	13.7	3.2	5.3	0.08	97.59	0.986	0.008	0.004	0.005		1.003	0.633	0.13	0.233	0.002	0.998
10	3 x 5	74.6	0.46	0.35	0.59	n.d.	13.9	2.8	5.1	n.d.	97.80	0.989	0.012	0.008	0.008		1.017	0.644	0.114	0.225		0.983
11	5 x 6	75	0.36	0.33	1.40	n.d.	13.9	2.3	4.4	n.d.	97.69	1.014	0.009	0.008	0.019		1.050	0.656	0.095	0.198		0.949
2. $Pt_{2.3}$ (Fe, Ni, Cu)$_{1.3}$ - isoferroplatinum?																						
12	10 x 10	82.9	0.63	0.43	0.60	0.2	10.9	1.1	2.6	n.d.	99.37	2.440	0.035	0.023	0.018	0.006	2.522	1.210	0.099	0.255		1.475
13*	4 x 8	81.2	0.75	0.50	0.56	n.d.	11.5	1	3.2	n.d.	98.71	2.350	0.041	0.027	0.017		2.435	1.165	0.089	0.308		1.562
14	8 x 9	83.4	0.67	0.45	0.51	n.d.	11	1.2	2.7	n.d.	99.93	2.430	0.037	0.024	0.015		2.506	1.121	0.107	0.262		1.490
15	10 x 10	81.8	0.6	0.48	0.50	n.d.	11.2	2.1	2.9	n.d.	99.58	2.345	0.033	0.025	0.015		2.418	1.121	0.185	0.276		1.582
16+	6 x 8	80.8	0.56	0.50	0.24	n.d.	12.5	1.1	2.6	n.d.	98.30	2.330	0.031	0.026	0.007		2.394	1.259	0.097	0.249		1.605
17	5 x 5	81	0.52	0.20	3.60	n.d.	11.4	0.5	1.2	n.d.	98.39	2.470	0.030	0.011	0.111		2.622	1.214	0.044	0.122		1.380
3. Pt_2 (Fe, Cu, Ni, Sb)$_2$ - tulameenite?																						
18	30 x 35	71.4	n.d.	0.65	n.d.	n.d.	5.5	12.9	2	6.9	99.35	1.915		0.032			1.947	0.515	1.062	0.178	0.297	2.052
19	10 x 10	73.8	0.44	0.39	0.29	0.3	11.1	9.7	2.9	n.d.	98.95	1.915	0.022	0.019	0.008	0.009	1.973	1.006	0.773	0.250		2.029

*n.d. = not detected. Ru was not detected; minimum detection limits in wt. % are: Rh, Pd, Ru 0.05; Os 0.10; and Sb 0.07. * and + =coexisting alloys.*
1 - With minor hollingworthite in silicate in contact with chromite; 2 - With isoferroplatinum and erlichmanite; 4 - With isoferroplatinum, Co-Ni-Fe sulphide and laurite; 5 - With platinian copper; 13 - c.f. 2; 14 - With some laurite; 15 - With tulameenite and platinian copper;16 - c.f.4; 18 - With some platinian copper; 19 - c.f. 15. Sample key: Analyses 1-4, 12-16, 18, 19: GN87 - 146B; Analyses 5-8: GN87-147B; Analyses 9-11: GN87-146A; Analysis 17: GN87-148A.

TABLE 10.2B
ELECTRON-MICROPROBE DATA ON PLATINUM ALLOYS IN PLACER NUGGETS

Anal No.	Weight per cent									Atomic proportions									
	Pt	Rh	Pd	Ir	Fe	Cu	Ni	Sb	Total	Pt	Rh	Pd	Ir	Sum	Fe	Cu	Ni	Sb	Sum
1. Pt(Fe, Cu, Ni) - tetraferroplatinum?																			
1	71	0.62	n.d.	6.5	16.4	4.6	0.22	n.d.	99.34*	0.94	0.01		0.09	1.04	0.76	0.19	0.01		0.96
2. Pt_3Fe and $Pt_{2.6}(Fe, Cu, Ni)_{1.4}$ - isoferrplatinum?																			
2	79.0	0.62	0.17	7.0	12.3	0.95	0.20	n.d.	100.24*	2.36	0.03	0.01	0.21	2.61	1.28	0.09	0.02		1.39
	79.2	0.66	0.18	7.0	12.8	0.92	0.21	n.d.	100.97*	2.33	0.04	0.01	0.21	2.59	1.31	0.08	0.02		1.41
4	90.2	-	-	n.d.	9.1	0.07	0.22	0.14	99.730	2.93				2.93	1.03	0.01	0.02	0.01	1.07
5	88.0	-	-	2.3	9.0	0.11	0.13	0.11	99.650	2.87			0.08	2.95	1.02	0.01	0.01	0.01	1.05
6	88.6	-	-	2.2	8.7	0.15	0.09	0.24	99.980	2.91			0.07	2.98	0.99	0.01	0.01	0.01	1.02
3. Pt_2FeCu - tulameenite?																			
7	69.9	0.6	n.d.	6.5	11.7	11	0.20	n.d.	99.900*	1.83	0.03		0.17	2.03	1.07	0.88	0.02		1.97

*Analyses 1, 2, 3, 7 from M12410 nugget #3; analyses 4, 5, 6 from Holland nugget. n.d. = not detected; - = not determined; * = Os not detected.*

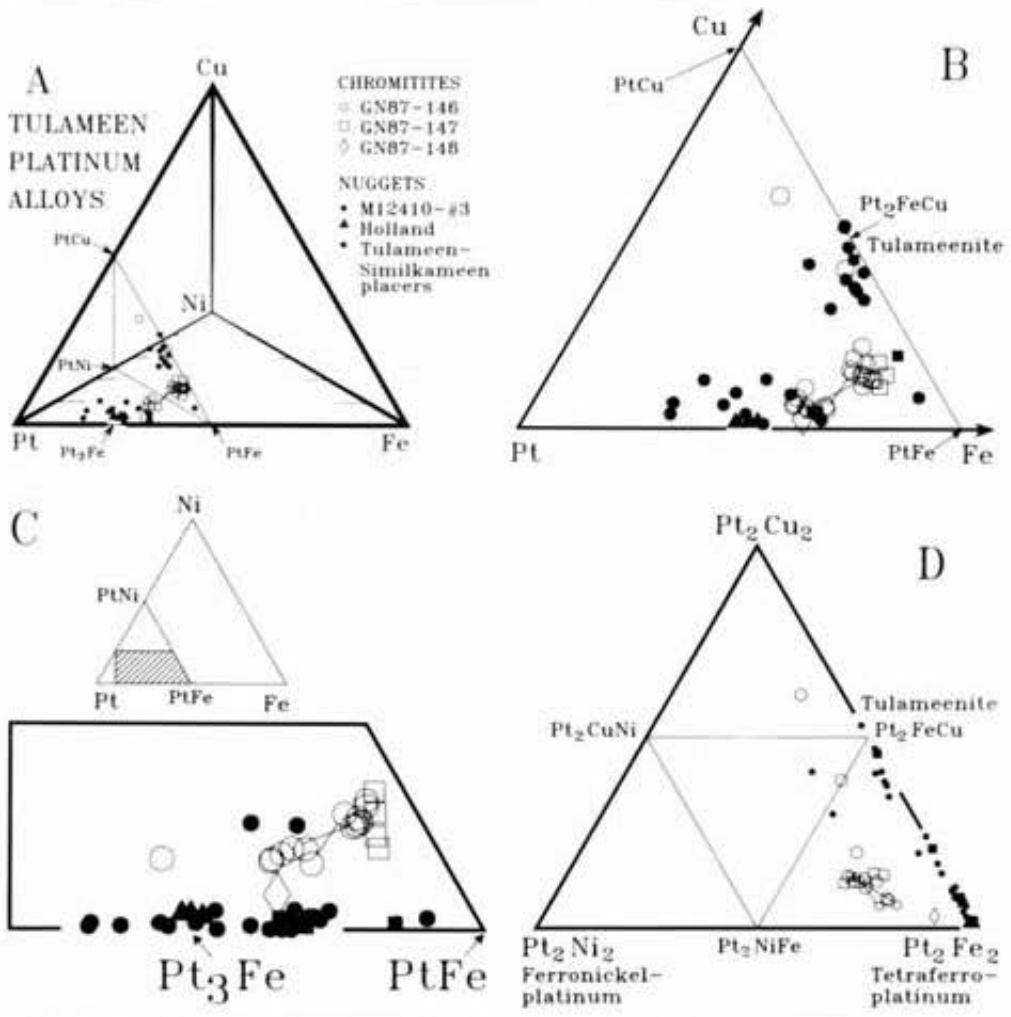

Figure 10.7. Plots of compositions of platinum alloys (atom %) that occur in Tulameen chromitites and placer nuggets. A. Alloys plotted in the Pt-Fe-Cu-Ni tetrahedron, showing ideal compositions of isoferroplatinum (Pt_3Fe) and tetraferroplatinum (PtFe). B. Cu-Pt-Fe projection of alloy compositions onto the face of the tetrahedron. C. Ni-Pt-Fe projfection onto base of tetrahedron. D. Pt_2Fe_2-Pt_2Cu_2-Pt_2Ni_2 equivalent plot of alloy compositons projected onto the PtFe-PtCu-PtNi plane in the tetrahedron (shown in A). Note that isoferroplatinum and tetraferroplatinum occupy the same point in this projection. Tie lines connect coexisting alloys (Analyses 2-13 and 4-16, Table 10.2A). Compositional data for Tulameen-Similkameenn placer grains taken from Cabri *et al.* (1973), Table 1), Cabri and Hey (1974, Table 1), and Cabri and Feather (1975, Table 2). For purposes of these plots, all platinum-group elements are included with Pt.

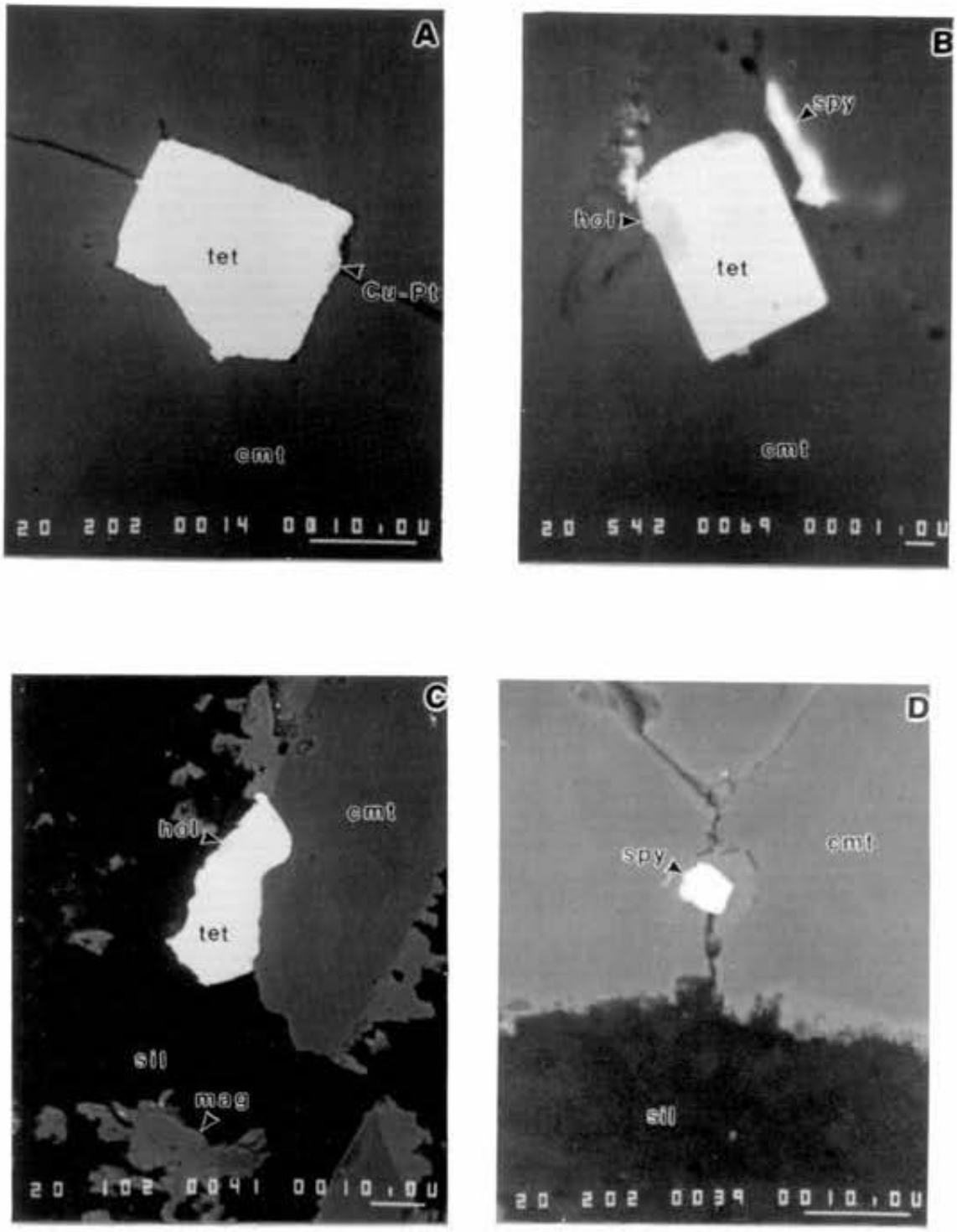

Photo 10.1. Scanning electron microscope (SEM) photomicrographs of PGM in chromitites: A. Subhedral inclusion of tetraferroplatinum(?) (tet) in chromite (cmt) with a thin, marginal zone of platinian copper (Cu-Pt) next to fracture (GN-147B); B. Euhedral inclusion of tetraferroplatinum (?) with marginal alteration to hollingworthite (hol). Nearby sperrylite (spy) occupies a fracture in host chromite (GN87-146); C. Anhedral tetraferroplatinum(?) with hollingworthite surrounded by chromite and serpentine (sil). Lighter grey zone at margin of chromite is area of "ferritchromite"-magnetite (mag) alteration (GN87-146B); D. Subhedral inclusion of sperrylite, probably a pseudormorph after platinum alloy, straddling a fracture in chromite lined with "ferritchromite"-magnetite (GN87-146B). Bar scale = 10 μmexcept in B (1 μm).

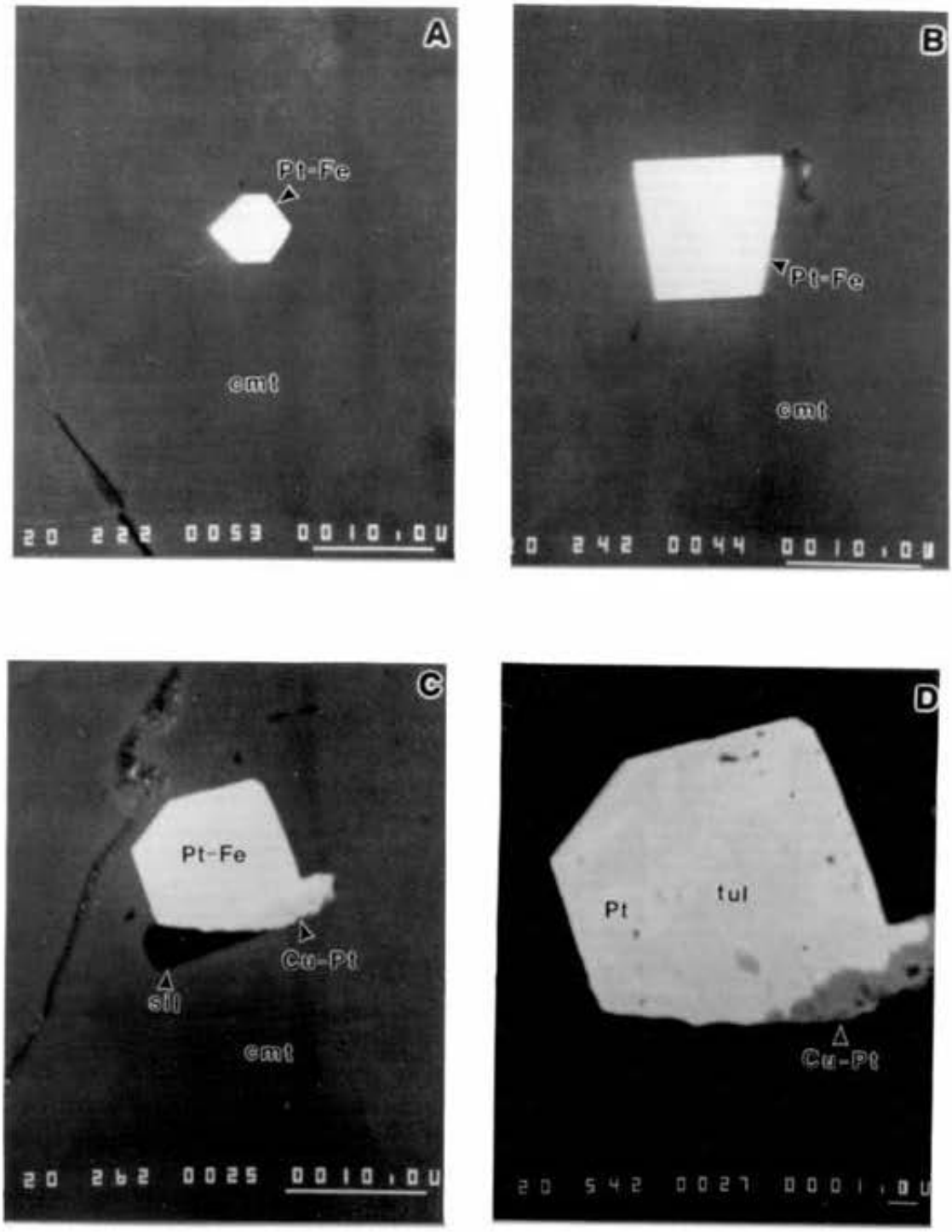

Photo 10.2. SEM photomicrographs of Pt-Fe alloys in chromitites: A. Euhedral isoferroplatinum(?) inclusion in chromite (cmt) (GN87-148A); B. Euhedral isoferroplatinum(?) inclusion (GN87-146B); C. Euhedral composite Pt-Fe alloy with peripheral replacement by platinian copper (Cu-Pt) and attached euhedral Mg-rich chlorite (sil) (GN87-146B); D.Magnification of C showing irregular intergrowth of tulameenite(?) (tul), isoferroplatinum(?) (pt) and platinian copper (Cu-Pt). Bar scale = 10 µmexcept in D (1 µm).

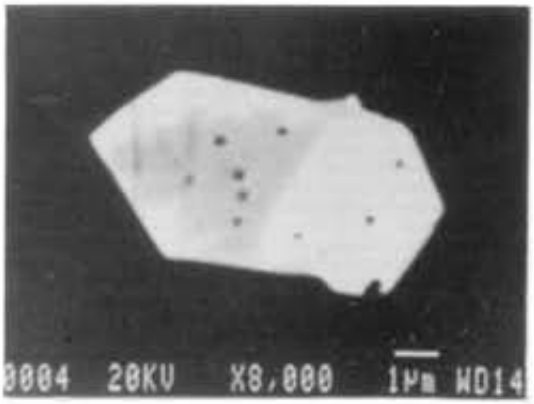

Photo 10.3. SEM image of two attached euhedral crystals of platinum alloy hosted by chromite (black) in Tulameen chromitite. Larger crystal has a core of "tetraferroplatinum" (dark grey) and rim of "isoferroplatinum" (white) in irregular contact with the core. The smaller crystal seems to consist entirely of isoferroplatinum, probably because the plane of the section traverses the rim of this crystal (*cf.* Analyses 2 and 13, Table 10.2A).

stoichiometry. Abundances of osmium and ruthenium are systematically below detection limits. The atomic proportions of ΣPGE (49.7-52.5 atom%) extend to the composition of a grain of ferroan platinum (ΣPGE=52.5%) in Similkameen placers (grain No. 9, Table 2, Cabri and Feather, 1975). However, platinum alloys in the chromitites contain twice as much copper and an order of magnitude more nickel than ferroan platinum in the placers.

Slight differences are observed among tetraferroplatinum compositions from different chromitites. For example, alloy grains in GN87-147 form a tight grouping in most plots (Figure 10.7) and are distinguished by a greater abundance of iridium and marginally higher iron than stoichiometrically similar grains of alloy in chromitite GN87-146 (Table 10.2A).

Grains of platinum alloy with compositions nearer $Pt_{2.5}(Fe, Ni, Cu)_{1.5}$ (60.5-65.6 atom% PGE) are tentatively assigned to isoferroplatinum, ideally Pt_3Fe. They contain small amounts of palladium, rhodium and iridium (up to 3.6 wt%), and one grain carries osmium, whereas ruthenium and antimony are routinely below detection limits (Table 10.2A). Absolute abundances of nickel and copper are consistently lower in isoferroplatinum than in tetraferroplatinum (Table 10.2A, Figures 10.7B and C), and Ni/Cu ratios are slightly higher in the former species (2.6 versus 1.7 atom %, respectively).

The majority of the grains of alloy seem to be homogeneous in composition. Rarely, coexisting alloys of Pt(Fe, Ni, Cu) and $Pt_{2.5}(Fe, Ni, Cu)_{1.5}$ are found within a single grain (Table 10.2A, Analyses 2-13 and 4-16; Figure 10.7). In one case, a euhedral crystal locked in chromite has a core of tetraferroplatinum surrounded by an irregular rim of isoferroplatinum (Photo 10.3). As discussed later, this rim may result from a high-temperature subsolidus reaction rather than a magmatic overgrowth formed prior to incorporation within chromite. Grains of relatively nickel and copper-free alloy of "Pt_2Fe" bulk composition were reported by Johan *et al.*, (1989) from primary mineralization in Alaskan-type intrusions near Fifield, Australia. The latter grains, however, comprise fine heterogeneous intergrowths of Pt_3Fe and PtFe that were accounted for by cooling within the miscibility gap in this part of the Pt-Fe system (*cf.* Cabri and Feather, 1975).

Grains of platinum alloy with appreciable iron and copper (and Sb in Analysis 18, Table 10.2A), and formulae that may be expressed as $Pt_2(Fe, Cu, Ni, Sb)_2$, are tentatively assigned to tulameenite (Pt_2FeCu). The antimony-rich grain contains 6.9 wt% antimony versus a maximum of 5.0 wt% in previously published analyses of tulameenite (Cabri *et al.*, 1973; Cabri and Hey, 1974). Minor substitution of rhodium, palladium, iridium and osmium occurs for platinum. One composition falls on the Pt_2FeCu-Pt_2NiFe tie line; the other plots within the Pt_2FeCu-Pt_2CuNi-Pt_2Cu_2 triangle (Figure 10.7D). Locally, tulameenite(?), accompanied by platinian copper, forms complex intergrowths with isoferroplatinum and has partly replaced the primary euhedral grain of Pt-Fe-Ni-Cu alloy (Analysis 15, Table 10.2A; Photo 10.2C and D).

Geversite ($PtSb_2$) is hosted by either chromite or serpentine, and locally occurs at chromite-serpentine contacts, where it forms anhedral intergrowths with other PGM (excluding Pt-Fe-Ni-Cu alloys) and base metal sulphides, arsenides and antimonides. Geversite has been identified in fractures, accompanied by serpentine and carbonate (Photo 10.4A and B), and may form relict cores of compound grains surrounded by breithauptite (Photo 10.4C), platinum oxide (Photo 10.4D) or platinian copper and hollingworthite (Photo 10.5A). Rarely, geversite occurs as subhedral inclusions in chromite that may represent a pseudomorph after a Pt-Fe-Ni-Cu alloy (Photo 10.4B). One large (30 µm) grain of geversite contains inclusions of irarsite. Microprobe analyses (Table 10.3) confirm rhodium, iridium, iron, cop-

TABLE 10.3
ELECTRON-MICROPROBE DATA ON GEVERSITE IN CHROMITITE

Anal. No.	Grain Size (µm)	Weight per cent									Atomic proportions							
		Pt	Rh	Ir	Fe	Cu	Ni	Sb	As	Total	Pt	Rh	Ir	Fe	Cu	Ni	Sum	Sb
1	10 x 25	42.9	n.d.	n.d.	0.80	0.25	0.22	54.9	1.2	100.27	0.93			0.06	0.02	0.01	1.02	1.9
2	8 x 10	41.4	0.24	0.14	0.92	n.d.	n.d.	55.5	0.28	98.48	0.92	0.01	<0.01	0.07			1.00	1.9
3	8 x 15	42.9	0.18	0.42	n.d.	n.d.	0.53	55.7	n.d.	99.73	0.95	0.01	0.01			0.04	1.01	1.9

n.d. = not detected; minimum detection limits in wt. % are: Fe, Cu, Ni 0.03; Rh 0.05; As, Ir 0.10.
1. GN87-146A: complex polymineralic grain with platinian copper, Ni antimonide and hollingworthite enclosed in magnetite-chromite.
2. GN87-148A: in contact with calcite-dolomite.
3. GN87-148A: in breithauptite with Pt oxide enclosed in serpentine.

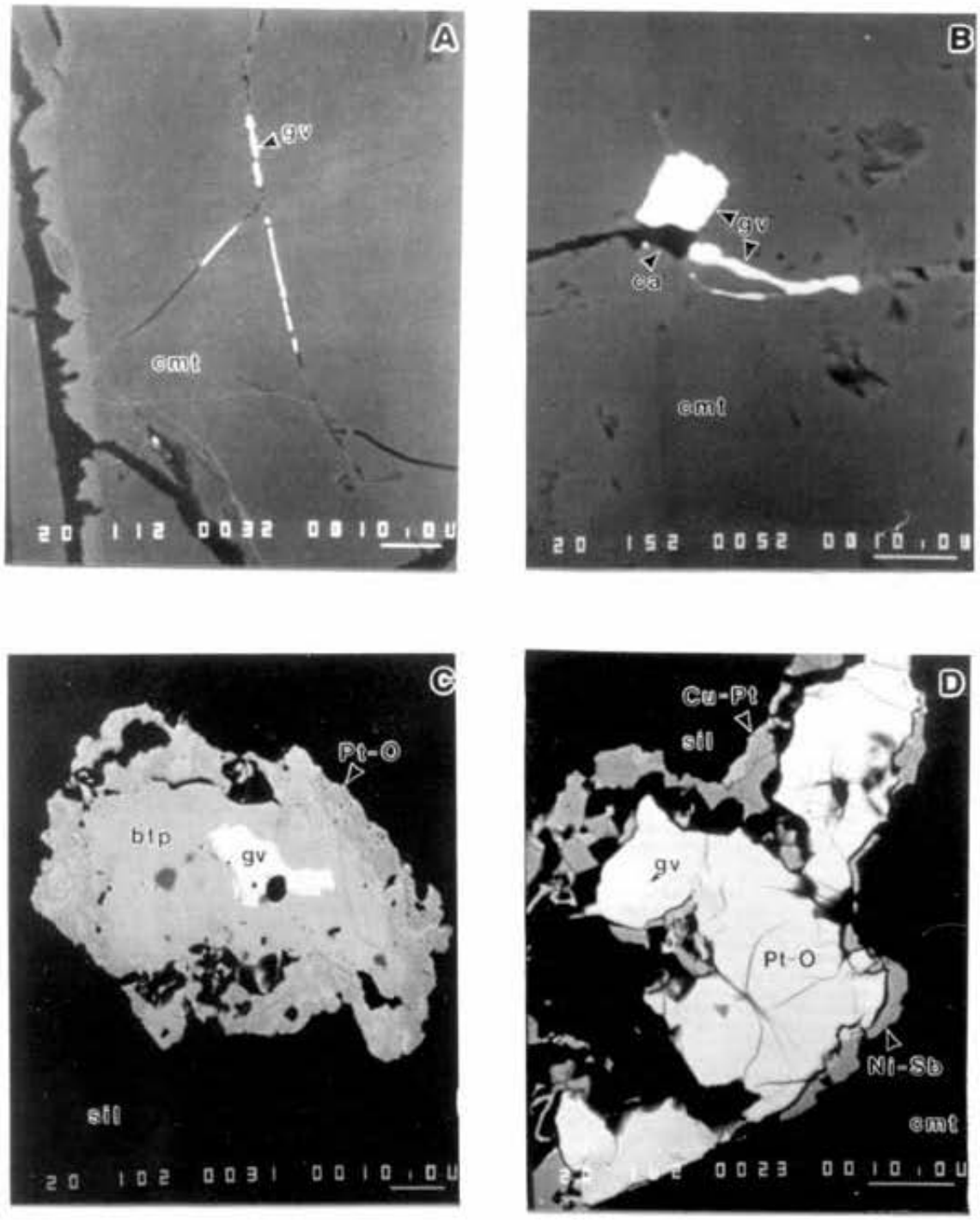

Photo 10.4. SEM photomicrographs of PGM in fractures and complex multimineralic intergrowths in chromitite: A. Fractures in chromite (cmt) filled by serpentine (black) and a platinum antimonide, probably geversite (gv). Note alteration of chromite to ferritchromite-magnetite (medium grey) along wide fractures at left (GN87-148); B. Fissure in chromite filled by geversite (gv) and calcite (ca) adjacent to subhedral geversite grain, probably a pseudomorph after primary platinum alloy in chromite (GN87-148A); C. Compound zoned grain of geversite and breithauptite (btp) with a platinum oxide rim enclosed in serpentine (GN87-148A); D. Composite grain of predominantly platinum oxide with relict geversite enclosed in a vein of serpentine in chromite. Thin discontinuous rims of platinian copper (Cu-Pt) and a nickel antimonide (Ni-Sb), probably breithauptite, also are present (GN87-148B). Bar scale = 10 µm.

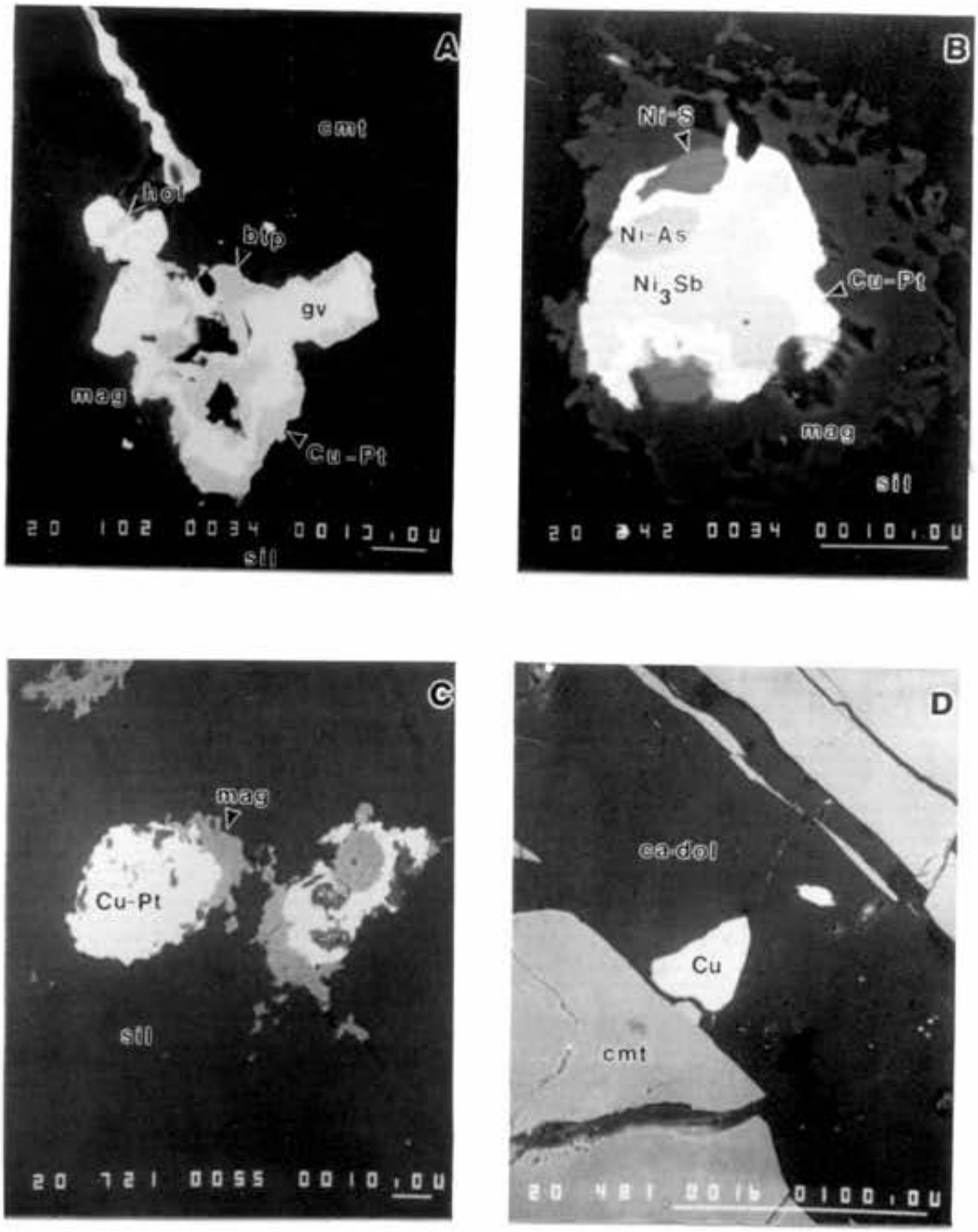

Photo 10.5. SEM photomicrographs of complex mineral intergrowths: A. Large altered grain with a core of geversite (gv) surrounded by irregular intergrowths of breithauptite (btp), platinian copper (Cu-Pt) and hollingworthite (hol) filling an irregular fissure in chromite (cmt) that is marginally altered to <169>ferritchromite<170>-magnetite (mag) (GN87-146A); B. Complex intergrowth of platinian copper, nickel antimonide (Ni3Sb), nickel arsenide (Ni-As) and nickel sulphide (Ni-S) enclosed by serpentine and magnetite (GN87-148A); C. Intergrowth of magnetite and platinian copper in serpentine (GN87-148A); D. Two anhedral grains of native copper (Cu) in a carbonate-filled (ca-dol) fracture in chromite (GN87-147B). Bar scale = 10 μm except in D (100 μm).

TABLE 10.4
ELECTRON-MICROPROBE DATA ON PLATINIAN COPPER IN CHROMITITE AND PLACER NUGGETS

Anal. No.	Grain Size (μm)	Weight percent Pt	Rh	Pd	Ir	Cu	Fe	Ni	Sb	Total	Atomic proportions Pt	Rh	Pd	Ir	Cu	Fe	Ni	Sb
1	13 x 30	33.0	0.10	0.07	-	65.6	0.17	0.40	0.15	99.49	0.14	<0.01	<0.01		0.85	<0.01	0.01	<0.01
2	8 x 40	34.9	0.10	0.05	-	61.9	0.59	2.90	1.30	99.13	0.15	<0.01	<0.01		0.83	0.01	<0.01	0.01
3	3 x 8	34.3	0.14	0.08	-	60.9	1.20	0.78	1.70	99.10	0.15	<0.01	<0.01		0.81	0.02	0.01	0.01
4	15 x 40	36.5	0.10	0.05	-	60.9	0.37	0.69	0.68	99.29	0.16	<0.01	<0.01		0.82	0.01	0.01	<0.01
5	10 x 18	30.4	0.09	0.08	-	59.2	2.10	3.70	3.20	98.77	0.13	<0.01	<0.01		0.77	0.03	0.05	0.02
6	10 x 25	40.1	0.85	0.18	8.6	48.0	2.50	0.07	n.d.	100.30	0.19	0.01	<0.01	0.04	0.71	0.04	<0.01	
7	10 x 25	42.9	0.57	0.24	5.6	48.2	2.20	0.07	n.d.	99.78	0.21	<0.01	<0.01	0.03	0.72	0.04	<0.01	
8	10 x 25	41.8	n.d.	0.30	n.d.	57.3	0.54	n.d.	n.d.	99.94	0.19		<0.01		0.80	0.01		
9	5 x 80	44.7	n.d.	0.45	n.d.	53.7	0.66	n.d.	n.d.	99.51	0.21		<0.01		0.78	0.01		
10	5 x 80	39.8	0.10	0.36	0.4	58.1	0.64	n.d.	n.d.	99.40	0.18	<0.01	<0.01	<0.01	0.80	0.01		

1. GN87-148A: in serpentine; 2. GN87-148B: with Pt oxide, geversite, serpentine and chromite; 3. GN87-148B; with Ni-antimonide and irarsite in chromite; 4. GN87-148A ; with magnetite in serpentine; 5. GN87-146: with Ni-arsenide in serpentine(?) between chromite grains; 6 - 8. M12410, nugget #3: 10 micrometre-wide ring-shaped inclusion in tulameenite; 9 and 10. M12410, nugget #3: as veinlets in tulameenite. n.d. = not detected; - = not determined.

TABLE 10.5
ELECTRON-MICROPROBE DATA ON PLATINUM OXIDE(?) IN CHROMITITE

Weight per cent							
Pt	Rh	Ir	Fe	Cu	Ni	Sb	O*	Total
78.7	0.28	0.92	0.33	4.1	4.4	2.6	8.67	100.00
76.2-80.3**		0.59-1.3		3.5-4.7	3.0-5. 5	2.1-3.0		

**Oxygen by difference. ** Range.*
GN87-148B: complex multimineralic grain with platinian copper, nickel antimonide, geversite(?) and nickel oxide, and surrounded by serpentine, magnetite, and chromite.

TABLE 10.6
ELECTRON-MICROPROBE DATA ON THREE Ni-Sb MINERALS IN CHROMITITE

Anal. No.	Grain Size (μm)	Weight per cent Ni	Cu	Fe	Ir	Pt	Rh	Sb	Total	Atomic proportions Ni	Cu	Fe	Ir	Pt	Rh	Sum	Sb
1	5 x 20	31.1	11.8	0.90	7.0	0.24	0.79	47.8	99.63	1.36	0.48	0.04	0.09	<0.01	0.02	1.99	1.01
2	30 x 60	31.1	0.32	n.d.	n.d.	1.7	0.14	65.9	99.16	0.97	0.01			0.02	<0.01	1.00	1.00
3	7 x 12	57.6	0.26	0.66	n.d.	n.d.	n.d.	40.5	99.02	2.95	0.01	0.04				3.00	1.00

n.d. = not detected; minimum detection limits in wt. % are: Fe 0.03; Rh 0.05; Ir, Pt, As 0.10; As was not detected.
1. GN87-148B: undetermined (Ni, Cu)$_2$Sb mineral complexly intergrown with platinian copper and irarsite enclosed in chromite.
2. GN87-148A: breithauptite in complex polymineralic grain with geversite and Pt oxide enclosed in serpentine.
3. GN87-148A: undetermined Ni$_5$Sb mineral in complex polymineralic grain with platinian copper, undetermined Ni arsenide and sulphide, surrounded by magnetite which is enclosed in serpentine.

TABLE 10.7
ELECTRON-MICROPROBE DATA ON AN UNUSUAL Ni ARSENIDE IN CHROMITITE

Anal. No.	Grain Size (μm)	Weight per cent Ni	Cu	Fe	As	Sb	Total	Atomic proportions Ni	Cu	Fe	Sum	As	Sb	Sum
1	5 x 8	58.8	0.22	4.1	33.3	3.2	99.62	6.47	0.02	0.47	6.96	2.87	0.17	3.04
2	10 x 23	60.8	0.37	1.5	34.3	1.9	98.87	6.72	0.04	0.17	6.93	2.97	0.10	3.07

1. GN87-146A: complex polymineralic grain with platinian copper, Ni sulphide and small Pt-Fe alloy grain in magnetite. 2. GN87-146B: complex polymineralic grain with undetermined Ni antimonide, platinian copper and geversite enclosed in magnetite-chromite.

per, nickel and arsenic as minor constituents; in addition, palladium and ruthenium were reported by St. Louis *et al.* (1986).

Minerals of the hollingworthite-irarsite (RhAsS-IrAsS) solid-solution series are also fairly common. Hollingworthite, associated with sperrylite, replaces the rim of platinum alloy grains in fractured chromite (Photos 10.1B and C). Hollingworthite and irarsite are also minor constituents of composite intergrowths of geversite, breithauptite, platinian copper, platinum oxide, and nickel arsenides and sulphides (Photo 10.5A). Small quantities of platinum, antimony, copper and nickel were detected by qualitative energy-dispersion analysis, but owing to small grain size, we cannot rule out contributions arising from secondary fluorescence of surrounding minerals.

Sperrylite ($PtAs_2$) is also found as a fracture filling, together with serpentine, carbonate and rare hollingworthite (Photo 10.1B). A subhedral crystal of sperrylite lying on a fracture in chromite appears to be completely enveloped by a "ferritchromite"-magnetite alteration zone (Photo 10.1D). This situation is analogous to the one involving geversite (Photo 10.4B) and may also represent replacement of a grain of primary Pt-Fe-Ni-Cu alloy. Minor amounts of ruthenium, iron, antimony and sulphur identified by qualitative energy-dispersion analysis may also be due to secondary fluorescence of neighboring minerals. Similar compositions were obtained by St. Louis *et al.* (1986), who found sperrylite to be one of the most abundant PGM in the Grasshopper Mountain chromitites.

Platinian copper forms a minor phase that occurs late in the paragenetic sequence. It contains up to 36.5 wt% platinum and small quantities of iron (≤2.1 wt%), nickel (≤3.7 wt%), antimony (≤3.2 wt%), rhodium and palladium (<0.15 wt% each; Table 10.4). This Cu-Pt alloy replaces parts of the rim of euhedral platinum alloys in fractured chromite crystals (Photos 10.1A, 10.2C and D), occurs as a thin discontinuous overgrowth on composite platinum oxide - geversite grains (Photos 10.4D and 10.5A), and forms intergrowths with magnetite and nickel sulphides, arsenides and antimonides (Photos 10.5B and C). A Cu-Pt alloy with up to 33 wt% platinum has been reported previously from Thetford Mines (Corrivaux and Laflamme, 1990) and Shetland ophiolites (Prichard *et al.*, 1986), where it also is associated with PGM-bearing chromitites.

Among the less abundant PGM are single grains of erlichmanite (OsS_2) and laurite (RuS_2), and an undefined platinum oxide, which forms the largest PGM grain observed to date (150 μm). The latter phase occurs within a serpentine-filled fissure in chromite and is associated with antimonides, nickel oxide(?) and platinian copper, and locally rims breithauptite (Photos 10.4C and D). Its composition is somewhat heterogeneous, with minor variations in rhodium, iridium, iron (<1.5 wt% each) and copper, nickel and antimony (2 - 5.5 wt%; Table 10.5). In addition to the PGM listed above, St. Louis *et al.* (1986) reported native platinum (Pt-Fe alloy, <20 atom% Fe), stumpflite (PtSb), and the very rare mineral genkinite [$(Pt, Pd)_4Sb_3$], as determined by qualitative energy-dispersion analyses.

BASE METAL MINERALS

Base metal sulphides, arsenides and antimonides, and native metals and metal oxides form a minor yet persistent mineral assemblage in partly serpentinized dunites and chromitites. These minerals typically occupy veinlets or interstices between chromite grains, textures similar to those described by St. Louis *et. al.* (1986; Photos 10.4C and D, 10.5A and B). The most widespread sulphide mineral is disseminated pyrite. Nickel sulphides include millerite or heazlewoodite and an undetermined Ni-Co-Fe sulphide intergrown with "ferritchromite"-magnetite and serpentine. Other nickel-bearing sulphides identified by St. Louis *et al.* (1986) are pentlandite, violarite and bravoite. Analyses of three nickel-antimony minerals, including breithauptite, are given in Table 10.6. They contain small quantities of platinum (≤1.7 wt %), rhodium (≤0.79 wt%) and iridium (up to 7.0 wt%) in addition to copper (≤11.8 wt %) and iron (≤0.9 wt%). Nickel arsenides include maucherite(?) and Ni_7As_3 that contains minor copper, iron and antimony (Table 10.7). Native metal and oxide phases include native copper, identified in calcium-magnesium carbonate veinlets (Photo 10.5D), native silver, and copper and nickel oxides.

PETROGRAPHY AND MINERALOGY OF PLACER NUGGETS

Aspects of the mineralogy of placer nuggets in the Tulameen and Similkameen rivers and their tributaries, and the PGM in particular, have been documented previously (Cabri *et al.*, 1973; Harris and Cabri, 1973; Cabri and Hey, 1974; Cabri and Feather, 1975; Raicevic and Cabri, 1976). Descriptions of specific nuggets given below augment these earlier observations. Results of electron-microprobe analysis of platinum alloys are given in Table 10.2B and plotted in Figure 10.7.

HOLLAND NUGGET

The Holland nugget is a rounded specimen, 4.5 millimetres in diameter, comprising cumulus chromite and minor olivine (<1 mm) set in a matrix of Pt-Fe alloy, probably isoferroplatinum, which contains up to 2.3 wt% palladium (Table 10.2B; Figure 10.7 and Photo 10.6A; *see also* Raicevic and Cabri, 1976; Figure 3). A single grain of laurite (0.5 mm) is included within the alloy. Osmium, platinum oxide and very fine intergrowths of tolovkite (IrSbS), geversite, sperrylite, pentlandite(?) and an undetermined palladium-antimony mineral were also observed. The few crystals of olivine that are present occur at the rim of the nugget. Chromite forms euhedral to subhedral grains with internal fractures and rims altered to magnetite. Magnetite also forms very fine grained intergrowths in Pt-Fe alloy. The ratio of chromite+olivine to PGM is approximately 1:1. Serpentine and magnesium-rich chlorite are trace constituents.

LINCOLN NUGGET

The Lincoln nugget (3 x 5 mm) also contains euhedral to subhedral cumulate chromite and olivine, and intercumulate Pt-Fe alloy, probably isoferroplatinum. Thin zones of magnetite separate the chromite crystals from the platinum alloy which contains relatively coarse intergrowths of mag-

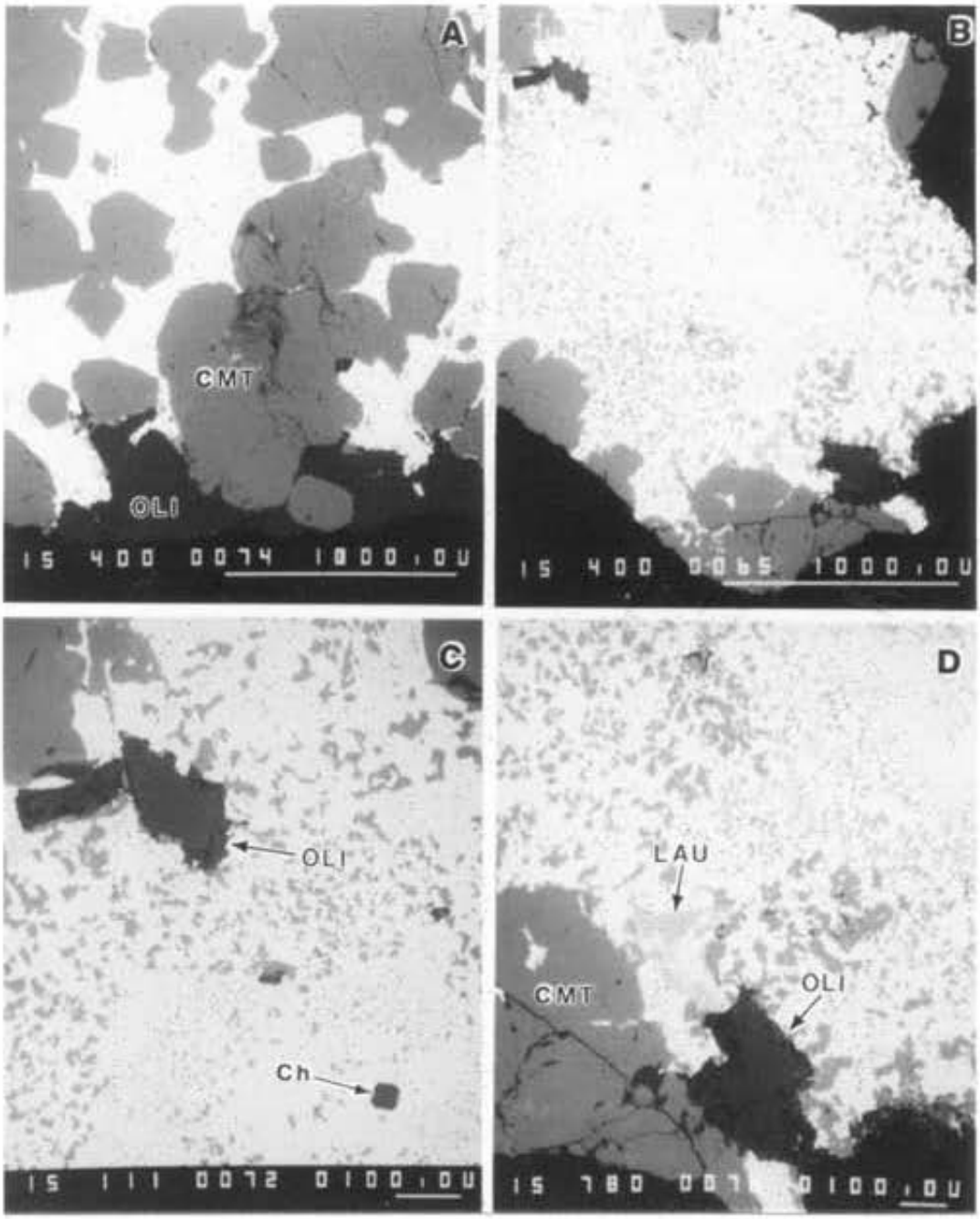

Photo 10.6. SEM photomicrographs of Holland and Lincoln nuggets. All of the chromite, in both nuggets, has a thin magnetite rim of variable thickness (10-25 μm) that cannot readily be seen on these photomicrographs. A. Subhedral chromite (cmt) and minor olivine (oli) included in platinum-iron alloy (white) containing fine intergrowths of magnetite (Holland nugget); B. platinum-iron alloy (white) with irregular intergrowths of magnetite bordered by chromite and olivine (Lincoln nugget); C. Enlargement of B showing olivine inclusion (oli), euhedral grain of chlorite (ch) and magnetite intergrowths in platinum-iron alloy; D. Enlargement of B showing an inclusion of laurite (L) in platinum-iron alloy near the contact with chromite-olivine. Bar scale = 1 mm in A-B, 100 μm in C-D.

netite that are particularly well developed adjacent to chromite (Photo 10.6B; *see also* Raicevic and Cabri, 1976, Figure 4). Inclusions of laurite and euhedral chlorite, possibly pseudomorphous after phlogopite, are also observed (Photos 10.6B-D). A single lath of osmium (25 x 100 µm) in Pt-Fe alloy was reported by Harris and Cabri (1973), and a few small inclusions of genkinite were also observed (not reported previously). Oxide alteration products of chromite are identical in composition to the magnetite intergrowths in Pt-Fe alloy (Table 10.8).

M12410 NUGGETS

Nugget 1 is a medium-size (3 x 4 mm) specimen comprising mainly Pt-Fe alloy (isoferroplatinum?) carrying generally fine-grained intergrowths of iridium (<5 to 20 x 20 µm), very thin laths of osmium, and minor laurite (Photo 10.7). Chromite is a subordinate constituent, forming subhedral to euhedral crystals and grain aggregates (<1 mm). Magnetite forms an intergrowth with Pt-Fe alloy and is a persistent alteration product of chromite. This nugget is particularly well endowed with a diverse assemblage of primary and secondary silicate inclusions (Photo 10.7D and described below).

Nugget 2 is the smallest (2 x 4 mm) of the three nuggets. It consists of Pt-Fe alloy (probably isoferroplatinum) with numerous fine-grained intergrowths of iridium, generally less than 5 µm in size, but reaching 20 x 100 µm. Chromite (<1 mm) is a minor constituent and locally exhibits euhedral margins rimmed by magnetite. No silicate minerals were observed.

Nugget 3 is the largest specimen (4 x 7 mm) and comprises approximately 50 vol% subhedral chromite embedded in a matrix of platinum alloy comprising principally tulameenite with minor isoferroplatinum(?) [$Pt_{2.6}(Fe,Cu,Ni)_{1.4}$] and rare tetraferroplatinum(?) [Pt(Fe,Cu,Ni), Photo 10.8]. The latter two alloys contain approximately 0.9 and 4.6 wt% copper, respectively, and similar amounts of iridium (6.5 - 7.0 wt%; Table 10.2B; Figure 10.7). Other PGM include fine-grained iridium (generally <5 µm in size, but reaching 30 x 40 µm) and thin laths of osmium set in platinum alloy. In addition, platinian copper with up to 44.7 wt% platinum and 8.6 wt% iridium is intergrown with magnetite and forms veinlets within, and rims around, tulameenite (Table 10.4; Photo 10.8D). Subhedral cumulate olivine and a variety of other silicate minerals enclosed in chromite and platinum alloy have also been identified (described below).

TABLE 10.8
ELECTRON-MICROPROBE DATA ON MAGNETITE IN PLATINUM NUGGETS

Anal. No.	1	2	3	4	5
SiO_2	-	-	0.26	0.27	-
TiO_2	-	-	-	-	-
Al_2O_3	-	-	-	-	-
Cr_2O_3	0.86**	0.63**	-	-	1.2**
Fe_2O_3*	68.3	68.2	68.4	68.6	67.8
FeO	28.5	28.3	28.7	28.2	28.8
MnO	-	0.18	0.18	0.25	0.30
MgO	1.5	1.4	1.4	1.7	1.1
Total	99.16	98.71	98.94	99.02	99.20
Cations per 32 Oxygen Atoms					
Si			0.080	0.083	
Ti					
Al					
Cr	0.209	0.154			0.292
Fe^{3+}	15.791	15.846	15.840	15.834	15.708
Fe^{2+}	7.313	7.309	7.390	7.240	7.417
Mn		0.047	0.047	0.065	0.078
Mg	0.687	0.644	0.643	0.778	0.505

* *Calculated assuming ideal stoichiometry.*
** *Part of the Cr_2O_3 reported could be due to fluorescence from the surrounding chromite.*
\- *not determined.*
1-2: Lincoln nugget, magnetite rim on chromite;
3-4: Lincoln nugget, magnetite intergrowth in Pt-Fe alloy;
5: Holland nugget, magnetite rim on chromite.

PLATINUM-GROUP MINERALS IN BEDROCK VERSUS PLACERS

The species of PGM in chromitites and placer deposits of the Tulameen region and their relative frequency are listed in Table 10.9. These data represent an important first step in an evaluation of the potential source(s) of PGE mineralization in the placers.

The principal PGM in both chromitites and placer nuggets are Pt-Fe-Cu-Ni alloys. However, the most abundant alloy species in chromitites is tetraferroplatinum [Pt(Fe,Ni,Cu)], closely followed by "isoferroplatinum" [$Pt_{2.5}(Fe,Ni,Cu)_{1.5}$], whereas "isoferroplatinum" [$Pt_{2.6}(Fe,Cu,Ni)_{1.4}$ to Pt_3Fe], native and ferroan platinum predominate in the placers (Raicevic and Cabri, 1976). In addition, geversite, sperrylite and rhodium-iridium sulpharsenides appear in greater abundance in the chromitites. Phases present in the placers yet apparently lacking in the chromitites include Ru-Ir-Os and Pt-Ir alloys, cooperite, tolovkite and an unnamed rhodium-antimony-sulphur mineral.

When all of the analytical data for Pt-Fe-Cu-Ni alloys are considered, it is clear that there is a considerable range of solid solutions (Figure 10.7). Except for a nickeloan variety of tulameenite(?), placer alloys are depleted in nickel relative to those in chromitites (Figures. 10.7C and D), but have a similar range of copper abundances (Figure 10.7B). Isoferroplatinum compositions in chromitites occupy the platinum-poor end of a continuous range of essentially Pt-Fe alloys that extend to native platinum, and a small compositional gap separates isoferroplatinum from tetraferroplatinum.

The mineralogical and compositional discrepancies between the PGM in chromitites and placers are perhaps not as striking as certain differences in grain size and texture. Platinum alloys in nuggets attain millimetre-scale dimensions and poikilitically enclose large primocrysts of chromite and olivine. In contrast, grains in the chromitites rarely exceed 30 µm across and are almost invariably enclosed in chromite. We note that the larger nuggets were obtained

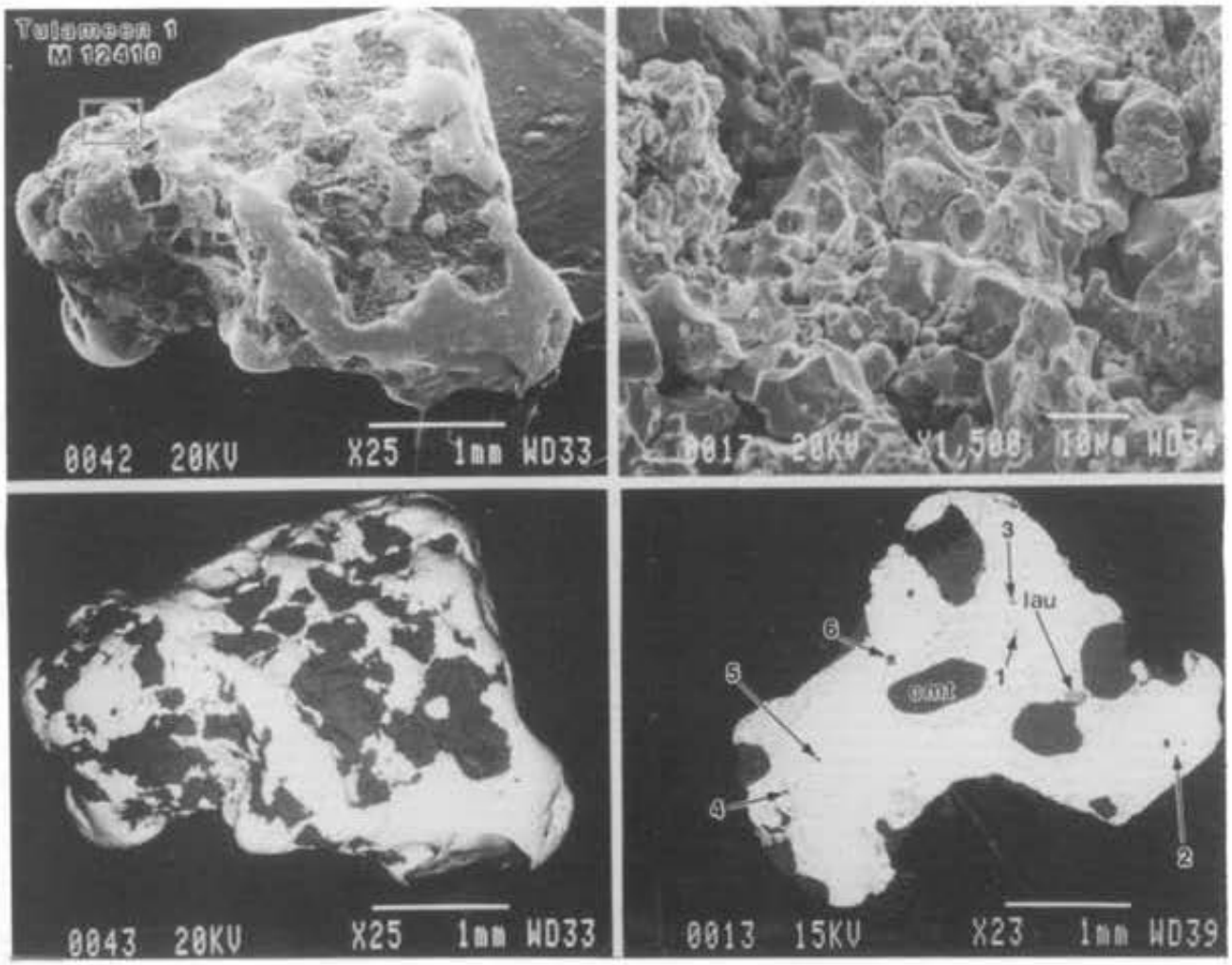

Photo 10.7. SEM photomicrographs of M12410 nugget 1: A. Low-magnification image of variably pitted surface of <169>knobby<170> nugget; B. High-magnification image of area outlined in A, showing irregular surface detail of platinum-iron alloy; C. Back-scattered electron image of A, clearly showing the chromite (dark grey) in the platinum-iron alloy matrix (white); D. Cross-section of nugget showing platinum-iron alloy with inclusions of laurite (lau), chromite (cmt) and very fine grained magnetite concentrated around chromite grains; arrows show the location of silicate inclusions that were analyzed (*cf.* Inclusion No.,Table 10.12, except Inclusion 6 which is an intergrowth of magnetite, chlorite and clinopyroxene). Bar scale = 1 mm except B (10 μm).

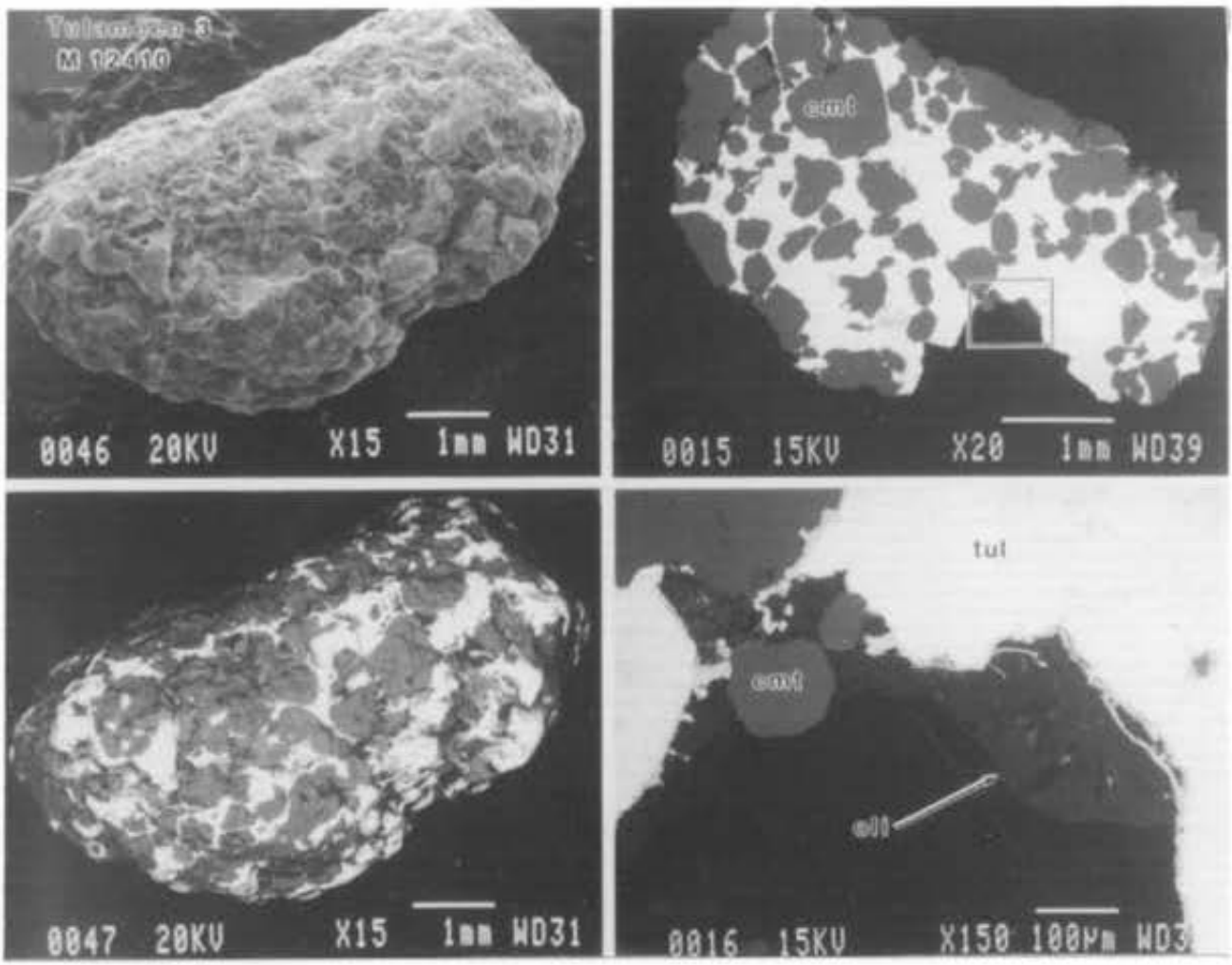

Photo 10.8. SEM photomicrographs of M12410 nugget 3: A. Low-magnification image of irregular surface features of nugget; B. Back-scattered electron image, clearly distinguishing chromite (dark grey) from platinum alloy (white) comprised mainly of tulameenite, minor isoferroplatinum(?) and rare tetraferroplatinum(?); C. Cross section of nugget showing subhedral chromite (cmt) set in matrix of platinum alloy; D. Enlargement of area outlined in C showing chromite and olivine (oli) in contact with tulameenite (tul), which is veined and rimmed by platinian copper (light grey). Bar scale = 1 mm except in D (100 µm).

TABLE 10.9
PLATINUM-GROUP MINERALS IN TULAMEEN CHROMITITES VERSUS PLACERS

Mineral	Ideal Formula	Minor Constituents	Chromitites[1]	Placers[1]	Ref.[2]
cooperite	PtS	Pd, Ni	-	x	6
Cu-Pt alloy	(Cu, Pt)	Pd, Rh, Fe, Ni, Sb	xx	x	1
erlichmanite	OsS_2	Pt, Pd, Rh, Ir	x	x	1, 6
genkinite	$(Pt, Pd)_4Sb_3$	Rh, S	x	x	1, 4
geversite	$PtSb_2$	Rh, Ir, Fe, Cu, Ni, As	xx	x	1, 6
hollingworthite-irarsite series	Rh-Ir(AsS)	Pt, Pd, Rh, Os, Ru, Sb, Cu, Ni, Co	xx	x	1, 4, 6
iridium	Ir	Pd, Rh, Os, Ru, Fe, Cu, Ni	-	x	5
iridosmine*	(Os, Ir)	Pt, Pd, Rh, Ru, Fe, Cu, Ni	-	xx	1, 5
isoferroplatinum	Pt_3Fe	Pd, Rh, Ir, Os, Cu, Ni, Sb	(xxx)	xxx	1, 2, 6
kotulskite*	PdTe	Pt, Sb, Bi	-	x	6
laurite	RuS_2	Rh, Ir, Os	x	x	1, 6
osmiridium**	(Ir, Os)	Pd, Rh, Ru, Fe, Cu, Ni	-	x	1, 5
osmium	Os	Pt, Pd, Rh, Ir, Ru, Fe, Cu, Ni	-	xx	5
platiniridium***	(Ir, Pt)	Os, Ru, Fe, Cu, Ni	-	x	7
platinum, ferroan	(Pt, Fe)>20 at. % Fe	Ir, Cu, Ni	-	xxx	2, 6
platinum, native	(Pt, Fe)>80 at. % Pt	Pd, Ir, Fe, Cu, Ni	x	xxx	2, 6
platinum oxide	(Pt, O)?	Rh, Ir, Fe, Cu, Ni, Sb	x	-	1
Pt-Fe-Cu-Ni alloys**	(Pt, Fe, Cu, Ni)	Pd, Rh, Ir, Sb	xxx	x	1
rutheniridosmine	(Ru, Os, Ir)	Pt, Pd, Rh, Fe, Cu, Ni	-	x	5
sperrylite	$PtAs_2$	Pd, Ni, Ru, Fe, Sb, S	xx	x	1, 4, 6
stumpflite	PtSb	Pd, Ru	x	-	4
tetraferroplatinum	PtFe	Pd, Rh, Ir, Cu, Ni, Sb	(xxx)	x	1
tolovkite***	IrSbS	Rh, As	-	x	3, 6
tulameenite	Pt_2FeCu	Pd, Rh, Ir, Os, Ni, Sb	xx	xx	1, 3
unnamed RhSbS	RhSbS	Pt, Ir, As	-	x	3, 6

* *found as inclusions in one grain of gold; not derived from the Tulameen ultramafic complex.*

** *see text for nomenclature.* ****Originally reported as unnamed IrSbS (6). Using the nomenclature of Harris and Cabri (1991): + = osmium; ++ = iridium; +++ = platinian iridium.*

1 *Frequency: xxx = most common; xx = common; x = infrequent to rare; (xxx) = probably present in Pt-Fe-Cu-Ni alloys but not confirmed by XRD.*

2 *References: 1. This study; 2. Cabri & Feather (1975); 3. Cabri et al. (1973); 4. St. Louis et al. (1986); 5. Harris & Cabri (1973); 6. Raicevic & Cabri (1976); 7. Cabri & Hey (1974).*

from placers near the eastern margin of the ultramafic complex, whereas material collected farther downstream typically occurs as fine flakes (-150 mesh; Raicevic and Cabri, 1976). We believe that these differences are best explained by inadequate sampling or complete erosion of high-grade lode occurrences. For example, the richer and more extensively exploited platinum deposits of the Urals contain sizeable concentrations of Pt-Fe alloys in bedrock, with textures matching the coarse intergrowths involving chromite and olivine in placer nuggets (*cf.* Duparc and Tikonowitch, 1920; Cabri and Genkin, 1991).

CHEMISTRY OF CHROMITE AND SILICATE MINERALS

Analyses were done on selected grains of chromite, olivine and other minor silicate inclusions in platinum nuggets in order to compare their compositions with cumulate minerals in the Tulameen complex and to determine more precisely the source of the PGE mineralization. The analytical results are presented in Tables 10.10 to 10.12.

CHROMITE

The compositions of chromiferous spinels in placer nuggets and Tulameen chromitites are given in Table 10.10 and plotted in Figures 10.8 and 10.9. Nugget spinels have high chromium (35.1 - 50.6 wt% Cr_2O_3), highly variable iron (11.9 - 28.2 wt% Fe_2O_3) and rather low aluminum (6.0 - 8.7 wt% Al_2O_3). The relatively high Fe^{3+} content of the spinel appears to be a general characteristic of Alaskan-type intrusions (Irvine, 1967). The Holland nugget contains the most chromium-rich spinel; the Lincoln nugget exhibits appreciable intergrain zoning (35.1 - 39.2 wt% Cr_2O_3). Spinel compositions within each M12410 nugget are fairly uniform. Variations in Cr/(Cr+Al) on the whole are limited (0.79 - 0.83) and even more uniform within individual nuggets. No systematic differences in composition have been detected between spinel grains that seem to be completely encapsulated by Pt-Fe alloys and grains in areas of more massive chromite.

Most spinel grains in the nuggets fall within the compositional field of Tulameen chromitites, although the Lincoln nugget exhibits some overlap with spinel compositions found in dunite, and the Holland nugget contains the most magnesium-rich, and ΣFe- and Fe^{3+}-poor spinel (Figures. 10.8 and 9). In general, chromite in the nuggets is quite distinct from the cumulus spinel in olivine and hornblende-rich clinopyroxenites, which approaches the pure magnetite endmember in the latter rock type (most clearly distinguished in Figure 10.8). Cumulus spinel is comparatively rare in the more clinopyroxene-rich olivine clinopyroxenites, and typically absent in olivine-free clinopyroxenites. The absence of a spinel phase may be related to a reaction relationship

TABLE 10.10
ELECTRON-MICROPROBE DATA ON CHROMITE IN CHROMITITES AND PLACER NUGGETS

	Nuggets													Chromitites		
	LINCOLN					HOLLAND		M12410						147	148	50
Analysis:	1	2	3	4	5	6	7 (n=8)*	8 (n=4)*	9 (n=2)*	10 (n=3)*	11 (n=2)*	12 (n=4)*	13 (n=3)	14 (n=16)*	15 (n=12)*	16 (n=8)*
SiO_2	0.16	0.31	0.25	0.30	0.24	0.18	0.22	0.26	0.27	0.24	0.32	0.21	0.35	0.27	0.19	0.19
TiO_2	0.68	0.88	0.69	0.86	0.83	0.84	0.59	0.56	0.58	0.50	0.29	0.47	0.35	0.78	0.42	0.51
Al_2O_3	6.10	6.20	6.00	6.60	6.20	6.10	8.70	7.90	8.00	6.70	6.70	7.60	7.70	6.31	7.28	7.45
Cr_2O_3	39.20	35.40	35.50	37.80	36.00	35.10	50.60	48.30	48.80	48.70	49.20	47.50	47.70	37.03	43.65	49.01
Fe_2O_3**	23.50	27.50	28.20	25.30	26.60	28.20	11.90	15.40	15.00	16.10	15.80	16.30	16.20	26.70	20.88	15.36
FeO	22.60	20.20	19.50	21.80	22.00	22.70	14.90	15.90	16.10	17.50	17.50	17.00	17.10	20.71	18.40	17.20
MnO	0.62	0.50	0.52	0.27	0.57	0.15	0.34	0.17	0.25	0.43	0.45	0.45	0.16	0.48	0.45	0.35
MgO	6.60	8.50	8.70	7.90	7.20	7.10	12.20	11.60	11.60	10.30	10.20	10.60	10.80	7.96	9.57	10.49
NiO	-	-	-	-	-	-	-	0.06	0.08	0.11	0.12	0.05	0.05	-	-	-
ZnO	-	-	-	-	-	-	-	0.13	0.11	0.13	0.15	0.12	0.13	-	-	-
Total	99.46	99.49	99.36	100.83	99.64	100.37	99.45	100.28	100.79	100.71	100.73	100.30	100.54	100.23	100.84	100.56
Cations per 32 Oxygen atoms																
Si	0.045	0.086	0.070	0.082	0.067	0.050	0.059	0.069	0.071	0.064	0.086	0.056	0.093	0.075	0.051	0.051
Ti	0.144	0.183	0.144	0.177	0.174	0.175	0.118	0.112	0.115	0.101	0.058	0.094	0.070	0.162	0.085	0.103
Al	2.011	2.018	1.955	2.125	2.033	1.991	2.710	2.466	2.484	2.113	2.114	2.394	2.413	2.042	2.301	2.338
Cr	8.670	7.727	7.757	8.162	7.919	7.685	10.573	10.111	10.162	10.304	10.415	10.035	10.025	8.037	9.255	10.318
Fe^{3+}	4.947	5.713	5.865	5.199	5.569	5.877	2.367	3.062	2.982	3.253	3.182	3.270	3.236	5.516	4.214	3.078
Fe^{2+}	5.287	4.664	4.507	4.979	5.119	5.257	3.294	3.526	3.538	3.909	3.916	3.792	3.811	4.755	4.127	3.801
Mn	0.147	0.117	0.122	0.063	0.135	0.036	0.077	0.038	0.056	0.097	0.102	0.102	0.036	0.110	0.103	0.079
Mg	2.752	3.498	3.584	3.216	2.986	2.931	4.806	4.579	4.554	4.109	4.071	4.222	4.280	3.257	3.825	4.164
Ni								0.013	0.017	0.024	0.026	0.011	0.011	0.000	0.000	0.000
Zn								0.025	0.021	0.026	0.030	0.024	0.026	0.000	0.000	0.000
Cr #	81.2	79.3	79.9	79.3	79.6	79.4	79.6	80.4	80.4	83.0	83.1	80.7	80.6	79.7	80.1	81.5
Mg #	34.2	42.9	44.3	39.2	36.8	35.8	59.3	56.5	56.3	51.3	51.0	52.7	52.9	40.7	48.1	52.1

TABLE 10.11
ELECTRON-MICROPROBE DATA ON OLIVINE IN PLATINUM NUGGETS

	Nuggets						Tulameen Complex	
	Lincoln				Holland	M12410-3	Dunite	Chromitite
	1	2	3	4	5	6 (n=3)*	7 (n=6)*	8 (n=7)*
SiO_2	41.50	41.90	41.40	41.20	41.40	41.70	40.50	41.54
TiO_2	-	-	-	-	-	-	0.01	0.01
Al_2O_3	-	-	-	-	-	-	0.08	0.12
FeO	6.70	5.20	6.10	5.40	4.80	5.80	10.69	5.95
MnO	-	-	-	-	-	-	0.24	0.09
MgO	51.90	52.90	52.30	52.30	53.20	52.40	47.97	52.10
CaO	-	-	-	-	-	-	0.22	0.19
Total	100.10	100.00	99.80	98.90	99.40	99.90	99.71	100.00
Cations per 4 Oxygen atoms								
Si	1.001	1.004	0.999	1.000	0.997	1.003	1.000	1.000
Ti							0.001	0.001
Al							0.003	0.004
Fe	0.136	0.105	0.124	0.110	0.097	0.117	0.221	0.120
Mn							0.006	0.002
Mg	1.865	1.889	1.881	1.892	1.910	1.879	1.766	1.869
Ca							0.006	0.005
XY	2.001	1.994	2.005	2.002	2.007	1.996	2.002	2.001
Z	1.001	1.004	0.999	1.000	0.997	1.003	1.000	1.000
Fo%	93.2	94.7	93.8	94.5	95.2	94.1	88.9	94.0

** Average of n spot analyses. Analyses of random grains at rim of nugget (1-3) and totally encapsulated within Pt-Fe alloy (4). Analysis 5: grain at rim of nugget. Analysis 6: olivine grain at rim of nugget in contact with tulameenite and platinian copper. Analyses 7 and 8 represent a microprobe traverse across a dunite-chromitite contact in a thin section of sample GN87-159 (location shown in Figure 10.6). - not determined.*

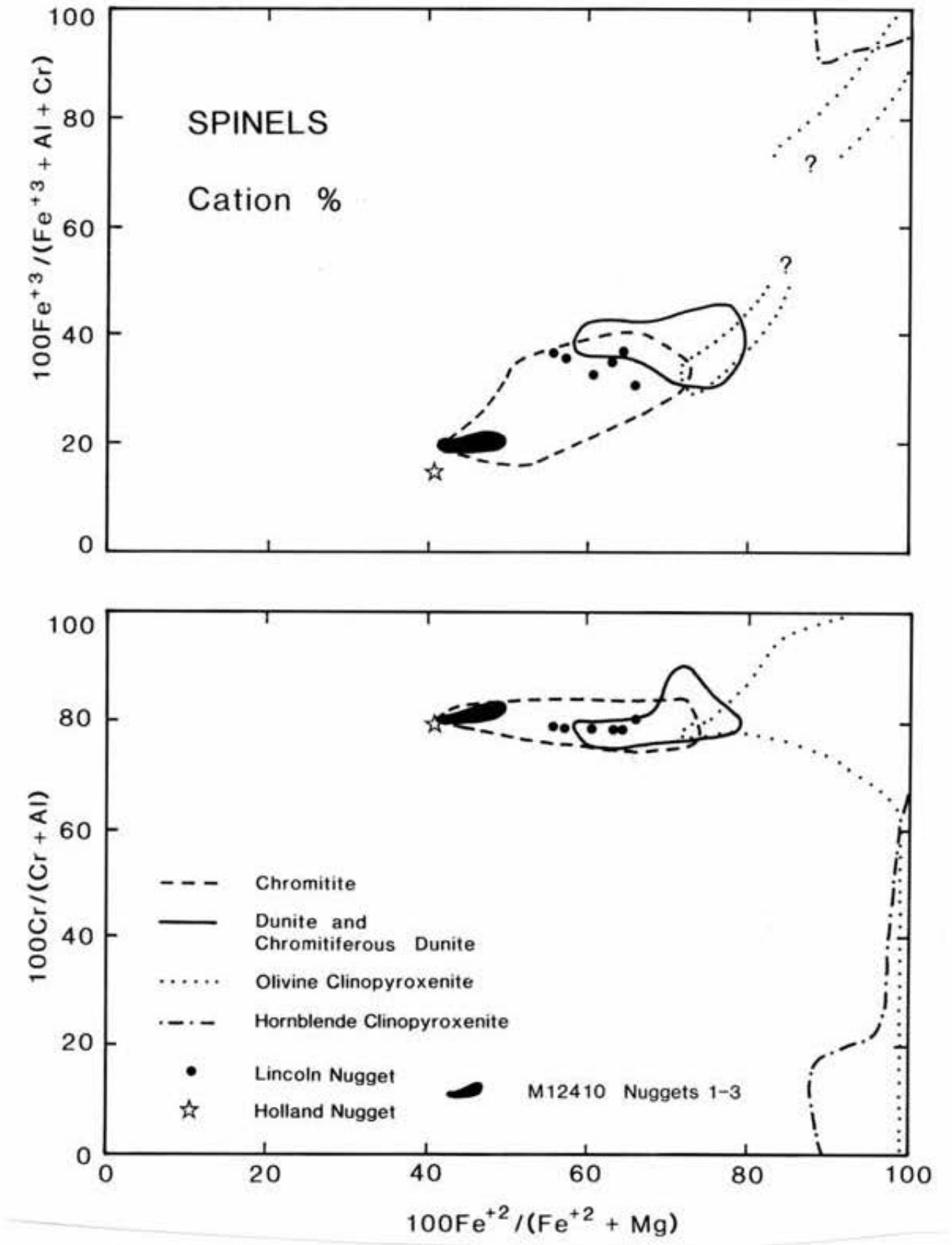

Figure 10.8. Plots of $Fe^{2+}/(Fe^{2+}+Mg)$ versus Cr/(Cr+Al) and $Fe^{3+}/(Fe^{3+}+Al+Cr)$ for chromiferous spinel in placer nuggets (32 analyses) in comparison to spinel compositions (264 analyses) in major rock types of the Tulameen complex.

TABLE 10.12
ELECTRON-MICROPROBE DATA ON MINOR SILICATE INCLUSIONS IN PLATINUM NUGGETS

	Nuggets												Tulameen Complex				
			M12410-1								M12410-3		163	179	88	88	88
Host:	PtFe	PtFe	PtFe	PtFe	PtFe	PtFe	PtFe	PtFe	Cmt	Cmt	Cmt	Cmt	Ol Cpxite		Hb Cpxite		
Incl. No.:	1	1	2a	2a	2b	2b	5	5	7	7	(n=6)*	5					
Mineral:	Hb	Bi	Cpx	Plag	Cpx	Plag	Ep	Cpx	Cpx	Phlog	Ch	Phlog	Cpx	Phlog	Cpx	Hb	Bi
SiO_2	42.10	35.20	54.00	69.00	53.10	68.50	38.50	53.80	54.60	39.90	30.70	38.60	54.42	38.79	52.05	41.40	37.30
TiO_2	0.52	1.30	0.00	0.06	0.09	0.00	0.18	0.09	0.06	0.22	0.06	0.30	0.14	0.80	0.27	1.88	2.97
Al_2O_3	10.60	13.30	0.59	19.50	0.15	19.90	25.10	1.00	0.73	13.80	14.70	15.00	0.75	14.91	2.15	12.40	15.80
Cr_2O_3	0.16	0.00	0.00	0.00	0.00	0.10	0.09	0.13	1.30	2.00	2.87	2.20	0.44	0.39	0.00	0.00	0.00
FeO	21.30	22.30	7.60	0.21	12.70	0.25	10.00	6.60	1.30	2.50	1.93	1.90	2.11	4.29	7.54	12.80	13.59
MnO	0.29	0.06	0.18	0.06	0.18	0.00	0.11	0.17	0.17	0.00	0.09	0.14	0.00	0.00	0.22	0.12	0.22
MgO	7.40	10.90	12.90	0.15	10.10	0.16	0.00	13.40	17.70	26.30	35.92	27.70	17.27	26.67	14.25	13.36	16.93
CaO	10.90	0.25	24.10	0.28	25.00	0.42	24.20	23.40	26.30	1.10	0.02	0.00	25.27	0.10	23.69	12.26	0.00
Na_2O	2.70	0.00	0.85	10.20	0.00	9.80	0.00	1.40	0.19	0.29	0.06	0.00	0.10	0.00	0.25	1.67	0.08
K_2O	1.00	7.90	0.00	0.30	0.00	0.00	0.00	0.00	0.00	7.20*	0.02	8.40	0.00	9.16	0.04	1.69	9.02
Total	96.97	91.21	100.22	99.76	101.32	99.13	98.18	99.99	102.35	93.31	86.37	94.24	100.50	95.11	100.46	97.58	95.91
	Cations per number of Oxygen atoms																
No. of Oxygens	23	22	6	8	6	8	25	6	6	22	28	22	6	22	6	23	22
Si	6.546	5.690	2.008	3.010	2.002	3.002	6.165	1.997	1.949	5.692	5.880	5.475	1.973	5.510	1.932	6.180	5.485
Ti	0.061	0.159	0.000	0.002	0.003	0.000	0.022	0.003	0.002	0.024	0.009	0.032	0.004	0.086	0.008	0.212	0.329
Al	1.943	2.534	0.026	1.003	0.007	1.028	4.737	0.044	0.031	2.320	3.319	2.508	0.033	2.496	0.095	2.182	2.739
Cr	0.020	0.000	0.000	0.000	0.000	0.000	0.012	0.004	0.037	0.226	0.435	0.247	0.013	0.044	0.000	0.000	0.000
Fe	2.770	3.015	0.237	0.008	0.401	0.010	1.340	0.205	0.039	0.299	0.310	0.226	0.064	0.510	0.234	1.598	1.672
Mn	0.039	0.009	0.006	0.003	0.006	0.000	0.015	0.006	0.006	0.000	0.015	0.017	0.000	0.000	0.007	0.016	0.028
Mg	1.715	2.626	0.715	0.010	0.568	0.011	0.000	0.742	0.942	5.592	10.254	5.856	0.933	5.647	0.789	2.973	3.711
Ca	1.816	0.044	0.960	0.014	1.010	0.020	4.152	0.931	1.006	0.169	0.005	0.000	0.982	0.016	0.942	1.961	0.000
Na	0.814	0.000	0.062	0.863	0.000	0.833	0.000	0.101	0.014	0.081	0.023	0.000	0.008	0.000	0.018	0.484	0.023
K	0.199	1.629	0.000	0.017	0.000	0.000	0.000	0.000	0.000	1.311	0.005	1.520	0.000	1.660	0.002	0.322	1.692
X	2.83	1.63					4.19			1.39		1.52		1.66		2.77	1.72
			2.01	0.92	1.99	0.87		2.03	1.98		12.25		2.03		2.03		
Y	5.09	6.08					6.09			6.32		6.38		6.31		5.16	5.96
Z	8.00	8.00	2.01	4.01	2.00	4.04	6.16	2.00	2.05	8.00	8.00	7.98	2.00	8.00	2.00	8.00	8.00
Ca (An)	28.8		50.2	(1.6)	51.0	(2.3)		49.6	50.6				49.6		47.9	30.0	
Mg (Ab)	27.2		37.4	(96.5)	28.7	(97.7)		39.5	47.4				47.2		40.1	45.5	
Fe (Or)	44.0		12.4	(1.9)	20.3	(0.0)		10.1	2.0				3.2		12.0	24.5	
Mg #	38.2	46.6	75.1		58.6			78.4	96.0	94.9	97.1	96.3	93.6	91.7	77.1	65.0	68.9

** Average of 6 random grain analyses. Mg # = 100 Mg/(Mg+Fe**). * low K_2O probably due to loss of K in electron beam. Hb - hornblende; Bi - biotite; Cpx - clinopyroxene; Plag - plagioclase; Ep - epidote; Phlog - phlogopite; Ch - chlorite; Cmt - chromite; PtFe - platinum-iron alloy; Ol Cpxite - olivine clinopyroxenite; Hb Cpxite - hornblende clinopyroxenite.*

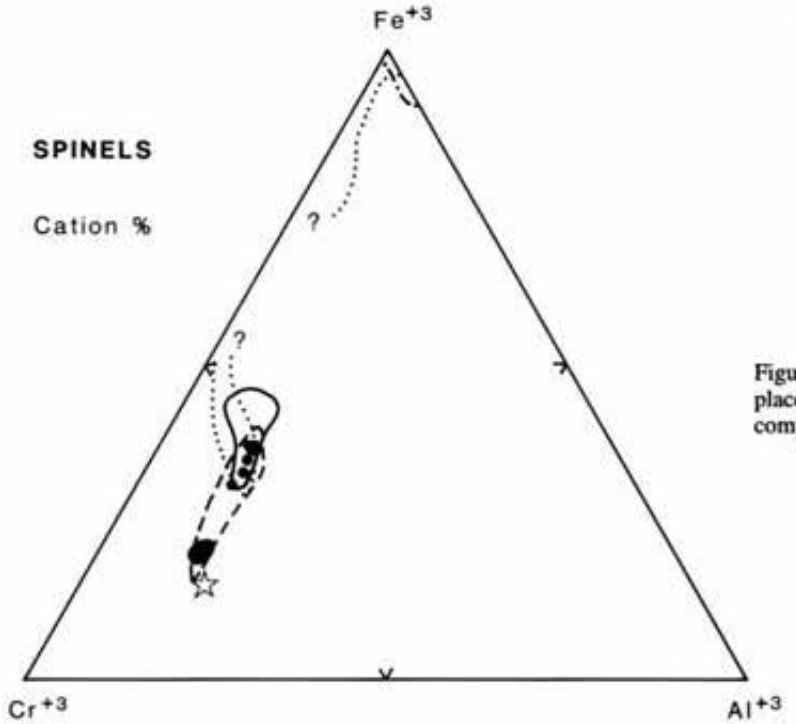

Figure 10.9. Fe^{3+}-Cr-Al plot of spinel compositions in placer nuggets and major rock types of the Tulameen complex. Same data and symbols as Figure 10.8.

between spinel and coexisting silicate melt at a point where chromium-bearing clinopyroxene becomes a dominant phase on the liquidus (Irvine, 1967; Hill and Roeder, 1974). The trend of spinel compositions in olivine clinopyroxenites away from the Cr-Al join in the cation plot (Figure 10.9), and toward "ferritchromite" or chrome-bearing to chrome-free magnetite, reflects loss of aluminum (and magnesium) and gain of Fe^{2+} and Fe^{3+} during low-temperature alteration (*e.g.*, Bliss and MacLean, 1975; Evans and Frost, 1975). As documented above, similar alteration is present at the margins of chromite grains in platinum nuggets. The compositional gap in the field for olivine clinopyroxenites (Figures 10.8 and 10.9) coincides with a sharp decrease in the modal abundance of spinel in clinopyroxenites (*c.f.* Hill and Roeder, 1974).

From the preceding data, it is clear that the abundance and composition of chromite in the nuggets point to a source of PGE-enriched placer material located within the dunite core of the Tulameen complex.

OLIVINE

Compositions of olivine grains in nuggets and ultramafic rocks of the Tulameen complex (Table 10.11) are plotted in Figure 10.10. The olivine in the nuggets has a composition extending from $Fo_{93.2}$ to $Fo_{95.2}$, with little variation among, or within, the individual nuggets. These compositions are distinct from those in olivine clinopyroxenite (Fo_{83-91}) or dunite (Fo_{88-91}), and closely match olivine compositions in the Tulameen chromitites (Fo_{92-95}; Figure 10.10). The limited number of dunite samples analyzed in this study is supplemented by data from Findlay (1963), who conducted more extensive sampling of the dunite core (Figure 10.6). Although Findlay's data were obtained on mineral separates by an x-ray-diffraction technique, his determinations are in good agreement with our microprobe analyses. The results clearly indicate that the dunite core as a whole is characterized by limited variation of olivine compositions.

The olivine compositions in these chromitites, however, are not primary. Numerous studies have pointed out the tendency for spinel and olivine to re-equilibrate under high-temperature, subsolidus conditions such that $Mg/(Mg+Fe^{2+})$ decreases in spinel and increases in olivine (*e.g.*, Irvine, 1965; Clark, 1978). All other factors being equal, the degree of subsolidus exchange during slow cooling is dictated by mass-balance considerations, namely the relative modal abundance of chromite and olivine within the effective equilibration volume. These effects can be quite pronounced on the scale of a single thin section. For example, Analyses 7 and 8 in Table 10.11 represent averages of olivine compositions in dunite and chromitite at opposite ends of the same thin section. Significant differences exist between cumulate olivine (Fo_{90}) in dunite that contains approximately 1 vol% spinel, and that trapped within part of a thin (3 cm) layer of chromitite containing approximately 5 vol% olivine primocrysts (Fo_{94}). From these data, it is evident that the highly magnesian compositions characteristic of olivine in the platinum nuggets are an unmistakable and predictable signature of their chromitite heritage.

SILICATE INCLUSIONS IN NUGGETS

In addition to olivine, M12410 Nuggets 1 and 3, and particularly Nugget 1, contain a number of inclusions of primary and secondary silicates (Photo 10.9). Representative compositions of the various minerals are given in Table 10.12 (*c.f.* Photo 10.7D) where the inclusion number identifies coexisting phases in specific inclusions. Silicates considered to be primary comprise clinopyroxene, hornblende, iron-magnesium mica (biotite-phlogopite) and plagioclase. Minerals indicative of secondary alteration principally include serpentine (compositions not given), chlorite and epidote, and trace amounts of quartz and sericite, and presumably represent the effects of subsequent regional metamorphism. Most inclusions are small (<200 μm across), incorporate more than a single mineral phase, and are hosted predominantly by platinum alloy (rarely chromite). They contain euhedral to anhedral crystals that rarely

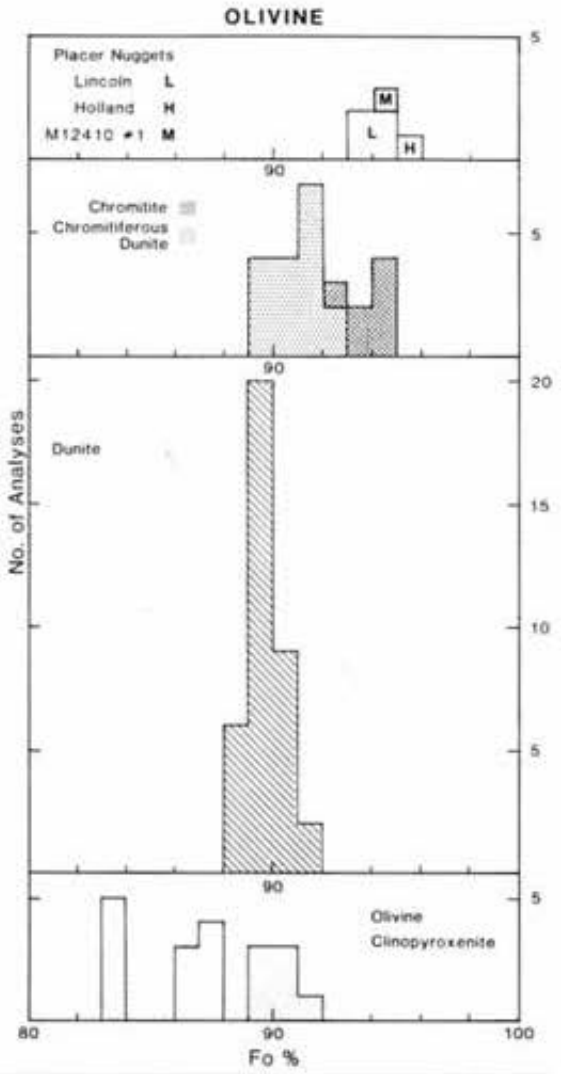

Figure 10.10. Histogram showing the distribution of olivine compositions (% forsterite) in placer nuggets (8 spot analyses) and ultramafic rocks (80 analyses) of the Tulameen complex.

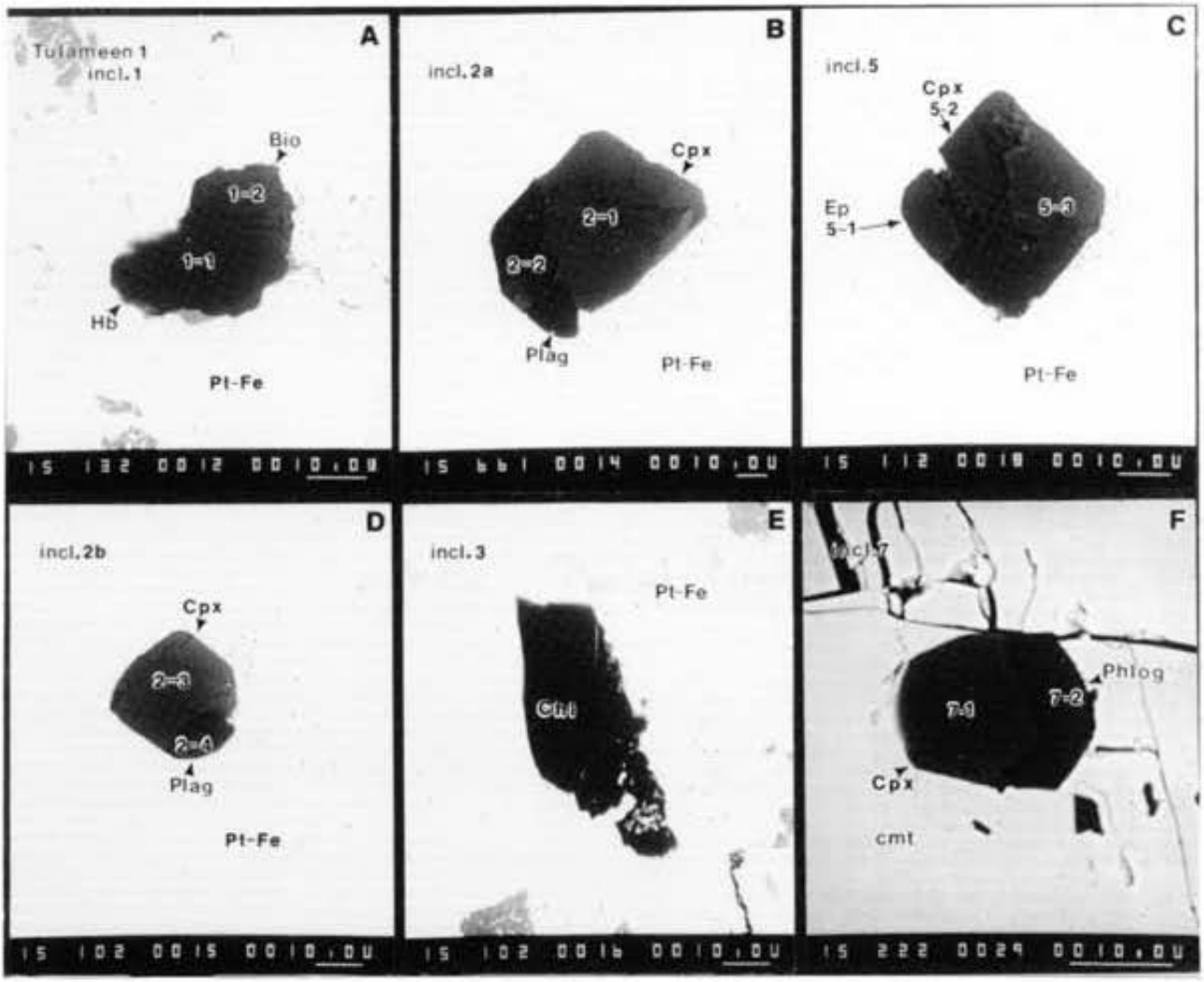

Photo 10.9. SEM photomicrographs of silicate inclusions hosted by platinum alloy (Pt-Fe) and chromite (cmt) in nugget M12410-1 (*cf.* Table 10.12 and Photo 10.7D). A. Coexisting iron-rich biotite (Bio) and ferroan hornblende (Hb). B. Coexisting euhedral crystals of iron-rich clinopyroxene (Cpx) and plagioclase (Plag). C. Subhedral clinopyroxene (Cpx) intergrown with epidote (Ep) and sericite (5-3) possibly pseudomorphous after plagioclase. D. Coexisting faceted crystals of iron-rich clinopyroxene (Cpx) and plagioclase (Plag). E. Anhedral chlorite (Chl), possibly pseudomorphous after phlogopite, and minor serpentine (lower right, not readily visible). F. Partly faceted diopside (Cpx) and magnesium-rich phlogopite (Phlog). Bar scale in μm.

exceed 100 μm in length and average about 20-50 μm (Photo 10.9).

Euhedral to subhedral clinopyroxene is a common inclusion mineral that occurs alone or is accompanied by plagioclase or phlogopite. Locally, it is intergrown with epidote and chlorite. In terms of the pyroxene quadrilateral (Morimoto, 1989), clinopyroxene compositions extend along the diopside-hedenbergite join from magnesium-rich diopside [100Mg/(Mg+Fe^{2+}) or Mg# = 96.0, Inclusion 7] to iron-rich diopside (Mg# = 58.6, Inclusion 2b), and are coincident with the trend for clinopyroxenes in ultramafic rocks of the Tulameen complex (Figure 10.11). The most iron-rich clinopyroxenes coexist with plagioclase (Inclusions 2a-b).

The plagioclase (inclusions 2a-b, Table 10.12) is almost pure albite (Ab_{96-98}) and most probably reflects subsolidus re-equilibration of an originally more calcic plagioclase under conditions of greenschist-facies metamorphism; calcium may have been incorporated locally in epidote which also is found within Pt-Fe alloy in the same nugget (Inclusion 5, Table 10.12, Photo 10.9C, Figure 10.11). A magmatic origin for these plagioclase compositions is difficult to reconcile with the extensive range of coexisting clinopyroxene compositions.

Single crystals of euhedral to subhedral phlogopite in chromite are more magnesian (Mg# 96.3 - 94.9) than cumulate phlogopite in olivine clinopyroxenite (Mg# 91.7; Table

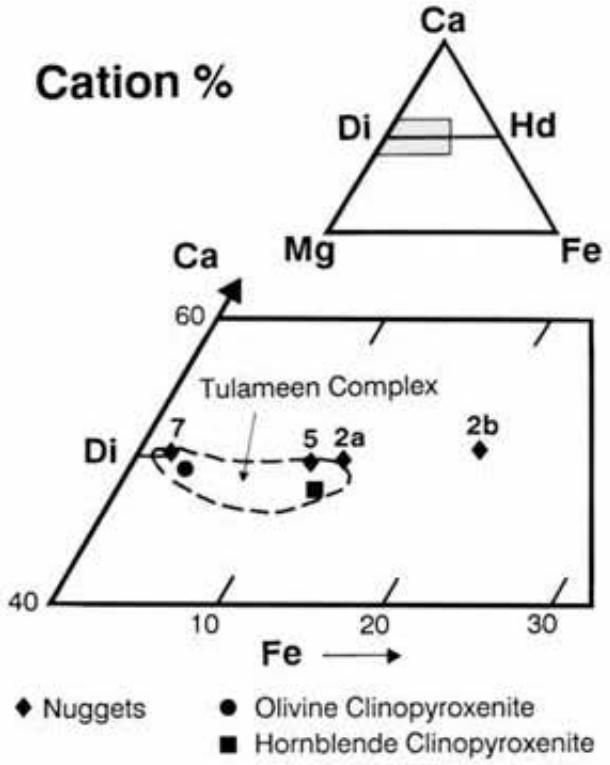

Figure 10.11. Ca-Mg-Fe plot of clinopyroxenes in platinum nuggets and ultramafic rocks of the Tulameen complex (G. T. Nixon, unpublished data). Numbers refer to Inclusion No. (Table 10.12). Representative compositions of pyroxenes in olivine and hornblende clinopyroxenites are given in Table 10.12.A.

10.12). This is also true for phlogopite coexisting with diopside (Inclusion 7), which falls at the most "primitive" end of the clinopyroxene trend (Figure 10.11).

Two 20-μm crystals of amphibole and biotite in Inclusion 1 are the most iron-rich silicates encountered. The biotite has relatively low titanium and Mg# = 47. Coexisting calcic amphibole [$(Na+Ca)_B = 1.91$, $Na_B = 0.09$] is ferroan pargasitic hornblende (Leake, 1978), with $(Na+K)_A = 0.92$, Si = 6.55 and Mg# = 38. In comparison, cumulate amphibole and biotite primocrysts in hornblende clinopyroxenites of the Tulameen complex are significantly more magnesian (Table 10.12). According to Leake's classification, the hornblende in the clinopyroxenites is a relatively magnesium-rich ferroan pargasite with reduced silica (6.18) and Mg# = 65.

Chlorite and epidote locally replace phlogopite and plagioclase, respectively. However, some chlorite may have been formed by reaction of serpentine and chromite to produce chlorite and "ferritchromite" (P.L. Roeder, personal communication, 1990). The chlorite is magnesium-rich clinochlore with little variation in Mg#. Both phases contain significant quantities of chrome, reaching 3.5 wt% Cr_2O_3 in chlorite and 4.1 wt% in epidote. Pan and Fleet (1989) reported up to 3.5 and 11.8 wt% Cr_2O_3 in chlorite and epidote, respectively, from metasomatically altered komatiites and komatiitic basalts in Ontario; Stockman and Hlava (1984) identified chromian chlorite (4.2 wt% Cr_2O_3) in PGE-bearing Alpine-type chromitites from southwestern Oregon. Thus, it appears that in the absence of primary silicates, chromium-bearing secondary minerals in placer nuggets may provide important clues as to the ultramafic provenance of the PGM.

ORIGIN OF PLATINUM NUGGETS: THE CHROMITITE CONNECTION

If the PGE-rich placer nuggets were derived from the chromitite horizons that were sampled in the core of the Tulameen complex, we would expect to see similar distributions of PGM in nuggets and chromitites. As pointed out above, and summarized in Table 10.9 and Figure 10.7, there are certain differences in the size, composition and relative abundance of PGM in placer and bedrock material. Discrepancies in the grain size of platinum alloys between nuggets and chromitites (mm-scale versus μm-scale, respectively) can be rationalized as an artifact of sampling bias. That the nuggets did in fact come from an igneous source is implied by the common incorporation of euhedral to subhedral crystals of cumulus chromite and minor olivine that are partly to completely enclosed by Pt-Fe alloy.

The compositions of chromite and olivine provide a more definitive argument for the origin of the PGM in the placers. The chromite found in nuggets exhibits significant variation in Mg# from nugget to nugget, but little difference in Cr/(Cr+Al). Within individual nuggets, however, compositions are more uniform. The majority of the grains analyzed plot in the field of Tulameen chromitites, although some overlap exists with spinel compositions in dunite. From chromite chemistry alone, it might be inferred that there is probably more than one hostrock (dunite and chromitite) with anomalous PGE abundances.

In this respect, olivine compositions are particularly informative. The olivine in nuggets is much more magnesian (Fo_{93-95}) than its counterpart in Tulameen dunite (Fo_{88-91}), but identical in composition to minor amounts of olivine trapped in cumulus chromitites. Thanks largely to earlier work by Findlay (1963), the distribution of olivines analyzed throughout the dunite core of the complex is unusually dense, which allows the construction of olivine isopleths (Figure 10.6). These data show that the anomalously magnesian olivine compositions are clearly unique to the chromitite environment. Furthermore, it has been shown in numerous studies that if chromite and olivine are allowed to re-equilibrate on cooling, the Mg# of olivine will increase in proportion to the modal abundance of chromite in the host, and an opposite and corresponding change occurs in coexisting chromite. Thus, the extremely magnesian compositions encountered in nugget olivine are a predictable consequence of cooling within a chromitite layer. Since it is not possible to rationalize the differences in PGM, placer nuggets must have been derived from chromitites that have not been sampled. The chromitite source of the PGM is no longer in question.

SIGNIFICANCE OF PRIMARY SILICATE INCLUSIONS

Besides chromite and olivine, primary inclusions in platinum alloys are represented by magnesium-iron mica (phlogopite-biotite), hornblende, clinopyroxene and plagioclase. Regional metamorphism was not sufficiently intense to obliterate the primary compositions of ferromagnesian silicates in the Tulameen complex, although plagioclase in the gabbroic rocks and in hornblende-rich pegmatites is commonly saussuritized (Findlay, 1963; Chapter 9). It seems likely, therefore, that the ferromagnesian silicates reveal certain peculiarities in the crystallization history of PGE-bearing chromitites, particularly nugget M12410-1 which contains the most extensive inclusion suite.

Whereas chromite and olivine are cumulus grains that have compositions compatible with early crystallization and re-equilibration within the chromitite environment, the inclusion minerals are more than an order of magnitude smaller (<100 μm) and compositionally diverse. Magnesium-rich, chromium-bearing phlogopite (Table 10.12) possibly has re-equilibrated with chromite during subsolidus cooling in exactly the same manner as olivine (P. L. Roeder, personal communication, 1990), or may have crystallized from the final few percent of trapped intercumulus melt (Roeder and Campbell, 1985). Considering the presence of iron-rich biotite in the same nugget, and coexisting ferroan pargasitic hornblende (Inclusion 1, Table 10.12), the former explanation seems unlikely. The extensive range of clinopyroxene compositions is also noteworthy (Figure 10.10). The iron-rich clinopyroxenes coexist with plagioclase (altered) and extend beyond the range of clinopyroxene compositions found in ultramafic rocks of the Tulameen complex. These clinopyroxenes, and probably the hydrous iron-rich silicates, evidently crystallized from melts of gabbroic or dioritic composition.

These observations may be rationalized with the textures and compositions of chromite and olivine if the silicate inclusions represent the fractionation products of primitive melt trapped in Pt-Fe alloy at the time of chromitite formation. From the olivine-chromite re-equilibration, we know that cooling was slow enough to permit high-temperature solid-state diffusion, and these conditions would certainly favour continued crystallization of any pockets of melt. The trapped liquid can be perceived as a microcosm of large-scale crystal-melt fractionation processes operating in Tulameen magma chambers. According to this hypothesis, the most iron-rich clinopyroxene compositions in the inclusions would represent the products of presumably closed-system evolution of felsic residual liquids, and may predict pyroxene trends in the syenogabbros and syenodiorites of the Tulameen complex should such a model apply. Compositional data for pyroxenes in the latter rocks are currently lacking.

Perhaps the most surprising aspect of the inclusion data is that cooling was sufficiently rapid to promote fractional crystallization of the trapped melt, although the implied thermal regime applies only to a single platinum nugget (M12410-1). Intriguingly, the platinum alloys serve as an almost ideal inert container for nature's crystallization experiments, analogous to those regularly conducted in modern petrological laboratories, except that we are left to derive the experimental conditions of the charge! However, the problems are compounded, because there has been more than one experiment: the products of metamorphism (and any deuteric changes that may have taken place) have formed subsequently both in the alloy (*e.g.*, magnetite) and from primary silicates (*e.g.*, chlorite and epidote).

PARAGENESIS OF THE PLATINUM-GROUP MINERALS

The mode of occurrence and textural relationships of the PGM and associated base metal minerals described earlier have been used to establish a tentative division of mineral parageneses (Table 10.13). The PGM are subdivided into two groups: predominantly platinum alloys that are considered to have segregated from high-temperature silicate melts, and other PGM and base-metal minerals that are considered to have formed during later metamorphism and serpentinization.

The euhedral nature of platinum alloys locked in chromite (*e.g.*, Photos 10.2A, B, 10.3), the large grains of intercumulate alloys in nuggets that enclose cumulate olivine and chromite (*e.g.*, Photos 10.6A, 10.7), and their demonstrated association with concentrations of chromite in the dunite core of the Tulameen complex, leave little doubt that these early PGM represent the products of high-temperature crystallization of primitive mantle-derived magmas.

The coprecipitation of Pt-Fe alloys and chromite in Alaskan-type intrusions has recently been addressed by Amossé *et al.* (1990), who investigated the solubility of platinum and iridium in a basaltic melt. Based on thermodynamic considerations and experimental data, they showed that an increase in oxygen fugacity decreases the solubility of platinum and iridium in the melt, and argued that Pt-Fe alloys with 10% iron may precipitate in platinum-saturated melts at typical basaltic liquidus temperatures and oxygen fugacities of approximately 10^{-4} kilopascals, conditions that

TABLE 10.13
PARAGENESIS OF PGM AND ASSOCIATED MINERALS IN THE TULAMEEN COMPLEX

Early PGM (High-T, magmatic)	Late PGM, Base and Precious Metals (Low-T, hydrothermal)
Cooperite	Cu oxide
Erlichmanite	Genkinite
Ir-Pt alloys	Geversite
Laurite	Ni sulphides
Pt-Fe-Cu-Ni alloys	Ni antimonides
Ru-Os-Ir alloys	Ni arsenides
	Native copper
	Native silver
	Ni oxide
	Platinian copper
	Pt oxide
	Rh-Ir(AsS)
	RhSbS
	Sperrylite
	Tolovkite
	Tulameenite

enhance the precipitation of chromite (Hill and Roeder, 1974). As platinum is more soluble than iridium under a wide range of oxygen and sulphur fugacities, the precipitation of Pt-Fe alloys in nature ought to be accompanied by iridium-rich phases. The predicted consequences of magmatic crystallization are observed in the Tulameen complex, in which the precipitation of chromite and Pt-Fe-Cu-Ni alloys (containing significant amounts of iridium in solid solution; Tables 10.2A and B) is accompanied by rare iridium and platinian iridium (formerly platiniridium; *cf.* Table 10.9). The preponderance of platinum-rich as opposed to iridium-rich phases in the chromitites of the Tulameen complex presumably reflects the high overall Pt/Ir ratio of parental magmas.

By analogy with the synthetic Pt-Fe system (Heald, 1967), the considerable range of platinum alloy compositions along the Pt-Fe join in Figure 10.7 is as expected if complete solid-solution exists at typical liquidus temperatures of basaltic systems (1300-1200°C). However, there is evidence that some of the early Pt-Fe-Cu-Ni alloy compositions may have undergone high-temperature subsolidus modification during cooling. The tie lines for two coexisting pairs of alloys from the same chromitite layer (Table 10.2A), including at least one zoned, euhedral crystal (Photo 10.3), straddle a compositional gap separating tetraferroplatinum [Pt(Fe,Ni,Cu)] and isoferroplatinum [$Pt_{2.5}(Fe,Ni,Cu)_{1.5}$] (Figure 10.7). These relationships suggest the presence of a miscibility gap in the system Pt-Fe-Ni-Cu, analogous to that implied to exist at low temperatures between pure Pt_3Fe and PtFe (Cabri and Feather, 1975). However, intimate, eutectic-like intergrowths of these alloys, such as those described by Johan *et al.* (1989) for nearly pure Pt-Fe phases, have not been observed.

Even though the faceted crystals that are contained in chromite, shown in Photo 10.3, appear to have grown from a melt, several internal features seem somewhat unusual for a growth phenomenon: the extremely variable thickness of the isoferroplatinum rim, its sharp contact with tetraferroplatinum in the core, and the highly irregular contact between these phases. We speculate that the zoning in this crystal may represent a reaction texture with its origin intimately linked to its chromite host. For example, Naldrett and Lehmann (1987) pointed out that where sulphide and chromite coexist, vacancies in the chromite lattice sites can be expected to take up iron on cooling and thus promote desulphurization reactions whereby the proportion of base metal sulphides decreases, and elements like copper, nickel and the platinum group are concentrated in the remaining sulphides. A similar mechanism may also explain the zoned inclusions of platinum alloys in chromite. Loss of iron from Pt-Fe alloy to fill vacancies in chromite could produce isoferroplatinum on cooling within a miscibility gap in the platinum alloy system. If this suggestion is viable, nickel and copper must be removed together with iron (*cf.* Figure 10.7B and C) and tetraferroplatinum may represent a relict, high-temperature composition. This explanation is only applied to the formation of isoferroplatinum in this particular chromitite.

Textural evidence suggests that the late PGM (Table 10.13) resulted from *in situ* metasomatic replacement of platinum alloy primocrysts (*e.g.*, Photos 10.1, 10.2C and D, 10.4B, 10.8D) and limited localized fracture-filling within the chromitite host (*e.g.*, Photos 10.1B, 10.4A and B). Thus, the mobility of PGE during hydrothermal alteration appears to be limited.

The only Pt-Fe-Cu-Ni alloy that is clearly secondary is tulameenite, which is intimately associated with platinian copper in both nugget and lode occurrences. Platinian copper is intergrown with a variety of products of late-stage crystallization that are enclosed in serpentine, including secondary magnetite that is presumably derived from the breakdown of olivine (Photo 10.5C). In one chromitite, tulameenite forms an intimate intergrowth with isoferroplatinum(?) and appears to partly replace the euhedral Pt-Fe-Ni-Cu alloy grain (Photos 10.2C and D). An equation can be written that describes this reaction in the presence of an aqueous fluid:

$$Pt_3Fe + 2Cu = Pt_2CuFe + (Cu, Pt)$$

isoferroplatinum — *fluid* — *tulameenite* — *platinian copper*

The presence of native copper in carbonate-serpentine veinlets that cut chromitites (Photo 10.5D) indicates a relatively high activity of copper and low sulphur fugacity in the fluid phase, and suggests that reactions of this type are indeed pertinent to the genesis of certain of the copper-rich PGM. The secondary nature of tulameenite in lode and placer deposits of the Urals was previously noted by Betekhtin (1961) who attributed its formation to the serpentinization of ultramafic massifs (*cf.* Cabri and Genkin, 1991).

Textural relationships among platinum alloys, sperrylite and geversite seem somewhat ambiguous. The latter two minerals are found as fracture fillings in chromite (Photos 10.1B, 10.4A and B) and as subhedral grains located on fractures (Photos 10.1D and 10.4B). In addition, geversite forms complex intergrowths with nickel antimonides and platinian copper (Photos 10.4C and 10.5A). The common association of geversite with base metal antimonides in serpentine suggests a low-temperature hydrothermal origin and is also compatible with the presence of geversite along fractures in chromite (Photo 10.4A). Where certain fractures exposed primary platinum alloys to the action of hydrothermal fluids, some grains were completely transformed to platinum antimonides and arsenides (Photos 10.1D and 10.4B). Breithauptite and platinian copper have locally formed later than geversite (Photos 10.4C and D, 10.5A), and these minerals are commonly intergrown with nickel arsenides and antimonides (Photo 10.5B). Equations of the type:

$$3Pt_3Fe + 10As + 8Sb + 2O_2 = 5PtAs_2 + 4PtSb_2 + Fe_3O_4$$

isoferroplatinum — *fluid* — *fluid* — *sperrylite* — *geversite* — *magnetite*

$$PtSb_2 + 4Ni = (Ni, Pt)Sb + Ni_3Sb$$

geversite — *fluid* — *breithauptite* — *Ni antimonide*

$$PtAs_2 + 2Ni + Cu = 2NiAs + (Cu, Pt)$$

sperrylite — *fluid* — *fluid* — *Ni arsenide* — *platinian copper*

can potentially explain these observations. Textural evidence for equilibrium between geversite and sperrylite is lacking.

Small quantities of platinum detected in nickel antimonides appear to decrease in proportion to increasing Ni/Sb ratios in the antimonides (Table 10.6). The nickel in antimonides and arsenides is readily available via serpentinization of olivine in host dunite. The copper and antimony may well have been derived from outside the Tulameen complex by leaching of Nicola Group hostrocks.

Rhodium sulpharsenides partly replace primary platinum alloys (Photo 10.1B and C) and probably formed more or less contemporaneously with platinum arsenides and antimonides. The formation of rare platinum oxide (*e.g.*, Photo 10.4C and D) provides clear evidence of alteration under conditions of locally high oxygen fugacity.

Intergrowths of magnetite in platinum alloy also appear to have formed in response to conditions of elevated oxygen fugacity, and are linked with serpentinization and hydrothermal alteration of chromite. The abundance of fine magnetite intergrowths in platinum alloy adjacent to chromite (Photos 10.6B and 10.7D) strongly suggests a low-temperature reaction relationship. Relevant equations may be represented by:

$$\underset{\textit{chromite}}{FeCr_2O_4} + \underset{\textit{tetraferro-platinum}}{18PtFe} + 10O_2 = \underset{\textit{isoferro-platinum}}{6Pt_3Fe} + \underset{\textit{ferrit-chromite}}{2Fe_2CrO_4} + \underset{\textit{magnetite}}{3Fe_3O_4}$$

$$\underset{\textit{chromite}}{FeCr_2O_4} + \underset{\textit{isoferro-platinum}}{6Pt_3Fe} + 4O_2 = \underset{\textit{ferrit-chromite}}{2Fe_2CrO_4} + \underset{\textit{magnetite}}{Fe_3O_4} + \underset{\textit{fluid}}{18Pt}$$

Platinum may be immobile, and loss of iron from tetraferroplatinum may form magnetite and ferritchromite in an isoferroplatinum reaction product. Alternatively, platinum may enter the fluid phase and take part in localized reactions involving antimonides and arsenides as described earlier. Another possibility is that part of the platinum enters the magnetite structure, as postulated by Cabri *et al.* (1981). The fine-grained nature of secondary magnetite in the Tulameen nuggets precluded confirmation of the latter hypothesis.

SULPHIDES

Sulphide minerals identified in lode and placer occurrences include extremely rare PGM (erlichmanite and laurite) and base metal sulphides (pyrite, millerite or heazlewoodite, pentlandite, violarite, bravoite, rare chalcopyrite and an undetermined Ni-Co-Fe sulphide). The presence of pyrrhotite has not been confirmed. Erlichmanite and laurite are associated with platinum alloys and are considered to have a high-temperature origin. Laurite, in particular, has been observed with a faceted morphology. In chromitites, the sulphides are invariably found in the interstices among chromite grains associated with serpentine, magnetite and secondary PGM; no sulphides have been observed to coexist with primary Pt-Fe-Cu-Ni alloys enclosed in chromite. In one nugget, however, pentlandite and chalcopyrite have been identified in Pt-Fe alloy, but not without other secondary oxides (magnetite) and PGM (*e.g.*, irarsite; *cf.* Raicevic and Cabri 1976).

St. Louis *et al.* (1986) made similar observations but proposed that some sulphides, in particular pentlandite, had a relatively high-temperature, magmatic origin. However, their illustration of this type of paragenesis (St. Louis *et al.* 1986, Figure 2B) involves an intergrowth of serpentine, magnetite, pentlandite, sperrylite and irarsite within a fractured area in chromite. Although the possibility of trace amounts of magmatic base metal sulphides, albeit remobilized, cannot be categorically ruled out, this mineral assemblage is quite consistent with a low-temperature, hydrothermal paragenesis, as implied earlier.

SUMMARY OF PGE MINERALIZATION IN THE TULAMEEN COMPLEX

Detailed study of the Tulameen complex has been directed toward a better understanding of the nature and origin of disseminated PGM in mafic-ultramafic intrusions of the Alaskan type, and their spatially associated placers. The anomalously high concentrations of PGE in Tulameen chromitites and placers is explained by the presence of discrete primary and secondary PGM. Key features of the primary PGM, predominantly represented by Pt-Fe alloys with minor but significant abundances of copper and nickel, are their idiomorphic habit in chromitites and coarsely crystalline texture in nuggets where platinum alloys enclose cumulus chromite and olivine. Secondary PGM, chiefly platinum arsenides and antimonides, rhodium-iridium sulfarsenides, tulameenite and platinian copper developed locally in PGE-enriched hostrocks by metasomatic replacement and limited remobilization of primary platinum alloys. The latter PGM were produced during subsequent serpentinization and regional metamorphism, and are associated with secondary low-temperature base metal sulphides, arsenides and oxides.

Although there are differences in the nature and frequency of the PGM between bedrock and placer occurrences, coexisting gangue minerals confirm their derivation from a common source. In particular, the compositions of chromite and olivine in placer nuggets match those observed in chromitites in the dunite core of the Tulameen complex. Olivine is especially diagnostic because of its well-known tendency to re-equilibrate with chromite on cooling, to produce anomalously magnesian compositions. Intriguingly, one nugget contains inclusions of other primary silicates with a wide range of compositions that crystallized from silicate melts trapped in platinum alloys at the time of chromitite formation. These crystallization products appear to mimic the liquid line of descent recorded by cumulate minerals in the ultramafic rocks of the Tulameen complex, and may predict the compositions of iron-rich clinopyroxenes in gabbroic to dioritic magmas that would evolve during comagmatic, closed-system fractional crystallization.

Finally, we stress that the high-temperature PGM segregated directly from a silicate melt and were not generated

by exsolution from chromite or magmatic sulphides. The common association of Pt-Fe alloys and chromitites in Alaskan-type intrusions suggests that whatever mechanism(s) triggers chromite precipitation in excess of normal cotectic proportions [*e.g.*, increase in $f(O_2)$] also enhances or initiates the precipitation of Pt-Fe alloys from primitive parental magmas of the Alaskan-type association.

ECONOMIC POTENTIAL OF ALASKAN-TYPE COMPLEXES - PGE AS AN EXPLORATION TOOL

Recently, Barnes (1990) has shown how the ratios of nickel and copper to PGE may be used to evaluate the potential of mafic and ultramafic rocks for a PGE deposit. Her diagrams are reproduced in Figures 10.12 to 14 which show fields for extrusive rocks (komatiites, high-MgO basalts and flood basalts) commonly considered to have formed by partial melting of mantle peridotite, and cumulate rocks from different geological environments. Also plotted are chromitites from an Alaskan-type complex (Tulameen) which may be compared to those from layered intrusions (LI) and ophiolites (OPH). Figure 10.12 appears to be the most effective discriminant for the various rock types with the notable exception of Alaskan-type chromitites which are best distinguished in Figure 10.14. However, the former diagram is probably less useful for exploration purposes as analysis for iridium is expensive and commercial laboratories routinely offer cheap analytical packages for platinum, palladium and rhodium. The most important ramification for exploration is that rocks which have Ni/Pd and Cu/Ir (or Cu/Rh or Cu/Pt) ratios lower than the trend for the extrusive rocks (Figures 10.12B, 10.13B and 10.14B) have experienced some PGE-enrichment process and could represent prime exploration targets. Conversely, rocks in which these same ratios are greater than those for the extrusive rocks are depleted in PGE and are expected to make poor prospecting targets. These conclusions pertain to magmatic ores and the diagrams are not intended for use with remobilized or hydrothermal deposits.

Factors affecting the distribution of nickel, copper and PGE in ultramafic and mafic rocks include partial melting and the segregation of olivine, chromite, sulphides and PGM

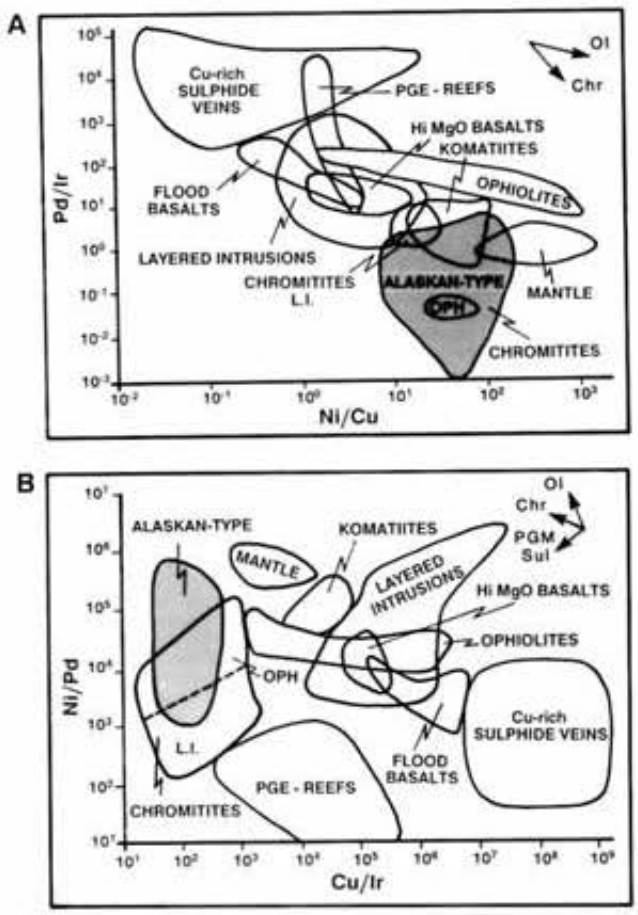

Figure 10.12. A. Pd/Ir versus Ni/Cu and B. Ni/Pd versus Cu/Ir plots for chromitites from Alaskan-type complexes (as represented by the Tulameen complex) and various mafic and ultramafic rock types, copper-rich sulphide veins and PGE reefs (after Barnes, 1990). Vectors indicate addition of olivine (Ol), chromite (Chr), sulphides (Sul) and platinum-group minerals (PGM).

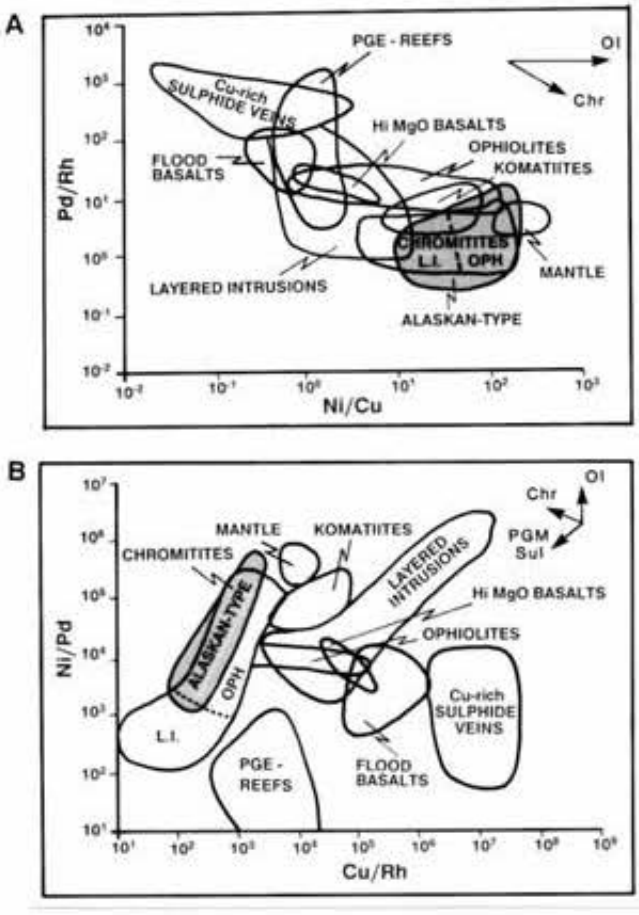

Figure 10.13. A. Pd/Rh versus Ni/Cu and B. Ni/Pd versus Cu/Rh plots for chromitites from Alaskan-type complexes (as represented by the Tulameen complex) and various mafic and ultramafic rock types, copper-rich sulphide veins and PGE reefs (after Barnes, 1990). Vectors as in Figure 10.12.

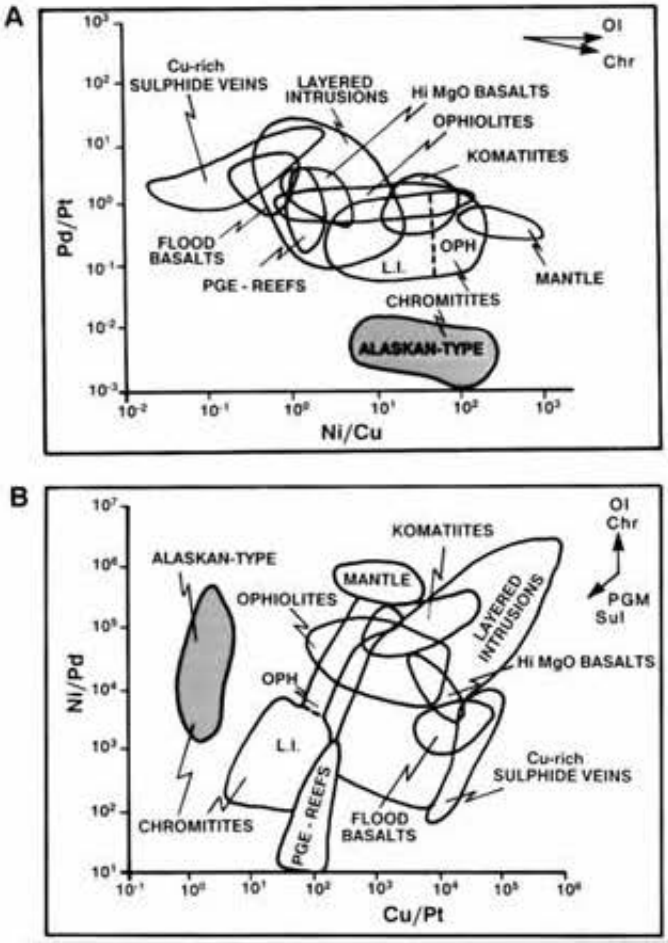

Figure 10.14. A. Pd/Pt versus Ni/Cu and B. Ni/Pd versus Cu/Pt plots for chromitites from Alaskan-type complexes (as represented by the Tulameen complex) and various mafic and ultramafic rock types, copper-rich sulphide veins and PGE reefs (after Barnes, 1990). Vectors as in Figure 10.11.

in early crystal cumulates. Progressive partial melting of mantle peridotite yields the trend for mafic extrusive rocks where komatiites represent the highest, and flood basalts the lowest degree of partial melting. The distinction of various magma types in these plots can be extremely useful (Barnes, 1990). For example, an intrusion might be considered a good target for a PGE deposit if samples from its chilled margin fall within the field of high-MgO basalt, as almost all of the world's most significant PGE deposits (*i.e.*, those hosted by large stratiform complexes such as the Bushveld and Stillwater complexes) are associated with this parental magma type. However, not all PGE-enriched sulphides are associated with the high-MgO magma type; exceptions include the Noril'sk-Talnakh intrusions (Naldrett, 1989) and the precious metal-enriched (gold-palladium) zones in the Skaergaard intrusion (Bird *et al.*, 1991), although the latter may be subeconomic.

In rocks formed by crystal accumulation, olivine and chromite are the main sources of variation in Figures 10.12A, 10.13A and 10.14A. Plagioclase and pyroxene fractionation are not thought to appreciably effect the Ni/Cu and inter-PGE ratios (Barnes, 1990). Accumulation of olivine or chromite drives resulting cumulates parallel or subparallel to the trend of extrusive rocks in the general direction of the field for mantle peridotite. Thus, if cumulate rocks are the only samples available, the trend for layered intrusions with PGE potential, for example, should project through the high-MgO basalt field.

Once the importance of olivine and chromite crystallization has been established, Figures 10.12B, 10.13B and 10.14B may be used to assess the role of sulphides. Because sulphides scavenge the PGE much more efficiently than they concentrate nickel and copper, the segregation of sulphides from a magma causes the Ni/Pd and Cu/Ir (or Cu/Rh or Cu/Pt) ratios to decrease in the sulphide-bearing cumulate (Barnes, 1990). Thus, a cumulate containing the first-formed sulphides should plot below the trend of extrusive rocks in these figures, and consequently point to processes favourable to the formation of a PGE deposit. Note that a second-stage sulphide-forming event in a system closed to renewed magma supply would be expected to yield PGE-poor cumulates.

The precipitation of PGM directly from a silicate melt was not specifically addressed by Barnes (1990), but has recently been advanced to account for certain PGE deposits in island arc (Peck and Keays, 1990) and ophiolitic (Corrivaux and Laflamme, 1990) settings. The distinctive field for chromitites of the Tulameen complex in Figure 10.14 reflects the accumulation of primary Pt-Fe-Cu-Ni alloys with very low Pd/Pt and Cu/Pt ratios that crystallized from sulphur-undersaturated liquids (discussed above). This diagram therefore appears to be most effective for evaluating the PGE potential of Alaskan-type complexes.

PGE MINERALIZATION IN ALASKAN-TYPE VERSUS STRATIFORM AND OPHIOLITIC COMPLEXES

In Alaskan-type complexes in general, the chromitite-PGE association appears to be the most widespread type of lode mineralization, though not the sole economic target (*cf.* Cox and Singer, 1986; Nixon and Hammack, 1991). In fact, PGE-enriched chromitites are even more important in other geological environments, such as stratiform mafic intrusions (*e.g.*, Bushveld complex, South Africa; Stillwater complex, Montana; and Bird River sill, Manitoba), and also have potential in the Alpine-type or ophiolitic (podiform) settings (*e.g.*, Shetland ophiolite, Prichard *et al.*, 1986). The podiform chromitites are usually impoverished in platinum and palladium relative to ruthenium, osmium, iridium (*e.g.*, Legendre and Augé, 1986), as are some stratiform chromitites (*e.g.*, Bird River and most Stillwater chromitites; Cabri and Laflamme, 1988; Talkington and Watkinson, 1986). However, certain stratiform chromitites (*e.g.*, those in the Middle and Upper Groups of the Bushveld complex and the A chromitite of the Stillwater complex) exhibit anomalous enrichment of platinum and palladium, although not as extreme as that encountered in the PGE-rich, sulphide-bearing reefs such as the Merensky (Bushveld) and J-M (Stillwater), which are characterized by extremely high Pt+Pd/(Ru+Os+Ir) ratios (Naldrett *et al.*, 1987; Lee and Parry, 1988).

In order to explain differences between the distribution and abundances of PGE in chromitites from layered intrusive and ophiolitic complexes, Naldrett and von Gruenewaldt (1989) proposed that the concentration of platinum and palladium in stratiform chromitites, and high Pt+Pd/(Ru+Os+Ir) ratios, reflect the former presence of base metal sulphides in the chromitites. The original process of concentration of the PGE is perceived to be that of collection by an iron-copper-nickel-rich sulphide liquid. Subsequent crystallization of non-sulphide PGM occurs during cooling at high temperatures, and the desulphurization reactions are driven by subsolidus uptake of sulphide-hosted iron by chromite (Naldrett and Lehmann 1987). They further concluded that such a process could account for high concentrations of PGE in chromitites with little or no visible sulphide, and that high Pt+Pd/(Ru+Os+Ir) ratios indicate appreciable original sulphide content.

The textural and mineralogical data presented here for the Tulameen complex do not support such a mechanism for chromitite-associated PGE mineralization in Alaskan-type intrusions. The PGE are primarily contained in Pt-Fe and Pt-Ir alloys, and, just as in the majority of Alaskan-type complexes, are not associated with primary magmatic base metal sulphides (Cabri 1981). We note that the high Pt+Pd/(Ru+Os+Ir) ratios of PGE-enriched chromitites in the Tulameen and other Alaskan-type complexes are typically accompanied by high Pt/Pd ratios (*e.g.*, Nixon and Hammack, 1991). The latter feature appears inconsistent with collection by base-metal sulphides, which are known to concentrate both platinum and palladium (*e.g.*, Makovicky *et al.*, 1986; Talkington and Watkinson, 1986; Naldrett, 1989). In the case of the Tulameen and many other Alaskan-type intrusions, the concentration of PGE in chromitites is best explained by the accumulation of platinum-rich alloys that segregated directly from the melt at an early stage in the evolution of the complex.

CHAPTER 11 MAGMATIC AND TECTONIC SETTING OF ALASKAN-TYPE COMPLEXES

THE LONGEVITY OF MESOZOIC ARC MAGMATISM IN QUESNELLIA AND STIKINIA

Alaskan-type complexes in British Columbia have been considered to be Late Triassic in age and generally coeval with widespread Upper Triassic to arc volcanic rocks of the Middle Triassic to Early Jurassic Rossland-Nicola-Takla-Stuhini groups in Quesnellia and Stikinia (Evenchick *et al.*, 1986; Irvine, 1976; Wheeler and McFeely, 1991; Woodsworth *et al.*, 1991). However, practically all of the geochronometric data used to support this contention are based on conventional K-Ar dating techniques that are prone to post-emplacement thermal resetting. The earliest attempt to date Alaskan-type complexes by U-Pb zircon techniques appears to have been made by Rublee and Parrish (1990) at the Tulameen complex. Preliminary results for slightly discordant zircon fractions in monzosyenites associated with this complex yield dates that straddle the Triassic-Jurassic boundary (204-212 Ma; Rublee and Parrish, 1990). However, the new U-Pb isotopic dates reported above for zircons extracted from late-stage quartz-feldspar-bearing pegmatites of Alaskan-type complexes in north-central British Columbia (Chapters 4 and 8) provide direct evidence for the longevity of arc magmatism in Quesnellia in early Mesozoic time.

The Lunar Creek Complex, located on the western margin of Quesnellia near the southern termination of the Kutcho fault (Figure 11.1), has yielded a U-Pb zircon age of 237±2 (2σ) Ma (Mid-Triassic - Ladinian - using the time scale of Harland *et al.*, 1990), which makes it the oldest known, directly dated Alaskan-type intrusion in British Columbia. Alaskan-type complexes of possibly similar age occur to the west in northern Stikinia (Figure 1.1). Potassium-argon dating of hornblende in hornblendite and hornblende clinopyroxenite of the Gnat Lakes complex, for example, has yielded isotopic ages of 230±10 (2σ) and 227±14 Ma, that is, early Late Triassic (Anderson, 1983). About 150 kilometres to the southwest at Mount Hickman, an Alaskan-type complex has been intruded by the Hickman batholith, the main phase of which has been dated by K-Ar on hornblende at 221±16 (2σ) Ma or mid-Late Triassic (Hickman pluton, Holbeck, 1988). A recently acquired, concordant U-Pb zircon date of 371±3 (2σ) Ma (J.M. Logan, personal communication, 1992) from the Forest Kerr - More Creek granitoid pluton, which incorporates a raft of ultramafic rock (phlogopite-olivine-hornblende clinopyroxenite) that is mineralogically consistent with an Alaskan-type affinity (Logan and Koyanagi, 1989), may indicate that an even older suite of Late Devonian Alaskan-type complexes is present in northern Stikinia. A parallel situation is now known to exist in southeastern Alaska where, although the majority of Alaskan-type intrusions are believed to be mid-Cretaceous, K-Ar dating has revealed a distinctly older group of early Paleozoic complexes (Loney *et al.*, 1987).

The youngest Alaskan-type intrusion thus far dated in British Columbia is the Polaris complex, situated at the eastern edge of Quesnellia (Figure 11.1), with a concordant U-Pb age of 186±2 (2σ) Ma (late Early Jurassic - earliest Toarcian). Recent work in the Nation Lakes area some 150 kilometres to the south, has recovered early and late Pleinsbachian ammonite faunas from intervolcanic shales presumed to lie near the top of the Takla Group in Quesnellia (Bellefontaine and Nelson, 1992). These fossils mark a Cordilleran-wide marine transgression in Pliensbachian time that occurred after the main phase of arc construction. Underlying volcanic lithologies are correlated with Lower Jurassic (Sinemurian) calcalkaline volcanic rocks in Stikinia (*i.e.*, Telkwa Formation of the Hazelton Group; Bellefontaine and Nelson, 1992). The latter lithologies were deposited contemporaneously with Lower Jurassic (Sinemurian-Pliensbachian) mafic-intermediate volcanic arc sequences in the Quesnel Terrane of southern British Columbia (*i.e.*, Elise Formation of the Rossland Group; Tipper, 1984; Höy and Andrew, 1989, 1991). Emplacement of the high-level Polaris complex at the beginning of the Toarcian therefore occurred during the waning stages of arc magmatism. Interestingly, in Quesnellia at least, mineralogical evidence suggests that parental magmas of the Polaris complex were of high-potassium affinity, as were some of the latest products of arc volcanism which have a decidedly shoshonitic character (Beddoe-Stephens and Lambert, 1981; Bellefontaine and Nelson, 1992).

In summary, available geologic and geochronometric data indicate that Alaskan-type complexes were emplaced throughout the entire span of early Mesozoic arc magmatism in Quesnellia at least, and possibly also in Stikinia. This magmatism began in the mid-Triassic and continued through to the accretion of island arc terranes at the end of the Early Jurassic (discussed below). Recently, Nelson and Mihalynuk (1992) have argued that faunal, geologic and isotopic linkages between Quesnellia and Stikinia are so strong as to imply that they constituted part of a festoon of volcanic arcs draped along the Cordilleran margin in Late Triassic to Early Jurassic time. The presence of Alaskan-type ultramafic complexes of similar age and tectonic setting is yet

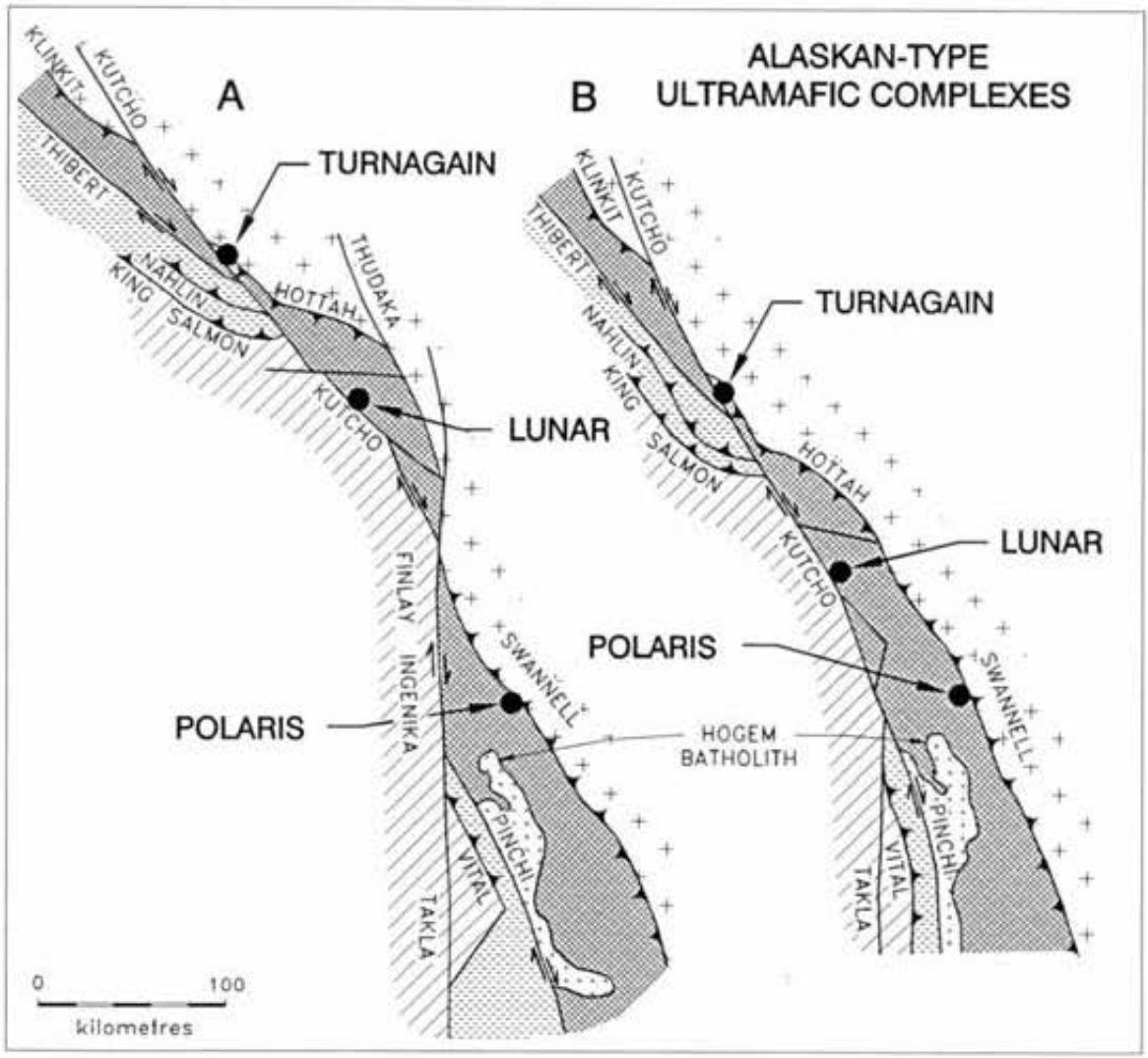

Figure 11.1 Partial restoration of Alaskan-type complexes in north-central British Columbia. A. Generalized terrane elements and major faults. B. Restoration of 60 kilometres of movement on the Thudaka fault and 50 kilometres on the Finlay and Ingenika faults (after Gabrielse, 1985). Patterns as in Figure 11.2

another common thread shared by these accreted arc terranes.

TIMING OF EARLY MESOZOIC DEFORMATION AND TERRANE ACCRETION

The U-Pb age of the Polaris complex places important constraints on the timing of contractional deformation associated with docking of accreted terranes, specifically Quesnellia, against the miogeoclinal margin of ancestral North America.

As described earlier (Chapter 8), the Polaris complex is a sill-like intrusion with a kinematically deformed thermal aureole exposed at its base. Here, mafic volcanic or volcaniclastic protoliths have been recrystallized to amphibolite, and carbonaceous shales to andalusite (chiastolite) schists. The amphibolites invariably exhibit a penetrative foliation and chiastolite porphyroblasts in the pelites have been flattened within the plane of the schistosity. Farther from the contact, these rocks pass downward into massive volcanics, foliated carbonates and fine-grained clastics with greenschist-grade metamorphic assemblages. The regional foliation imprinted in the hostrocks is concordant with fabrics in the aureole. The kinematics (C/S fabrics) of ductile shear zones within the aureole indicate eastward transport of the Polaris complex together with its wallrocks. These textural features indicate that eastward-verging deformation occurred while the thermal aureole was hot. However, penetrative fabrics have not been observed within the complex, suggesting that solidification was essentially complete prior to deformation. As the zircons that yield the U-Pb age of 186±2 Ma are concordant and come from a late feldspathic pegmatite near the roof of the intrusion, this date represents

the final stages of crystallization of the complex. Furthermore, the intrusion was emplaced at a relatively high-level (subvolcanic?) within the crust and so is unlikely to have experienced protracted cooling. Therefore, the early Toarcian date is considered to be a good approximation of the timing of the deformation event.

The regional schistosity and eastward-verging deformation in this part of the Lay Range is correlated with the earliest phase of deformation recognized in the Ingenika Group east of the Swannell fault. Here, Bellefontaine (1989, 1991) has documented an early, approximately synmetamorphic foliation associated with northeast-vergent, tight to isoclinal folds overprinted by second-phase, post-metamorphic open folds and minor structures associated with the Swannell thrust. At this latitude, the Swannell fault appears to be a southwesterly vergent suture that places Upper Proterozoic miogeoclinal rocks of the Cassiar Terrane upon the Harper Ranch Subterrane (Lay Range assemblage) of Quesnellia (Figure 11.1). This sequence of northeastward overthrusting of allochthonous terranes followed by southwestward back-thrusting and back-folding of allochthonous and autochthonous miogeoclinal sequences is well known in the Omineca crystalline belt and has been linked to the accretion of Quesnellia, or the Intermontane Superterrane, to the pericratonic margin (Monger *et al.*, 1982; Brown *et al.*, 1986; Price, 1986; Murphy, 1989).

From the correlations detailed above, the earliest phase of deformation associated with this accretionary event is precisely dated at 186±2 Ma or earliest Toarcian. This timing is supported by the recent results of U-Pb dating by Murphy *et al.* (1995) on syntectonic to post-tectonic granitoid plutons in the southern part of the Omineca Belt (Kootenay Arc and Cariboo Mountains). Based on less precise zircon dates and existing biochronological data, they propose that northeastward overthrusting of Quesnellia onto the North American continental margin took place in mid-Toarcian time (*ca.* 183 Ma) and that subsequent backthrusting of allochthonous and autochthonous rocks ceased by the end of the Aalenian (*ca.* 174 Ma). Deformation of similar age is widespread in the Intermontane Belt. In northern Stikinia, for example, a regional angular unconformity occurs at the base of strata of uppermost Pliensbachian or Toarcian age (Henderson and Perry, 1981; Gabrielse, 1991). Volcaniclastic rocks and lavas directly overlying this unconformity have yielded a concordant zircon date of 185±2 Ma (D.A. Brown, unpublished data). Folding, thrusting and synkinematic metamorphism at the northern edge of Stikinia, associated with southward-directed overthrusting of Cache Creek Terrane along the King Salmon fault, occurred between early Toarcian and middle Bajocian (Thorstad and Gabrielse, 1986; Gabrielse, 1991). The synchronicity of these events in terranes of the Intermontane Belt and the miogeocline suggests that either contraction affected a broad "soft" zone of accreted terranes that had amalgamated by late Early Jurassic time; or accretion to the North American continental margin was contemporaneous with the final phases of amalgamation of the Intermontane Superterrane (Cordey *et al.*, 1987, 1991). The presence of deformation of similar age in the Insular Belt may imply that Stikinia was already amalgamated to the outboard terranes of Wrangellia and Alexander (Insular Superterrane) prior to final closure of the Cache Creek ocean basin in the late-Early to early-Middle Jurassic (Murphy *et al.*, 1995; Van der Heyden, 1992).

TECTONIC SETTING OF THE TURNAGAIN COMPLEX AND STRIKE-SLIP DISPLACEMENTS IN CENTRAL BRITISH COLUMBIA

The Turnagain Alaskan-type complex has been studied in detail by Clark (1975, 1978, 1980) and a geologic map based partly on Clark's work has been published by Nixon *et al.* (1989). The tectonic setting of this ultramafic complex imposes some important constraints on Mesozoic to (?)Early Tertiary strike-slip motions along major transcurrent faults in north-central British Columbia.

The regional setting of the Turnagain complex is shown in Figures 11.2 and 11.3. The northern and eastern margins of the complex are bounded by a high-angle reverse(?) fault which places locally serpentinized and talc-carbonate-altered dunite against black carbonaceous phyllite. At the northwestern contact of the intrusion, lowermost amphibolite-grade metavolcanic and metasedimentary rocks in the hangingwall of the fault are juxtaposed against lower to middle greenschist-grade assemblages in the footwall. These amphibolite-grade rocks may represent vestiges of a kinematically deformed thermal aureole similar to that developed beneath the Polaris complex (Chapter 8). Southeast of the Turnagain complex, Clark (1975) documented another small Alaskan-type "ring complex" intruding graphitic slate and exhibiting a narrow but pronounced thermal aureole involving cordierite-anthophyllite assemblages. Gabrielse (1991) concluded that Mississippian to Upper Triassic rocks forming the allochthonous sliver northeast of the Kutcho fault and west of the Rainbow fault were of oceanic affinity. However, in view of the presence of Alaskan-type intrusions and arc-related silicic volcanics (originally correlated with the Kutcho Formation by Gabrielse *et al.*, 1979), it seems probable that this allochthon represents part of Quesnellia, probably the Harper Ranch Subterrane, as also inferred by Wheeler and McFeely (1991). In this case, the high-angle reverse fault delineating the eastern margin of the Turnagain complex must extend to the southeast. This fault is taken to mark the eastern extremity of Quesnellia and its southern extension has been placed arbitrarily at the base of the volcanic package in the south (H. Gabrielse, 1992, personal communication; Figure 11.3). The Turnagain allochthon is considered to represent an extension of the eastward-verging Hottah-Klinkit system which implies right-lateral offset of approximately 65 kilometres along this part of the Kutcho fault rather than 100 kilometres as estimated by Gabrielse (1985). The tectonic setting of the Turnagain complex is directly analogous to that of the Polaris complex farther south. In fact, the lithologies which host these intrusions are so strikingly similar as to suggest a direct correlation with the Lay Range assemblage (Harper Ranch Subterrane) described by Monger (1973). The black phyllite unit in fault contact with the Turnagain complex forms part of a well-foliated sequence of Lower Paleozoic fine-grained clastics that passes eastwards into interbedded siltstones, carbonates

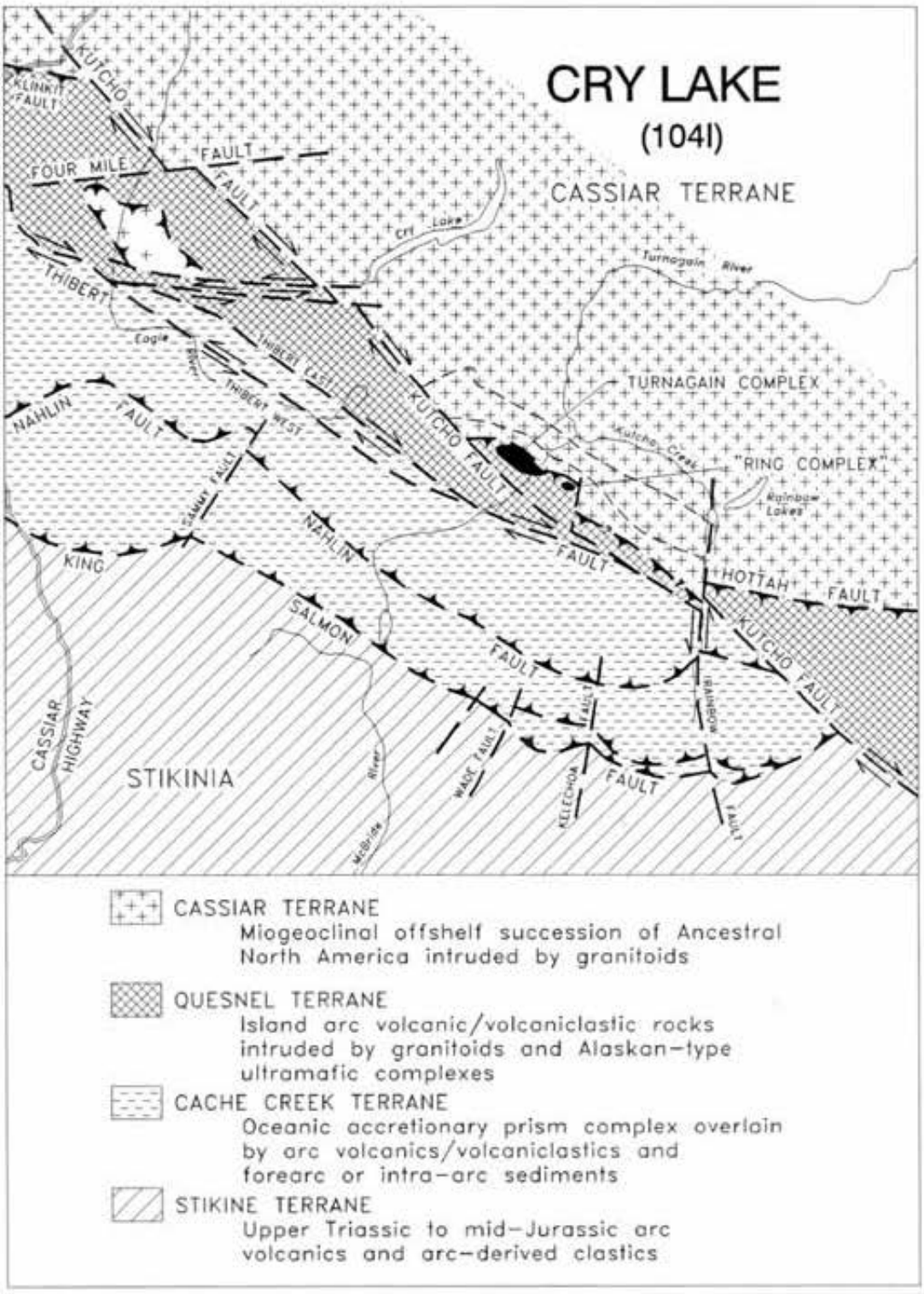

Figure 11.2. Simplified terrane map, Cry Lake map-area, showing setting of Turnagain Alaskan-type complex and a smaller "ring complex" described by Clark (1975).

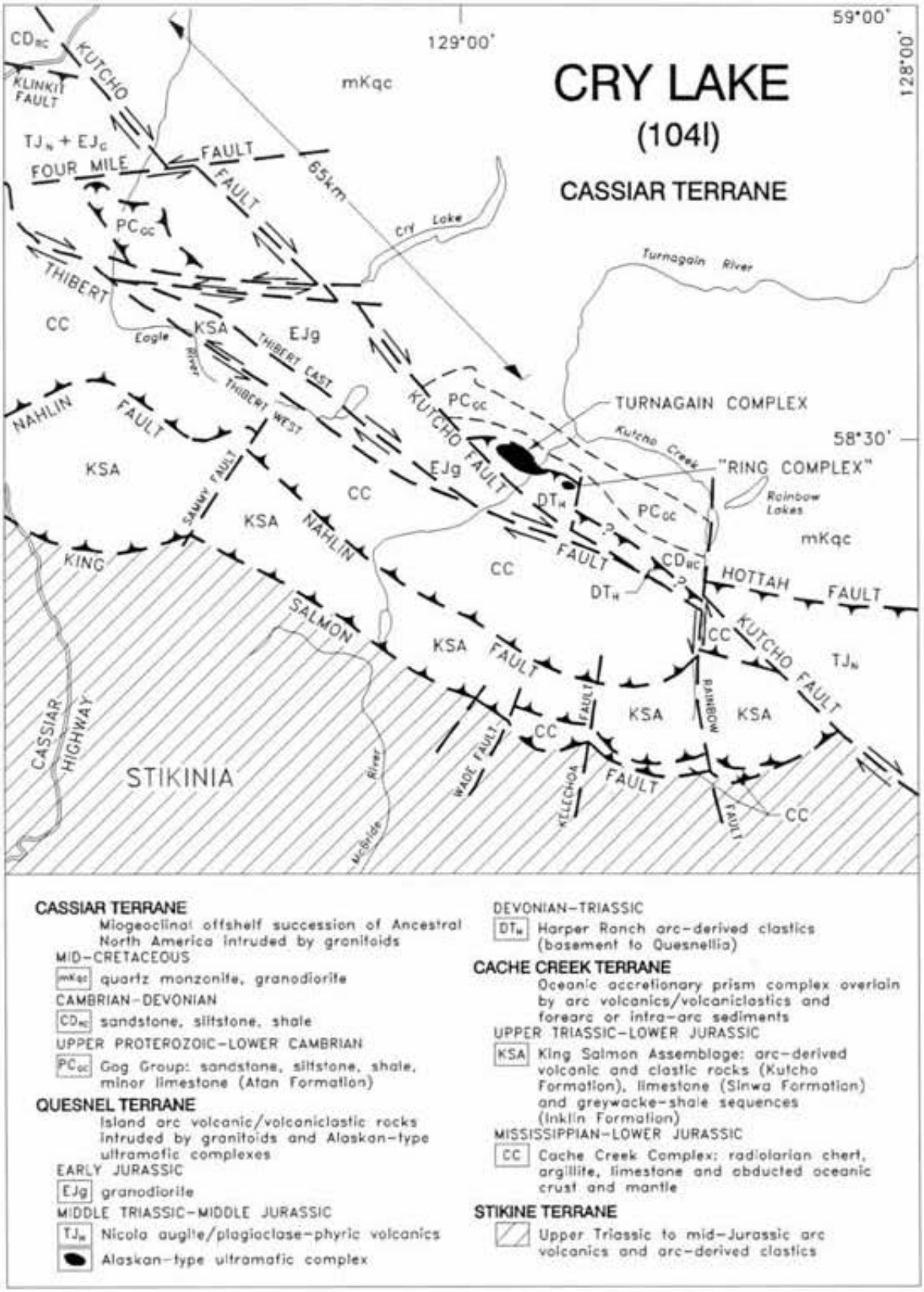

Figure 11.3. Tectonostratigraphic assemblages and major faults in the Cry Lake map area, north-central British Columbia (modified after Thorstad and Gabrielse, 1986; Gabrielse *et al.*, 1979; and Gabrielse, 1991).

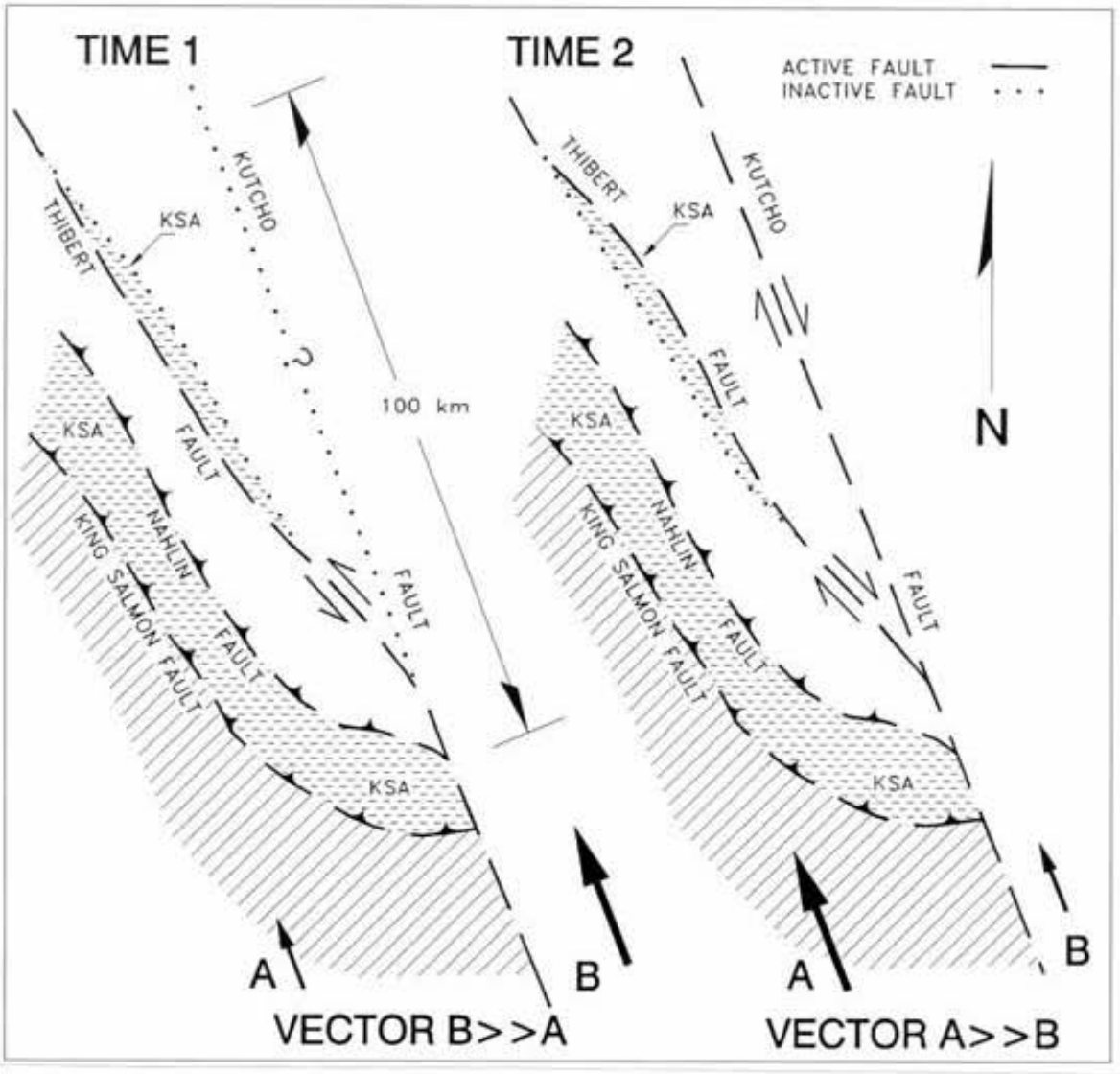

Figure 11.4. Schematic terrane motions and development of strike-slip faulting in north-central British Columbia. *See* text for explanation.

and micaceous quartzites assigned to the Lower Cambrian Atan Formation (Gabrielse *et al.*, 1979). The exact position of the fault boundary between lithologies representing the Cassiar Terrane (Atan Formation) and Quesnellia is not well known. The sedimentary rocks east of Quesnellia are considered to represent the offshelf equivalents of displaced miogeoclinal sequences of ancestral North America (Gabrielse, 1991; Wheeler and McFeely, 1991).

Almost all of the major stike-slip faults in the Canadian Cordillera, including the Kutcho-Thibert fault system, have been demonstrated to have right-lateral displacements since at least the mid-Cretaceous (Gabrielse, 1985). However, permissive evidence for left-lateral strike-slip is found along the Thibert fault west of the Turnagain complex.

In the Cry Lake map area on the western side of the Cache Creek Terrane, Monger and Thorstad (1978) coined the name King Salmon assemblage for an apparently continuous succession of Upper Triassic to Lower Jurassic rocks bounded by the Nahlin and King Salmon southward-verging thrust faults. Three lithological divisions were recognized: dominantly mafic to silicic arc-related volcanic and volcaniclastic rocks of the Kutcho Formation; sparsely fossiliferous carbonate of the Sinwa Formation; and greywacke, siltstone, shale and local conglomerate of the Inklin Formation (Figure 11.3). A northwest-trending sliver of these three lithologically distinctive subdivisions was also identified at the eastern margin of the Cache Creek accretionary complex (Gabrielse, 1962; Gabrielse *et al.*, 1979; Figure 11.3). The latter authors noted that the eastern margin of this sliver is intruded by Early Jurassic granodiorite whereas the western margin is in fault contact with the Cache Creek complex (Thibert fault). Later, Thorstad and

Gabrielse (1986) and Gabrielse (1991) placed the trace of the Thibert fault along the eastern margin of this rock package and re-interpreted the western contact to be in stratigraphic continuity with the Cache Creek, thereby placing King Salmon lithologies within the Cache Creek Terrane (Wheeler *et al.*, 1991). In contrast, Wheeler and McFeeley (1991) consider that the Thibert fault defines the western limit of this sliver, which they place within Quesnellia and correlate with Lower Jurassic clastic rocks of the Hall Formation. These discrepancies are probably best reconciled by accepting the original lithological correlations made by Gabrielse *et al.* (1979), and regarding the sliver of King Salmon assemblage rocks at the eastern margin of the Cache Creek Group to be completely bounded by steeply dipping strike-slip faults (H. Gabrielse, personal communication, 1992; Figure 11.3). As the major outcrops of King Salmon lithologies lie along the western margin of the Cache Creek Terrane and end abruptly at the Kutcho fault, similar assemblages along the Thibert fault may represent a tectonic sliver that has been displaced northward by left-lateral translation.

One scenario for sinistral displacement along the Kutcho-Thibert fault system is depicted in Figure 11.4 and involves differences in the rate of northward motion of fault-bounded blocks in the accreted and displaced pericratonic terranes relative to the craton. Block A (Cache Creek and Stikine terranes) west of the Thibert fault, and Block B (Quesnel and Cassiar terranes) to the east, moved northward at different rates (Vectors A and B, Figure 11.4) relative to ancestral North America (fixed, not shown). This results in left-lateral offset of approximately 100 kilometres along the Thibert-Kutcho fault system. At some later time, Block B decelerated relative to A and the Thibert fault jumped eastward thereby effecting the transfer of a sliver of King Salmon rocks to Block A (Cache Creek Terrane) and resulting in dextral offsets along the Thibert and Kutcho faults (Figure 11.4). Cumulative displacement relative to ancestral North America can be accommodated by more inboard faults (*e.g.*, Tintina - Northern Rocky Mountain Trench system - not shown). Provided that late dextral motion was entirely confined to the Thibert East splay, sinistral kinematic fabrics might be preserved adjacent to the Thibert West branch (Figure 11.3). A similar tectonic history has been interpreted in southern British Columbia where late Mesozoic (post-Albian) sinistral motion along a strand of the Yalakom fault is succeeded by dextral displacement (Eocene?) along the main fault trace (Miller, 1988; P. Schiarizza, personal communication, 1992).

Based on constraints provided by stratigraphic and structural correlations and isotopic dating of plutons, Gabrielse (1985) determined that pre-Late Cretaceous and younger(?) dextral displacements along the Thibert and Kutcho faults were linked to movements along the Thudaka-Finlay-Ingenika fault system. Accommodating about 125 kilometres of dextral offset on the latter system restores the trace of the Hottah-Swannell thrust faults and the Kutcho-Pinchi fault trace (Gabrielse, 1985; Figure 11.1B). As noted earlier, the Hottah-Klinkit fault trace can be restored by 65 kilometres of motion along the Kutcho fault; further displacement of approximately 110 kilometres along the Thibert-Kutcho-Takla system is required in order to restore the trace of the Nahlin-Vital fault (Gabrielse, 1985).

Ave-Lallemant and Oldow (1988) have related strike-slip displacements along the Cordilleran margin to transpressional tectonics and shown that this hypothesis is consistent with both absolute and relative motions of Pacific ocean basin plates (Engebretson *et al.*, 1985). During the Triassic to mid-Cretaceous, Cordilleran suspect terranes were moving southward with respect to North America due to left-oblique convergence, and thereafter northward as convergence became right-oblique. Since Gabrielse (1985) has inferred that motions on most of the major faults shown in Figure 11.1 probably terminated by Late Cretaceous, sinistral displacement along the Thibert-Kutcho fault system would presumably correspond to relative differences in the rates of southward migration of fault-bounded blocks (*i.e.*, this requires southward-directed and reverse vectors for Blocks A and B in Figure 11.4). Strike-slip motion on many of these faults may have been initiated as early as the late-Early Jurassic contractional deformation accompanying terrane accretion (Ave-Lallemant and Oldow, 1988; Gabrielse, 1991).

REFERENCES

Albee, A.L. and Ray, L. (1970): Correction Factors for the Electronprobe Microanalysis of Silicates, Oxides, Carbonates and Sulfates; *Analytical Chemistry*, Volume 42, pages 1408-1414.

Amossé, J., Allibert, M., Fischer, W. and Piboule, M. (1990): Experimental Study of the Solubility of Platinum and Iridium in Basic Silicate Melts - Implications for the Differentiation of Platinum-group Elements During Magmatic Processes; *Chemical Geology*, Volume 81, pages 45-53.

Anderson, R.G. (1979): Distribution and Emplacement History of Plutons within the Hotailuh Batholith in the Cry Lake and Spatsizi Map Areas, North-central British Columbia; *Geological Survey of Canada*, Paper 79-1A, pages 393-395.

Anderson, R.G. (1980): Satellitic Stocks, Volcanic and Sedimentary Stratigraphy, and Structure around the Northern and Western Margins of the Hotailuh Batholith, North-central British Columbia; *Geological Survey of Canada*, Paper 80-1A, pages 37-40.

Anderson, R.G. (1983): The Geology of the Hotailuh Batholith and Surrounding Volcanic and Sedimentary Rocks, North-central British Columbia; unpublished Ph.D. thesis, *Carleton University*, Ottawa, 669 pages.

Anderson, R.G. (1984): Late Triassic and Jurassic Magmatism along the Stikine Arch and the Geology of the Stikine Batholith, North-central British Columbia; *Geological Survey of Canada*, Paper 84-1A, pages 67-73.

Anderson, R.G. (1988): A Paleozoic and Mesozoic Stratigraphic and Plutonic Framework for the Iskut Map Area (104B), Northwestern B.C.; *in* Geology and Metallogeny of Northwestern British Columbia, *Geological Association of Canada, Cordilleran Section Meeting*, Smithers, B.C., pages A1-A3.

Anderson, R.G. Loveridge, W. D. and Sullivan, R. W. (1982): U-Pb Isotopic Ages of Zircon from the Jurassic Plutonic Suite, Hotailuh Batholith, North-central British Columbia; *Geological Survey of Canada*, Paper 82-1C, pages 133-137.

Armstrong, J.E. (1946): Aiken Lake (South Half), British Columbia; *Geological Survey of Canada*, Paper 46-11.

Armstrong, J.E. and Roots, E.F. (1948): Geology and Mineral Deposits of Aiken Lake Map Area, British Columbia; *Geological Survey of Canada*, Paper 48-5, 46 pages.

Ave-Lallement, H. G. and Oldow, J. S. (1988): Early Mesozoic Southward Migration of Cordilleran Transpressional Terranes; *Tectonics*, Volume 7, pages 1057-1075.

Barnes, S.J. (1990): The Use of Metal Ratios in Prospecting for Platinum-group Element Deposits in Mafic and Ultramafic Intrusions; *Journal of Geochemical Exploration*, Volume 37, pages 91-99.

Barnes, S.-J., Boyd, R., Korneliussen, A., Nilsson, L.-P., Often, M., Pedersen, R. B. and Robins, B. (1988): The Use of Mantle Normalization and Metal Ratios in Discriminating Between the Effects of Partial Melting, Crystal Fractionation and Sulphide Segregation on Platinum-group Elements, Gold, Nickel and Copper; *in* Geoplatinum '87, Prichard, H.M., Potts, P.J., Bowles, J. F. W. and Cribb, S. J., Editors; *Elsevier Publishing Company*, pages 113-144.

Beddoe-Stephens, B. and Lambert, R. St. J. (1981): Geochemical, Mineralogical, and Isotopic Data Relating to the Origin and Tectonic Setting of the Rossland Volcanic Rocks, Southern British Columbia; *Canadian Journal of Earth Sciences*, Volume 18, pages 858-868.

Bellefontaine, K.A. (1989): Tectonic Evolution of Upper Proterozoic Ingenika Group, North-central British Columbia; *in* Geological Fieldwork 1988, *B.C. Ministry of Energy, Mines and Petroleum Resources*, Paper 1989-1, pages 221-226.

Bellefontaine, K.A. (1991): The Boundary between the Omineca Crystalline Belt and the Intermontane Belt in Aiken Lake Map-area North-central British Columbia: An Example of Flake Tectonics; unpublished M.Sc. thesis, *McGill University*, 77 pages.

Bellefontaine, K.A. and Minehan, K. (1988): Summary of Fieldwork in the Ingenika Range, North-central British Columbia (94D/09; 94C/12); *in* Geological Fieldwork 1987, *B.C. Ministry of Energy, Mines, and Petroleum Resources*, Paper 1988-1, pages 195-198.

Bellefontaine, K.A. and Nelson, J. (1992): New Paleontologic and Lithogeochemical Data from the Nation Lakes Area and its Implications for the Quesnel and Stikine Arcs; *Southern Cordillera Transect (Lithoprobe) and Cordilleran Tectonics Workshop*, Edmonton, Alberta, Abstracts, page 84.

Bence, A.E. and Albee, A.L. (1968): Empirical Correction Factors for the Electron Microanalysis of Silicates and Oxides; *Journal of Geology*, Volume 76, pages 382-403.

Betekhtin, A. G. (1961): Mikroskopische Untersuchungen an Platinerzen aus dem Ural; *Neues Jahrbuch fur Mineralogie Abhandlungen*, Volume 97, pages 1-34.

Bird, D.K., Brooks, C.K., Gannicott, R. A. and Turner, P. A. (1991): A Gold-bearing Horizon in the Skaergaard Intrusion, East Greenland; *Economic Geology*, Volume 86, pages 1083-1092.

Bliss N.W. and Maclean, W.H. (1975): The Paragenesis of Zoned Chromite from Central Manitoba; *Geochimica Cosmochimica Acta*, Volume 39, pages 973-990.

Brown, D.A. and Gunning, M.H. (1989): Geology of the Scud River Area, Northwestern British Columbia (104G/5 and 6), *in* Geological Fieldwork 1988, *B.C. Ministry of Energy, Mines and Petroleum Resources*, Paper 1989-1, pages 251-267.

Brown, R.L., Journeay, J.M., Lane, L.S., Murphy, D.C. and Rees, C.J. (1986): Obduction, Backfolding, and Piggyback Thrusting in the Metamorphic Hinterland of the Canadian Cordillera; *Journal of Structural Geology*, Volume 8, pages 255-268.

Cabri, L.J. (1981): Nature and Distribution of Platinum-group Element Deposits; *Episodes*, Volume 2, pages 31-35.

Cabri, L.J. and Feather C.E. (1975): Platinum-Iron Alloys: Nomenclature Based on a Study of Natural and Synthetic Alloys; *Canadian Mineralogist*, Volume 13, pages 117-126.

Cabri, L.J. and Genkin, A. D. (1991): Re-examination of Pt Alloys from Lode and Placer Deposits, Urals; *Canadian Mineralogist*, Volume 29, pages 419-425.

Cabri, L.J. and Harris, D.C. (1975): Zoning in Os-Ir Alloys and the Relation of the Geological and Tectonic Environment of the Source Rocks to the Bulk Pt:Pt+Ir+Os Ratio for Placers; *Canadian Mineralogist*, Volume 13, pages 266-274.

Cabri, L.J. and Hey, M.H. (1974): Platiniridium - Confirmation as a Valid Mineral Species; *Canadian Mineralogist*, Volume 12, pages 299-303.

Cabri, L.J. and Laflamme, J.H.G. (1988): Mineralogical Study of the Platinum-group Element Distribution and Associated Minerals from Three Stratigraphic Layers, Bird River Sill, Manitoba; *Canada Centre for Mineral and Energy Technology*, Report CM88-1E, 52 pages.

Cabri, L.J., Criddle, A.J., Laflamme, J.H.G., Bearne, G. S. and Harris, D.C. (1981): Mineralogical Study of Complex Pt-Fe Nuggets from Ethiopia; *Bulletin de Minéralogie*, Volume 104, pages 508-525.

Cabri, L.J., Owens, D.R. and Laflamme, J.H.G. (1973): Tulameenite, a New Platinum-Iron-Copper Mineral from Placers in the Tulameen River Area, British Columbia; *Canadian Mineralogist*, Volume 12, pages 21-25.

Cabri, L.J., Rosenweig, A. and Pinch, W.W. (1977): Platinum-group Minerals from Onverwacht. 1. Pt-Fe-Cu-Ni Alloys; *Canadian Mineralogist*, Volume 15, pages 380-384.

Cameron, A. E., Smith, D. H. and Walker, R. L. (1969): Mass Spectrometry of Nanogram-size Samples of Lead; *Analytical Chemistry*, Volume 41, pages 525-526.

Camsell, C. (1913): Geology and Mineral Deposits of the Tulameen District, British Columbia; *Geological Survey of Canada*, Memoir 26, 188 pages.

Church, B.N. (1974): Geology of the Sustut Area, *in* Geology, Exploration and Mining in British Columbia 1973, *B.C. Ministry of Energy, Mines and Petroleum Resources*, pages 411-455.

Church, B.N. (1975): Geology of the Sustut Area; *in* Geology, Exploration and Mining in British Columbia 1974, *B.C. Ministry of Energy, Mines and Petroleum Resources*, pages 305-309.

Clark, T. (1975): Geology of an Ultramafic Complex on the Turnagain River, Northwestern British Columbia; unpublished Ph.D. thesis, *Queen's University*, 453 pages.

Clark, T. (1978): Oxide Minerals in the Turnagain Ultramafic Complex, Northwestern British Columbia; *Canadian Journal of Earth Sciences*, Volume 15, pages 1893-1903.

Clark, T. (1980): Petrology of the Turnagain Ultramafic Complex, Northwestern British Columbia; *Canadian Journal of Earth Sciences*, Volume 17, pages 744-757.

Cordey, F., Gordey, S. P. and Orchard, M. J. (1991): New Biostratigraphic Data for the Northern Cache Creek Terrane, Teslin Map-area, Southern Yukon; *Geological Survey of Canada*, Paper 91-1E, pages 67-76.

Cordey, F., Mortimer, N., DeWever, P. and Monger, J.W.H. (1987): Significance of Jurassic Radiolarians from the Cache Creek Terrane, British Columbia; *Geology*, Volume 15, pages 1151-1154.

Corrivaux, L. and Laflamme, J.H.G. (1990): Minéralogie des éléments du Groupe du Platine dans les Chromitites de l'Ophiolite de Thetford Mines; *Canadian Mineralogist*, Volume 28, pages 579-595.

Cox, D.P. and Singer, D.A., Editors (1986): Mineral Deposit Models; *U.S. Geological Survey*, Bulletin 1693, 379 pages.

Davis, D.W. (1982): Optimum Linear Regression and Error Estimation Applied to U-Pb Data; *Canadian Journal of Earth Sciences*, Volume 19, pages 2141-2149.

Duparc, L. and Tikonowitch, M.N. (1920): Le Platine et les Gîtes Platinifères de l'Oural et du Monde; *Sonor*, Genève.

Eadie, E.T. (1976): K-Ar and Rb-Sr Geochronology of the Northern Hope Batholith, British Columbia; unpublished B.Sc. thesis, *The University of British Columbia*, 46 pages.

Eales, H.V. (1987): Upper Critical Zone Chromitite Layers at R.P.M. Union Section Mine, Western Bushveld Complex; *In* Evolution of Chromium Ore Fields, Stowe, C.W., Editor, *Van Nostrand Reinhold*, New York, pages 144-168.

Eastwood, G.E.P. (1959): Magnetite in Lodestone Mountain Stock; *B.C. Minister of Mines*, Annual Report, Lode Metals, pages 39-53.

Engebretson, D.C., Cox, A. and Gordon, R.G. (1985): Relative Motions Between Oceanic and Continental Plates in the Pacific Basin; *Geological Society of America*, Special Paper 206, 59 pages.

Evans, B.W. and Frost, B.R. (1975): Chrome-spinel in Progressive Metamorphism - a Preliminary Analysis; *Geochimica Cosmochimica Acta*, Volume 39, pages 959-972.

Evenchick, C.A., Monger, J.W.H. and Friday, S.J. (1986): Potential Hosts to Platinum Group Element Concentrations in the Canadian Cordillera; *Geological Survey of Canada*, Open File 1433.

Ewing, T.E. (1980): Paleogene Tectonic Evolution of the Pacific Northwest; *Journal of Geology*, Volume 88, pages 619-638.

Ferri, F. and Melville, D.M. (1994): Bedrock Geology of the Germansen Landing - Manson Creek Area, British Columbia (94N/9, 10, 15; 94C/2); *B.C. Ministry of Energy, Mines and Petroleum Resources*, Bulletin 91, 147 pages.

Ferri, F., Dudka, S. and Rees, C. (1992a): Geology of the Uslika Lake Area, Northern Quesnel Trough, B.C. (94C/3, 4, 6); *in* Geological Fieldwork 1991, *B.C. Ministry of Energy, Mines and Petroleum Resources*, Paper 1992-1, pages 127-146.

Ferri, F., Dudka, S., Rees, C. and Meldrum, D. (1993a): Geology of the Aiken Lake and Osilinka River Areas, Northern Quesnel Trough (94C/2, 3, 5, 6, 12); *in* Geological Fieldwork 1992, *B.C. Ministry of Energy, Mines and Petroleum Resources*, Paper 1993-1, pages 109-134.

Ferri, F., Dudka, S., Rees, C. and Meldrum, D.G. (1993b): Preliminary Geology and Geochemistry of the Aiken Lake and Osilinka River Areas (94C/2, 3, 5, 6, 12); *B.C. Ministry of Energy, Mines and Petroleum Resources*, Open File 1993-2.

Ferri, F., Dudka, S., Rees, C., Meldrum, D. and Wilson, M. (1992b): Geology and Geochemistry of the Uslika Lake Area, British Columbia (94C/3, 4, 6); *B.C. Ministry of Energy, Mines and Petroleum Resources*, Open File 1992-11.

Findlay, D.C. (1963): Petrology of the Tulameen Ultramafic Complex, Yale District, British Columbia; unpublished Ph.D. thesis, *Queen's University*, 415 pages.

Findlay, D.C. (1969): Origin of the Tulameen Ultramafic-Gabbro Complex, Southern British Columbia; *Canadian Journal of Earth Sciences*, Volume 6, pages 399-425.

Foster, F. (1974): History and Origin of the Polaris Ultramafic Complex in the Aiken Lake Area of North-central British Columbia; unpublished B.Sc. thesis, *The University of British Columbia*, 66 pages.

Friedman, R.M. and van der Heyden, P. (1992): Late Permian U-Pb Dates for the Farwell and Northern Mt. Lytton Plutonic Bod-

ies, Intermontane Belt, British Columbia; *Geological Survey of Canada*, Paper 92-1A, pages 137-144.

Gabrielse, H. (1962): Cry Lake, British Columbia; *Geological Survey of Canada*, Map 29-1962.

Gabrielse, H. (1985): Major Dextral Transcurrent Displacements Along the Northern Rocky Mountain Trench and Related Lineaments in North-central British Columbia; *Geological Society of America*, Bulletin, Volume 96, pages 1-14.

Gabrielse, H. (1991): Late Paleozoic and Mesozoic Terrane Interactions in North-central British Columbia; *Canadian Journal of Earth Sciences*, Volume 28, pages 947-957.

Gabrielse, H. and Dodds, C.J. (1974): Operation Findlay; *Geological Survey of Canada*, Paper 74-1A, pages 13-16.

Gabrielse, H. and Yorath, C.J. (1991): Tectonic Synthesis, Chapter 18; *in* Geology of the Cordilleran Orogen in Canada; Gabrielse, H. and Yorath, C. J., Editors, *Geological Survey of Canada*, Geology of Canada, Number 4, pages 677-705.

Gabrielse, H., Anderson, R.G., Leaming, S.F., Mansy, J.L., Monger, J.W.H., Thorstad, L.E. and Tipper, H.W. (1979): Cry Lake, British Columbia; *Geological Survey of Canada*, Open File 610.

Gabrielse, H., Wanless, R.K., Armstrong, R.L. and Erdman, L.R. (1980): Isotopic Dating of Early Jurassic Volcanism andPlutonism in North-central British Columbia; *Geological Survey of Canada*, Paper 80-1A, pages 27-32.

Genkin, A.D. and Evstigneeva, T.L. (1986): Associations of Platinum-group Minerals of the Noril'sk Copper-Nickel Sulfide Ores; *Economic Geology*, Volume 81, pages 1203-1212.

Gray, F., Page, N.J., Carlson, C.A., Wilson, S.A. and Carlson, R.R., (1986): Platinum-group Element Geochemistry of Zoned Ultramafic Intrusive Suites, Klamath Mountains, California and Oregon; *Economic Geology*, Volume 81, pages 1252-1260.

Greig, C. J. (1989): Geology and Geochronometry of the Eagle Plutonic Complex, Coquihalla Area, Southwestern British Columbia (92H/6, 7, 10, 11); unpublished M.Sc. thesis, *The University of British Columbia*, 423 pages.

Greig, C.J. (1992): Jurassic and Cretaceous Plutonic and Structural Styles of the Eagle Plutonic Complex, Southwestern British Columbia, and their Regional Significance; *Canadian Journal of Earth Sciences*, Volume 29, pages 793-811.

Greig, C.J., Armstrong, R.L. , Harakal, J.E., Runkle, D. and van der Heyden, P. (1992): Geochronometry of the Eagle Plutonic Complex and the Coquihalla Area, Southwestern British Columbia; *Canadian Journal of Earth Sciences*, Volume 29, pages 812-829.

Hanson, G. and McNaughton, D. A. (1936): Eagle-McDame Area, Cassiar District, British Columbia; *Geological Survey of Canada*, Memoir 194, 16 pages.

Harland, W. B., Armstrong, R. L., Craig, L. E., Smith, A. G. and Smith, D. G. (1990): A Geologic Time Scale 1989; *Cambridge University Press*, 263 pages.

Harris, D. C. and Cabri, L. J. (1973): The Nomenclature of the Natural Alloys of Osmium, Iridium, and Ruthenium Based on New Compositional Data of Alloys from Worldwide Occurrences; *Canadian Mineralogist*, Volume 12, pages 104-112.

Harris, D. C. and Cabri, L. J. (1991): Nomenclature of Platinum-group Element Alloys: Review and Revision; *Canadian Mineralogist*, Volume 29, pages 231-237.

Heald, E.F. (1967): Thermodynamics of Iron-Platinum Alloys; *Transactions of the Metallurgical Society (AIME)*, Volume 239, pages 1337-1340.

Henderson, C. M. and Perry, D. G. (1981): A Lower Jurassic Heteroporid Bryozoan and Associated Biota, Turnagain Lake, British Columbia; *Canadian Journal of Earth Sciences*, Volume 18, pages 457-468.

Hill, R. and Roeder, P. (1974): The Crystallization of Spinel from Basalt Liquid as a Function of Oxygen Fugacity; *Journal of Geology*, Volume 82, pages 709-729.

Hoffmann, S. J. and Wong, R. H. (1986): Geochemical Assessment Report of the Gold, Silver, Platinum and Palladium Potential of the NIK 1 - 4 Claims; *B.C. Ministry of Energy, Mines and Petroleum Resources*, Assessment Report 15194, 63 pages.

Holbeck, P. M. (1988): Geology and Mineralization of the Stikine Assemblage, Mess Creek Area, Northwestern British Columbia; unpublished M.Sc. thesis, *The University of British Columbia*, 184 pages.

Höy, T. and Andrew, K.P.E. (1989): The Rossland Group, Nelson Map-area, Southeastern British Columbia; *in* Geological Fieldwork 1988, *B.C. Ministry of Energy, Mines and Petroleum Resources*, Paper 1989-1, pages 33-43.

Höy, T. and Andrew, K.P.E. (1991): Geology of the Rossland Area, Southeastern British Columbia; *in* Geological Fieldwork 1990, *B.C. Ministry of Energy, Mines and Petroleum Resources*, Paper 1991-1, pages 21-31.

Hulbert, L.J., Duke, M.J., Eckstrand, O.R., Lydon, J.W., Scoates, R.F.J., Cabri, L.J. and Irvine, T.N. (1988): Geological Environments of the Platinum-group Elements; *Geological Association of Canada*, Cordilleran Section Workshop, Vancouver, 151 pages.

Irvine, T.N. (1965): Chromian Spinel as a Petrogenetic Indicator. 1. Theory; *Canadian Journal of Earth Sciences*, Volume 2, pages 648-672.

Irvine, T.N. (1967): Chromian Spinel as a Petrogenetic Indicator. 2. Petrologic Applications; *Canadian Journal of Earth Sciences*, Volume 4, pages 71-103.

Irvine, T.N. (1974a): Petrology of the Duke Island Ultramafic Complex, Southeastern Alaska; *Geological Society of America*, Memoir 138, 240 pages.

Irvine, T.N. (1974b): Ultramafic and Gabbroic Rocks in the Aiken Lake and McConnell Creek Map-areas, British Columbia; *Geological Survey of Canada*, Paper 74-1A, pages 149-152.

Irvine, T.N. (1976): Alaskan-type Ultramafic-Gabbroic Bodies in the Aiken Lake, McConnell Creek and Toodoggone Map-areas; *Geological Survey of Canada*, Paper 76-1A, pages 76-81.

Irvine, T.N. (1986): Layering and Related Structures in the Duke Island and Skaergaard Intrusions: Similarities, Differences, and Origins; *in* Origins of Igneous Layering, Parsons, I., Editor, NATO ASI Series, Volume 196, pages 185-245.

Irvine, T.N. and Baragar, W. R. A. (1971): A Guide to the Chemical Classification of the Common Volcanic Rocks; *Canadian Journal of Earth Sciences*, Volume 8, pages 523-545.

Johan, Z., Ohnenstetter, M., Slansky, E., Barron, L.M. and Suppel, D. (1989): Platinum Mineralization in the Alaskan-type Intrusive Complexes near Fifield, New South Wales, Australia. 1. Platinum-group Minerals in Clinopyroxenites of the Kelvin Grove Prospect, Owendale Intrusion; *Mineralogy and Petrology*, Volume 40, pages 289-309.

Jones, H.M. (1970): Geological and Geochemical Report on the West Nos. 1-14 Mineral Claims; *B.C. Ministry of Energy, Mines, and Petroleum Resources,* Assessment Report 2548, 10 pages.

Kleinspehn, K. L. (1985): Cretaceous Sedimentation and Tectonics, Tyaughton-Methow Basin, Southwestern British Columbia; *Canadian Journal of Earth Sciences*, Volume 22, pages 154-174.

Krogh, T. E. (1973): A Low-contamination Method for Hydrothermal Decomposition of Zircon and Extraction of U and Pb for Isotopic Age Determinations; *Geochimica Cosmochimica Acta*, Volume 37, pages 485-494.

Krogh, T. E. (1982): Improved Accuracy of U-Pb Zircon Ages by the Creation of More Concordant Systems Using an Air Abrasion Technique; *Geochimica Cosmochimica Acta*, Volume 46, pages 637-649.

Krogh, T. E., and Davis, G. L. (1975): The Production and Preparation of ^{205}Pb for Use as a Tracer for Isotope Dilution Analyses; *Carnegie Institute of Washington,* Yearbook 74, pages 416-417.

Laflamme, J.H.G. (1990): The Preparation of Materials for Microscopic Study; *in* Advanced Microscopic Studies of Ore Minerals, Jambor, J.L. and Vaughan, D.J., Editors, *Mineralogical Association of Canada*, Short Course 17, pages 37-68.

Lay, R. (1932): Aiken Lake Area, North-central British Columbia; *B.C. Ministry of Energy, Mines, and Petroleum Resources,* Bulletin 1, 32 pages.

Leake, B. E. (1978): Nomenclature of Amphiboles; *American Mineralogist,* Volume 63, pages 1023-1053.

Lee, C.A. and Parry, S.J. (1988): Platinum-group Element Geochemistry of the Lower and Middle Group Chromitites of the Eastern Bushveld Complex; *Economic Geology*, Volume 83, pages 1127-1139.

Legendre, O. and Augé, T. (1986): Mineralogy of Platinum-group Mineral Inclusions in Chromitites from Different Ophiolitic Complexes; *in* Metallogeny of Basic and Ultrabasic Rocks, Gallagher, M.J., Ixer, R.A., Neary, C.R. and Prichard, H.M., Editors, *Institution of Mining and Metallurgy*, pages 361-372.

Le Maitre, R.W., Editor (1989): A Classification of Igneous Rocks and Glossary of Terms; *Blackwell Scientific Publications*, Oxford, 193 pages.

Logan, J. M. and Koyanagi, V. A. (1989): Geology and Mineral Deposits of the Galore Creek Area (104G/3 and 4); *in* Geological Fieldwork 1988, *B.C. Ministry of Energy, Mines, and Petroleum Resources,* Paper 1989-1, pages 269-284.

Loney, R. A., Himmelberg, G. R. and Shew, N. (1987): Salt Chuck Palladium-bearing Ultramafic Body, Prince of Wales Island; *United States Geological Survey*, Circular 998, pages 126-127.

Lord, C.S. (1948): McConnell Creek Map-area, British Columbia; *Geological Survey of Canada*, Memoir 26, 72 pages.

Macdonald, A. J. (1986): The Platinum Group Element Deposits: Classification and Genesis; *Geoscience Canada*, Volume 14, pages 155-166.

Makovicky, M., Makovicky, E. and Rose-Hansen, J. (1986): Experimental Studies on the Solubility and Distribution of Platinum Group Elements in Base-metal Sulphides in Platinum Deposits; *in* Metallogeny of Basic and Ultrabasic Rocks, Gallagher, M.J., Ixer, R.A., Neary, C.R. and Prichard, H.M., Editors, *Institution of Mining and Metallurgy*, pages 415-425.

Malinsky, D. (1966): Copper Pass Mines Ltd., Induced Polarization Survey, Dalvenie, Mac, and New Deal Claims, Stikine Plateau Area; *B.C. Ministry of Energy, Mines, and Petroleum Resources,* Assessment Report No. 899, 11 pages.

Mansy, J.L. and Gabrielse, H. (1978): Stratigraphy, Terminology and Correlation of Upper Proterozoic Rocks in Omineca and Cassiar Mountains, North-central British Columbia; *Geological Survey of Canada*, Paper 77-19.

McDougall, I. (1974): The ^{40}Ar/^{39}Ar Method of K-Ar Age Determination of Rocks using HIFAR Reactor; *Atomic Energy in Australia*, Number 17, pages 9-18.

Meyer, W. and Overstall, R. (1973): Geological, Geochemical and Geophysical Survey on the ARD Claims, McConnell Creek Area, Omineca Mining Division; *B.C. Ministry of Energy Mines and Petroleum Resources*, Assessment Report 4707, 13 pages.

Miller, M. G. (1988): Possible Pre-Cenozoic Left-lateral Slip on the Yalakom Fault, Southwestern British Columbia; *Geology*, Volume 16, pages 584-587.

Minehan, K. (1989): Takla Group Volcano-sedimentary Rocks, North-central British Columbia; *in* Geological Fieldwork 1988, *B.C. Ministry of Energy, Mines and Petroleum Resources,* Paper 1989-1, pages 227-232.

Monger, J.W.H. (1973): Upper Paleozoic Rocks of the Western Canadian Cordillera; *Geological Survey of Canada*, Paper 73-1A, pages 27-28.

Monger, J.W.H. (1976): Lower Mesozoic Rocks in McConnell Creek Map Area (94D), British Columbia; *Geological Survey of Canada*, Paper 76-1A, pages 51-55.

Monger, J.W.H. (1977): The Triassic Takla Group in McConnell Creek Map-area, North-central British Columbia, *Geological Survey of Canada*, Paper 76-29, 45 pages.

Monger, J.W.H. (1985): Structural Evolution of the Southwestern Intermontane Belt, Ashcroft and Hope Map Areas, British Columbia; *in* Current Research, Part A, *Geological Survey of Canada*, Paper 85-1A, pages 349-358.

Monger, J.W.H. (1989): Geology , Hope, British Columbia; *Geological Survey of Canada*, Map 41-1989, Sheet 1.

Monger, J.W.H. and Church, B. N. (1977): Revised Stratigraphy of the Takla Group, North-central British Columbia; *Canadian Journal of Earth Sciences*, Volume 14, pages 318-326.

Monger, J.W.H. and Paterson, I. A. (1974): Upper Paleozoic and Lower Mesozoic Rocks of the Omineca Mountains; *Geological Survey of Canada,* Paper 74-1A, pages 19-20.

Monger, J.W.H. and Thorstad, L. (1978): Lower Mesozoic Stratigraphy, Cry Lake and Spatsizi Map-areas, British Columbia; *Geological Survey of Canada*, Paper 78-1A, pages 21-24.

Monger, J.W.H., Price, R.A. and Templeman-Kluit, D.J. (1982): Tectonic Accretion and the Origin of the Two Major Metamorphic and Plutonic Welts in the Canadian Cordillera; *Geology*, Volume 10, pages 70-75.

Monger, J.W.H., Richards, T. A. and Paterson, I. A. (1978): The Hinterland Belt of the Canadian Cordillera: New Data from Northern and Central British Columbia; *Canadian Journal of Earth Sciences*, Volume 15, pages 823-830.

Monger, J.W.H, Wheeler, J. O., Tipper, H. W., Gabrielse, H., Harms, T., Struik, L. C., Campbell, R. B., Dodds, C. J., Gehrels, G. E. and O'Brien, J. (1991): Cordilleran Terranes, Chapter 8, Upper Devonian to Middle Jurassic Assem-

blages; *in* Geology of the Cordilleran Orogen in Canada, Gabrielse, H., and Yorath, C. J., Editors, *Geological Survey of Canada*, Geology of Canada, Number 4, pages 281-327.

Morimoto, N. (1989): Nomenclature of Pyroxenes; *Canadian Mineralogist*, Volume 27, pages 143-156.

Mortimer, N. (1986): Late Triassic, Arc-related, Potassic Igneous Rocks of the North American Cordillera; *Geology*, Volume 14, pages 1035-1038.

Murphy, D. C. (1989): Crustal Paleorheology of the Southeastern Canadian Cordillera and Its Influence on the Kinematics of Jurassic Convergence; *Journal of Geophysical Research*, Volume 94, pages 15723-15739.

Murphy, D. C., van der Heyden, P., Parrish, R. R., Klepacki, D. W., McMillan, W., Struik, L. C. and Gabites, J. (1995): New Geochronological Constraints on Jurassic Deformation of the Western Edge of North America, Southeastern Canadian Cordillera; *in* Jurassic Magmatism and Tectonics of the North American Cordillera, *Geological Society of America*, Special Paper 299, pages 159-171.

Naldrett, A.J. (1989): Magmatic Sulfide Deposits; *Oxford University Press*, New York, 186 pages.

Naldrett, A.J. and Lehmann, J. (1987): Spinel Non-stoichiometry as the Explanation for Ni-, Cu- and PGE-enriched Sulphides in Chromitites; *In* Geoplatinum '87, Prichard, H.M., Potts, R.J., Bowles, J.F.W. and Cribb, S.J., Editors, *Elsevier*, London, pages 93-110.

Naldrett, A.J. and Von Gruenewaldt, G. (1989): The Association of PGE with Chromitite in Layered Intrusions and Ophiolite Complexes; *Economic Geology*, Volume 84, pages 180-187.

Naldrett, A.J., Cameron, G., von Gruenewaldt, G. and Sharpe, M.R. (1987): The Formation of Stratiform PGE Deposits in Layered Intrusions; *in* Layered Intrusions, Parsons, I., Editor, *NATO Advanced Scientific Institute, Series* C, Volume 196, pages 313-397.

Nelson, J. and Mihalynuk, M. (1992): The Cache Creek Ocean: Closure or Enclosure?; *Southern Cordillera Transect (Lithoprobe) and Cordilleran Tectonics Workshop*, Edmonton, Alberta, Abstracts, page 83.

Nixon, G.T. (1988): Geology of the Tulameen Ultramafic Complex; *B.C. Ministry of Energy, Mines, and Petroleum Resources*, Open File 1988-25.

Nixon, G.T., (1990): Geology and Precious Metal Potential of Mafic-Ultramafic Rocks in British Columbia: Current Progress; *in* Geological Fieldwork 1989, *B.C. Ministry of Energy, Mines and Petroleum Resources*, Paper 1990-1, pages 353-358.

Nixon, G.T. and Hammack, J.L. (1991): Metallogeny of Mafic-Ultramafic Rocks in British Columbia with Emphasis on Platinum-group Elements; *in* Ore Deposits, Tectonics and Metallogeny in the Canadian Cordillera, *B.C. Ministry of Energy, Mines and Petroleum Resources*, Paper 1991-4, pages 125-161.

Nixon, G.T., Ash, C.H., Connelly, J.N. and Case, G. (1989): Geology and Noble Metal Geochemistry of the Turnagain Ultramafic Complex, Northern British Columbia; *B.C. Ministry of Energy, Mines, and Petroleum Resources*, Open File 1989-18.

Nuttall, C. (1991): Petrology of the Lunar Creek Mafic-Ultramafic Alaskan-type Complex in North-Central British Columbia; B.Sc. thesis, *Queen's Univesity*, Kingston, Ontario, 68 pages.

O'Neil, J.J. and Gunning, H.C. (1934): Platinum and Allied Metal Deposits of Canada; *Geological Survey of Canada*, Economic Geology Series 13, 165 pages

Pan, Y. and Fleet, M.E. (1989): Cr-rich Calc-silicates from the Hemlo Area, Ontario; *Canadian Mineralogist*, Volume 27, pages 565-577.

Parrish, R.R. and Monger, J.W.H. (1992): New U-Pb Dates from Southwestern British Columbia; *in* Radiogenic Age and Isotopic Studies, Report 5, *Geological Survey of Canada*, Paper 91-2, pages 87-108.

Peck, D. C. and Keays, R. R. (1990): Insights into the Behavior of Precious Metals in Primitive, S-undersaturated Magmas: Evidence from the Heazlewood River Complex, Tasmania; *Canadian Mineralogist*, Volume 28, pages 553-577.

Preto, V.A. (1975): The Nicola Group: Mesozoic Volcanism Related to Rifting in Southern British Columbia; *in* Volcanic Regimes in Canada, Baragar, W.R.A., Coleman, L.G. and Hall, J.M., Editors, *Geological Association of Canada*, Special Paper 16, pages 38-57.

Preto, V.A. (1979): Geology of the Nicola Group between Merritt and Princeton; *B.C. Ministry of Energy, Mines, and Petroleum Resources*, Bulletin 69, 90 pages.

Price, R. A. (1986): The Southeastern Canadian Cordillera: Thrust Faulting, Tectonic Wedging and Delamination of the Lithosphere; *Journal of Structural Geology*, Volume 8, pages 239-254.

Price, R.A., Parrish, R.R., Monger, J.W.H. and Roddick, J.A. (1987): Cordilleran Cross-section: Calgary to Vancouver; *in* Guidebook for Scientific Excursion A1, 19th General Assembly, *International Union of Geodesy and Geophysics*, 96 pages.

Prichard, H.M., Neary, C.R. and Potts, P.J. (1986): Platinum Group Minerals in the Shetland Ophiolite; in Metallogeny of Basic and Ultrabasic Rocks, Gallagher, M.J., Ixer, R.A., Neary, C. R. and Prichard, H.M., Editors, *Institution of Mining and Metallurgy*, pages 395-414.

Raicevic, D. and Cabri, L.J. (1976): Mineralogy and Concentration of Au- and Pt-bearing Placers from the Tulameen River Area in British Columbia; *Canadian Institute of Mining and Metallurgy*, Bulletin, Volume 69, pages 111-119.

Reynolds, N.W. (1967): Copper Pass Mines Ltd., Geochemical Report No. 1, Stikine Plateau Property; *B.C. Ministry of Energy, Mines, and Petroleum Resources*, Assessment Report 896, 14 pages.

Rice, H.M.A. (1947): Geology and Mineral Deposits of Princeton Map Area, British Columbia; *Geological Survey of Canada*, Memoir 243, 136 pages.

Richards, T.A. (1976a): McConnell Creek Map Area (94D/E), Geology; *Geological Survey of Canada*, Open File 342.

Richards, T.A. (1976b): Takla Group (Reports 10-16): McConnell Creek Map Area (94D, East Half), British Columbia; *Geological Survey of Canada*, Paper 76-1A, pages 43-50.

Roddick, J.C. and Farrar, E. (1971): High Initial Argon Ratios in Hornblendes; *Earth and Planetary Science Letters*, Volume 12, pages 208-214.

Roddick, J.C. and Farrar, E. (1972): Potassium-Argon Ages of the Eagle Granodiorite, Southern British Columbia; *Canadian Journal of Earth Sciences*, Volume 9, pages 596-599.

Roed, M.A. (1966a): Copper Pass Mines Ltd., Geologic Report No. 1, Dalvenie, Mac, and New Deal Claims, Stikine Plateau

Area; *B.C. Ministry of Energy, Mines, and Petroleum Resources*, Assessment Report 898, 24 pages.

Roed, M.A. (1966b): Copper Pass Mines Ltd., Geologic Report No. 2, Stikine Plateau and Pine Point Properties; *B.C. Ministry of Energy, Mines, and Petroleum Resources*, Assessment Report 897, 32 pages.

Roeder, P.L. and Campbell, I.H. (1985): The Effect of Postcumulus Reactions on Composition of Chrome-spinels from the Jimberlana Intrusion; *Journal of Petrology*, Volume 26, pages 763-786.

Roots, E. F. (1954): Geology and Mineral Deposits of Aiken Lake Map Area, British Columbia; *Geological Survey of Canada*, Memoir 274, 246 pages.

Rublee, V.J. (1986): Occurrence and Distribution of Platinum-group Elements in British Columbia; *B.C. Ministry of Energy, Mines, and Petroleum Resources*, Open File 1986-7, 94 pages.

Rublee, V.J. (1994): Chemical Petrology, Mineralogy and Structure of the Tulameen Complex, Princeton Area, British Columbia; M.Sc. thesis, *University of Ottawa*, Ottawa, Ontario, 183 pages.

Rublee, V.J. and Parrish, R.R. (1990): Chemistry, Chronology and Tectonic Significance of the Tulameen Complex, Southwestern British Columbia; *Geological Association of Canada - Mineralogical Association of Canada*, Abstracts with Programs, Volume 15, page A114.

Ryback-Hardy, V. (1972): Geological-Geochemical Report on the South Group of the West Property; *B.C. Ministry of Energy, Mines, and Petroleum Resources*, Assessment Report 3835, 10 pages.

Slansky, E., Johan, Z., Ohnenstetter, M., Barron, L. M. and Suppel, D. (1991): Platinum Mineralization in the Alaskan-type Intrusive Complexes near Fifield, N. S. W., Australia. 2. Platinum-group Minerals in Placer Deposits at Fifield; *Mineralogy and Petrology*, Volume 43, pages 161-180.

Souther, J. G. (1972): Telegraph Creek Map-area, British Columbia (104G); *Geological Survey of Canada*, Paper 71-44, 38 pages.

Souther, J.G. (1991): Volcanic Regimes, Chapter 14; *in* Geology of the Cordilleran Orogen in Canada, Gabrielse, H. and Yorath, C.J., Editors, *Geological Survey of Canada*, Geology of Canada, Number 4, pages 457-490.

St. Louis, R. M., Nesbitt, B. E. and Morton, R. D. (1986): Geochemistry of Platinum Group Elements in the Tulameen Ultramafic Complex, Southern British Columbia; *Economic Geology*, Volume 81, pages 961-973.

Steiger, R. H. and Jäger, E. (1977): Subcommision on Geochronology: Convention on the Use of Decay Constants in Geo- and Cosmochronology; *Earth and Planetary Science Letters*, Volume 36, pages 359-362.

Stevens, R. D., Delabio, R. N. and Lachance, G. R. (1982): Age Determinations and Geological Studies; *Geological Survey of Canada*, Paper 82-2, 56 pages.

Stockman, H.W. and Hlava, P.F. (1984): Platinum-group Mnerals in Alpine Cromitites from Suthwestern Oregon; *Economic Geology*, Volume 79, pages 491-508.

Talkington, R.W. and Watkinson, D.H. (1986): Whole-rock Platinum-group Element Trends in Chromite-rich Rocks in Ophiolitic and Stratiform Igneous Complexes; *in* Metallogeny of Basic and Ultrabasic Rocks, Gallagher, M.J., Ixer, R.A., Neary, C. R. and Prichard, H.M., Editors, *Institution of Mining and Metallurgy*, pages 427-440.

Taylor, H. P. Jr. (1967): The Zoned Ultramafic Complexes of Southeastern Alaska; *in* Ultramafic and Related Rocks, P. J. Wyllie, Editor, *John Wiley and Sons Inc.*, New York, pages 97-121.

Thorstad, L. (1980): Upper Paleozoic Volcanic and Volcaniclastic Rocks in Northwest Toodoggone Map Area, British Columbia; *Geological Survey of Canada*, Paper 80-1B, pages 207-211.

Thorstad, L. and Gabrielse, H. (1986): The Upper Triassic Kutcho Formation, Cassiar Mountains, North-central British Columbia; *Geological Survey of Canada*, Paper 86-16, 53 pages.

Tipper, H. W. (1984): The Age of the Jurassic Rossland Group of Southeastern British Columbia; *Geological Survey of Canada*, Paper 84-1A, pages 631-632.

Travers, W.B. (1978): Overturned Nicola and Ashcroft Strata and their Relation to the Cache Creek Group, Southwestern Intermontane Belt, British Columbia; *Canadian Journal of Earth Sciences*, Volume 15, pages 99-109.

Travers, W.B. (1982): Possible Large-scale Overthrusting near Ashcroft, British Columbia: Implications for Petroleum Prospecting; *Bulletin of Canadian Petroleum Geology*, Volume 30, pages 1-8.

Van der Heyden, P. (1992): A Middle Jurassic to Early Tertiary Andean-Sierran Arc Model for the Coast Belt of British Columbia; *Tectonics*, Volume 11, pages 82-97.

Wanless, R.K., Stevens, R. D., Lachance, G. R. and Delabio, R. N. (1979): Age Determinations and Geological Studies: K-Ar Isotopic Ages, Report 14; *Geological Survey of Canada*, Paper 79-2, 67 pages.

Wanless, R.K., Stevens, R.D., Lachance, G.R. and Edmonds, C.M. (1968): Age Determinations and Geologic Studies, K-Ar Isotopic Ages, Report 8; *Geological Survey of Canada*, Paper 67-2A, 141 pages.

Wheeler, J.O. and McFeely, P. (1991): Tectonic Assemblage Map of the Canadian Cordillera and Adjacent Parts of the United States of America; *Geological Survey of Canada*, Map 1712A.

Wheeler, J. O., Brookfield, A.J., Gabrielse, H., Monger, J.W.H., Tipper, H. W. and Woodsworth, G. J. (1991): Terrane Map of the Canadian Cordillera; *Geological Survey of Canada*, Map 1713A.

White, G. V. (1987): Olivine Potential in the Tulameen Ultramafic Complex, Preliminary Report; *in* Geological Fieldwork 1986, *B.C. Ministry of Energy Mines and Petroleum Resources*, Paper 1987-1, pages 303-307.

Wong, R.H., Godwin, C.I. and McTaggart, K.C. (1985): 1977 - Geology, K-Ar Dates and Associated Sulphide Mineralization of Wrede Creek Zoned Ultramafic Complex (94D/9E), *in* Geology in British Columbia 1977-1981, *B.C. Ministry of Energy, Mines and Petroleum Resources*, pages 148-155.

Woodsworth, G.J. (1976): Plutonic Rocks of McConnell Creek (94D West Half) and Aiken Lake (94C East Half) Map Areas, British Columbia; *Geological Survey of Canada*, Paper 76-1A, pages 69-73.

Woodsworth, G.J., Anderson, R. G., Armstrong, R. L., Struik, L. C. and Van der Heyden, P. (1991): Plutonic Regimes, Chapter 15; *in* Geology of the Cordilleran Orogen in Canada; Gabrielse, H. and Yorath, C.J., Editors, *Geological Survey of Canada*, Geology of Canada, Number 4, pages 491-531.

APPENDICES

APPENDIX A

INTERIM REPORTS ON ALASKAN-TYPE COMPLEXES

Hammack, J.L., Nixon, G.T., Wong, R.H., Paterson, W.P.E. and Nuttall, C. (1990): Geology and Noble Metal Geochemistry of the Wrede Creek Ultramafic Complex (94D/9); *B.C. Ministry of Energy, Mines, and Petroleum Resources*, Open File 1990-14 (Map, 1:16 000).

Hammack, J.L., Nixon, G.T., Wong, R.H. and Paterson, W.P.E. (1990): Geology and Noble Metal Geochemistry of the Wrede Creek Ultramafic Complex, North-central British Columbia; *in* Geological Fieldwork 1989, *B.C. Ministry of Energy, Mines, and Petroleum Resources*, Paper 1990-1, pages 405-415.

Hammack, J.L., Nixon, G.T., Paterson, W.P.E. and Nuttall, C. (1991): Geology and Noble Metal Geochemistry of the Lunar Creek Alaskan-type Complex, North-central British Columbia; *in* Geological Fieldwork 1990, *B.C. Ministry of Energy, Mines, and Petroleum Resources, Paper* 1991-1, pages 217-233.

Nixon, G.T., Cabri, L.J. and Laflamme, J.H.G. (1989): Tulameen Placers 92H/7, 10: Origin of Platinum Nuggets in Tulameen Placers: A Mineral Chemistry Approach with Potential for Exploration; *in* Exploration in British Columbia 1988, *B.C. Ministry of Energy, Mines and Petroleum Resources*, pages B83-B89.

Nixon, G.T., Ash, C.H., Connelly, J.N. and Case, G. (1989): Alaskan-type Mafic-ultramafic Rocks in British Columbia: the Gnat Lakes, Hickman, and Menard Creek Complexes; *in* Geological Fieldwork 1988, *B.C. Ministry of Energy, Mines, and Petroleum Resources*, Paper 1989-1, pages 429-442.

Nixon, G.T., Ash, C.H., Connelly, J.N. and Case, G. (1989): Preliminary Geology and Noble Metal Geochemistry of the Polaris Mafic-ultramafic Complex, British Columbia; *B.C. Ministry of Energy, Mines, and Petroleum Resources*, Open File 1989-17 (Map 1:16 000).

Nixon, G.T., Ash, C.H., Connelly, J.N. and Case, G. (1989): Geology and Noble Metal Geochemistry of the Turnagain Ultramafic Complex, Northern British Columbia; *B.C. Ministry of Energy, Mines, and Petroleum Resources*, Open File 1989-18 (Map 1:16 000).

Nixon, G.T. and Hammack, J.L. (1991): Metallogeny of Ultramafic-mafic Rocks in British Columbia with Emphasis on the Platinum-group Elements; *in* Ore Deposits, Tectonics and Metallogeny in the Canadian Cordillera, *B.C. Ministry of Energy, Mines and Petroleum Resources, Paper* 1991-4, pages 125-161.

Nixon, G.T., Cabri, L.J. and Laflamme, J.H.G. (1990): Platinum-group-element Mineralization in Lode and Placer Deposits Associated with the Tulameen Alaskan-type Complex, British Columbia; *Canadian Mineralogist*, Volume 28, pages 503-535.

Nixon, G.T., Hammack, J.L., Connelly, J.N., Case, G. and Paterson, W.P.E. (1990):Geology and Noble Metal Geochemistry of the Polaris Ultramafic Complex, North-central British Columbia; *Geological Fieldwork 1989, B.C. Ministry of Energy, Mines, and Petroleum Resources, Paper* 1990-1, pages 387-404.

Nixon, G.T., Hammack, J.L. and Paterson, W.P.E. (1990): Geology and Noble Metal Geochemistry of the Johanson Lake Ultramafic Complex, North-central British Columbia; *in* Geological Fieldwork 1989, *B.C. Ministry of Energy, Mines, and Petroleum Resources*, Paper 1990-1, pages 417-424.

Nixon, G.T., Hammack, J.L., Ash, C.H., Connelly, J.N., Case, G., Paterson, W.P.E. and Nuttall, C. (1990): Geology of the Polaris Ultramafic Complex (94C/5, 12); *B.C. Ministry of Energy, Mines, and Petroleum Resources, Open File* 1990-13 (2 Map Sheets, 1:16 000 and 1:8 000).

Nixon, G.T., Hammack, J.L., Paterson, W.P.E. and Nuttall, C. (1990): Preliminary Geology and Noble Metal Geochemistry of the Lunar Creek Ultramafic Complex (94E/13, 14); *B.C. Ministry of Energy, Mines, and Petroleum Resources*, Open File 1990-12 (Map 1:16 000).

APPENDIX B

U-Pb ANALYTICAL TECHNIQUES

All U-Pb zircon analyses were performed in the Geochronology Laboratory of the Royal Ontario Museum by Heaman. Rock samples were pulverized in a jaw crusher and Bico disk mill using stringent cleaning procedures for all equipment. Zircon concentrates were obtained by a combination of density and magnetic mineral separation procedures. The rock powder was initially passed over a Wilfley table to obtain a heavy mineral concentrate. This concentrate was further processed using standard mineral separation techniques including a Franz isodynamic separator and heavy liquids (bromoform, methylene iodide). The zircon grains selected for analysis were hand-picked using a binocular microscope, and generally only transparent grains devoid of cracks, alteration, inclusions and other imperfections were chosen. All zircon fractions were given an air abrasion treatment following the procedure outlined by Krogh (1982).

The zircon fractions were washed in nitric acid, weighed on disposable aluminum weighing boats, and dissolved in Parr-type teflon bombs at 220°C using a mixture of HF and 8N HNO_3 (15:1). Prior to dissolution, a calibrated amount of $^{205}Pb/^{235}U$ tracer solution (Krogh and Davis, 1975) was added to each sample in order to determine concentrations by isotope dilution. The uncertainty in the concentrations listed in Tables 4.1 and 8.1 are approximately 1% (2σ) for most fractions and 10% for fractions weighing less than 10 micrograms. Uranium and lead were isolated from the dissolved sample solutions by anion exchange chromatography generally following the procedures of Krogh (1973) except that columns approximately 1/10th of the size of those reported were used. The total procedural blanks for Pb and U are typically in the range 2-10 and 1-5 picograms, respectively.

Both uranium and lead were loaded together onto outgassed Re filaments in a mixture of silica gel and phosphoric acid (silica gel technique of Cameron *et al.*, 1969). The isotopic ratios were measured with a VG354 mass spectrometer in a single collector mode using Faraday or Daly photomultiplier detector systems. All U and Pb isotopic data were corrected for mass discrimination by a factor of +0.13%/amu based on replicate measurements of NBS standards. Isotopic data determined using the Daly detector were also further corrected by a factor of +0.3%/amu. U-Pb age calculations and error estimation follow the procedure of Davis (1982). All errors are reported at the 95% confidence level. The uncertainty in the $^{207}Pb/^{206}Pb$ and U/Pb ratios are generally less than 0.1% and 0.5% respectively. The uranium decay constants and isotopic composition of uranium used are those recommended by Steiger and Jäger (1977): $^{238}U = 1.55125 \times 10^{-10}$ yr^{-1}; $^{235}U = 9.8485 \times 10^{-10}$ yr^{-1}; and $^{238}U/^{235}U = 137.88$.

APPENDIX C

LOCATION OF GEOCHEMICAL SAMPLE SITES, TULAMEEN COMPLEX

Locality[1]	Sample[2]	Easting[3]	Northing[3]	Lat.[4]	Long.[4]
71	3	660687	5475484	49-24-46	120-57-05
12	7	654042	5489416	49-32-23	120-52-15
13	9	653121	5489297	49-32-20	120-53-01
27	10	652642	5488449	49-31-53	120-53-26
29	11A	652323	5488317	49-31-49	120-53-42
29	11B	652323	5488317	49-31-49	120-53-42
30	12	651964	5488214	49-31-46	120-54-00
49	19	649994	5485996	49-30-36	120-55-41
49	20	649994	5485996	49-30-36	120-55-41
36	22	651180	5487482	49-31-23	120-54-40
35	24	651434	5487767	49-31-32	120-54-27
26	28	652178	5488467	49-31-54	120-53-49
24	29A	652072	5488681	49-32-01	120-53-54
24	29B	652072	5488681	49-32-01	120-53-54
22	30	652032	5488680	49-32-01	120-53-56
23	32	651730	5488671	49-32-01	120-54-11
32	33	651747	5488085	49-31-42	120-54-11
33	34	651929	5488028	49-31-40	120-54-02
32	35	651747	5488085	49-31-42	120-54-11
15	36	651713	5489289	49-32-21	120-54-11
14	37	651932	5489357	49-32-23	120-54-00
18	38	651897	5489170	49-32-17	120-54-02
18	39	651897	5489170	49-32-17	120-54-02
20	40	651941	5489048	49-32-13	120-54-00
20	41	651941	5489048	49-32-13	120-54-00
16	45	650731	5489169	49-32-18	120-55-00
41	48	653768	5487029	49-31-06	120-52-32
37	51	653174	5487383	49-31-18	120-53-01
11	55	650742	5489478	49-32-28	120-54-59
21	56	650715	5489014	49-32-13	120-55-01
5	59	654079	5490962	49-33-13	120-52-11
3	60	653276	5491650	49-33-36	120-52-50
1	68	653411	5491840	49-33-42	120-52-43
2	69	653792	5491881	49-33-43	120-52-24
4	70	655503	5491095	49-33-16	120-51-00
6	71	656017	5490708	49-33-03	120-50-35
50	73	653364	5485658	49-30-22	120-52-54
48	77	653594	5486066	49-30-35	120-52-42
43	79	654068	5486388	49-30-45	120-52-18
44	80	654108	5486389	49-30-45	120-52-16
45	81	653929	5486322	49-30-43	120-52-25
47	84	653612	5486128	49-30-37	120-52-41
46	86	653630	5486221	49-30-40	120-52-40
53	87	657999	5484059	49-29-26	120-49-06
53	88	657999	5484059	49-29-26	120-49-06
52	90	658016	5484152	49-29-29	120-49-05
51	92	657175	5484715	49-29-48	120-49-46
57	93A	656839	5480997	49-27-48	120-50-08
58	93B	656802	5480873	49-27-44	120-50-10
60	97	656902	5480906	49-27-45	120-50-05

56	101	655750	5481028	49-27-50	120-51-02
62	102A	657533	5479966	49-27-14	120-49-35
62	102B	657533	5479966	49-27-14	120-49-35
59	103	656678	5480962	49-27-47	120-50-16
55	114	656157	5483697	49-29-16	120-50-38
54	117	658630	5483799	49-29-17	120-48-35
61	124	659132	5480415	49-27-27	120-48-15
64	125	659495	5479004	49-26-41	120-47-59
63	126	659455	5479002	49-26-41	120-48-01
63	127	659455	5479002	49-26-41	120-48-01
67	128A	659246	5478564	49-26-27	120-48-12
67	128C	659246	5478564	49-26-27	120-48-12
68	129	659068	5478466	49-26-24	120-48-21
69	130	658868	5478398	49-26-22	120-48-31
65	131	657642	5478981	49-26-42	120-49-31
66	132	658117	5478593	49-26-29	120-49-08
70	133	659192	5478346	49-26-20	120-48-15
7	143	652373	5490142	49-32-48	120-53-37
8	144	652354	5490110	49-32-47	120-53-38
9	145	652392	5490173	49-32-49	120-53-36
10	146	652058	5489886	49-32-40	120-53-53
19	147	652056	5489237	49-32-19	120-53-54
20	148	651941	5489048	49-32-13	120-54-00
42	149	650741	5488798	49-32-06	120-55-00
40	150	651111	5487078	49-31-10	120-54-44
38	151	651206	5487266	49-31-16	120-54-39
39	152	651228	5487205	49-31-14	120-54-38
34	159	651755	5487776	49-31-32	120-54-11
31	160	652328	5488163	49-31-44	120-53-42
25	163	651234	5488441	49-31-54	120-54-36
72	166	652425	5488289	49-31-48	120-53-37
73	167	652584	5488355	49-31-50	120-53-29
74	168	652623	5488387	49-31-51	120-53-27
75	170	652643	5488388	49-31-51	120-53-26
76	171	652663	5488419	49-31-52	120-53-25
77	172	652683	5488420	49-31-52	120-53-24
78	173	652683	5488420	49-31-52	120-53-24
79	174	652683	5488420	49-31-52	120-53-24
80	175	652663	5488419	49-31-52	120-53-25
81	176	652683	5488420	49-31-52	120-53-24
82	177	652683	5488420	49-31-52	120-53-24
83	179	652702	5488451	49-31-53	120-53-23
84	180	652702	5488451	49-31-53	120-53-23
85	181	652702	5488451	49-31-53	120-53-23
86	182	652702	5488451	49-31-53	120-53-23
28	183	652644	5488357	49-31-50	120-53-26
21	185A	650654	5489043	49-32-14	120-55-04
17	187	650470	5489162	49-32-18	120-55-13

[1] Sample sites shown on Map 5 and Figure 9.6

[2] Prefix GN87-

[3] NTS 92H/10 and 92H/7, UTM Zone 10

[4] Degrees-minutes-seconds

APPENDIX D

SAMPLE PREPARATION AND MICROBEAM TECHNIQUES

Chromitite specimens were initially examined in polished thin section with a Nanolab 7 scanning electron microscope at the University of British Columbia. Subsequently, the nuggets and six chromitite chips from three samples (GN87-146, -147, and -148) were selected for quantitative analysis, and sliced and mounted in cold-setting araldite. The samples were polished on a temperature-controlled Dürener polisher using lead laps, with final buffing using 0.05 m gamma alumina (Laflamme, 1990).

Electron microprobe analyses were done at CANMET on a JEOL733 microanalyzer system. The silicate and spinel analyses were carried out by energy-dispersion spectrometry at 15 kV, with a beam (Faraday cup) current of 12 nA, and using the following x-ray lines (and standards): Fe$K\alpha$ (metal or amphibole #1), Cr$K\alpha$, Ni$K\alpha$ and Zn$K\alpha$ (metals), Al$K\alpha$ (Al_2O_3), Si$K\alpha$ (SiO_2), Mn$K\alpha$ (rhodochrosite), Ti$K\alpha$ (TiO_2), Mg$K\alpha$ (MgO), K$K\alpha$ (orthoclase), CaKa (wollastonite) and Na$K\alpha$ ($NaNbO_3$). Ni and Zn were done by wavelength dispersion spectrometry. Counting times were of the order of 100 s. Analyses of all the PGM and PGE-bearing minerals were carried out by wavelength dispersion spectrometry at 20 kV, with a beam current of 20 nA, using the following x-ray lines (and standards): Pt$L\alpha$ and Fe$K\alpha$ (PtFe or Pt_3Fe), PdLa , Rh$L\alpha$, Ru$L\alpha$, Ir$L\alpha$, Os$M\alpha$, Cu$K\alpha$, NiKα and Sb$L\alpha$ (metals), As$L\alpha$ (InAs), and S$K\alpha$ (pyrite). Raw data were corrected using the ZAF program supplied by Tracor Northern and additional corrections were performed for enhancement of the following primary x-ray lines by secondary lines: Ru$L\beta_1$ and PtM_2 N_4 on Rh$L\alpha_1$; IrL1 on Cu$K\alpha$; Ru$L\beta_2$ and Rh$L\beta_1$ on Pd$L\alpha_1$; and Ru$L\alpha_{II}$ and Sb$L\beta_1$ on As$L\alpha$.Additional electron-microprobe analyses were performed at Queen's University on spinel and olivine in chromitites, dunites and clinopyroxenites using an ARL-SEMQ microanalyzer fitted with an energy-dispersion spectrometer and a Tracor Northern x-ray analysis system. Ten-element analyses were performed simultaneously using an accelerating potential of 15 kV, a beam current of about 20 nA, and counting times of 200 s. Materials used as standards include synthetic glass (Queen's University reference number S-204), chromite (S-164) and olivine (S-68). X-ray intensities were corrected for matrix effects using the procedures of Bence and Albee (1968) and alpha correction factors of Albee and Ray (1970).

BRITISH COLUMBIA
Ministry of Employment and Investment
Energy and Minerals Division
Geological Survey Branch

Geological Survey Branch

BULLETIN 93

Map 1

GEOLOGY OF THE LUNAR CREEK ALASKAN-TYPE COMPLEX

NTS 94E/13,14

Geology by G.T. Nixon, J.L Hammack
W.P.E. Paterson and C. Nuttall

Scale 1:20 000

0 1000
Metres

LEGEND

INTRUSIVE ROCKS

LATE TRIASSIC TO EARLY JURASSIC

GUICHON SUITE GRANITOIDS

HBM — Hornblende-biotite quartz monzonite, monzonite and monzodiorite

Fp — Feldspar porphyry

STIKINE SUITE(?) GRANITOID

HM — Hornblende monzodiorite-foilated

LUNAR CREEK COMPLEX

MID-TRIASSIC

HGD — Dark to pale grey, medium to coarse grained, predominantly hornblende diorite or gabbro with subordinate clinopyroxene-hornblende gabbro or diorite, minor clinopyroxene leucogabbro and hornblende-feldspar-quartz pegmatite; HGDa pale grey, medium grained biotite-hornblende quartz diorite/monzonite; HGDb well-foliated diorite or gabbro similar to unit HGD but older than units HGD and HGDa

Um — Undifferentiated medium to coarse grained, thickly layered hornblende diorite or gabbro, hornblende clinopyroxenite, clinopyroxenite, hornblende-olivine clinopyroxenite and olivine clinopyroxenite

HPx — Dark greenish grey, medium to coarse grained hornblende clinopyroxenite, locally feldspathic

CPx — Dark to medium greenish grey, medium to coarse grained clinopyroxenite, locally feldspathic

OPx — Dark to medium greenish grey, medium to coarse grained, olivine clinopyroxenite with subordinate clinopyroxenite

ImU — Layered mixed units: thinly to thickly stratified, medium to coarse grained dunite/olivine wehrlite and olivine clinopyroxenite/clinopyroxenite; ImUa: replacement dunite/wehrlite locally crosscutting the layering

cmU — Chaotic mixed units: dark to medium greenish grey and buff weathering mottled outcrops comprising irregular blocks and schlieren of medium grained dunite/olivine wehrlite and olivine clinopyroxenite/clinopyroxenite; cmUa: dunite to wehrlite-rich domains; cmUb: clinopyroxenite-rich domains

Du — Pale buff weathering, medium grained, weakly serpentinized dunite cut by abundant olivine clinopyroxenite and clinopyroxenite dikes; Dua: contains minor chromitite schlieren; Dub: contains minor olivine wehrlite

STRATIFIED ROCKS

MIDDLE TRIASSIC TO LOWER JURASSIC

TAKLA GROUP

TJT — Middle greenischist to lowermost amphibolite grade volcanic, volcaniclastic, and sedimentary rocks:
TJTa dark grey to greenish grey augite and plagioclase-phyric actinolitic schists, and amphibole-biotite wacke or tuff;
TJTb dark grey to black well-foliated amphibolite

DEVONIAN TO LOWER PERMIAN

ASITKA GROUP (Basement of Stikine Terrane)

DPA — Greenschist grade volcanic, volcaniclastic, and sedimentary rocks; brownish grey weathering, thinly bedded sandy limestone, medium grey chert, dark grey-green quartz-actionlite schist, hornblende-plagioclase porphyry, actinolitic and saussuritized lithic wacke and/or feldspathic tuff

SYMBOLS

- Geological boundary (defined or approximate, inferred or assumed)
- High-angle fault or shear zone (defined or approximate, inferred or assumed)
- Bedding attitude (tops unknown, inclined, vertical)
- Magmatic layering
- Limit of extensive outcrop
- Schistosity or foliation attitude (inclined, vertical)
- Mineral lineation
- Dike attitude (inclined, vertical)
  - Dike: We-wehrlite; Cp-clinopyroxenite; Mz-hornblende-biotite monzonite/monzodiorite:
  - Fp-feldspar porphyry; Md-hornblende microdiorite; Qf-quartz-feldspar leucogranite;
  - Lm-leuco-monzodiorite; Lg-leucodiorite/leucogabbro
  - (Qf, Lm and Lg may be differentiates of the gabbroic rocks; Mz is probably related to HBM; and Fp and Md are of dubious affinity)
- Strike and dip of quartz vein
- Chromitite localities
- Geochemical assay site (see report for details)
- Field station
- U-Pb isotopic date (zircon) ± 2 σerror — 237±2Ma
- Contours (every 20m)

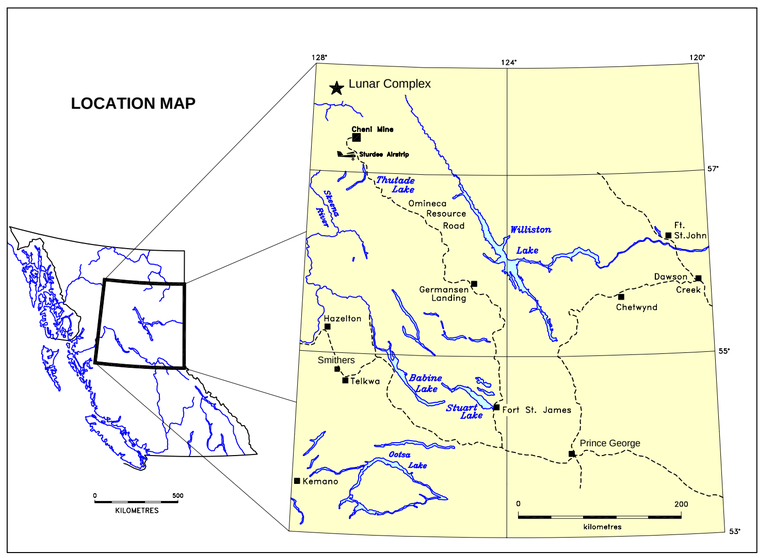

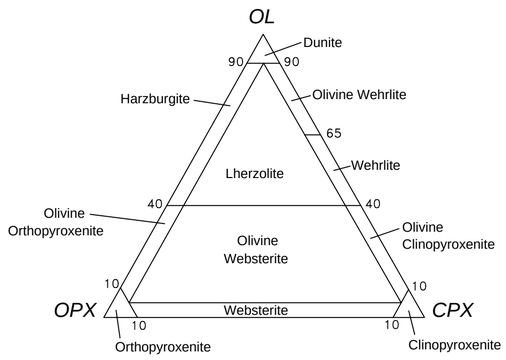

CLASSIFICATION OF ULTRAMAFIC ROCKS

Note: The geology was mapped and fitted to a 1:50 000 NTS (NAD 27) digitized topographic base.

BRITISH COLUMBIA

Ministry of Employment and Investment
Energy and Minerals Division
Geological Survey Branch

Geological Survey Branch

BULLETIN 93

Map 2

GEOLOGY OF THE WREDE CREEK ALASKAN-TYPE COMPLEX

NTS 94D/9

Geology by J.L. Hammack, G.T. Nixon
R.H. Wong, W.P.E. Paterson, and C. Nuttall

Scale 1:20 000

0 1000
Metres

LEGEND

INTRUSIVE ROCKS

MIDDLE JURASSIC

QM — Hornblende-bearing quartz monzonite/monzonite/quartz diorite/diorite: buff-white weathering, white to pale grey, medium grained, equigranular; includes rare plagioclase porphyry

WREDE CREEK COMPLEX

LATE TRIASSIC (?)

HD — Hornblende diorite or gabbro/clinopyroxene-hornblende diorite or gabbro (10-40% plagioclase; 50-90% hornblende; 0-30% clinopyroxene) and hornblendite/clinopyroxene hornblendite (0-10% plagioclase; 50-100% hornblende; 0-50% clinopyroxene); pale grey to black weathering, fine to coarse grained

HPx — Hornblende clinopyroxenite (50-90% clinopyroxene; 10-50% hornblende): medium brown weathering, coarse grained

uCPx — Undifferentiated clinopyroxenite includes hornblende clinopyroxenite (50-90% clinopyroxene; 10-50% hornblende)clinopyroxenite (90-100% clinopyroxene)/olivine clinopyroxenite (60-90% clinopyroxene; 10-40% olivine)/olivine-hornblende clinopyroxenite (50-90% clinopyroxene; 10-50% hornblende; 5-15% olivine): dark to medium grey-green weathering, medium to coarse grained

OPx — Olivine clinopyroxenite (10-40% olivine; 60-90% clinopyroxene): medium to pale grey-green weathering, medium to coarse grained

We — Wehrlite (40-65% olivine; 35-60% clinopyroxene): dark to medium brown weathering, predominantly medium grained or medium to coarse grained

Du — Dunite (90-100% olivine; 0-10% clinopyroxene): pale buff-orange weathering, dark grey to black, fine to medium grained

STRATIFIED ROCKS

MIDDLE TRIASSIC TO LOWER JURASSIC
TAKLA GROUP

TJT — Brown to dark grey weathering, medium grey-green and dark grey augite and augite-plagioclase crystal tuffs, flows and volcanic breccia

UPPER PALEOZOIC (Mississippian-Permian)
LAY RANGE ASSEMBLAGE (HARPER RANCH SUBTERRANE)

MPLA — Phyllite, phyllitic quartzite, chlorite schist, chert, lithic tuff, volcanic breccia and minor pillow basalt

UPPER PROTEROZOIC TO PALEOZOIC
EAGLE BAY ASSEMBLAGE (KOOTENAY TERRANE)

BPEA — Metamorphosed mafic to intermediate volcanic rocks, chlorite schist and limestone

SYMBOLS

- Geological boundary (defined or approximate, inferred or assumed)
- Geological boundary inferred from aeromagnetic data
- High-angle fault or shear zone (defined or approximate, inferred or assumed)
- Bedding attitude (tops unknown, inclined, vertical)
- Magmatic layering
- Schistosity or foliation attitude (inclined, vertical)
- Dike attitude (Di, diorite, quartz diorite, monzonite and quartz monzonite; We, wehrlite; Du, dunite; Hb, hornblende-feldspar pegmatite) (inclined, vertical)
- Chromitite schlieren (inclined, vertical)
- Geochemical sample site (see report for details)
- Chromitite geochemical sample site (see report for details)
- Other chromitite localities
- Outcrop
- Contours (every 20m)

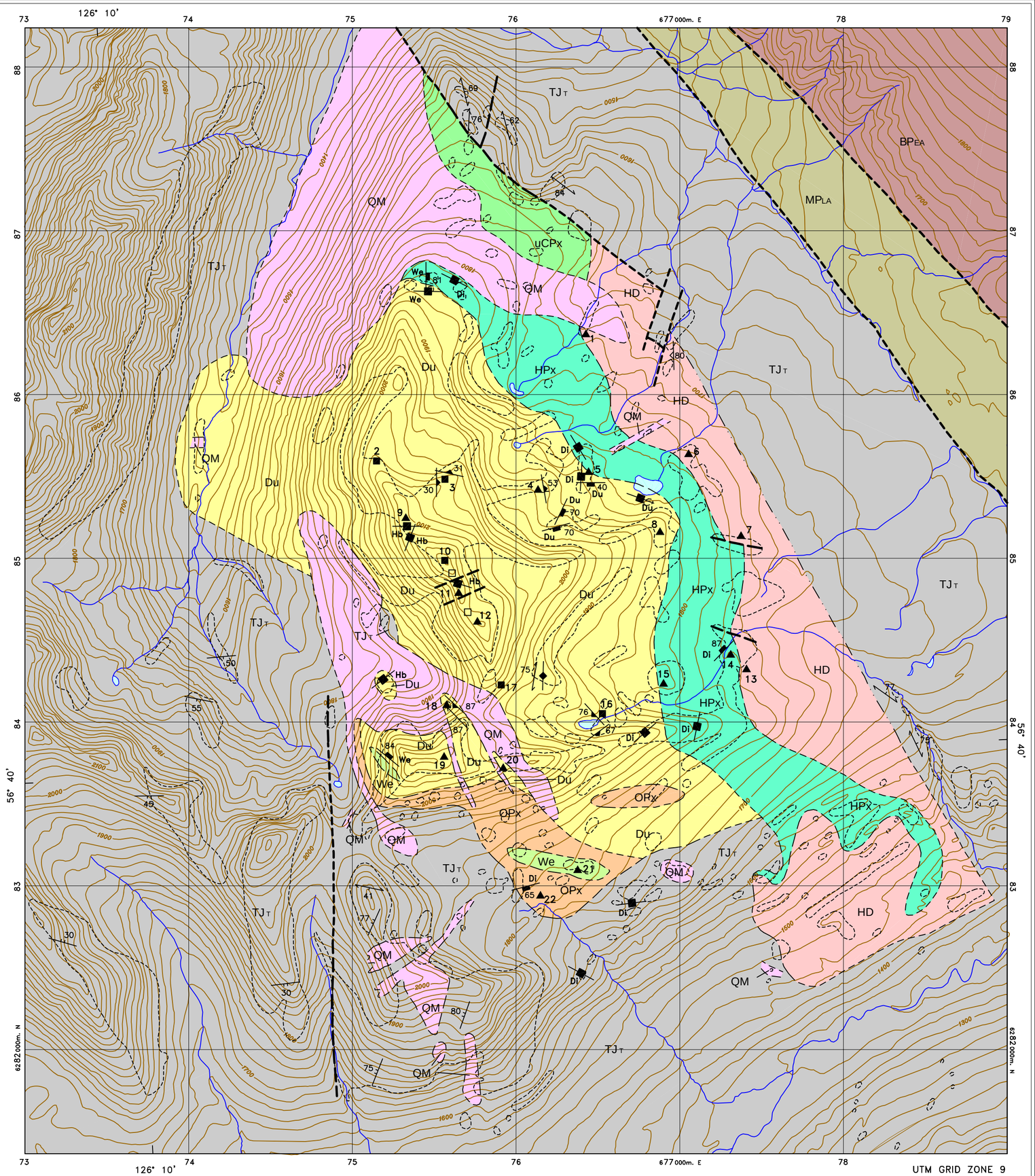

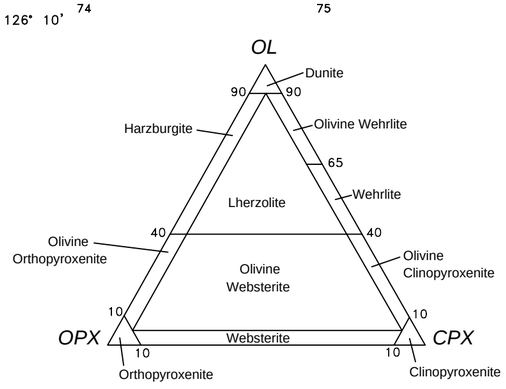

CLASSIFICATION OF ULTRAMAFIC ROCKS

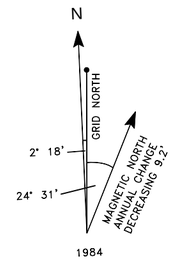

Note: The geology was mapped and fitted to a 1:50 000 NTS (NAD 27) digitized topographic base.

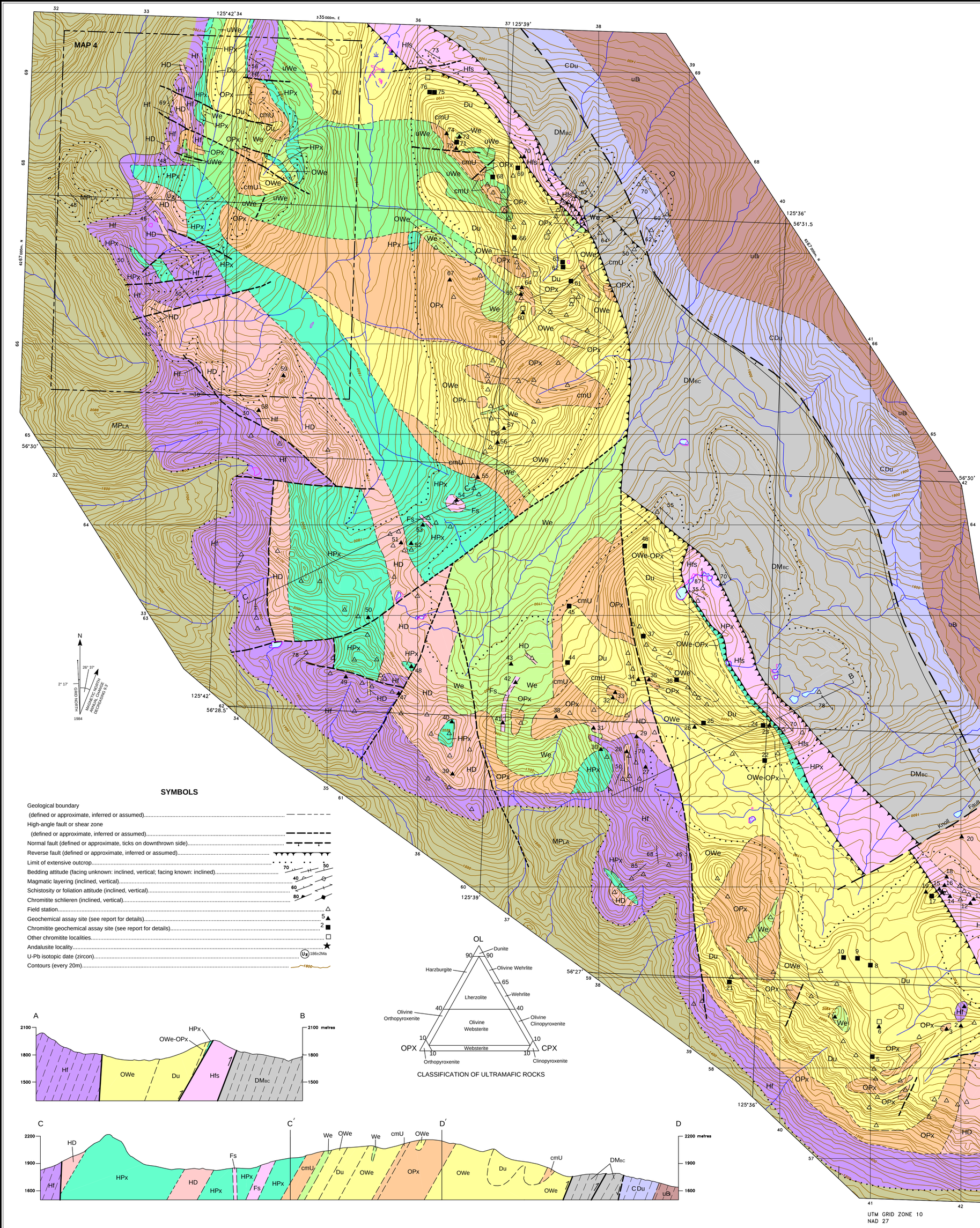

SYMBOLS

- Geological boundary (defined or approximate, inferred or assumed)
- High-angle fault or shear zone (defined or approximate, inferred or assumed)
- Normal fault (defined or approximate, ticks on downthrown side)
- Reverse fault (defined or approximate, inferred or assumed)
- Limit of extensive outcrop
- Bedding attitude (facing unknown: inclined, vertical; facing known: inclined)
- Magmatic layering (inclined, vertical)
- Schistosity or foliation attitude (inclined, vertical)
- Chromitite schlieren (inclined, vertical)
- Field station
- Geochemical assay site (see report for details)
- Chromitite geochemical assay site (see report for details)
- Other chromitite localities
- Andalusite locality
- U-Pb isotopic date (zircon) — Uz 186±2Ma
- Contours (every 20m)

CLASSIFICATION OF ULTRAMAFIC ROCKS

UTM GRID ZONE 10
NAD 27

BRITISH COLUMBIA
Ministry of Employment and Investment
Energy and Minerals Division
Geological Survey Branch

Geological Survey Branch

BULLETIN 93

Map 3

GEOLOGY OF THE POLARIS ALASKAN-TYPE COMPLEX

NTS 94C/5

Geology by G.T. Nixon, J.L. Hammack, C.H. Ash
J.N. Connelly, G. Case, W.P.E. Paterson and C. Nuttall*

Scale 1:20 000

0 — 1000 Metres

LEGEND

POLARIS COMPLEX

EARLY JURASSIC

- **Fs** — Felsic intrusions: syenite/leucomonzonite, pale grey to cream weathering; many thin, medium grained to locally pegmatitic dikes (not shown) in western part of complex
- **HD** — Hornblende-bearing diorite or gabbro, equigranular to locally mylonitic, dark to medium grey weathering, fine to medium grained, rare local layering, includes minor clinopyroxene-hornblende diorite or gabbro and feldspathic hornblendite
- **HPx** — Hornblende clinopyroxenite (90-50% clinopyroxene; 50-10% hornblende) clinopyroxene hornblendite (90-50% hornblende; 50-10% clinopyroxene) and minor hornblende-olivine clinopyroxenite, hornblendite and feldspathic hornblendite: dark to medium grey-green or black weathering, medium to coarse grained
- **cmU** — Chaotic mixed olivine wehrlite-wehrlite-minor dunite and olivine clinopyroxenite-clinopyroxenite: mottled brown and pale grey-green weathering, medium to coarse grained
- **OPx** — Olivine clinopyroxenite (40-10% olivine; 90-60% clinopyroxene) to clinopyroxenite (10-0% olivine; 100-90% clinopyroxene): medium to pale grey-green weathering, medium to coarse grained, locally pegmatitic
- **uWe** — Undifferentiated olivine wehrlite to wehrlite: dark to medium brown weathering, medium to coarse grained, rare clinopyroxene megacrysts
- **We** — Wehrlite (65-40% olivine; 60-35% clinopyroxene) with minor olivine clinopyroxenite: dark to medium brown weathering, medium to coarse grained, rare pegmatitic clinopyroxene
- **OWe** — Olivine wehrlite (90-65% olivine; 35-10% clinopyroxene): dark to medium brown weathering, generally medium grained
- **Du** — Dunite (100-90% olivine; 10-0% clinopyroxene): pale buff weathering, generally medium grained
- **Hf | Hfs** — Contact Metamorphic Aureole: Hf, Hornfelsed volcanic and sedimentary rocks of the Lay Range Assemblage; Hfs, strongly foliated rocks in the basal metamorphic aureole, locally includes amphibolite and mica and andalusite schist; protolith in part includes minor sills of gabbro/diorite and clinopyroxenite

STRATIFIED ROCKS

UPPER PALEOZOIC

Lay Range Assemblage (Mississippian to Permian)

- **MPLA** — Metasedimentary and metavolcanic rocks including flows, tuffs and subvolcanic intrusions (augite and/or plagioclase-phyric and hornblende-phyric),laminated to thickly bedded, tuffaceous siltstone and sandstone, phyllite, shale and mudstone, minor impure limestone, chert and conglomerate; predominantly dark grey to green weathering, generally fine grained, locally graded and cross bedded

Big Creek Group (Upper Devonian to Lower Mississippian)

- **DMBC** — Shale, mudstone, siltstone, sandstone, wacke, chert, conglomerate and minor limestone and felsic tuff; predominantly black to dark grey; thinly bedded and wavy bedded

- **CDu** — Undifferentiated Cambrian to Devonian rocks of the Atan, Razor Back, Echo Lake and Otter Lakes Groups, includes limestone and dolostone, shale, siltstone, sandstone, impure quartzite, phyllite and minor schist

UPPER PROTEROZOIC

Ingenika Group

- **uBi** — Limestone, sandstone, quartzite, siltdstone, slate, phyllite and schist

*Geology east of Polaris taken from Ferri, F., Dudka, S., Rees, C. and Meldrum, D. (1993): Preliminary Geology of the Aiken Lake and Osilinka River Areas, British Columbia (NTS 94C/2,3,5,6 and 12); Ministry of Energy, Mines and Petroleum Resources, Open File 1993-2

Note: The geology was mapped and fitted to a 1:50 000 NTS (NAD 27) digitized topographic base.

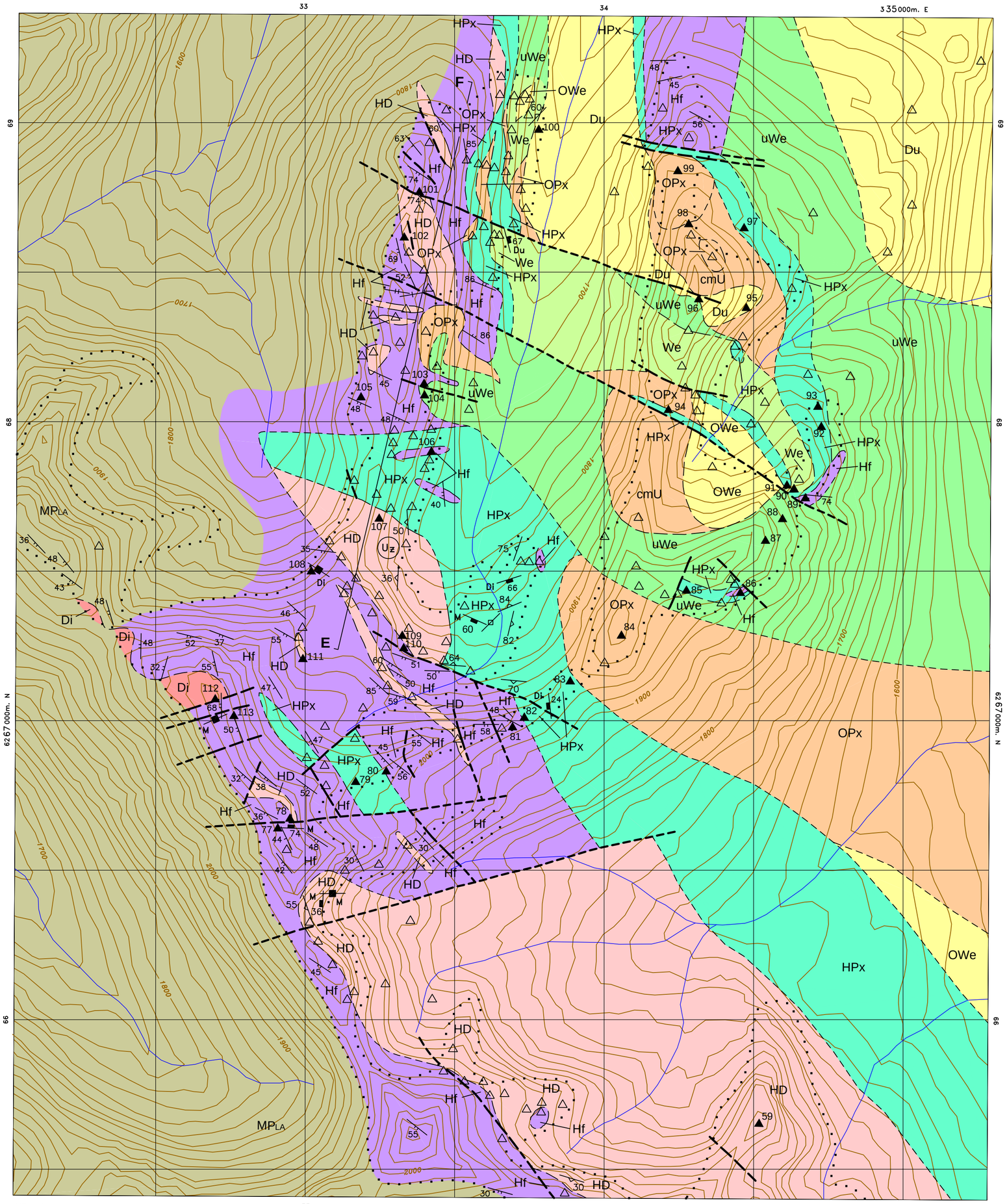

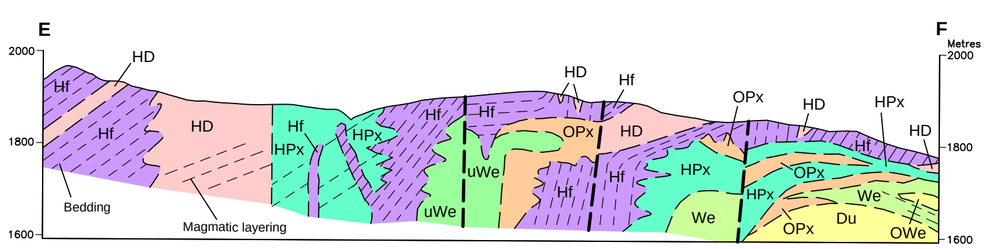

Note: The geology was mapped and fitted to a 1:50 000 NTS (NAD 27) digitized topographic base.

BRITISH COLUMBIA
Ministry of Employment and Investment
Energy and Minerals Division
Geological Survey Branch

Geological Survey Branch

BULLETIN 93

Map 4

GEOLOGY OF THE NORTHWESTERN PART OF THE POLARIS ALASKAN-TYPE COMPLEX

NTS 94C/5

Geology by G.T. Nixon, J.L. Hammack, C.H. Ash
J.N. Connelly, G. Case, W.P.E. Paterson and C. Nuttall

Scale 1:10 000

0 — 1000
Metres

LEGEND

INTRUSIVE ROCKS

JURASSIC (?)

Di — Hornblende diorite: grey-brown weathering, medium grained, locally epidotized

POLARIS COMPLEX

EARLY JURASSIC

HD — Hornblende-bearing diorite or gabbro, equigranular to locally mylonitic, dark to medium grey weathering, fine to medium grained, rare local layering, includes minor clinopyroxene-hornblende diorite or gabbro and feldspathic hornblendite

HPx — Hornblende clinopyroxenite (90-50% clinopyroxene; 50-10% hornblende) clinopyroxene hornblendite (90-50% hornblende; 50-10% clinopyroxene) and minor hornblende-olivine clinopyroxenite, hornblendite and feldspathic hornblendite: dark to medium grey-green or black weathering, medium to coarse grained

cmU — Chaotic mixed olivine wehrlite-wehrlite-minor dunite and olivine clinopyroxenite-clinopyroxenite: mottled brown and pale grey-green weathering, medium to coarse grained

OPx — Olivine clinopyroxenite (40-10% olivine; 90-60% clinopyroxene) to clinopyroxenite (10-0% olivine; 100-90% clinopyroxene): medium to pale grey-green weathering, medium to coarse grained, locally pegmatitic

uWe — Undifferentiated olivine wehrlite to wehrlite: dark to medium brown weathering, medium to coarse grained, rare clinopyroxene megacrysts

We — Wehrlite (65-40% olivine; 60-35% clinopyroxene) with minor olivine clinopyroxenite: dark to medium brown weathering, medium to coarse grained, rare pegmatitic clinopyroxene

OWe — Olivine wehrlite (90-65% olivine; 35-10% clinopyroxene): dark to medium brown weathering, generally medium grained

Du — Dunite (100-90% olivine; 10-0% clinopyroxene): pale buff weathering, generally medium grained

Hf — Contact Metamorphic Aureole
Hornfelsed volcanic and sedimentary rocks of the Lay Range Assemblage

STRATIFIED ROCKS

UPPER PALEOZOIC

Lay Range Assemblage (Mississippian to Permian)

MPLA — Metasedimentary and metavolanic rocks including flows, tuffs and subvolcanic intrusions (augite and/or plagioclase-phyric and hornblende-phyric),laminated to thickly bedded, tuffaceous siltstone and sandstone, phyllite, shale and mudstone, minor impure limestone, chert and conglomerate; predominantly dark grey to green weathering, generally fine grained, locally graded and cross bedded

SYMBOLS

Geological boundary
(defined or approximate, inferred or assumed)

High-angle fault or shear zone
(defined or approximate, inferred or assumed)

Limit of extensive outcrop

Bedding attitude
(Facing known: inclined, vertical; facing unknown: inclined, vertical)

Magmatic layering (inclined, vertical)

Schistosity or foliation attitude (inclined, vertical)

Dike attitude (M-mafic; Di-diorite, quartz diorite, monzonite and quartz monzonite; Du-dunite; inclined, vertical)

Field station

Geochemical assay site (see report for details)

U-Pb isotopic date (zircon) — 186±2Ma

Contours (every 20m)

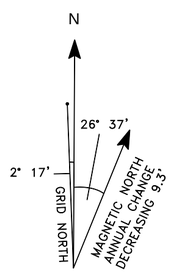

BRITISH COLUMBIA
Ministry of Employment and Investment
Energy and Minerals Division
Geological Survey Branch

Geological Survey Branch

BULLETIN 93

Map 5

GEOLOGY OF THE TULAMEEN ALASKAN-TYPE COMPLEX

NTS 92H/7, 10

Geology by D.C. Findlay (1963)* as modified by G.T. Nixon

Scale 1:20 000

0 1000
Metres

LEGEND

INTRUSIVE ROCKS

TERTIARY (Eocene)

Egd — Granodiorite (unfoliated)

LATE JURASSIC TO MID-CRETACEOUS

TKegd — Eagle Plutonic Complex: granodiorite (foliated)

TULAMEEN COMPLEX

LATE TRIASSIC

Pg — Mafic pegmatite (locally feldspathic)

Sd — 'Syenodiorite' (monzonite-monzodiorite), variably saussuritized

Gb — Gabbro-'syenograbbo'(monzogabbro-monzodiorite), variably saussuritized

Um — Undifferentiated mafic-ultramafic rocks (gabbro or diorite/ hornblende clinopyroxenite/hornblendite)

HPx — Hornblende clinopyroxenite (includes minor hornblendite, clinopyroxenite, mafic pegmatite and magnetite schlieren)

HOPx — Hornblende-olivine clinopyroxenite

OPx — Olivine clinopyroxenite (includes minor olivine wehrlite/wehrlite

Du — Dunite (variably serpentinized; includes minor olivine wehrlite/ wehrlite)

STRATIFIED ROCKS

TERTIARY (Eocene)

PRINCETON GROUP

EPR — Shales,arkosic sandstones and conglomerates, coal seams and seat earths, laharic breccias, rhyolitic to basaltic lava flows

UPPER TRIASSIC

NICOLA GROUP

ut N — Metasedimentary and metavolcanic rocks

ut Nv — Metavolcanic units

ut Nm — Marble

MYLONITIC ROCKS

My — Undifferentiated ductily deformed Nicola and ultramafic-mafic rocks

SYMBOLS

Geological boundary (defined or approximate, inferred or assumed)

Unconformity (inferred)

High-angle fault (defined or approximate, inferred)

Foliation strike and dip (inclined, vertical)

Bedding strike and dip (inclined: tops unknown, tops known)

Chromite schlieren strike and dip (inclined, vertical)

Minor fold attitude (plunge of axis, dip of axial plane, vertical axial plane, folded chromitite schlieren)

Mineral lamination strike and dip (inclined, vertical)

Mineral lineation (plunge indicated)

Dike strike and dip (<2m width, >2m width)

Dikes and minor intrusions: M=mafic; F=felsic; H=intermediate, hornblende-phyric; Cp=clinopyroxenite

Magnetite prospect

Sulphide occurrence

Geochemical assay site (see report for details)

Chromitite/chromitiferous dunite assay site (see report for details)

Contours (every 100 feet)

*Findlay, D.C. (1963): Petrology of the Tulameen Ultramafic Complex, Yale District, British Columbia, Unpublished Ph. D. Thesis, Queen's University, Kingston, Ontario.

N
1° 42'
GRID NORTH
20° 34'
MAGNETIC NORTH
ANNUAL CHANGE DECREASING 4.5'
1977

OL
Dunite
Harzburgite
Olivine Wehrlite
Lherzolite
Wehrlite
Olivine Orthopyroxenite
Olivine Websterite
Olivine Clinopyroxenite
OPX
Websterite
CPX
Orthopyroxenite
Clinopyroxenite

CLASSIFICATION OF ULTRAMAFIC ROCKS

UTM GRID ZONE 10
NAD 27

Note: The geology was mapped and fitted to a 1:50 000 NTS (NAD 27) digitized topographic base.